Titre: Title:	Identification robuste de fonctions de transfert par déconvolution pour l'interprétation d'essais de réponse thermique
Auteur: Author:	Gabriel Dion
Date:	2023
Type:	Mémoire ou thèse / Dissertation or Thesis
Référence: Citation:	Dion, G. (2023). Identification robuste de fonctions de transfert par déconvolution pour l'interprétation d'essais de réponse thermique [Thèse de doctorat, Polytechnique Montréal]. PolyPublie. https://publications.polymtl.ca/57118/

URL de PolyPublie: PolyPublie URL:	https://publications.polymtl.ca/57118/
Directeurs de recherche: Advisors:	Philippe Pasquier, & Denis Marcotte
Programme: Program:	Génie minéral

POLYTECHNIQUE MONTRÉAL
affiliée à l'Université de Montréal

Identification robuste de fonctions de transfert par déconvolution pour l'interprétation d'essais de réponse thermique

GABRIEL DION
Département des génies civil, géologique et des mines

Thèse présentée en vue de l'obtention du diplôme de *Philosophiæ Doctor*
Génie minéral

Décembre 2023

POLYTECHNIQUE MONTRÉAL
affiliée à l'Université de Montréal

Cette thèse intitulée :

Identification robuste de fonctions de transfert par déconvolution pour l'interprétation d'essais de réponse thermique

présentée par **Gabriel DION**
en vue de l'obtention du diplôme de *Philosophiæ Doctor*
a été dûment acceptée par le jury d'examen constitué de :

Massimo CIMMINO, président
Philippe PASQUIER, membre et directeur de recherche
Denis MARCOTTE, membre et codirecteur de recherche
Gabriel FABIEN-OUELLET, membre
Bertrand FRANÇOIS, membre externe

DÉDICACE

"Le doute est à l'origine de la sagesse."
- René Descartes

REMERCIEMENTS

Tout d'abord, j'offre mes sincères remerciements à mon directeur Philippe Pasquier, qui a su me guider avec ses suggestions, ses critiques constructives et ses remarques pertinentes lors de nos nombreuses rencontres durant les quatre dernières années. Ses précieux conseils m'ont permis d'achever mon doctorat avec un sentiment de fierté envers le travail que j'ai accompli.

Mes prochains remerciements s'adressent à mon co-directeur Denis Marcotte, qui m'a énormément aidé techniquement et qui a toujours su me communiquer authentiquement ses conseils, autant pour des équations, des résultats ou les nombreux textes qu'il a révisés. La qualité des documents que j'ai produits a largement été augmentée par son aide.

J'adresse mes remerciements aux membres du jury Massimo Cimmino, Gabriel Fabien-Ouellet et Bertrand François pour avoir consacré leur temps et leur énergie à la révision de cette thèse.

Je tiens ensuite à exprimer ma gratitude envers mes collègues de bureau, Léo Cerclet, Louis Jacques, Gabrielle Beaudry, Christopher Rose et Stéphanie Robert pour leur support à la fois technique et émotionnel tout au long de mon projet de recherche. Les rencontres en ligne au vif de la pandémie de la COVID-19 ont permis de maintenir une certaine productivité malgré ces moments éprouvants.

J'aimerais aussi signifier ma reconnaissance sans borne envers ma compagne, Jade qui a été mon pilier et ma source d'énergie dès les premiers mois de mon projet de recherche. Son écoute, son empathie et son ouverture ont été des composantes irremplaçables à ma réussite.

Finalement, ce projet a été réalisable grâce au soutien du Conseil de recherche en sciences naturelles et en génie du Canada, l'Institut de l'énergie Trottier, Forage FTE, Marmott Énergies, Richelieu Hydrogéologie et Versaprofiles.

RÉSUMÉ

Les efforts globaux pour combattre le réchauffement climatique tentent, entre autres, de réduire la quantité d'énergie utilisée pour le chauffage et la climatisation des bâtiments, ce qui diminuera les émissions de gaz à effet de serre associées à cette activité. Pour atteindre cet objectif, les systèmes géothermiques de basses températures ont été ciblés comme une technologie prometteuse, diminuant la consommation d'un bâtiment pour le chauffage et la climatisation par un facteur de 3 à 5. Pour dimensionner et concevoir ces systèmes, l'essai de réponse thermique est largement employé, car il permet d'identifier les paramètres thermiques du sol à l'endroit où un système géothermique sera conçu. Il s'agit d'un test *in situ* où la différence de température entre l'entrée et la sortie d'un échangeur de chaleur souterrain permet le calcul des propriétés thermiques du sol. À l'aide de ces paramètres et de la demande énergétique en chauffage et en climatisation du bâtiment, des simulations sont effectuées pour répondre à un certain pourcentage de la demande énergétique du bâtiment selon différentes configurations, longueurs de forage et conditions d'opération. Ainsi, évaluer précisément les paramètres thermiques du sol mène à des simulations et un dimensionnement précis du système géothermique.

Pour interpréter un essai de réponse thermique, un modèle direct émulant le transfert de chaleur dans le sol, ainsi qu'une méthode d'inversion sont employés. Les modèles représentent les processus d'échange de chaleur dans le sol et dans l'échangeur de chaleur souterrain à l'aide de divers paramètres, tandis que les méthodes d'inversion optimisent la valeur des paramètres thermiques pour que le modèle direct s'ajuste aux données expérimentales de l'essai. Une autre approche utilise les fonctions de transfert, qui représentent la réponse thermique de l'échangeur de chaleur souterrain à une charge unitaire et constante de chaleur. Ainsi, ces dernières peuvent être utilisées pour simuler les températures en sortie de l'échangeur de chaleur souterrain selon le patron de charges thermiques, soit pour reproduire un essai de réponse thermique, ou pour tester la réponse de l'échangeur à différents patrons de charges et conditions d'opération. Préalablement aux travaux de cette thèse, les fonctions de transfert étaient évaluées à l'aide de modèles analytiques ou numériques. Chacune de ces approches comporte des inconvénients, qui concernent soit la précision de la reconstruction avec les fonctions de transfert ou le temps de calcul avec les modèles numériques.

L'objectif principal de ce projet de recherche est de développer une méthodologie par déconvolution permettant d'améliorer l'interprétation des données expérimentales d'un essai de réponse thermique pour différents échangeurs de chaleur souterrain. La méthode retenue doit

être précise et rapide, s'appliquer à différents types d'échangeurs de chaleur souterrains et pour différents types d'essais de réponse thermique. Pour atteindre cet objectif, un algorithme de déconvolution robuste a été développé permettant l'obtention de fonctions de transfert à court terme pouvant être utilisées directement à la simulation des systèmes géothermiques.

Les premiers travaux de ce projet de recherche ont été d'identifier et de développer la méthode de déconvolution la plus adaptée aux données expérimentales d'un essai de réponse thermique pour des conditions d'opération stationnaires. La méthode d'optimisation établie itère sur la position de noeuds positionnés sur la fonction de transfert et minimise une fonction comprenant des termes d'ajustement des températures et de régularisations permettant d'améliorer l'efficacité de l'algorithme et le réalisme des fonctions de transfert obtenues. Des contraintes linéaires d'inégalité sont aussi incluses pour que la fonction de transfert respecte certaines propriétés mathématiques, telles que la positivité, la croissance continue et la décroissance de la dérivée première après quelques heures d'essais. La validation de la méthode de déconvolution a été faite à l'aide de plusieurs essais de réponse thermique générés à partir d'un modèle numérique, ainsi que des essais réels sur le terrain. La méthode a été appliquée à des échangeurs de chaleur souterrains de types puits en boucle fermée et puits à colonne permanente, résultant en une fonction de transfert par essai qui respecte les contraintes d'optimisation établies. Les températures reconstruites à l'aide de ces fonctions ont un manque ajustement de moins de 0.10 °C avec les températures de l'essai, ce qui est conforme avec la précision des capteurs de température.

Lors de l'opération d'un système géothermique, les conditions d'opérations sont variées pour fournir la charge de chauffage ou de climatisation souhaitée au bâtiment. Cela permet de minimiser les coûts d'exploitation, ce qui est particulièrement important pour les puits à colonne permanente, où le débit de circulation est plus élevé que pour les puits en boucle fermée. Une fonction de transfert représente l'échange de chaleur pour des conditions d'opération fixes. Ainsi, lorsque ces dernières changent, plusieurs fonctions sont nécessaires et la méthode de déconvolution validée doit être modifiée pour considérer la non-stationnarité de l'essai. Les travaux réalisés durant cette thèse ont abordé cette problématique en utilisant un algorithme de convolution non stationnaire comme modèle direct. Ainsi, la déconvolution itère sur les noeuds de plusieurs fonctions de transfert, qui sont définies pour chaque séquence de conditions d'opérations. L'algorithme interprète la première séquence d'un essai de réponse thermique comme étant stationnaire, puis optimise les fonctions pour les autres séquences. Pour cela, le processus d'optimisation déterminé rend des ajustements de températures aussi précis que 0.10 °C. Cette approche a été validée par des essais de réponse thermique non stationnaires générés numériquement et des essais de terrain.

Pour dimensionner un échangeur de chaleur souterrain, des notions sur la géologie locale, l'écoulement souterrain et la distribution verticale des propriétés thermiques et hydrogéologiques du site aident les concepteurs à choisir l'emplacement et la profondeur à laquelle forer pour minimiser les coûts de construction et maximiser l'échange thermique possible. Pour évaluer la distribution verticale des propriétés thermiques du sol, les essais de réponses thermiques distribués sont couramment employés. Dans ces derniers, une fibre optique installée dans l'échangeur de chaleur souterrain permet d'enregistrer les signaux de températures à différentes profondeurs. L'interprétation de ces essais traduit les variations verticales des propriétés physique, géologique et hydrogéologique par un profil de conductivités thermiques en fonction de la profondeur dans l'échangeur de chaleur souterrain. Lors de ce projet de recherche, la méthode de déconvolution a été appliquée à ce type d'essai pour obtenir des fonctions de transfert pour chaque unité géologique d'un site. L'interprétation de ces fonctions montre une précision supérieure sur l'estimation des conductivités thermiques comparée à celles obtenues en interprétant les signaux de températures. De plus, l'interprétation à l'aide des fonctions de transfert est plus robuste lorsque le débit de circulation dans l'échangeur de chaleur souterrain est faible, un effet qui éloigne les données expérimentales des hypothèses des modèles de transfert de chaleur. Finalement, les fonctions de transfert permettent d'identifier nettement l'instant où le transfert de chaleur passe du puits au sol environnant.

Les travaux de recherche effectués contribuent significativement à l'interprétation efficace des essais de réponse thermique, qu'ils soient réguliers ou distribués, dans différentes conditions d'opération (stationnaires ou instationnaires) et sur différents types d'échangeurs de chaleur souterrains, tels que les puits en boucle fermée et les puits à colonne permanente. Une discussion approfondie des résultats met en évidence diverses stratégies et méthodologies à considérer pour appliquer adéquatement la déconvolution. La méthode de déconvolution proposée s'intègre dans le processus de conception d'un système géothermique, en facilitant l'interprétation des essais sur le terrain et en aidant à la simulation et au dimensionnement du système à construire.

ABSTRACT

Global efforts to combat global warming are aiming, among other targets, to reduce the amount of energy used to heat and cool buildings, thereby lowering the greenhouse gas emissions associated with this activity. To achieve this goal, low-temperature geothermal systems have been identified as a promising technology, limiting a building's consumption for heating and cooling by a factor of 3 to 5. To size and design these systems, the thermal response test is widely used, as it allows to identify the thermal parameters of the ground at the location where a geothermal system is to be built. The thermal response test is *in-situ* and the temperature difference between the inlet and outlet of a ground heat exchanger is used to calculate the thermal properties of the soil. Using these parameters and the heating/cooling thermal load of the building, simulations are carried out to meet a certain percentage of the building's energy demand for different configurations, borehole lengths and operating conditions. In this way, precise assessment of the ground's thermal parameters leads to accurate simulations and correct sizing of the geothermal system.

To interpret a thermal response test, both a direct model emulating heat transfer in the ground and an inversion method are employed. The models represent the heat exchange processes in the soil and in the ground heat exchanger using various parameters, while the inversion methods optimize the value of the thermal parameters so that the direct model fits the experimental data. Another approach uses transfer functions that define the thermal response of the ground heat exchanger to a constant and unitary heat pulse. They can then be used to simulate temperature signals at the outlet of the ground heat exchanger, according to a thermal load, either to reproduce a thermal response test, or to test the exchanger's response to different heat load and operating conditions. Prior to this thesis, transfer functions were evaluated using analytical or numerical models. Each of these approaches has drawbacks, which relate either to the reconstruction accuracy with the transfer functions or the computation time for numerical models.

The main objective of this research project is to develop a deconvolution methodology to improve the interpretation of experimental data from a thermal response test for different ground heat exchangers. The chosen method must be accurate and fast, applicable to different types of ground heat exchangers and different types of thermal response tests. To achieve this goal, a robust deconvolution algorithm has been developed to obtain short-term transfer functions that can be used directly to simulate geothermal systems.

The initial work of this research project is to identify and develop a deconvolution method

that is best suited to the experimental data from a thermal response test for stationary operating conditions. The selected optimization method iterates over the position of nodes on the transfer function to minimize a function including temperature adjustment and regularization terms to improve the efficiency of the algorithm and the realism of the resulting transfer functions. Linear inequality constraints are also included to ensure that the transfer function respects certain mathematical properties, such as positivity, continuously growing and negative first derivative after a few hours of test. The deconvolution method has been validated using several thermal response tests generated from a numerical model, as well as field tests. The method was applied to ground heat exchanger of either closed-loop or standing column well types, resulting in a transfer function that respects the chosen optimization constraints for each test. The temperatures reconstructed using these functions have a misfit of less than 0.10 °C with the experimental ones, which is consistent with the accuracy of the temperature sensors.

When operating a geothermal system, operating conditions are varied to provide the desired heating or cooling load to the building. In doing so, operating costs can be minimized, which is particularly relevant for standing column wells, where circulation rates are much higher than in closed-loop systems. To reproduce these operating conditions, thermal response tests can be conducted by changing operating conditions. The validated deconvolution method must then be modified to interpret non-stationay thermal response tests. The subsequent work in this thesis addresses this issue by using a non-stationary convolution algorithm as a direct model. Thus, deconvolution iterates over the nodes of several transfer functions, which are defined for each sequence of operating conditions. The algorithm interprets the first sequence as stationary and then optimizes the functions for the remaining sequences. To do this, the optimization process results in temperature adjustments as accurate as 0.10 °C.

When sizing a ground heat exchanger, knowledge of the local geology, groundwater flow and vertical distribution of the site's thermal and hydrogeological properties helps designers to choose the location and depth of the ground heat exchanger to minimize construction costs and maximize possible heat exchange. Distributed thermal response tests are commonly used to assess the vertical distribution of soil thermal properties. In these tests, a fiber-optic cable is installed in the ground heat exchanger to record temperature signals at different depths. Their interpretation translates the vertical variations of physical, geological and hydrogeological properties into a profile of thermal conductivity estimations as a function of depth. During this research project, the deconvolution method was applied to this type of test to obtain transfer functions for each geological layer of a site. The interpretation of these functions shows a marked improvement in the accuracy of estimated thermal conductivity compared with those obtained by interpreting temperature signals. Furthermore, the results

of the interpretation using transfer functions are more robust when the flow rate in the ground heat exchanger is low, an effect that dissociate the experimental data from assumptions used in heat transfer models. Finally, the transfer functions clearly identify the point at which heat transfer occurs from the borehole to the surrounding soil.

The research carried out has contributed significantly to the effective interpretation of thermal response tests, whether regular or distributed, under different operating conditions (stationary or non-stationary) and on different types of ground heat exchangers, such as closed-loop and standing column wells. An in-depth discussion of the results highlights various strategies and methodologies to correctly apply the deconvolution method. The proposed deconvolution method is integrated into the design process of a geothermal system, facilitating the interpretation of field tests and helping in simulation and sizing of the system to be built.

TABLE DES MATIÈRES

LISTE DES TABLEAUX

LISTE DES FIGURES

LISTE DES SIGLES ET ABRÉVIATIONS

ÉCS	Échangeur de chaleur souterrain
EDP	Essai de pompage
ERT	Essai de réponse thermique
GES	Gas à effet de serre
PBF	Puits en boucle fermée
PCP	Puits à colonne permanente
RMSE	*Root-mean-squared error*
SLI	Source linéique infinie

LISTE DES ANNEXES

CHAPITRE 1 INTRODUCTION

Les dernières décennies ont montré une augmentation mondiale des efforts pour réduire les impacts négatifs du réchauffement climatique, principalement en diminuant les émissions de gaz à effet de serre (GES) [2]. Ces gaz, essentiellement le CO_2, proviennent anthropologiquement des systèmes de production d'énergie qui brûlent des énergies fossiles [3]. Au Canada, suivant l'accord de Paris en 2015 [4], une loi a été adoptée, visant la carboneutralité d'ici 2050 [5]. Au Québec, le Plan pour une économie verte aspire notamment à réduire les émissions de GES provenant du chauffage des bâtiments de 50 % d'ici 2030 [6]. Ainsi, pour atteindre ces ambitieux objectifs, une refonte substantielle des méthodes de chauffage et de climatisation devra être engagée dans les prochaines années [7].

À l'échelle globale en 2022, l'énergie produite est utilisée à 44 % pour le chauffage de l'eau et des bâtiments, ce qui correspond à 39 % des émissions de CO_2 [7]. Ces proportions sont toutefois bien changeantes d'une région à l'autre. Par exemple, en 2020 au Québec et en 2021 au Canada, seulement 10 % des émissions de CO_2 résultent de l'utilisation de l'énergie dans les bâtiments [8, 9] [1]. Ce faible pourcentage comparé aux autres pays s'explique par les hautes émissions du secteur du transport, puisque le Canada est un pays vaste, ainsi qu'un secteur industriel énergivore qui relâche une grande quantité de CO_2. Au Québec spécifiquement, le réseau de distribution électrique est alimenté à 95 % par des sources hydro-électriques renouvelables, ce qui est un atout majeur pour décarboner le chauffage des bâtiments [6, 10]. Dans ce secteur, 61 % et 43 % de l'énergie est utilisée pour le chauffage par les bâtiments résidentiels et commerciaux/institutionnels, respectivement [10]. De plus, en 2022, les bâtiments résidentiels et commerciaux/institutionnels s'alimentent à 23 % et 36 % respectivement par des combustibles fossiles [10]. En conséquence, réduire ces derniers pourcentages et accroître l'utilisation de l'électricité pour chauffer les bâtiments augmentera la charge et la demande énergétique en pointe sur le réseau de distribution électrique [9].

Dans l'objectif d'électrifier le secteur du bâtiment, une solution à la demande grandissante en électricité pour le chauffage et la climatisation est d'employer des thermopompes et des thermopompes géothermiques [6, 11]. Ces appareils permettent d'échanger de la chaleur entre un bâtiment et une autre source, soit l'air extérieur ou le sol. L'intérêt envers cette technologie est l'efficacité énergétique supérieure des thermopompes par un facteur 3 à 5, comparé à des plinthes électriques chauffantes [11, 12]. Ainsi, en utilisant une thermopompe, la surcharge

1. Le rapport Dion *et al.*, 2021b (référence [8]) provient de l'Institut canadien pour des choix climatiques et non de l'auteur de cette thèse.

sur le réseau de distribution électrique et l'appel de puissance en périodes de basses températures extérieures seraient atténués [9]. Un des avantages des thermopompes *géothermiques* est l'usage du sol comme réservoir thermostable, permettant leurs emplois lors de basses températures extérieures où les thermopompes air-air cessent de fonctionner dû à une faible efficacité [12, 13]. Au Canada, des températures extérieures de -20 °C et moins surviennent fréquemment en hiver. Donc, les systèmes géothermiques de basse température utilisant une thermopompe géothermique sont d'un intérêt majeur pour diminuer la consommation énergétique globale du secteur du bâtiment.

En contrepartie aux systèmes utilisant une thermopompe air-air, les systèmes géothermiques de basse température utilisant une thermopompe géothermique sont plus coûteux dû à la nécessité de creuser ou forer le sol. Un tel système relie une thermopompe à un échangeur de chaleur souterrain (ÉCS). Cette structure permet l'échange d'énergie entre un fluide qui circule dans l'ÉCS, le sol et l'aquifère. Il existe divers types d'ÉCS, se regroupant principalement en échangeurs horizontaux et verticaux. Ces derniers ont les principaux avantages de n'utiliser qu'un faible espace en surface et d'être thermostables dès que le forage dépasse une vingtaine de mètres de profondeur [14]. Les ÉCS verticaux se séparent typiquement en systèmes en boucle fermée et en systèmes en boucle ouverte.

Les puits en boucle fermée (PBF) font circuler un fluide caloporteur dans une ou deux paires de tuyaux en "U", fixés dans un coulis de sable et bentonite et qui permet un transfert de chaleur par conduction avec le sol [12]. Un ÉCS est dit ouvert lorsque l'eau d'un l'aquifère est utilisée comme fluide caloporteur. Un système typique pompe l'eau d'un premier puits et l'injecte dans un second. Un ÉCS ouvert et n'ayant qu'un seul puits pompe l'eau de l'aquifère en surface et la réinjecte au fond du même forage, transférant ainsi la chaleur par conduction et advection [15]. Ce système de puits à colonne permanente (PCP) peut donc être moins profond qu'un PBF grâce à l'effet bénéfique de l'advection, ce qui permet d'économiser sur les coûts de forage. De plus, en déviant une partie du débit de circulation hors du puits d'opération, un processus appelé saignée, un cône de rabattement se forme autour du PCP, favorisant l'écoulement de l'aquifère vers le puits et stabilisant les températures. Ainsi, la performance d'un PCP peut être augmentée, réduisant davantage la profondeur de forage requise et l'empreinte en surface pour un système à plusieurs puits [16, 17].

La figure 1.1 schématise à la fois les composants en surface et souterrain d'un système géothermique. Ainsi, la thermopompe géothermique relie un bâtiment à l'ÉCS, qui est dimensionné à l'aide des propriétés thermiques du sol telles que la conductivité thermique et la résistance équivalente du puits [18]. La bonne performance d'un système géothermique dépend de plusieurs éléments, tels que l'évaluation de la demande énergétique du bâtiment, le choix

approprié de la thermopompe et la précision sur l'estimation des paramètres thermiques du sol [19, 20]. Moghanni et al. (2023) [21] identifient le choix de la thermopompe comme étant le facteur le plus influent sur le coefficient de performance du système et le climat extérieur comme étant le facteur principal affectant la capacité maximale de chaleur pouvant être transmise au bâtiment par l'ÉCS. Le profil de consommation énergétique du bâtiment se calcule à l'aide d'outils en mécanique du bâtiment incluant, entre autres, la surface totale, le pourcentage de fenestration, l'isolation et les températures de consignes [22].

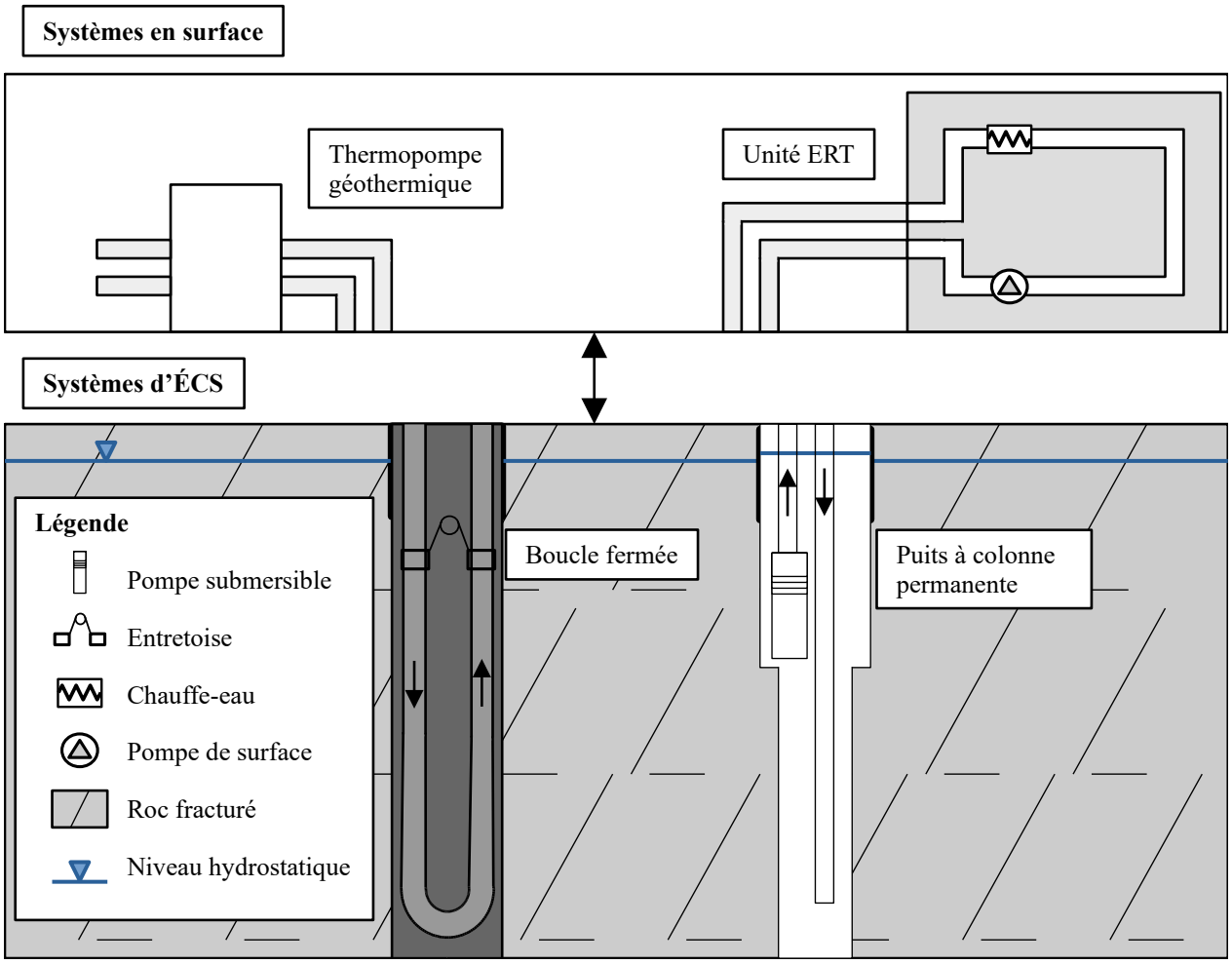

FIGURE 1.1 Schémas représentant les éléments en surface et souterrain d'un système géothermique de basse température. Systèmes en surface : une thermopompe géothermique pouvant être connectée à un bâtiment (gauche) et une unité de réponse thermique (droite). Systèmes d'échangeur de chaleur souterrain : un puits en boucle fermée (à gauche) et un puits à colonne permanente (à droite). Schéma non à l'échelle.

Les paramètres thermiques du sol s'identifient à l'aide de méthodes en laboratoire ou d'essais *in situ* [23]. La méthode la plus courante pour les estimer est l'essai de réponse thermique

(ERT) [24–26]. Ce test consiste à chauffer et circuler un fluide caloporteur dans l'ÉCS et à évaluer la dispersion de chaleur dans le sol [27]. Pour ce faire, les températures à l'entrée et à la sortie de l'ÉCS, le débit de circulation et la chaleur induite dans le fluide caloporteur sont mesurés. Ensuite, à l'aide d'une méthode d'interprétation, les propriétés thermiques, comme la conductivité thermique du sol et la résistance thermique du puits, sont calculées [28]. À l'aide de ces propriétés et de la demande énergétique du bâtiment, différentes variables de dimensionnement, telles que la longueur totale de forage, le nombre de puits, leur diamètre et le type de coulis, sont établies pour répondre à une certaine portion de la demande énergétique du bâtiment [29].

Pour obtenir des paramètres thermiques justes à l'aide d'un d'ERT, ce dernier doit être réalisé à l'aide d'un montage adéquat et bien construit [18,30]. Le test doit idéalement maintenir des conditions d'opérations constantes, telles que le débit de circulation, pour satisfaire aux hypothèses des modèles de transfert de chaleur utilisés dans l'interprétation. La figure 1.1 montre en surface une unité d'ERT, qui peut être connectée à un ÉCS similairement à une thermopompe. L'unité doit être bien isolée pour que les températures extérieures n'affectent pas les températures du fluide caloporteur durant l'essai et elle doit permettre l'enregistrement de toutes les variables nécessaires à l'interprétation. Un ERT de bonne qualité a une haute fréquence d'enregistrement (de 30 secondes à 2 minutes), des paramètres d'opération (c.-à-d., le débit de circulation, la puissance de chauffage et, dans le cas de PCP, le débit de saigné) les plus constants possibles ainsi qu'une durée totale de plusieurs jours pour assurer une évolution stable du régime thermique. La durée recommandée d'un essai est le sujet de plusieurs études, avec des durées d'essais variant entre 12 heures et 7 jours, avec un consensus à 3 jours [25, 31–34].

Concernant les méthodes d'interprétations, elles doivent être adaptées aux données expérimentales de l'essai, bien représenter le transfert thermique dans l'ÉCS, être précises, mais sans être trop complexes [35,36]. Pour interpréter un ERT, un modèle de transfert de chaleur (modèle direct) tente de reproduire l'échange thermique dans le sol et une méthode itérative (modèle inverse) optimise la valeur des propriétés thermiques du modèle direct pour reproduire les données expérimentales de l'ERT [37, 38]. Les modèles directs analytiques ou numériques ont chacun leurs avantages et inconvénients, tels que résumés dans le tableau 1.1.

Le concept de fonction de transfert peut alternativement être employé pour simuler un système géothermique en opération ou un ERT. Ces fonctions représentent la réponse d'un système lorsqu'une charge de chauffage unitaire et constante est appliquée. Pour un système géothermique de basse température, une fonction de transfert est la réponse de l'ÉCS suite à une charge de 1 °C, 1 W/m ou 1 W ajouté au fluide caloporteur entre la sortie et l'entrée

Tableau 1.1 Avantages et inconvénients des modèles de transfert de chaleur analytiques et numériques

Avantages	
Analytique	- Simple à implémenter sur différents logiciels
	- Se calcule rapidement
	- Beaucoup de littérature sur la précision
Numérique	- Intègre beaucoup de paramètres thermiques/hydrauliques
	- Couple différentes physiques
	- Représente plus précisément la géométrie/géologie de l'ÉCS et du site
Inconvénients	
Analytique	- Hypothèses limitantes sur la nature du transfert de chaleur
	- Difficulté à représenter toutes les composantes de l'ÉCS
	- Peut devenir très complexe
Numérique	- Long à modéliser/tester
	- Nécessite une grande charge de calcul
	- Doit être refait pour chaque site à l'étude
	- Expertise requise pour créer le modèle

de l'échangeur [39, 40]. En recourant à une superposition temporelle, les températures d'opération d'un système géothermique ou d'un ERT peuvent être calculées, sachant le patron de chauffage appliqué à l'ÉCS et la fonction de transfert le décrivant [41, 42]. Il est courant de distinguer les fonctions de transfert à court et long pas de temps. Une fonction de transfert à long terme, également nommée *g-function* par Eskilson (1987) [39], traite des pas de temps allant de l'heure jusqu'aux décennies [43]. Ces intervalles sont employés pour valider les températures au sol lors de l'opération d'un système géothermique. À l'opposé, une fonction de transfert à court terme contient des pas de temps allant des secondes aux jours [40, 44]. Ces périodes sont importantes à étudier, car elles présentent les effets du changement de température dans le fluide le long des tuyaux de l'ÉCS, l'échange de chaleur à l'intérieur du coulis, ainsi que l'impact thermique du changement rapide des consignes d'opération sur l'ÉCS [44]. En région nordique, les pointes de consommation électrique se produisent sur des périodes de quelques heures. Ces périodes doivent spécialement être analysées lors de la conception d'un système géothermique pour que, lors d'importantes demandes en chauffage, la température du fluide caloporteur évite d'atteindre la température limite d'opération, arrêtant ainsi la thermopompe. Pour simuler ces périodes, il est nécessaire de connaître la fonction de transfert à court terme de l'ÉCS. Ainsi, son évaluation précise est primordiale pour dimensionner correctement un système géothermique.

Pour simuler les températures d'un ÉCS à l'aide des fonctions de transfert, une technique de convolution peut être utilisée, permettant un calcul rapide [45–47]. De plus, si une fonction de transfert est définie à la sortie de l'ÉCS, elle regroupe toutes les composantes du transfert de chaleur à la fois dans l'ÉCS, le sol et l'aquifère. Ces avantages ont fait des approches de conception et de dimensionnement par fonction de transfert une norme dans l'industrie de la géothermie de basse température [22, 48]. Des désavantages majeurs à leur emploi sont que les fonctions de transfert sont majoritairement définies à la paroi de l'ÉCS, nécessitant une étape supplémentaire pour calculer les températures à la sortie de l'échangeur et que les fonctions sont habituellement calculées à l'aide de modèles analytiques ou numériques, comportant chacun leurs limitations (voir tableau 1.1). À noter que dans les modèles analytiques ou numériques, les paramètres thermiques sont obtenus en interprétant un ERT. Sur l'ensemble des publications obtenant des fonctions de transfert, un seul cas mentionne des fonctions expérimentales, c'est-à-dire acquises à l'aide de données expérimentales. Cimmino et Bernier (2015) [49] ont utilisé un modèle réduit où, en maintenant constantes les conditions d'opération et de chauffage, des fonctions de transfert sont simulées directement.

Un ERT représente la période caractéristique d'une fonction de transfert à court terme. Aussi, jusqu'aux travaux proposés par ce projet, les méthodes pour évaluer ces fonctions reposent principalement sur l'emploi de modèles analytiques ou numériques. La problématique de ce projet de recherche vise donc à déterminer expérimentalement la fonction de transfert à court terme à la sortie d'un ÉCS de type PBF ou PCP. Pour ce faire, la méthode développée permettra d'acquérir ces fonctions directement à partir des données d'un ERT, sans utiliser de modèle de transfert de chaleur. Par ailleurs, peu de recherches étudient l'impact du changement des conditions d'opérations sur les fonctions de transfert lors de la simulation des températures d'un ÉCS, un aspect déterminant spécialement pour l'efficacité des PCP. Enfin, aucune étude n'a encore identifié les fonctions de transfert à différentes profondeurs d'un ÉCS ou n'offre de comparaison entre l'application d'une méthode d'interprétation sur les températures d'un ÉCS ou sur une fonction de transfert expérimentale.

Apporter une contribution aux éléments ci-dessus aiderait à interpréter efficacement un ERT, à simuler précisément les températures d'un ÉCS et à dimensionner exactement un système géothermique. Ce dernier point est critique pour éviter un sur-dimensionnement (entraînant des coûts trop élevés) ou un sous-dimensionnement (diminuant l'impact positif du système sur le chauffage et la climatisation) du système géothermique. En contexte nordique, tel qu'au Québec, l'instauration à plus grande échelle des systèmes géothermiques correctement dimensionnés offre une solution durable à l'augmentation de l'appel de puissance en pointe de consommation et à la surcharge sur le réseau de distribution électrique dans un objectif d'électrification du secteur du bâtiment. Ces systèmes aideront aussi à diminuer les émissions

de GES associées au chauffage et à la climatisation des bâtiments.

CHAPITRE 2 REVUE DE LITTÉRATURE / LITERATURE REVIEW

Ce chapitre présente une revue de la littérature des recherches pertinentes aux travaux de ce projet de recherche. Plus précisément, cette revue traite des ERT, de leur interprétation, de l'obtention et l'utilisation des fonctions de transfert ainsi que de l'emploi de la déconvolution dans des domaines des géosciences.

2.1 Essai de réponse thermique

Comme mentionné en introduction, l'ERT est la méthode *in situ* la plus couramment utilisée pour estimer les propriétés thermiques d'un ÉCS, telles que la conductivité thermique du sol et la résistance thermique du puits [28, 35]. Le concept d'ERT a été introduit par Mogensen (1983) [24] et standardisé par les travaux de Austin et al. (2000) [25] et Gehlin (2002) [26]. Ce test peut s'appliquer à la fois sur des ÉCS de types PBF ou PCP, où la principale différence entre ces échangeurs est que la puissance de chauffage doit être plus élevée pour un PCP, puisqu'il y a un plus grand volume d'eau à chauffer et que les PCP sont plus profonds.

Durant cet essai, un fluide caloporteur circule dans l'ÉCS et les variables suivantes sont enregistrées à intervalles réguliers : les températures à l'entrée et à la sortie de l'ÉCS, le débit de circulation et la puissance de chauffage induite au fluide caloporteur [18, 27]. La séquence typique d'un ERT comprend la recirculation en début d'essai pour homogénéiser la température dans l'ÉCS, la période de chauffage où le chauffe-eau est activé, et la période de restitution où le chauffage est arrêté tout en maintenant la circulation du fluide dans l'échangeur. Avant la recirculation, le profil vertical de température est habituellement mesuré permettant d'évaluer le gradient géothermique [1, 50]. L'objectif de ce test est d'obtenir des données expérimentales du site à l'étude pour calculer les propriétés thermiques du sol qui sont ensuite utilisées pour dimensionner l'ÉCS qui sera connecté au système géothermique [51].

Dans la majorité des ERT, le chauffage de l'eau se fait à l'aide d'un chauffe-eau par résistance thermique dû à la simplicité du montage dans l'unité d'ERT [18]. Pour mesurer la puissance thermique (Q), un wattmètre peut être installé sur le chauffe-eau. Si cet instrument n'est pas utilisé, la formule de la chaleur spécifique $Q = VC_f\Delta T$ est employée, puisque la puissance de chauffage est directement proportionnelle à la différence de température entre la sortie et l'entré du chauffe-eau (ΔT). Cette équation nécessite également le débit de circulation dans l'ÉCS (V), et la capacité thermique volumétrique du fluide caloporteur C_f.

Un chauffe-eau par résistance thermique résulte en une puissance de chauffage plus ou moins variable dans le temps, dû aux variations du courant électrique alimentant les résistances thermiques [52]. Une autre approche proposée dans la littérature est un test de *performance* thermique, où la température à l'entrée de l'ÉCS est maintenue constante, plutôt que la puissance de chauffage du chauffe-eau [53]. Ce type de montage est davantage utilisé pour évaluer la performance thermique d'un ÉCS [53], mais Choi et al. (2019) [54] ont mis de l'avant que cet essai permet de calculer les propriétés thermiques du sol avec autant, sinon plus, de précision qu'un ERT classique. Beier (2021) [55] obtient, par inversion, des propriétés thermiques similaires en analysant à la fois des essais de réponse ou de performance thermique. Pour effectuer l'essai de performance thermique, la principale différence au montage est l'ajout d'un réservoir maintenu à température constante avant l'entrée de l'ÉCS.

Un ERT peut aussi être effectué sans la circulation d'un fluide caloporteur. Par exemple, Raymond et al. (2010) [56], Raymond et Lamarche (2015) [57] et Raymond et al. (2015) [58] proposent d'utiliser des câbles chauffants insérés le long d'un forage. Ce faisant, la température est émise uniformément et radialement sur toute la profondeur du forage. Cette technique s'approche davantage des hypothèses des modèles de transfert thermique, qui seront vues à la section suivante, puisque la température ne varie pas en fonction de la profondeur comme en utilisant un fluide caloporteur. Ainsi, cela s'éloigne des conditions d'opération réelle d'un système géothermique. Dans le même ordre d'idée, Acũna et al. (2019) [59] et Acũna et Palm (2013) [60] ont développé l'usage de la fibre optique pour mesurer une distribution verticale de la température dans les tuyaux d'entrée et de sortie d'un ÉCS en boucle fermée ou coaxial. L'emploi d'une fibre optique chauffante a été démontré par Vélez Márquez et al. (2018) [61] et simplifie le montage expérimental employant ces outils.

On désigne communément deux types d'ERT où les températures sont mesurées en fonction de la profondeur : les ERT distribués (ERTD) et les ERT améliorés [62], qui sont des méthodes de mesures actives [63]. L'avantage principal de ces essais est que la distribution verticale des températures permet de calculer une distribution verticale de propriétés thermiques du sol, telle qu'un profil de conductivités thermiques [64, 65]. Lors de la conception du système géothermique, la connaissance des propriétés thermiques en fonction des unités géologiques aide à identifier quelle profondeur atteindre pour des ÉCS subséquents, puisque les unités géologiques ayant de hautes conductivités thermiques ou hydrauliques peuvent être ciblées [65]. Pour un PCP, un ERTD se fait en plaçant une fibre optique dans le puits en contact avec la formation rocheuse, dans la conduite d'injection et dans le puits de réinjection [1].

Pour assurer un enregistrement de qualité des données d'un ERT, les erreurs de mesure causées par la précision et la justesse des instruments doivent être limitées [66]. De plus, la

possibilité qu'une interruption de courant survienne doit être minimisée [67, 68]. Ces erreurs sont habituellement réduites par une bonne calibration des capteurs, l'utilisation d'équipement de qualité et un suivi minutieux d'une méthodologie d'essai robuste. En particulier, les biais systématiques d'un capteur doivent être corrigés en comparant les valeurs du capteur à celles d'un autre dans un environnement identique. Une dérive temporelle s'amende en calibrant le capteur avant et après un essai.

Il existe aussi des sources d'erreurs inhérentes aux modèles de transfert de chaleur et à la méthode d'interprétation utilisés pour acquérir les propriétés thermiques de l'ÉCS. Witte (2013) [66] identifie ces sources comme : les erreurs sur le modèle de transfert de chaleur employé pour représenter l'échange d'énergie dans le sol, la déviation sur les paramètres qui sont fixés dans le modèle choisi ainsi que la propagation de ces erreurs en intégrant toutes les composantes de l'analyse. Ainsi, le modèle de transfert de chaleur et la méthode d'interprétation des données de l'ERT doivent être choisis pour réduire le biais entre les paramètres thermiques estimés et les paramètres réels de l'ÉCS. Le reste de cette section mettra en évidence les modèles et méthodes utilisés pour interpréter un ERT et montrera le besoin de développer des outils plus flexibles et robustes.

2.1.1 Modèles de transfert de chaleur

L'objectif d'un ERT est d'étudier le transfert de chaleur dans le sol près d'un site où un système géothermique de basse température sera construit. Ce transfert peut être représenté, sous différentes hypothèses et contraintes, par un modèle de transfert de chaleur qui inclut les propriétés thermiques et géométriques du sol et de l'ÉCS. Une approche classique est d'évaluer la température à la paroi du forage $T(t, r_b)$ et de la réconcilier avec la température moyenne du fluide T_f en posant que la différence entre ces deux signaux est le produit d'une résistance et de la puissance de chauffage :

$$T_f(t) - T(t, r_b) = q(t) \cdot R_b \tag{2.1}$$

où T_f est la température moyenne du fluide ($(T_{in} + T_{out})/2$), q est la puissance de chauffage divisé par la longueur du forage (Q/H) et R_b est la résistance équivalente à la paroi du forage (r_b) [26]. Le modèle de transfert de chaleur le plus élémentaire simplifie l'ÉCS en une ligne d'extension infinie chauffant un milieu homogène et isotrope [69, 70]. Cette source linéique infinie (SLI) évalue la température à un rayon r de la ligne. On peut donc calculer $T(t, r_b)$

sous les hypothèses ci-dessus. L'équation 2.1 incluant la SLI s'écrit tel que [24] :

$$T_f(t) - T_0 = \bar{q} R_b + \frac{\bar{q}}{4\pi k} \int_x^\infty \frac{e^{-u}}{u} du \tag{2.2}$$

où $\bar{q}$ est la puissance de chauffage moyenne par unité de longueur du forage durant l'ERT, T_0 est la température initiale du fluide dans l'ÉCS avant la période de chauffage, k est la conductivité thermique du sol, $x = r_b^2 C_s/(4kt)$ où C_s la capacité thermique volumétrique du sol.

En modifiant les inconnus R_b et k (C_s est habituellement fixé) dans l'équation 2.2, les températures expérimentales d'un ERT peuvent être reproduites [24, 26]. Cette technique est souvent employée dû à sa simplicité, mais rend des paramètres thermiques qui peuvent être biaisés dus aux hypothèses limitantes de ce modèle [32,36,66,71]. L'utilisation de la résistance thermique pour représenter le transfert de chaleur dans l'échangeur empêche de modéliser les effets transitoires survenant dans le puits, lesquels sont importants pour le contrôle à court terme du système.

Ainsi, d'autres modèles analytiques ont été développés pour décrire le transfert de chaleur dans le sol. Ces modèles sont (non exhaustivement) la source cylindrique infinie [55,69,72], la source linéique finie [45,73–79], la SLI mobile [45,70,80–82] et la source linéique finie mobile [83–85]. L'objectif principal de ces modèles est d'augmenter la précision de la reconstruction des températures d'un ERT en considérant davantage de paramètres et conditions frontières, tels que l'écoulement souterrain, une géologie non homogène, différentes configurations de l'ÉCS (c.-à-d., distance entre les tuyaux, matériaux de remplissage, diamètres du puits), un gradient géothermique, etc.

Plus la quantité de paramètres d'un modèle analytique est grande, plus le modèle est complexe, ce qui peut mener à des erreurs lors de son élaboration, lors du calcul ou sur la sensibilité du modèle face à certains paramètres [86]. En revanche, les modèles de simulations numériques sont plus flexibles pour incorporer un éventail de paramètres à la fois géologique, géométrique, hydrogéologique et thermique. Les avantages d'un modèle numérique sont de pouvoir étudier l'impact de certains paramètres sur la réponse d'un ÉCS [87–90]. Plus spécifiquement, les modèles numériques permettent l'analyse des effets transitoires lorsque le flux de chaleur varie grandement au fil du temps, ce qui est difficilement évaluable avec des modèles analytiques [31, 40, 44]. Il est aussi possible de coupler différentes physiques dans un modèle numérique, ce qui est spécialement pertinent pour les PCP. Par exemple, Beaudry et al. (2019) [1] et Robert et al. (2022) [91] combinent un modèle hydrogéologique (loi de Darcy) et modèle d'écoulement thermique en milieu poreux. Eppner et al. (2017) [92] et Cerclet et

al. (2023) [93] ajoutent un modèle géochimique aux deux précédents. Finalement, il est aussi possible de faire des simulations à plus grande échelle pour étudier les interactions entre des ÉCS [94].

Il existe aussi les modèles de transfert thermique de type résistance et capacités thermiques, qui intègrent les paramètres thermiques, géométriques et hydrogéologiques d'un échangeur de chaleur souterrain sous forme de résistances et de capacités thermiques [47, 95–99]. Il est donc possible d'intégrer les paramètres de tous les matériaux de l'ÉCS, du sol et de l'aquifère.

À noter que pour les PCP, il n'y a toujours pas de modèle analytique permettant de représenter adéquatement l'échange de chaleur conductif dans le sol, advectif dans le puits ainsi que l'effet de la saignée. Seul un modèle de résistance et capacités thermiques a été proposé [97]. Donc, leur simulation se fait à l'aide de modèles numériques [16, 94, 100–102].

Des revues récentes des modèles de transfert de chaleur sont présentées dans, entre autres, Spitler et Gehlin (2015) [18], Cui et al. (2018) [103], Franco et Conti (2020) [104], et Zhang et al. (2021) [105]. Outre les méthodes analytiques et numériques présentées ci-dessus, l'approche utilisant les fonctions de transfert, ou g-functions, constitue une méthode directe simple et efficace pour évaluer les températures d'un ÉCS sous un patron de charge connu. Cette approche sera détaillée à la section 2.2.

Une fois le modèle de transfert de chaleur choisi, les paramètres de ce dernier doivent être calibrés pour recréer les données expérimentales de l'ERT avec la plus grande précision possible, tout en s'assurant que les valeurs des paramètres sont compatibles au contexte géologique et hydrogéologique du site étudié. Pour cela, une pléthore d'algorithmes d'inversions sont utilisables.

2.1.2 Méthodes d'inversion

L'objectif d'une méthode d'inversion pour interpréter un ERT est d'identifier la valeur des paramètres du modèle de transfert de chaleur qui maximisent l'ajustement entre les températures simulées et expérimentales [106]. La méthode d'inversion la plus élémentaire est l'essai-erreur, où les paramètres d'un modèle sont modifiés manuellement jusqu'à ce que l'ajustement entre le modèle et les données expérimentales satisfasse l'analyste. Cette méthode, bien que simple, est peu efficace en temps d'optimisation. Il y a aussi des règles empiriques qui approximent les paramètres optimaux en fonction de quelques données rapides à obtenir [48, 107]. Ces méthodes ne nécessitent pas d'expertise particulière, mais tendent à sur-dimensionner les systèmes géothermiques pour assurer le rendement souhaité.

Les deux principales catégories de méthodes pour interpréter un ERT sont la méthode de

la pente et les méthodes de calibration des paramètres par optimisation. Pour la méthode de la pente, l'objectif est de minimiser les moindres carrés entre une régression linéaire en échelle logarithmique de la SLI et les températures expérimentales de l'ERT. Ensuite, les paramètres thermiques sont calculés à l'aide des paramètres de la régression [24,26]. Toutefois, l'approximation de premier ordre de la SLI peut mener à des erreurs de plus de 2 % sur la température comparée à l'équation complète pour tous les temps avant $t_c = 5r_b^2 c/k$ [108] et une erreur sur l'estimation de la conductivité thermique pouvant atteindre 26 % [36]. Il s'agit cependant d'une méthode simple et rapide à utiliser, qui est encore la norme dans l'industrie [34].

La seconde catégorie d'algorithmes d'optimisation, qui s'applique à la fois aux modèles analytiques et numériques [37], rassemble diverses méthodes où le but est de minimiser itérativement la valeur d'une fonction objectif. Cette fonction intègre principalement l'ajustement entre des données expérimentales et simulées et, parfois, des contraintes limitant la plage de valeurs admissibles des paramètres thermiques [109]. Une fonction objectif type [109] est la racine de l'erreur quadratique moyenne ou *root-mean-square error* (RMSE) entre des données expérimentales (y) et des données simulées (y_{ref}) :

$$\mathrm{RMSE} = \sqrt{\frac{1}{n}\sum \left(y - y_{ref}\right)^2} \tag{2.3}$$

Ainsi, ces méthodes tentent de maximiser l'ajustement entre les températures expérimentales et calculées à l'aide du modèle direct, en modifiant les paramètres thermiques de ce dernier. La figure 2.1 décrit généralement comment ces méthodes d'optimisation des paramètres procèdent pour converger. Un élément clé de ces méthodes est l'algorithme employé pour naviguer dans l'espace des paramètres et trouver l'optimum global. L'espace des paramètres comprend l'ensemble des valeurs que peuvent avoir les paramètres d'optimisation, et l'optimum est défini par le maximum ou le minimum de la fonction objectif [110]. Zhang et al. (2014) [109] et Zhang et al. (2021) [105] ont revu plusieurs articles utilisant des algorithmes tels que Simplex, Levenberg-Marquardt, Quasi-Newton et autres.

Un concept majeur pour les méthodes d'optimisation est l'utilisation d'une fonction multiobjectif [111]. Ces fonctions intègrent plusieurs termes pondérés (tel que l'équation 2.3) pour optimiser plusieurs objectifs simultanément. Par exemple, les aspects économiques et thermiques peuvent être joints [112–114] et la corrélation entre les paramètres peut être étudiée [115].

Un aspect important à noter pour des méthodes d'optimisation est que l'optimum d'une fonction objectif peut ne pas correspondre à des valeurs uniques des paramètres [116]. Une

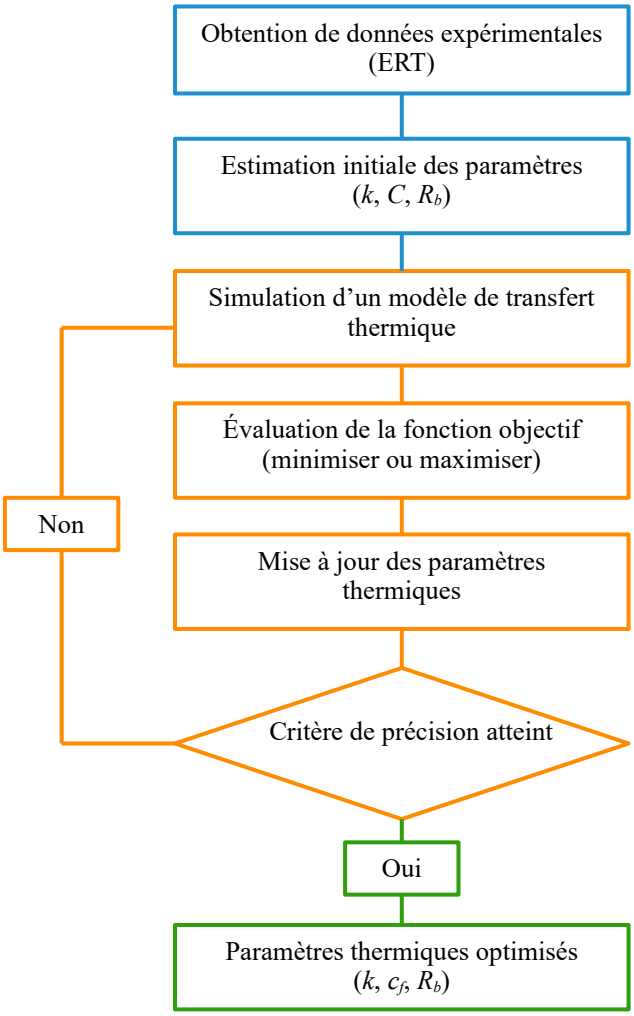

FIGURE 2.1 Méthodologie d'optimisation pour les méthodes d'estimation des paramètres pour interpréter un essai de réponse thermique.

des causes de ce phénomène est la corrélation entre les paramètres, qui implique que plusieurs combinaisons de paramètres peuvent atteindre un optimum semblable. Par exemple, une corrélation a été notée entre la conductivité thermique et la résistance du puits [32, 88], la capacité thermique volumétrique [117, 118] ainsi que d'autres paramètres [115]. Pour comprendre et réduire ce phénomène, des méthodes stochastiques plutôt que déterministes peuvent être employées. En l'occurrence, les méthodes d'inférence bayésienne ont notamment été utilisées pour quantifier la corrélation entre différents paramètres thermiques [32, 71, 118] et hydrogéologiques [119] d'un ÉCS.

Pour reproduire les températures d'un ERT, la combinaison d'un modèle de transfert de chaleur adéquat et d'une méthode d'interprétation doit être employée. Ces dernières sont

exigeantes en temps de calcul. Une façon simple d'accélérer la simulation est d'utiliser le concept de fonction de transfert couplé à une convolution.

2.2 Fonction de transfert

Le concept des fonctions de transfert en géothermie de basse température, souvent référé sous l'appellation g-function [39], est utile à la simulation d'un ÉCS sur plusieurs décennies sous différents patrons de charge pour valider les températures de l'ÉCS . Les g-fonctions décrivent la réponse thermique d'un ÉCS ou d'un groupe d'ÉCS à une impulsion de chaleur unitaire. Ainsi, les fonctions de transfert sont l'équivalent d'un modèle de transfert thermique permettant de simuler la température du sol en fonction de charges thermiques variables. Pour cela, la technique de superposition temporelle est utilisée [41]. À titre d'exemple, l'équation 2.2 s'écrit, pour une charge variable et une fonction de transfert g telle que :

$$T_f(t_i) - T_0 = q(t_i)R_b + \sum_{i=1}^{n} (q(t) - q(t_{i-1})) \cdot g(t - t_{i-1}, r) \tag{2.4}$$

où r désigne le rayon du puits et q la charge thermique. À noter que l'ensemble des processus décrivant le transfert de chaleur dans le sol est résumé par la fonction de transfert g et la résistance thermique du puits R_b. L'utilisation de la résitance thermique équivalente du puits empêche de représenter la phase transitoire du transfert de chaleur se déroulant dans le puits. Le paramètre g est la fonction de transfert décrivant l'évolution de la température à la paroi de l'ÉCS et dépend des paramètres thermiques du sol et du modèle de transfert de chaleur adopté (source linéique infinie ou finie, source cylindrique infinie ou finie, modèle numérique, etc.). Par exemple, la fonction de transfert pour le modèle de la SLI de l'équation 2.2 s'écrit tel que :

$$g(t, r) = \frac{1}{4\pi k} \int_x^\infty \frac{e^{-u}}{u} du \tag{2.5}$$

Des équations 2.4 et 2.5, plusieurs faits peuvent être ressortis. D'une part, l'ensemble des processus décrivant le transfert de chaleur dans le sol est résumé par la g-function, qui s'exprime par une exponentielle intégrale, et d'autre part que la conductivité thermique du sol est explicitement utilisée pour calculer cette fonction. La fonction de transfert g décrit seulement l'échange de chaleur à la paroi du forage, et donc, n'intègre pas les matériaux de l'ÉCS. Pour obtenir une fonction de transfert en sortie d'ÉCS, la résistance du puits comme décrite à l'équation 2.1 doit être intégrée à la fonction de transfert. La section 2.2.2 présente davantage de détails sur ce point.

Deux principales méthodes sont employées pour calculer la réponse d'un puits selon une

fonction de transfert et une charge variable à l'aide de la superposition temporelle. L'une est l'agrégation des charges [99, 120–122], l'autre est un produit de convolution [45, 96, 123]. Ce dernier s'exprime dans le domaine de Fourier avec l'équation suivante [123] :

$$\Delta T(t) = (f * g)(t) = \mathcal{F}^{-1}\left(\mathcal{F}(f) \cdot \mathcal{F}(g)\right) \tag{2.6}$$

où $\mathcal{F}$ et $\mathcal{F}^{-1}$ sont respectivement la transformée de Fourier et son inverse et $*$ est le produit de convolution. Le paramètre f est une fonction par impulsion de la charge thermique appliquée au fluide de l'ÉCS et qui s'écrit, pour une charge thermique en W/m par $f = q(t_i) - q(t_{i-1})$, ou pour une charge thermique en °C par $f = \Delta T(t_i) - \Delta T(t_{i-1})$. La fonction impulsion f permet donc de simuler des températures ΔT selon un patron de charge spécifique appliqué à la fonction de transfert g. En appliquant la transformée de Fourier, les signaux f et g sont convertis en fréquence, et la convolution se résout alors par une multiplication. À noter que, dans l'équation 2.6, ΔT est l'équivalent de la variable $T(t, r_b)$ de l'équation 2.1. Ainsi, la fonction de transfert g est encore définie à la paroi du forage.

Pour effectuer la superposition temporelle et obtenir la réponse de l'ÉCS à l'aide des équations 2.4 ou 2.6, la fonction de transfert du sol, d'un ÉCS ou d'un groupe d'ÉCS doit d'abord être obtenue. La littérature sépare deux types de fonctions de transfert, celles à long terme et celles à court terme. La principale différence entre les deux est l'échelle de temps représentée, soit des heures aux décennies pour les longues, et des secondes aux jours pour les courtes. Le reste de cette section présente l'état de la science pour générer ces fonctions.

2.2.1 Fonction de transfert à long terme

Suite aux travaux d'Eskilson (1987) [39], nombre d'approches ont été proposées pour développer et utiliser les fonctions de transfert à long terme (c.-à-d. des pas de temps des heures aux décennies). Des modèles analytiques courants, la source linéique finie est le plus employé pour générer des fonctions de transfert à long terme [78, 124–126]. Les objectifs des dernières méthodes proposées sont d'améliorer la précision, le temps de calcul et de réduire la mémoire vive requise pour simuler les fonctions, tel que décrit par Spitler et al. (2020) [43], ainsi que d'étendre les modèles pour différentes configurations de champ d'ÉCS en considérant les interactions thermiques entre eux [127, 128].

L'utilisation de modèles numériques pour générer les g-functions a aussi fait l'objet de plusieurs publications, entre autres, tel que proposé originalement par Eskilson (1987) [39], mais aussi par Monzó et al. (2015) [89], Yavuzturk et Chiasson (2002) [101], Zanchini et al. (2023) [129] et Beaudry et al. (2022) [102]. Ce dernier article génère des g-functions pour

un champ de PCP pour ensuite simuler dynamiquement l'effet de l'advection dans les puits, l'impact de la saignée et les interactions thermiques et hydrogéologiques entre les PCP et l'aquifère. Bien que cette approche donne des résultats précis et considère les interactions de plusieurs physiques, elle reste néanmoins longue à employer autant en temps de développement du modèle qu'en temps de calcul. Il s'agit néanmoins de la méthode de prédilection pour les projets complexes, puisque les g-functions sont davantage ajustées aux conditions réelles du site étudié.

Certains modèles complexes, tels que les réseaux de neurones artificiels, permettent d'obtenir des g-functions pour des agencements prédéterminés de champs de PBF [130]. Plus la base de données d'entraînement est large, plus le réseau sera polyvalent et pourra prédire la fonction de transfert pour une grande combinaison de paramètres. Ces modèles nécessitent toutefois un long développement et entraînement, surtout lorsque le nombre de paramètres augmente, car les combinaisons sont décuplées. Finalement, d'autres méthodes basées sur des interpolations de tables [131] ou sur une forme polynomiale d'une source cylindrique finie [132, 133] ont aussi été proposées. Ces méthodes sont aussi limitées par le nombre de paramètres utilisés pour générer les tables d'interpolation.

2.2.2 Fonction de transfert à court terme

Les bâtiments ont fréquemment des demandes énergétiques qui varient rapidement selon la température extérieure, les consignes des différents espaces du bâtiment ainsi que des opérations s'effectuant dans le bâtiment. La demande énergétique en chauffage ou en climatisation est ensuite transférée en charge thermique à l'ÉCS (ou au champ d'ÉCS). Lorsque ce dernier est sollicité, les premiers matériaux échangeant de la chaleur sont le fluide caloporteur et les matériaux de l'ÉCS [44]. Ainsi, lors de la simulation d'un système géothermique, les variations rapides de la demande thermique à l'ÉCS doivent être représentées par de courts pas de temps (c.-à-d., des secondes aux minutes), sachant que la capacité d'échange thermique de l'ÉCS a un impact non négligeable sur l'efficacité, la robustesse et le dimensionnement d'un système géothermique [87, 134].

Pour un système géothermique où les demandes énergétiques varient rapidement et dynamiquement au cours du temps, la simulation de la réponse de l'ÉCS se fait à l'aide des fonctions de transfert à court terme. À cet effet, Yavuzturk et Spitler (1999) [40] et Yavuzturk et al. (1999) [135] ont proposé un premier modèle numérique évaluant ces fonctions et qui permet d'évaluer la consommation énergétique du système. Suite à leur démonstration, l'évaluation de la réponse à court terme d'un ÉCS est devenue un sujet de recherche d'intérêt. Les modèles tentent de représenter précisément l'impact des matériaux de l'ÉCS, du temps de résidence

du fluide, de son débit et de l'interaction entre l'ÉCS et le sol sur la fonction de transfert à court terme.

De façon analogue aux g-functions, les avancées techniques menant à l'obtention des fonctions de transfert à court terme sont réparties en modèles analytiques [44, 74, 136–140], en modèles numériques [40, 91, 101, 135, 141–143] et en modèles de résistance et capacités thermiques [47, 98, 99, 144, 145]. Les avantages et limitations de chacun de ces modèles sont similaires à ceux présentés au tableau 1.1. À noter que le moment le moins bien représenté sur les fonctions de transfert par les modèles analytiques est l'instant où le fluide caloporteur retourne pour la première fois à la thermopompe (ou au chauffe-eau lors d'un ERT). À ce temps de résidence, il y a un changement de régime marqué sur la fonction de transfert qui n'est visible qu'à l'aide d'un modèle numérique.

Pasquier et al. (2018) [98] ont mis de l'avant une caractéristique importante à l'utilisation des fonctions de transfert. L'objectif des simulations est de calculer les températures à la sortie de l'ÉCS et non à la paroi du puits. Ainsi, la convolution décrite à l'équation 2.6 peut être réécrite telle que :

$$T_{out}(t) - T_0 = (f * g_{out})(t) \tag{2.7}$$

où g_{out} est la fonction de transfert à la sortie de l'ÉCS. Cette dernière représente donc la réponse du sol *et* de l'ÉCS (matériaux de construction, propriétés thermiques du puits et de l'ÉCS, dimensions de l'échangeur et vitesse de circulation du fluide caloporteur). À l'aide de modèles numériques, il est aisé d'obtenir cette fonction, tandis que pour les modèles analytiques, une résistance du puits doit être utilisée pour obtenir une fonction de transfert équivalente.

Les fonctions de transfert à court terme ont une échelle temporelle adéquatement représentée par un ERT, qui varie de 12 heures à 7 jours [32, 146]. Ainsi, les modèles évaluant ces fonctions sont couramment validés en simulant des températures pour reproduire les données expérimentales d'un ERT. À noter qu'il n'y a toutefois pas d'étude démontrant l'obtention de fonctions de transfert pour un profil vertical de températures, tel que lors d'un ERTD.

Pour simuler un système géothermique sur tout type d'échelle temporelle, il est possible de joindre les fonctions à court et long termes [98, 99, 142, 145, 147]. Les techniques combinent les portions courte et longue (et parfois une portion intermédiaire) obtenues à l'aide de différents modèles de transfert thermique (analytique, résistances et capacités thermiques ou numérique). Pour ce faire, la portion à long terme est ajustée pour que son premier pas de temps corresponde au dernier de la fonction de transfert à court terme.

Comme pour les g-functions, les algorithmes précédents n'obtiennent pas de fonctions de

transfert expérimentales, c'est-à-dire directement des données d'un ERT. Un modèle de transfert thermique est toujours utilisé pour représenter le transfert de chaleur. Tel que mentionné par Witte (2013) [66], une des erreurs lors de l'analyse d'un ERT provient du modèle choisi, parce qu'ils incorporent certainement des limitations. La seule instance où une fonction de transfert a été obtenue expérimentalement est par Cimmino et Bernier (2015) [49], qui ont réalisé un essai de 168 heures sur un modèle réduit d'un ÉCS. Bien que les conditions d'opération ont été maintenues assez constantes, les auteurs ont noté que même de petites variations, notamment sur la température ambiante dans la pièce où le modèle réduit se trouvait, entraînent des variations sur la fonction de transfert expérimentale.

2.2.3 Stationnarité et non-stationnarité

Dans l'analyse d'un système géothermique, les modèles de transfert de chaleur analytique supposent un système stationnaire. Ce dernier est défini par deux principales propriétés [148] :

Système linéaire Il y a une relation linéaire entre les entrants et les extrants du système. Dans l'équation 2.6 (ou l'équation 2.7), cela équivaut au fait que la variable ΔT est linéairement corrélée au changement dans la variable f, et donc, que g est invariable.

Temporellement invariant La réponse du système est toujours la même, peut importe le temps t. Ainsi, la fonction de transfert g est stationnaire et valide à tout temps t.

Pour un système géothermique, un système linéaire est rencontré lorsque les paramètres d'opération imposés à l'ÉCS sont maintenus constants. Ces paramètres sont principalement la vitesse de circulation du fluide caloporteur, le débit de saignée dans un PCP et les variations externes de températures (définies comme des conditions frontières invariables). Ainsi, lorsqu'un système géothermique opère ou lors d'un ERT, il est impossible, en pratique, d'obtenir des conditions d'opération qui respectent les propriétés d'un régime stationnaire. Lors d'un ERT, les paramètres sont toutefois maintenus le plus constants possible pour qu'un régime quasi stationnaire s'établisse. Ce faisant, les modèles analytiques tels que les équations 2.4 et surtout 2.6 et 2.7, qui respectent strictement la définition d'un système stationnaire, sont jugées valides et peuvent être utilisées pour représenter un ERT.

Un cas pratique survient lorsque le calcul de la fonction de charge f de l'équation 2.6 utilise l'équation de la chaleur spécifique $Q = VC_f\Delta T$ pour convertir des W aux °C. Dans ce cas, le débit de circulation V, définissant la stationnarité de la fonction de transfère, se retrouve dans l'équation de la fonction impulsion. Ainsi, pour que l'approche par convolution soit valide, le débit de circulation doit être le plus stable possible. L'idéal serait de ne considérer que le wattage ajouté au fluide caloporteur de l'ÉCS pour omettre d'ajouter l'impact de la variation du débit de circulation dans la fonction de charge.

Lors de l'opération d'un système géothermique, la non-stationnarité des conditions d'opérations est recherchée pour offrir la performance la mieux adaptée aux demandes énergétiques du bâtiment. Pour cela, des simulations numériques sont habituellement réalisées, où les conditions d'opérations, tel que le débit de circulation [149–151] et le débit de saignée pour un PCP [152] changent en fonction du temps. Beaudry et al. (2021) [143] ont formulé une méthode de convolution non-stationnaire utilisant plusieurs fonctions de transfert pour reproduire le signal de température d'un ÉCS sous différentes conditions d'opération. La méthodologie fait une combinaison non stationnaire de plusieurs produits de convolution et une correction est ajoutée pour émuler l'effet d'une convolution non stationnaire. Leur approche s'applique à la fois au système géothermique en marche ou à un ERT non stationnaire. Beaudry et al. (2022) [102] utilisent cette méthode pour étudier l'efficacité économique d'un système à plusieurs PCP opérant plusieurs débits de circulation et de saignée. Leur recherche montre les gains d'efficacité à utiliser dynamiquement les différents débits pour répondre à la demande énergétique du bâtiment. À noter que dans leur méthodologie, les fonctions de transfert générées pour chaque combinaison de débits de circulation et de saignée proviennent d'un modèle numérique.

Ainsi, aucune recherche ne porte sur le problème inverse, soit d'identifier plusieurs fonctions de transfert pour différentes combinaisons de conditions d'opérations d'un système géothermique à partir de données d'opérations. Ce type de données peut être obtenue à partir d'ERT ou de l'enregistrement d'un système géothermique en fonction.

2.3 Déconvolution

L'équation 2.7 permet la simulation des températures à la sortie d'un ÉCS, lorsque la fonction de transfert g_{out} et la fonction incrémentale de charge f sont connues. Cette opération s'applique en situation stationnaire et utilise la superposition temporelle pour considérer des charges variables. Pour un ERT, les températures T_{out} et T_0 ainsi que le patron de charge f sont connus. Ainsi, l'inconnue est la fonction de transfert à court terme g_{out} et elle peut être calculée par le processus contraire de la convolution : la déconvolution. Cette technique est fréquente dans le domaine du traitement de signal et est simplement l'inverse d'un produit de convolution. Mathématiquement, la déconvolution s'écrit, à partir de l'équation 2.7, telle que :

$$g_{out}(t) = \left((T_{out} - T_0) * f^{-1} \right)(t) \tag{2.8}$$

Une particularité de la déconvolution est que l'équation 2.8 décrit un système *mal posé*, c'est-à-dire que du bruit sur les données connues (ici, T_{out} et f) cause de grandes fluctuations

sur la réponse g_{out} [153]. De façon similaire, le bruit d'enregistrement sur les données a été identifié par Witte (2013) [66] comme l'un des quatre facteurs ayant un impact sur la qualité des paramètres thermiques obtenus.

Cette section présente quelques applications notables de méthodes de déconvolution dans divers domaines des géosciences, ainsi que son utilisation dans le domaine de la géothermie de basse température au moment de la rédaction de cette thèse.

2.3.1 Application en géoscience

Géophysique

L'utilisation de méthodes de déconvolution en géophysique est un domaine de recherche riche. Les applications sont variées, mais souvent centrées sur l'inversion de données sismiques obtenues à l'aide d'un sismographe [154]. En effet, ces données sont particulièrement bruitées, et la déconvolution a pour but de les filtrer pour améliorer la lisibilité et interprétabilité des sectionss sismiques [155,156]. Beaucoup de filtres s'appliquent pour des systèmes stationnaires [154], mais des méthodes non stationnaires ont été proposées, telles que, le domaine des ondelettes [157, 158], la déconvolution de Gabor [159, 160], une transformée-S [161] ou une filtration inverse-Q dans le domaine temporel [162]. La théorie de Margrave (1998) [163] est, entre autres, à l'origine de la méthode de convolution non stationnaire développée par Beaudry et al. (2021) [143].

La nature et la qualité des données (c.-à-d. l'amplitude du bruit sur les données originales) font cependant que les méthodes de déconvolution dans ce domaine ne sont pas directement applicables aux données d'un ERT.

Hydrogéologie

En hydrogéologie, la déconvolution est utilisée pour obtenir des fonctions de transfert d'aquifères ou de rivières. De ces fonctions, différents paramètres hydrauliques peuvent être calculés, tels que le temps de résidence de l'eau [164–166], le ratio du taux d'infiltration sur le taux d'écoulement de surface [167], la diffusivité verticale hydraulique [168] ainsi que la distribution du temps de transport entre une rivière et un puits adjacent en filtration sur berge [169].

Les techniques de déconvolution des articles mentionnés ci-dessus sont toutes basées sur des méthodes d'optimisation où une fonction objectif est déterminée pour ajuster la différence entre un modèle direct et des données expérimentales. Sonnewald et al. (2014, 2015) [164,165] utilisent une fonction objectif d'entropie maximale qui encourage le lissage de la fonction

obtenue en plus de l'ajustement des données. Cirpka et al. (2007) [169] utilisent une contrainte par multiplicateur de Lagrange pour assurer le lissage de la fonction de transfert. Finalement, Meresescu et al. (2018) [166] revoient plusieurs types de contraintes et choisissent d'appliquer des contraintes de positivité et de causalité.

Les données hydrogéologiques s'apparentant plus étroitement aux données d'un ERT, les méthodes de déconvolution par optimisation peuvent donc être utilisées en géothermie. Auquel cas, les contraintes de positivité, de causalité et les notions sur l'obtention d'une fonction lisse seraient avantageuses à exploiter.

Pétrolier

En exploitant un puits pétrolier, la relation entre le débit et la pression en fond de forage peut être représentée par un système stationnaire, si les conditions d'opération sont maintenues constantes. Les données expérimentales peuvent donc être représentées par un système de convolution où la fonction de transfert est la réponse en pression du réservoir de pétrole pour un débit unitaire [170]. Ce type d'essais est analogue aux ERT.

Une succession de méthodes de déconvolution pour obtenir la fonction de transfert d'un puits pétrolier ont été produites dans les années 2000 [170–175]. La méthodologie de base, décrite par von Schroeter et al. (2001) [171], propose un système d'optimisation non linéaire avec une fonction objectif exprimant les moindres carrés des erreurs entre les données expérimentales et la réponse du modèle de convolution. Seule une contrainte de positivité est utilisée et elle provient implicitement d'une transformation en exposant de l'équation de convolution. Des recherches subséquentes [172, 174] améliorent la méthodologie originale en considérant explicitement le premier pas de temps ainsi qu'en utilisant une fonction objectif régularisée de Tikhonov, favorisant le lissage de la fonction de transfert et aidant la convergence de l'algorithme. Finalement, une approche sur la dérivée des données de pression retire l'impact de la pression initiale dans le réservoir et améliore encore une fois la performance de la déconvolution pour ce type d'application [175].

La version finale de ces méthodes de déconvolution s'applique adéquatement aux données d'un ERT. L'approche par optimisation et les contraintes appliquées sont conséquentes avec la nature du problème de transfert de chaleur dans le sol. La section suivante décrit comment ces approches de déconvolution ont été transférées à l'interprétation d'ERT.

2.3.2 Application en géothermie de basse température

Une première méthode pour obtenir expérimentalement la réponse thermique d'un ÉCS a été proposée par Monteyne et al. (2014) [176]. L'objectif de l'algorithme proposé est d'approximer un modèle de la fonction de réponse fréquentielle qui traduit une fonction de transfert. L'approche considère différentes résistances thermiques se trouvant dans un ÉCS de type PBF et itère sur la réponse fréquentielle dans le domaine spectral. L'algorithme est ensuite validé sur des données d'un système géothermique et obtient des ajustements des températures acceptables allant de 0.17 °C à 0.36 °C. Les principales limites de la méthode sont que les fonctions de transfert ne sont pas explicitées dans le domaine temporel, même s'il est mentionné dans l'article que cela est possible, l'approche est relativement complexe et la fonction de réponse fréquentielle du modèle n'a pas pu être comparée à une réponse connue pour valider sa reconstruction.

Grâce à la similitude entre les données d'un ERT et celles de l'exploitation d'un réservoir pétrolier, la méthodologie proposée par Beier (2020a) [177] est calquée sur celle de Pimonov et al. (2010) [174]. L'approche par optimisation utilise une fonction multiobjectif où l'équation de convolution est posée sous une formulation par exposant. Ainsi, l'inversion assure une contrainte de positivité sur le problème. La conductivité thermique est évaluée à l'aide de la dérivée de l'approximation de premier ordre de la SLI et la résistance effective du puits est évaluée à l'aide d'un modèle de transfert thermique composite [146].

Les limitations de l'approche de Beier (2020a) [177] sont que les courbes de température comprennent la température initiale du sol (donc ne commencent pas à 0), une interpolation linéaire est utilisée pour compléter les valeurs qui servent à générer la courbe de température plutôt qu'une interpolation lisse. Ainsi, la dérivée des courbes de température est discontinue aux noeuds. La fonction objectif tente aussi de minimiser le RMSE entre la dérivée des températures expérimentales et obtenues par déconvolution. Or, la dérivée des températures expérimentales est reconnue comme étant un signal très bruité [108]. Pour considérer cela, une dérivée modifiée de Bourdet est utilisée [178]. Cette approche lisse la dérivée bruitée, modifiant ainsi le facteur signal sur bruit. Donc, la fonction objectif minimise l'ajustement entre deux signaux où l'information du signal réel est partiellement voilée par un filtrage. Finalement, la plus grande contrainte à la méthode de Beier (2020a) [177] est l'amincissement du jeu de données lors de l'optimisation. Dans l'exemple disponible en annexe de l'article, 100 données expérimentales sont utilisées dans la déconvolution. Autrement, les calculs sont trop lourds pour converger rapidement. Il est cependant inadapté de représenter les particularités de l'échange thermique d'un essai de plusieurs jours à l'aide d'un nombre aussi restreint de données expérimentales.

2.4 Synthèse

Pour dimensionner un système géothermique, une des premières étapes consiste à évaluer les paramètres thermiques du sol à l'aide d'un ÉCS sur lequel un ERT est effectué. Ensuite, ces propriétés thermiques sont utilisées pour simuler la réponse de l'ÉCS et du sol sous la demande thermique en chauffage et en climatisation du bâtiment.

Pour interpréter un ERT, un modèle de transfert thermique est employé pour reproduire les températures expérimentales de l'essai. Ensuite, une méthode d'inversion est choisie pour optimiser les paramètres thermiques et géométriques du modèle pour ajuster la réponse de ce dernier aux températures expérimentales de l'ERT. Les modèles de transfert thermique analytiques sont rapides, mais simplifient la réalité expérimentale de l'essai tandis que les modèles de simulation numériques sont précis et peuvent intégrer davantage de paramètres, mais sont longs à calibrer et nécessitent une lourde charge de calcul. De plus, il n'existe toujours pas de modèle analytique validé pour simuler adéquatement un PCP. Ainsi, un modèle numérique doit être employé dans ces cas-là.

Les fonctions de transfert à la sortie de l'ÉCS englobent l'ensemble des processus du transfert de chaleur dans l'ÉCS et dans le sol pour des conditions d'opération fixes. En les utilisant conjointement à une méthode de superposition temporelle comme modèle direct pour simuler un ÉCS, les températures expérimentales de l'opération d'un système géothermique ou d'un ERT peuvent être reproduites avec exactitude. Simuler des températures avec des conditions d'opération constantes ou non peut être fait à l'aide de méthodes de convolution stationnaire ou non stationnaire, pour des ÉCS de type PBF ou PCP. La limitation principale de ces approches est que les fonctions de transfert sont obtenues à l'aide de modèles analytiques (source linéique finie) ou de modèles numériques, comprenant leurs limitations respectives. Une seule étude sur un modèle réduit en laboratoire d'un ÉCS présente l'obtention de fonctions de transfert expérimentales [49].

Les méthodes de déconvolution, utilisées dans divers domaines des géosciences, permettent d'obtenir des fonctions de transfert à l'aide de données expérimentales dans plusieurs contextes différents. En géothermie de basse température, l'approche par déconvolution n'avait été étudiée qu'à deux reprise avant ce projet de recherche en utilisant des méthodes provenant des domaines du traitement de signal et de l'exploitation pétrolière [177]. Les approches proposées peuvent être améliorée sur plusieurs aspects.

De plus, un ÉCS exploité avec des conditions d'opérations non stationnaires peut-être représenté par une convolution non stationnaire, qui inclut une fonction de transfert pour chaque combinaison de conditions d'opérations. Cependant, les fonctions de transfert doivent être

produites à l'aide d'un modèle numérique. Finalement, aucune mention n'a été faite dans la littérature de l'obtention de fonctions de transfert expérimentale à différentes profondeurs lors d'un ERTD et du gain de l'évaluation des propriétés thermiques des unités géologiques en utilisant les fonctions de transfert plutôt que les signaux de température.

CHAPITRE 3 OBJECTIFS ET DÉMARCHE DE RECHERCHE

Pour réduire l'utilisation de combustibles fossiles lors du chauffage et la climatisation des bâtiments, l'électrification de ce secteur est un scénario envisagé. Dans cette situation, l'implantation de la géothermie de basse température a le potentiel de réduire considérablement la demande énergétique sur le réseau de distribution électrique. Cet effet est dû à la haute efficacité des thermopompes géothermiques et l'utilisation du sol comme réservoir thermostable. Dans les régions nordiques, tels que le Québec, les pics de consommation énergétique hivernaux seront aussi atténués par l'utilisation généralisée des systèmes géothermiques.

Un frein au déploiement à plus grande échelle de cette technologie est la complexité du design d'un système géothermique. Comme solution, des améliorations techniques peuvent être apportées à la méthodologie de dimensionnement des ÉCS. L'évaluation précise de l'échange et des propriétés thermiques d'un ÉCS mène à une meilleure capacité à dimensionner un système géothermique performant et durable. C'est dans cette optique que les outils développés dans ce projet de recherche ont été pensés. Ces derniers doivent permettre la simulation dynamique d'un système géothermique, en plus d'être flexibles, performants et utiles pour des ÉCS de types PBF ou PCP. Ce dernier est considéré, car il offre un potentiel important en termes d'efficacité énergétique, de bas coûts, et d'implémentation en milieu urbain.

Ces motifs de recherche mettent en évidence l'importance d'exploiter les données expérimentales d'un ERT, l'essai *in situ* de prédilection pour évaluer les propriétés thermiques de l'ÉCS, pour assurer un dimensionnement adéquat. L'utilisation de fonctions de transfert et d'une convolution permet de simuler précisément la réponse d'un ÉCS en fonction d'un patron de charge déterminé. Obtenir une fonction de transfert expérimentale d'un ÉCS à l'aide d'une méthode de déconvolution appliquée à un ERT a le potentiel de contribuer à faciliter le dimensionnement d'un ÉCS en améliorant la simulation du système géothermique.

3.1 Objectif général

L'objectif général de ce projet de recherche est de développer, tester et valider un algorithme de déconvolution flexible, robuste et performant, permettant d'obtenir des fonctions de transfert expérimentales d'un ÉCS en utilisant les données d'un ERT sous différentes conditions d'opérations et pour plusieurs types d'ÉCS. À l'aide de ces fonctions de transfert expérimentales, les simulations de la réponse d'un ÉCS à différentes charges seront plus précises, aidant au dimensionnement d'un système de géothermie de basse température.

3.2 Objectifs spécifiques

1. **Développer une méthode de déconvolution des données expérimentales d'un ERT**

   À l'aide des données expérimentales d'un ERT, une équation de convolution peut être écrite entre la réponse thermique du puits, l'impulsion de chaleur perturbant thermiquement le puits et la fonction de transfert de l'ÉCS. En utilisant les deux premiers signaux, la fonction de transfert d'un ERT peut être extraite, par inversion, à partir de l'équation de convolution. En s'appuyant sur des applications semblables dans divers domaines des géosciences, le premier objectif spécifique est le suivant :

   Établir, tester et valider expérimentalement la méthode de déconvolution la plus adaptée aux données expérimentales d'un ERT pour reconstruire précisément et rapidement les fonctions de transfert de différents types d'ÉCS. Cet objectif vise à résoudre les situations où les conditions d'opérations sont stationnaires, donc où les débits de circulation dans l'ÉCS sont maintenus constants dans le temps.

2. **Obtenir un ensemble de fonctions de transfert sur un ERT non stationnaire**

   La simulation dynamique d'un système géothermique implique des changements dans les conditions d'opération imposées à l'ÉCS. Ces changements visent à fournir la demande énergétique souhaitée au bâtiment, assurant ainsi la durabilité du système conçu. Dans le but d'obtenir des fonctions de transfert expérimentales à partir de données d'opération d'un ÉCS pour effectuer des simulations non stationnaires, le second objectif spécifique est le suivant :

   Étendre la méthode de déconvolution pour inclure l'interprétation d'ERT où les conditions d'opérations sont non stationnaires. Cette approche utilise une méthode de convolution non stationnaire et obtient un ensemble de fonctions de transfert pour chaque combinaison de conditions d'opération. Ainsi, des signaux beaucoup plus réalistes peuvent être interprétés, permettant ensuite la simulation dynamique des systèmes géothermiques. Cette approche doit aussi être validée expérimentalement sur des ÉCS de type PBF et PCP.

3. **Déterminer les fonctions de transfert et les propriétés d'un ÉCS à l'aide d'un ERTD**

   Lorsqu'un ERT est interprété, les propriétés moyennes de l'ÉCS sont calculées. L'utilisation de données d'un ERTD permet aussi d'obtenir la distribution verticale des propriétés d'un ÉCS. Les méthodes d'interprétation supposent toutefois des conditions d'opération idéalistes qui sont difficiles à maintenir lors d'essais de terrain, tel

qu'une puissance de chaleur radiale constante sur toute la profondeur de l'échangeur. Le troisième objectif spécifique est le suivant :

Appliquer la déconvolution aux données d'un ERTD pour obtenir une distribution verticale de fonctions de transfert selon les horizons géologiques d'un site. Aussi, un but est de démontrer l'application de méthodes d'interprétation connues sur des fonctions de transfert plutôt que sur des signaux de température, à la fois en surface et sur le profil de température vertical de l'ERTD. Ce faisant, mettre en évidence les gains à utiliser les fonctions de transfert expérimentales pour retrouver les propriétés thermiques du sol et aider au choix de la profondeur la plus appropriée au forage d'un champ d'ÉCS.

L'atteinte des trois objectifs spécifiques est présentée par un article scientifique par objectif. Ces derniers sont reproduits aux chapitres 4, 5 et 6 de cette thèse. Les articles des chapitres 4 et 5 ont été publiés, tandis que l'article présenté au chapitre 6 a été accepté pour publication. Les trois articles ont été soumis, respectivement, aux revues : *Geothermics*, *Science and Technology for the Built Environment* et *Applied Thermal Engineering*. Le chapitre 7 discute des principaux résultats obtenus en indiquant les avantages des méthodes développées, les bénéfices à les utiliser pour interpréter un ERT, tout en soulignant certaines limites aux algorithmes. De plus, certaines recommandations favorisant l'obtention de données optimales, ainsi que quelques paramètres à considérer pour appliquer la déconvolution sont énoncées. Finalement, le chapitre 8 présente une conclusion générale faisant état des principales contributions et suggérant des travaux et applications futurs.

CHAPITRE 4 ARTICLE 1 - DECONVOLUTION OF EXPERIMENTAL THERMAL RESPONSE TEST DATA TO RECOVER SHORT-TERM *g*-FUNCTION

Gabriel Dion[1*], Philippe Pasquier[1], Denis Marcotte[1]

Geothermics, January 8th 2022

[1] Department of Civil, Geological and Mining Engineering, Polytechnique Montréal, P.O. Box 6079 Station Centre-Ville, Montréal, Canada H3C 3A7

[*] Corresponding author email: gabriel.dion@polymtl.ca

Keywords: Temperature response deconvolution, Thermal Response Test, Short-term *g*-function, Ground heat exchanger

4.1 Abstract

The thermal parameters of the ground and the borehole, combined with a thermal model such as the infinite line source, enable fitting a short-term *g*-function by using a unit heating profile. This classical method is sensitive to model errors. The approach developed in this work extracts the short-term *g*-function and its derivative directly by deconvolution of thermal response test data, without having to specify a thermal model. The method minimizes a least squares-based multi-objective function on a set of nodes. The approach is robust to random power fluctuations affecting the thermal response test and allows using different heating and cooling scenarios. Results show that the deconvolved short-term *g*-functions display expected characteristics, and the temperature reconstructions have an error of less than 0.1 °C across various numerical and field test cases, an accuracy hardly attainable by classical analytic approaches.

4.2 Introduction

The building and construction sector represented 35% of the global energy consumption and it resulted in 38% of the carbon dioxide emissions globally in 2019 [179, 180]. Knowing that heating and cooling represent approximately 40% of this energy consumption [181], a keen interest has risen in the last decade for alternative technologies that could enhance energy efficiency in the building sector [182]. Ground-source heat pump (GSHP) systems are a suitable way to reduce a building's energy required for heating or cooling, due to the high

efficiency of heat pumps combined with a ground heat exchanger (GHE) [20]. The GHE and the heat pump allow respectively to exploit the ground as a thermal reservoir [12] and to exchange energy with buildings of sizes varying from a residential house to an industrial complex.

To size a GHE, ground thermal parameters, such as thermal conductivity, are required [27]. To obtain them, it is common to perform a thermal response test (TRT) [24, 25]. Such field test is usually conducted with a mobile rig and consists in circulating a heated fluid inside a testing borehole to retrieve a TRT data set [18]. The data set is usually composed of the entering and leaving water temperature at the surface of the test borehole, the volumetric flow rate and the heating power. The data set can then be interpreted by various methods to recover the desired thermal parameters [103]. Different thermal variables can be extracted from the information of a TRT. For example, the thermal conductivity and volumetric heat capacity of the ground and grout [118, 183, 184], the borehole thermal resistance [185], and the ground initial temperature [186] can be identified.

During the last decade, the quality and quantity of information extracted from a TRT data set has improved [38], notably on the thermal parameter estimation of the ground and borehole. Choi et al. (2018) [32] used a Bayesian inference framework that reduces parameter estimation's error as a TRT gets longer. Pasquier et Marcotte (2020) [118] enhanced the estimation of the volumetric heat capacity with a Bayesian inference approach considering correlated residuals. Pasquier (2018) [108] presented four different first-order approximations that allow the recovery of the thermal conductivity within 10% of reference values using the time derivative. Beier (2018, 2019, 2020a) [51, 177, 187] also used a logarithmic temperature derivative to improve parameter estimation. Its use also allowed to separate three different periods that occur during a TRT. Luo et al. (2020) [68] worked on interrupted TRTs and how to obtain satisfactory thermal parameter values in such cases. Li et al. (2020) [188] used a Monte-Carlo experiment with a stepwise algorithm to decrease the error on the parameter estimated. Beier (2021) [55] recently published a composite heat transfer model for parameter estimation with controlled inlet temperature. Jia et al. (2019) [189] used a modified TRT rig to provide constant heating or cooling load. Choi et al. (2021) [186] proposed a modification to the TRT rig to lessen the impact of the initial water temperature estimation. Franco et Conti (2020) [104] review various TRT analysis methods and proposed a TRT routine combined with a geotechnical analysis, so that both procedures could benefit from each other.

The previous advances tried to minimize various effects that may be observed on the data set recovered from a TRT. One of these effects is the measurement error on every recorded

variables, which is of high frequency and affects the data at every recorded time step [66]. This error can be partly removed by a low-pass filter. Another effect is the heating power and flow rate variations that mostly originate from the fluctuation of the supplied electric power [190]. These variations are typically handled by using the temporal superposition principle [41], which is equivalent to a convolution product [45,123]. These mathematical operations involve an excitation function and a transfer function. The latter, also called a system's impulse function, a response function, g-function or Green's function, is the thermal response of a GHE to a unit impulse signal. In a GSHP system, a transfer function can describe the heat exchange capacity of the geological material surrounding a test borehole [39], as well as borehole material and dimensions [191]. Hence, the transfer function allows the prediction of the ground behaviour under a heating load, which is important when considering fluctuating parameters.

The original formulation of the transfer function is the so-called g-function proposed by Eskilson (1987) [39] that considers long time step (i.e. between hours and years). Large time steps limit the analysis of rapidly varying processes that are inherent to GSHP operation [87]. To improve the temporal resolution of the g-function, Yavuzturk et Spitler (1999) [40] used a numerical model that includes short time steps. The use of short-time steps allows the consideration of the fluid residence time in the borehole, as well as the properties and geometry of the components of the borehole (i.e. the grout, piping and circulating fluid). The short-time g-function (STgF) can then better predict the borehole outlet fluid temperature, which allows a better control and operation of the GSHPs. Javed et Claesson (2011) [44] pointed that the operation and performance of a GSHP depend on the heat transfer occurring underground. As such, the short-term response of the ground and the borehole modifies the fluid temperature and influences the performance of the GSHP. Thus, considering the short-term thermal response has a significant importance, which justifies identifying the STgF at a given building site.

Several approaches have been used so far to obtain STgFs. For instance, Yavuzturk et Spitler (1999) [40] employed a 2D finite volume model on a closed-loop borehole. Javed et Claesson (2011) [44] implemented an analytical model that considers the thermal properties as well as boundary conditions of the GHE in the Laplace domain. Li et Lai (2012b, 2013) [137, 192] and Li et al. (2014) [147] developed a complete g-function where the short-term portion is based on a composite-medium line-source model. Their method is only applied to closed-loop boreholes. Wei et al. (2016) [139] presented a simplified composite infinite line source model for short time-steps g-function. De Rosa et al. (2015) [144] used a thermal network with a vertical discretization to calculate the STgF. Brussieux et Bernier (2018) [142] developed a hybrid approach with finite volume numerical method and the cylindrical heat source

model to obtain STgF. Quite recently, Pasquier et al. (2018) [98] developed an artificial neural network trained with a STgF database that was produced by a thermal resistance and capacity model [47, 96]. An advantage of the method is its ability to compute the borehole outlet temperature almost instantaneously, allowing more accurate prediction of the heat pump coefficient of performance.

Recently, Cruz-Peragon et al. (2020) [140] generated experiment-based STgFs using the experimental data of a TRT. The technique used extracts the thermal conductivity and borehole thermal resistance with the graphic interpretation method [24]. Then, the STgF is constructed with an analytical solution or the exponential integral function. As pointed out in the article, such a method limits the quality of the recovered STgF, since only the linear part of semi-logarithmic plot is taken into account, which omits the short-term temperature variations. The reconstructed STgF also has negative values on early times, which is also pointed out in the article as an inconvenient since the solution retrieved does not respect the mathematical properties of a transfer function.

Since the experimental data of a TRT may be expressed as a convolution product [45], a deconvolution algorithm can be applied to extract directly the STgF [193]. To this end, Beier (2020a) [177] used a deconvolution methodology based on a petroleum problem to extract the thermal parameters of the ground. The technique used is a naturally constrained, multi-objective optimization strategy on a TRT data set to recover the temperature variation and its logarithmic first derivative. The practical implementation published with the article executes a thinning of the data set, likely to lighten the computation burden of the algorithm. Another shortcoming of the algorithm is that the transfer function second derivative is discontinuous on the selected nodes, since a linear interpolation is performed between the nodes. Furthermore, a transformation to the convolution integral allows a natural positivity constraint, at the expense of making the equation non-linear. In consequence, as the number of nodes grows, the computation takes longer to converge. Considering these limitations a different deconvolution approach could be applied to the full experimental data of a TRT to obtain better STgFs and their derivatives in a shorter computing time. The convolution equation could be expressed on the borehole outlet fluid temperature instead of the mean temperature between the entry and exit points of the GHE.

The goal of this paper is to present a deconvolution method to recover the STgF and its smooth derivative at the borehole outlet directly from the entire experimental TRT data set, bypassing the need of defining a thermal model and estimating its parameters. The proposed method uses known constraints on a set of nodes, such as positivity, smoothness and the strictly increasing nature of a transfer function, to guide the deconvolution algorithm. It is

applicable to different types of GHEs and can evaluate a STgF with time-varying heat loads and high frequency sampling rate TRTs. The deconvolved borehole outlet STgF can predict the temperature variations of the fluid entering the heat pump.

4.3 Methodology

This section first presents some mathematical considerations on the convolution and deconvolution. The deconvolution algorithm developed in this work is then presented, outlining the parameters and variables of the problem. The last part of the section presents how to obtain an initial guess to use with the deconvolution algorithm.

4.3.1 Direct Deconvolution

Following the works of Pasquier et Marcotte (2014) [47] and Pasquier et al. (2018) [98], the GHE output fluid temperature variation can be expressed as the convolution of an excitation function f and a transfer function g with Eq. 4.1:

$$T(t_i) = (f * g)(t_i) = \sum_{j=1}^{i} f(t_j) g(t_{i-j+1}) \tag{4.1}$$

where $T = T_{out} - T_0$ (°C) is the temperature variation at the borehole outlet, T_{out} (°C) is the exiting GHE fluid temperature, T_0 (°C) is the initial ground temperature, t_i is the time step vector with length $i = 1, ..., m$, g (-) is the borehole outlet STgF and f (°C) is the incremental temperature function. The latter is an impulse function characterizing the temperature variation at each time step of the TRT, as described with Eq. 4.2:

$$f(t_i) = \Delta T(t_i) - \Delta T(t_{i-1}) = \frac{Q(t_i) - Q(t_{i-1})}{\bar{V} \cdot C_f} \tag{4.2}$$

where ΔT (°C) is the ground inlet and outlet temperature difference ($T_{in} - T_{out}$), Q (W) is the heating power transmitted to the heat carrying fluid, V ($m^3 \cdot s^{-1}$) is the flow rate of the circulating fluid and C_f ($J \cdot m^{-3} \cdot K^{-1}$) is the volumetric heat capacity of the fluid. The last equality in Eq. 4.2 stems from the energy conservation principle under the assumption of no heat loss in the above ground piping. The incremental temperature function requires as input the heating rate $Q(t_i)$ and the flow rate $V(t_i)$, which is usually taken as a constant, simplifying Eq. 4.2 with $V(t_i) = V$. These variables fluctuate in time due to intrinsic electric power variations, which causes heating power and flow rates variations, or even equipment interruption due to power outages. It is worth noting that all the previous variables are

either known constants (C_p, ρ) or measured directly during a TRT (T_{out}, T_0, Q, V).

The aim of the current deconvolution algorithm is to obtain $\hat{g}$, an estimation of the real STgF g. Figure 4.1 illustrates an example of the direct convolution and deconvolution operations originating from Eq. 4.1. The convolution is shown from left to right where the function g is convolved with function f to obtain the temperature variation T. The deconvolution is shown from right to left where the measured (i.e. experimental) temperature $T_{exp} = T_{out} - T_0$ is convolved with f^{-1} to obtain $\hat{g}$. Since deconvolution is not a real operator [193], solving directly Eq. 4.1 for $\hat{g}$ leads to an ill-posed problem, where the errors in the experimental data are amplified. Such a direct deconvolution algorithm usually results in unstable STgFs that does not necessarily possess the desired smoothness and positivity. To account for error propagation, a robust deconvolution algorithm needs to be used.

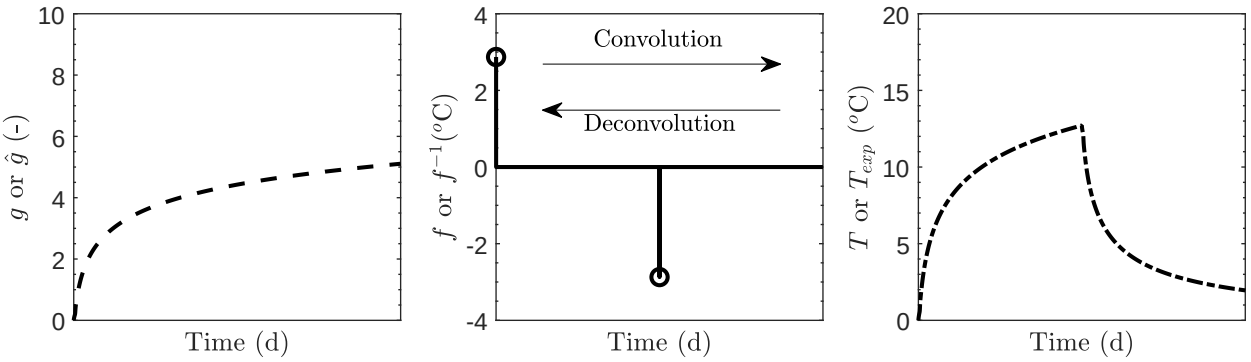

Figure 4.1 Illustration of the direct convolution of functions f and g to obtain T (from left to right), and of the direct deconvolution of functions T_{exp} and f^{-1} to obtain $\hat{g}$ (from right to left).

4.3.2 Multi-objective constrained iterative deconvolution algorithm

The classical approach in inversion is to express the problem as an objective function to optimize, i.e. minimize the difference between the left and right side of Eq. 4.1, with respect to different variables directing the minimization [35]. In this work, a multi-objective function is minimized under a series of constraints. The following subsections describe the deconvolution algorithm developed to obtain $\hat{g}$ from the data set obtained with a TRT.

The STgFs $\hat{g}$ being smooth and strictly increasing, they can conveniently and accurately be represented as a piecewise cubic Hermite interpolating polynomial (PCHIP), which ensures exact interpolation at the nodes and preserve $C2$ continuity of $\hat{g}$ [194]. First, a series of nodes are selected $\tau_j,\ j = 1, ..., n$ from the time vector of length m to lessen the significance of the rapid variation caused by natural variations and measurement errors (circles in Fig.

4.2(Left)). In the approach, the abscissas and number of nodes n are chosen by the user. Initial $\hat{g}(\tau_j)$ values are assigned at these nodes and then, the PCHIP interpolator is applied to obtain $\hat{g}(t_i)$ at all measurement times. The optimization of the objective function bears solely on the ordinates of the nodes $\hat{g}(\tau_j), \forall j = 1, ..., n$ that parametrize the curve $\hat{g}(t_i), \forall i = 1, ..., m$. However, the latter is used to compute the objective function to consider all the variations present in the TRT experimental data. When the optimization converges, the optimized $\hat{g}(\tau_j)$ can be interpolated with PCHIP to obtain $\hat{g}(t_i),\ \forall i = 1, ..., m$. It is stressed that the optimization uses the same temporal resolution as the TRT. The nodes $\hat{g}(\tau_j)$ are the one being optimized, but using the complete temperature and heating power vectors retrieved from the TRT.

The number of nodes n needs not be large, as a STgF is smooth by definition. The fact that both $\hat{g}$ and its first derivative often vary quickly at early times suggests to concentrate more nodes at the beginning of the time series as obtained with a logarithmic spacing of the nodes. In a petroleum reservoir inversion context, Pimonov et al. (2010) [174] recommended 10 nodes per logarithmic cycle (i.e. per unit when expressed in the log basis), or around 40 nodes, which is considered in this article for the TRT cases. See Fig. 4.2 in section 4.3.3 for a visualization of the nodes position.

To obtain the estimated $\hat{g}$, the multi-objective function to minimize is defined as:

$$E(t_1, ..., t_m) = E_{\hat{T}} + E_{\hat{g}'} + E_{\hat{g}''} \tag{4.3}$$

where:

$$E_{\hat{T}} = \left[\sum_{i=1}^{m} W_T(t_i) \cdot \left(\hat{T}(t_i) - T_{exp}(t_i)\right)^2\right]^{1/2} \tag{4.4}$$

$$E_{\hat{g}'} = P_{\hat{g}'} \cdot \left[\sum_{i=1}^{m} (\hat{g}')^2\right]^{1/2} \tag{4.5}$$

$$E_{\hat{g}''} = P_{\hat{g}''} \cdot \left[\sum_{i=1}^{m} (\hat{g}'')^2\right]^{1/2} \tag{4.6}$$

The objective function comprises three terms. $E_{\hat{T}}$ is the main objective to minimize, as it measures the misfit between the m convolved $\hat{T} = (f * \hat{g})$ and experimental T_{exp}. The m weights W_T enable putting more emphasis, if desired, on some parts of the TRT, like the beginning of the heating and recovery phases. The terms $E_{\hat{g}'}$ and $E_{\hat{g}''}$ are respectively the norms of the first and second derivatives of $\hat{g}$. The first and second derivatives are forward differences of level 1 and 2, respectively. These terms help prevent unwanted variations and

improve the smoothness of $\hat{g}$. $P_{\hat{g}'}$ and $P_{\hat{g}''}$ are positive relative weights on the norms to balance the contribution of their respective terms in the global objective function. Appropriate weights W and P will be discussed in section 4.6.2.

Knowing that $\hat{g}$ is positive and strictly increasing by definition, the following constraints are imposed on $\hat{g}(\tau_j)$ and its first and second derivatives:

$$0 < \hat{g}(\tau_j) < \hat{g}(\tau_{j+1}) \ \forall j = 1, ..., n-1 \tag{C1}$$

$$\begin{aligned} 0 < \hat{g}'(\tau_j) < \hat{g}'(\tau_{j+1}) \ \forall j = 1, ..., z-1 \\ 0 < \hat{g}'(\tau_{j+1}) < \hat{g}'(\tau_j) \ \forall j = z, ..., n-1 \end{aligned} \tag{C2}$$

where constraint $C1$ imposes both positivity and positive first derivative on $\hat{g}$. Constraint $C2$ reflects the property of a STgF's first derivative obtained with an infinite or finite, line or cylindrical-source model to present a single inflexion point at short times. It is then apparent to a positive and negative second derivative respectively before and after the inflexion point of $\hat{g}'$. In constraint $C2$, z is the position of the first node following the maximum of the STgF first derivative, calculated directly from $\hat{g}(\tau_j)$. The value of z can change at each iteration, allowing flexibility of the optimization process. Figure 4.2(Right) illustrates this last constraint using the first derivative of an infinite line source model.

Eq. 4.3 can then be minimized by a non-linear programming solver. The selected one is the *interior-point* algorithm [195] and the problem can then be written as:

$$\hat{g} = \arg\min_{\hat{g}} E\left(t_1, ..., t_m \middle| \ \text{C1,C2}\right) \tag{4.7}$$

It is stressed that the constraints C1 and C2 are enforced on the *nodes* τ_j of $\hat{g}$. Although forcing the constraints on the nodes helps the interpolated $\hat{g}(t_i)$ to mostly respect them, C2 is not always respected over the whole function, as will be discussed in section 4.6.1.

4.3.3 Initial solution on nodes τ_j

The optimization process on specified nodes benefits from an initial solution that respects the constraints imposed. For this, a fast two-step procedure is used to generate an initial $\hat{g}(\tau_j)$ guess with the desired properties. First, an estimate of $\hat{g}(t_i)$ is calculated directly using sequential formulation derived from Eq. 4.1. To help the direct approach handing acceptable noisy initial solution, a low-pass filter is applied to the experimental data set of the TRT prior to the calculation of Eq. 4.8. The filtered data can also be used for the complete

iterative deconvolution. Applied filters will be discussed in section 4.4.1 and their impacts are discussed in section 4.6.1.

$$\hat{g}_0(t_i) = \begin{cases} \dfrac{T_{exp}\left(t_1\right)}{f\left(t_1\right)} & \text{for } i = 1 \\ \dfrac{T_{exp}\left(t_i\right) - \sum_{p=2}^{i} f\left(t_p\right) \cdot g\left(t_{i-p+1}\right)}{f\left(t_1\right)} & \text{for } 2 \leq i \leq m \end{cases} \tag{4.8}$$

Note that convolving this $\hat{g}_0$ with f would fit perfectly the entire temperature variation, meaning $\hat{T} = T_{exp}$. However, due to measurement errors in the TRT data set, the $\hat{g}_0$ function so obtained is not smooth, nor does it respect the desired constraints, but it presents the general shape wanted.

The second step consists of a least-squares fit of an exponential integral equation, defined with $\hat{g}_0(x_1, x_2, \tau) = x_1 \int_u \frac{e^{-u}}{u} du$ where $u = x_2/\tau$, to the sequential formulation of Eq. 4.8. Variables x_1 and x_2 are dimensionless parameters to obtain the least squares fit on the nodes τ_j. The exponential integral is used for common usage in heat transfer model, such as in the infinite line source [69]. The fit is then apparent to solving $\hat{g}_0(\tau_j) = \arg\min_{\hat{g}_0} \parallel \hat{g}_{0,exp\ int} - \hat{g}_{0,seq} \parallel_2^2$.

Although other approaches could have been used to get the initial solution, this simple method hands satisfactory initial guess to implement in the iterative minimization rapidly. Figure 4.2 shows the first inversion and the selected nodes used to fit the exponential integral equation.

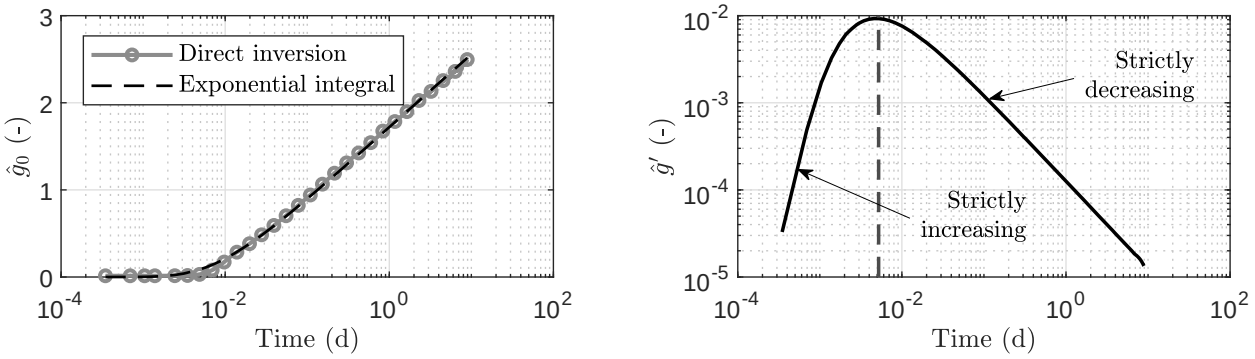

Figure 4.2 (Left) Direct calculation of $\hat{g}_0$ from Eq. 4.8 and exponential integral function fit on the selected nodes τ_j (grey circles). (Right) First derivative of an ILS model with the constraints $C1$ and $C2$.

4.3.4 Summary of the method

The above presented deconvolution methodology can be summarized in the following steps:

1. Following a TRT, extract the experimental data set composed of the initial ground temperature T_0, the GHE outlet water temperature T_{out}, the circulating flow rate V and the heating power Q.
2. Calculate the incremental temperature function with either the second or third term of Eq. 4.2.
3. Optionally, apply a low-pass filter, such as a moving average, as a preprocessing step, to remove part of the measurement error on V, Q or T or a combination. This point is further discussed in section 4.4.3.
4. Determine the number of nodes used to parametrize $\hat{g}$, common values are between 25 and 60, depending on the duration of the TRT and its sampling rate that jointly determine the number of logarithmic cycles on the time axis. A generic number of nodes is 40.
5. Calculate the initial solution at the nodes using the two-step procedure composed of a direct deconvolution using Eq. 4.8, followed by the least-squares fit with an exponential integral equation on the selected nodes. It is recommended to apply a low-pass filter on the incremental temperature function before calculating Eq. 4.8 to enhance computing stability.
6. Find $\hat{g}$ by optimizing the objective function (Eq. 4.7) on the selected nodes subjected to the prescribed constraints $C1$ and $C2$. Each iteration requires:
   (a) With the initial (or previous iteration) $\hat{g}(\tau_j)$, interpolate at every time step $\hat{g}(t_i)$ by PCHIP.
   (b) Convolve the current $\hat{g}(t_i)$ with f to obtain the $\hat{T}$ with Eq. 4.1.
   (c) Compute the objective function (Eq. 4.7).
7. With the optimized $\hat{g}(\tau_j)$, use PCHIP to obtain the final interpolated function $\hat{g}(t_i)$.

4.4 Validation scenarios

This section presents numerical and field validation scenarios used to assess the performance of the deconvolution algorithm on retrieving the borehole outlet $\hat{g}$. To illustrate how flexible the proposed algorithm is, the validation scenarios use both closed-loop and standing column well GHEs, as well as time-varying heat loads profiles. To improve the results of the algorithm, different approaches that use low-pass filters are presented to mitigate the effect of measurement errors. The validation procedure consists of the following steps:

1. Define the numerical and experimental test cases to be used as validation scenarios (see section 4.4.1 and 4.4.2).

2. Apply the procedure described at section 4.3.4 on each test case to retrieve the borehole outlet $\hat{g}$ and the temperatures $\hat{T}$.
3. Assess the performance of the algorithm with the visual quality of $\hat{g}$ and its first derivative, as well as with the *root-mean-square-error* (RMSE) between $\hat{g}$ and g_{exp} (numerical) and $\hat{T}$ and T_{exp} (numerical and field) (see section 4.5).

4.4.1 Numerical test cases

To obtain some reference numerical solutions (g_{exp} and T_{exp}), the 2D axisymmetric finite element model of Beaudry et al. (2019) [1] was used to emulate the response of a standing column well (SCW). The model integrates the fluid flow within the borehole and heat transfer in the borehole and surrounding geological media.

It is worth noting that the temperature load applied to obtain the reference g_{exp} is a constant ΔT=1 °C. Hence, the incremental temperature function would be an initial impulse of 1°C and 0°C for the remaining values.

The numerically generated TRTs have durations of 7 days with recordings every minute. The initial ground temperature T_0 is set to 11 °C and the flow rate is fixed at $V = 100$ L/min. The variations caused by the electricity grid fluctuation and measurement errors caused by the equipment are integrated to the simulated experimental data. First, the variations are known to have auto-correlation between each of their values [118]. To simulate this effect, an exponential covariance function [196] is used to add correlated variations on the heating power Q for the length of the test cases. The heating power profile is then used in the numerical model and the temperatures T_{out} are retrieved, considering the auto-correlation of the variations. Second, to simulate measurement errors, a white Gaussian noise is added on Q and T_{out} at each time step. The data set thus created will be used in the deconvolution algorithm to obtain $\hat{g}$ and $\hat{T}$. Table 4.1 and Fig. 4.3 present a summary of the 4 numerical test cases. The main difference between each case is the heating power profile. The "Numerical" column of the Table 4.2 presents input values in used in the numerical model.

4.4.2 Field test cases

To further assess the deconvolution algorithm performance, four field TRT test cases are added to the numerical ones as validation scenarios. The first three TRTs were performed on single closed-loop boreholes with a single U-tube and the last TRT was performed on a SCW. The four field test cases were performed in the province of Quebec, Canada and have lengths varying from 5 to 10 days. Figure 4.4 presents the field heating power profile Q and

Table 4.1 Heating profile used to compute the temperature with the numerical model to form the TRT numerical test cases.

Cases	Description
1	Constant heating at 24 kW for 7 days.
2	Heating at 24 kW for 3.5 days and recovery at 0 kW for 3.5 days.
3	Pulse steps between 24 kW and 0 kW every 24 hours.
4	Sinusoidal test with a mean of 15 kW and an amplitude of 5 kW with cycles of 1 day.

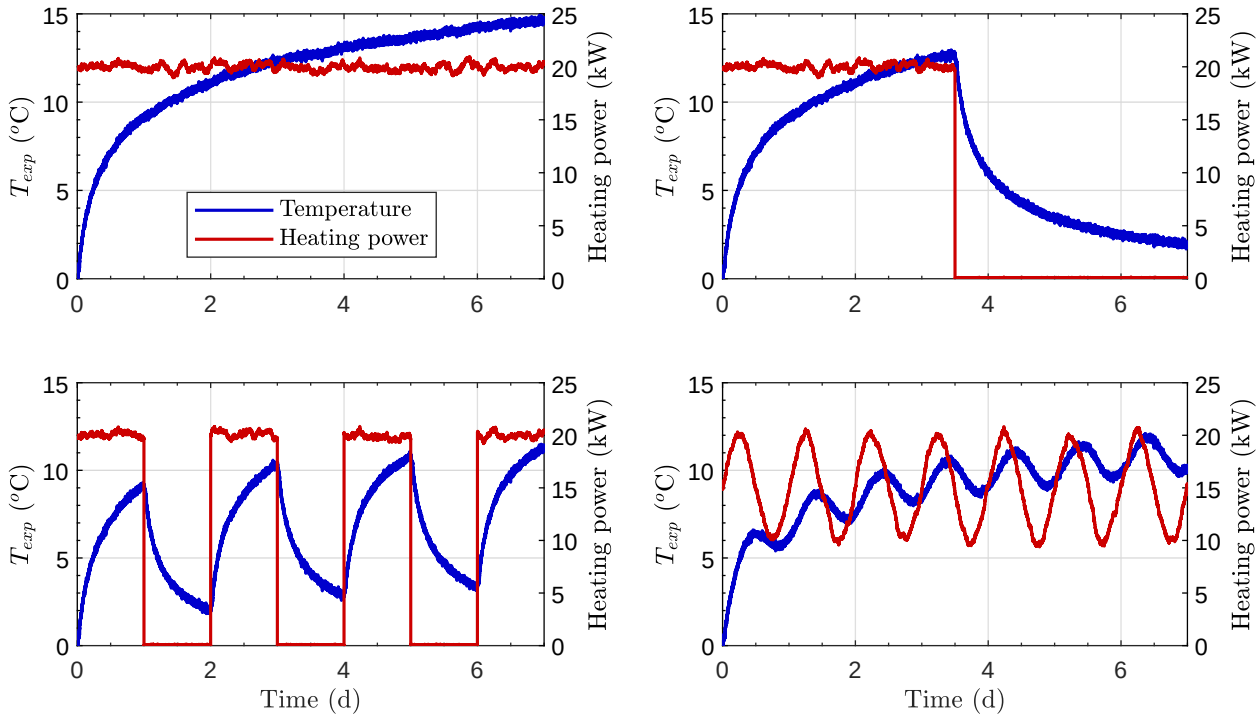

Figure 4.3 Experimental temperatures measured at the outlet of a SCW and used for the numerical test cases: (Top-left) constant heating, (Top-right) heating-recovery, (Bottom-left) pulse steps and (Bottom-right) sinusoidal heating pattern. The numerical temperatures include short-term variations and measurement errors and were obtained with a constant flow rate of 100 L/min.

temperature response T_{exp} for the field TRTs. It is worth noting that cases 1 and 2 are from the same site, but correspond to two different boreholes. Hence, the geological environment is similar for these two TRTs. The second TRT presents an electric shut down at 3.5 days where the heating power and flow rate were equivalent to 0. Impact of this unplanned power outage can also be seen on the recorded temperatures. The third test presents an initial high heating input when the heater is started, but stabilizes afterward. The flow rates were taken

as constants with an average over the duration of the TRTs. The mean values are, for cases 1 through 4 respectively, 26.0 L/min, 24.7 L/min, 12.3 L/min and 97.8 L/min. It can be observed that these four data sets presents various effects that will test the robustness of the deconvolution algorithm. Table 4.2 lists information about the boreholes, the soil and the TRT for the field test cases.

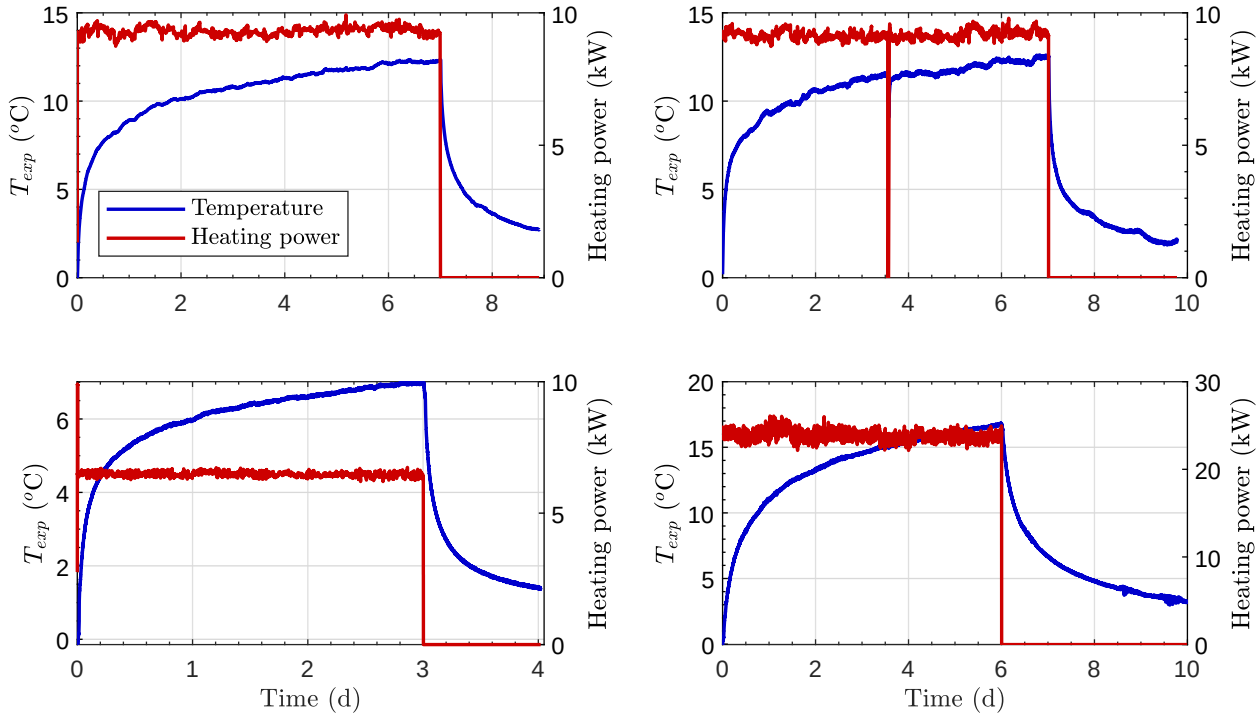

Figure 4.4 Experimental temperatures measured at the outlet of closed-loop boreholes (three first figures) and SCW (last figure) used for the field test cases. Flow rate for the test cases are respectively $V = 26.0$ L/min, $V = 24.7$ L/min, $V = 12.3$ L/min and $V = 97.8$ L/min.

Table 4.2 Borehole geometry and thermal properties of the numerical and field TRTs used in the deconvolution algorithm.

Parameters	Symbol	Unit	Numerical	Field 1	Field 2	Field 3	Field 4
Initial ground temperature	T_0	°C	11.00	7.47	7.17	9.48	12.48
Soil thermal conductivity	k_s	W/(m·K)	2.76	3.05	3.05	3.30	2.74 ± 0.25
Soil heat capacity	C_s	MJ/(m^3·K)	2.00	2.00	2.00	1.70	2.00
Grout thermal conductivity	k_g	W/(m·K)	-	1.65	1.65	0.50	-
Grout heat capacity	C_g	MJ/(m^3·K)	-	2.00	2.00	1.90	-
Borehole radius	r_b	m	0.083	0.051	0.051	0.076	0.083
Borehole length	H	m	215.0	152.4	152.4	155.4	215.0
Circulation flow rate	V	L/min	100.0	23.7	23.7	12.3	97.8
Half pipe spacing	D	m	-	0.029	0.029	0.100	-
Bleed ratio	β	%	0	-	-	-	0
TRT duration	-	d	7	9	10	4	10
Type/configuration	-	-	SCW	Single U-tube	Single U-tube	Single U-tube	SCW

4.4.3 Filtering

Knowing that the unfiltered temperature and heating power signals have high frequency measurement errors, smoothing them with a low-pass filter helps lessening the errors amplitudes. Removing part of the measurement errors, while not deforming the initial signal, could enhance the precision of the deconvolution algorithm on recreating the temperatures. The two studied low-pass filters are the moving average (MA) and Gaussian kernel moving average (GMA) [193, 197]. These two filters are selected because of their usually good performance with time series and ease of implementation. Table 4.3 summarizes the three approaches applied to the numerical and experimental test cases, which are comprised of the unfiltered (NF standing for No Filter) and filtered values using both the MA and GMA filters.

Table 4.3 Low-pass filtering approaches applied to the numerical and field test cases.

Approach	**Description**
1 (NF)	Measured data, composed of natural variations and measurement errors.
2 (MA)	Moving average filter, centered with 5 points before and after the evaluated one.
3 (GMA)	Gaussian window moving average filter, centered with 5 points before and after the evaluated one.

4.5 Results

The deconvolution algorithm presented in section 4.3 is applied to the eight test cases described in section 4.4. The *root-mean-square-error* (RMSE) between the calculated $\hat{g}$ and field g_{exp} and between the reconstructed $\hat{T}$ and experimental T_{exp} is used to assess the performance of the algorithm.

4.5.1 Numerical test cases

Table 4.4 presents the RMSE for $\hat{g} - g_{exp}$ and $\hat{T} - T_{exp}$ with the three filtering approaches. Results show that filtering seems to give better results than the unfiltered approach to the reconstruct $\hat{g}$. However, the differences between the filters are not significant enough to identify a best filter. Also, filtering does not seem to have a large impact on the error on $\hat{T}$ for all the test cases. When comparing the different heating patterns, the sinusoidal test case shows the lowest RMSE for both $\hat{g}$ and $\hat{T}$ when used with filtering. However, the differences between the test cases' RMSEs are not significant, suggesting that the heating pattern does not have a large impact to obtain a satisfactory $\hat{g}$.

Table 4.4 RMSE on the transfer function $\hat{g}$ and the temperature $\hat{T}$ for each filtering approaches and the four numerical test cases.

Numerical cases	RMSE for $\hat{g}$ (-)			RMSE for $\hat{T}$ (°C)		
	NF	MA	GMA	NF	MA	GMA
1 (Constant)	0.026	0.011	0.011	0.113	0.101	0.101
2 (Step)	0.014	0.010	0.010	0.106	0.101	0.101
3 (Pulsated)	0.016	0.009	0.008	0.108	0.102	0.102
4 (Sinusoidal)	0.015	0.008	0.008	0.105	0.101	0.101

Figure 4.5(Top) shows the numerical g_{exp} and reconstructed $\hat{g}$ for the numerical test cases. The functions show typical transfer function's characteristics, such as starting 0 and being strictly increasing. The first derivative of $\hat{g}$ and g_{exp} are shown in Fig. 4.5(Middle). All the reconstructed $\hat{g}$ are smooth, even smoother than the numerical curve at early time steps. Note that this numerical curve itself is subject to small numerical errors related to the discretization of the domain and time steps adopted at the beginning of the numerical simulation. Figure 4.5(Bottom) shows the reconstructed and numerical temperature variations. The temperatures reconstructed with the $\hat{g}$ are nearly coincident to numerical temperatures in all test cases. To observe this, Fig. 4.6 shows the residual between the $\hat{g}$ and g_{exp} and between $\hat{T}$ and T_{exp}. This result confirms the good performance of the algorithm to recover both $\hat{g}$ and $\hat{T}$ when numerically generated data are used, since residuals are small. It is worth noting that while the STgFs are well reconstructed at large time steps, the early time steps show the largest discrepancy. Yet, these errors are small and are mostly attributed to the performance of the numerical model at short time steps.

4.5.2 Field test cases

For the field test cases, the known STgFs are, of course, unavailable. Thus, the RMSE is computed using only the reconstructed ($\hat{T}$) and measured (T_{exp}) temperature signals. As shown in Table 4.5, the RMSEs are smaller than 0.1 °C and filtering does not appear to have an effect on the reconstructed temperature signal. It must be emphasized that the objective of the deconvolution algorithm is not, per se, minimizing the temperature RMSE (see section 4.6.2), but rather to estimate a STgF and its first derivative displaying the desired characteristics (i.e. positivity and increasing smooth function at all times) whilst providing acceptable temperature reconstruction.

Figure 4.7(Top) shows the STgFs obtained with the deconvolution algorithm. They show the main desired characteristics of such functions (i.e. positivity and strictly growing). Figure

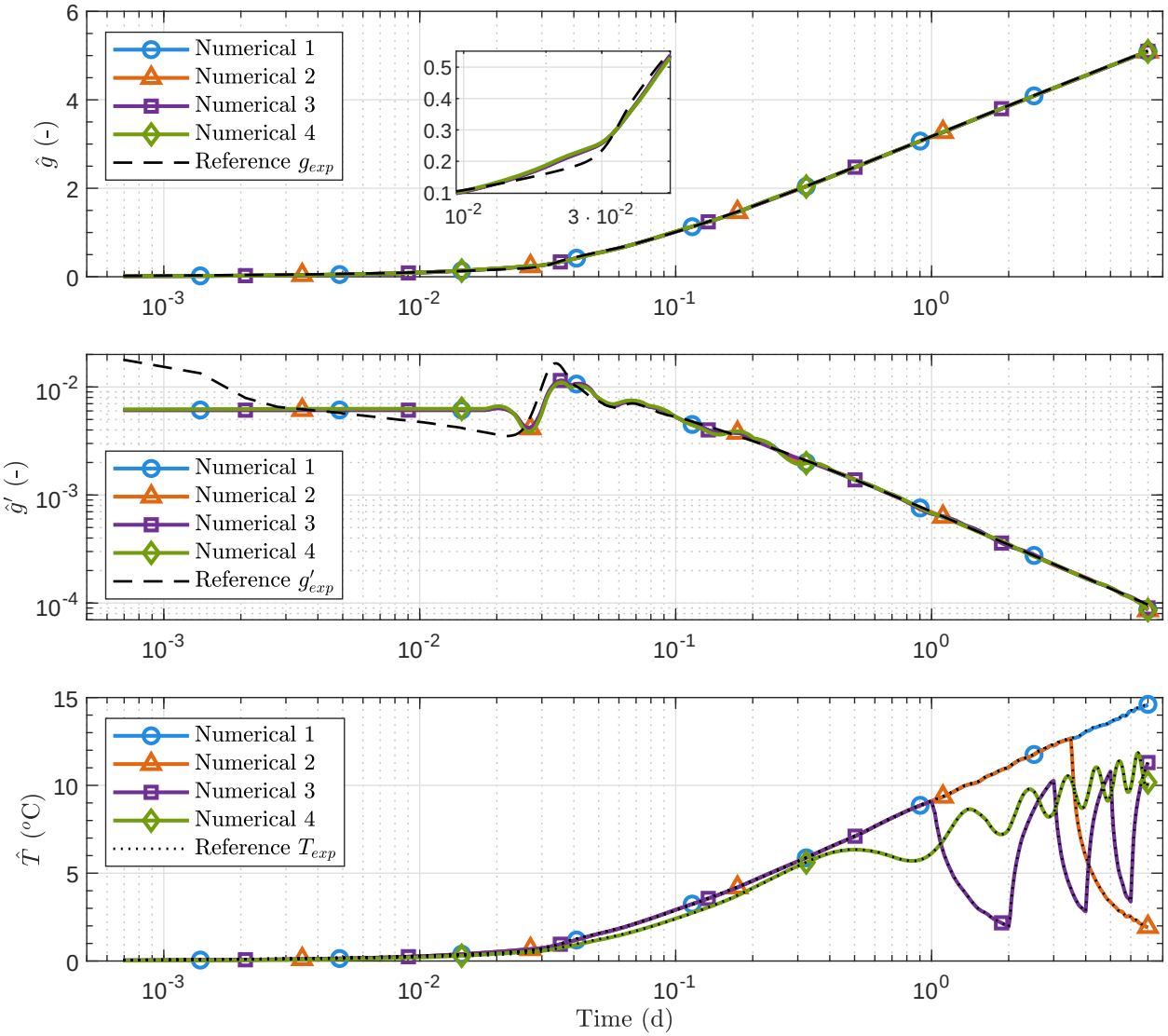

Figure 4.5 Results of the deconvolution for the numerical test cases with the moving average (MA) filter: (Top) $\hat{g}$, (Middle) $\hat{g}'$ and (Bottom) $\hat{T}$.

Table 4.5 RMSE on the temperature $\hat{T}$ for each filtering approaches and the field test cases.

field cases	RMSE for $\hat{T}$ (°C)		
	NF	MA	GMA
1	0.040	0.040	0.040
2	0.096	0.096	0.096
3	0.023	0.022	0.022
4	0.061	0.061	0.060

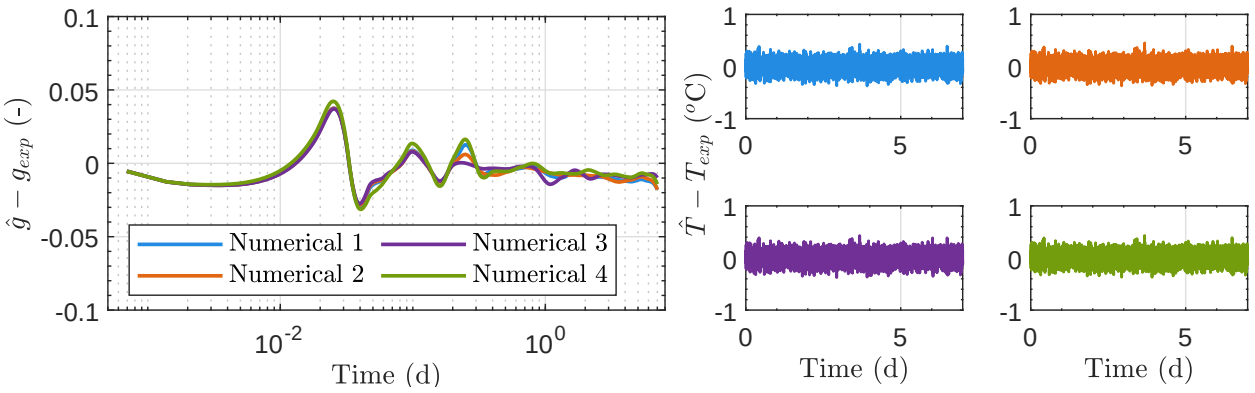

Figure 4.6 Residuals of (Left) g_{exp} and (Right) T_{exp} for the numerical test cases and with the moving average (MA) filter.

4.7(Middle) shows the first derivative of $\hat{g}$. While not being completely smooth, the derivatives are noiseless, which is the desired output. Figure 4.7(Bottom) shows the fit between the field and reconstructed temperatures. Whilst the different fits appear to be good, it is difficult to judge the difference between the curves. So, Fig. 4.8 shows the discrepancy between the field and reconstructed temperatures. Note that the residuals are centered around a value of 0 °C. Figure 4.9 shows the benefits of using the derivative of $\hat{g}$ instead of the derivative of T_{exp}. On this figure, T'_{exp} is divided by the initial impulse on the incremental temperature function $f(t_1)$, so that it matches $\hat{g}'$.

4.6 Discussion

4.6.1 Results analysis

For both the numerical and field test cases, results show the great accuracy of the method on various GHE types, heating power scenarios and TRT conditions (i.e. TRT duration, power outage and various level of measurement noise). The $\hat{g}$s show expected results that consider the geological material as well as the borehole influence, as displayed by the characteristics bumps at the end of the residence time, when the $\hat{g}$ values start to increase (∼43 minutes for the numerical test cases (SCW) and ∼15 minutes for the field test cases 1, 2 and 3 (closed-loop)). This effect was anticipated since the functions are computed at the borehole outlet. The variations between each $\hat{g}$ represent the effects of the ground and GHE thermal exchange properties (i.e. thermal parameters of the ground and GHE), as well as GHE depth and circulation flow rate.

It is worth noting that $\hat{g}$ is obtained using a $\Delta T = 1°C$ between the inlet and outlet borehole

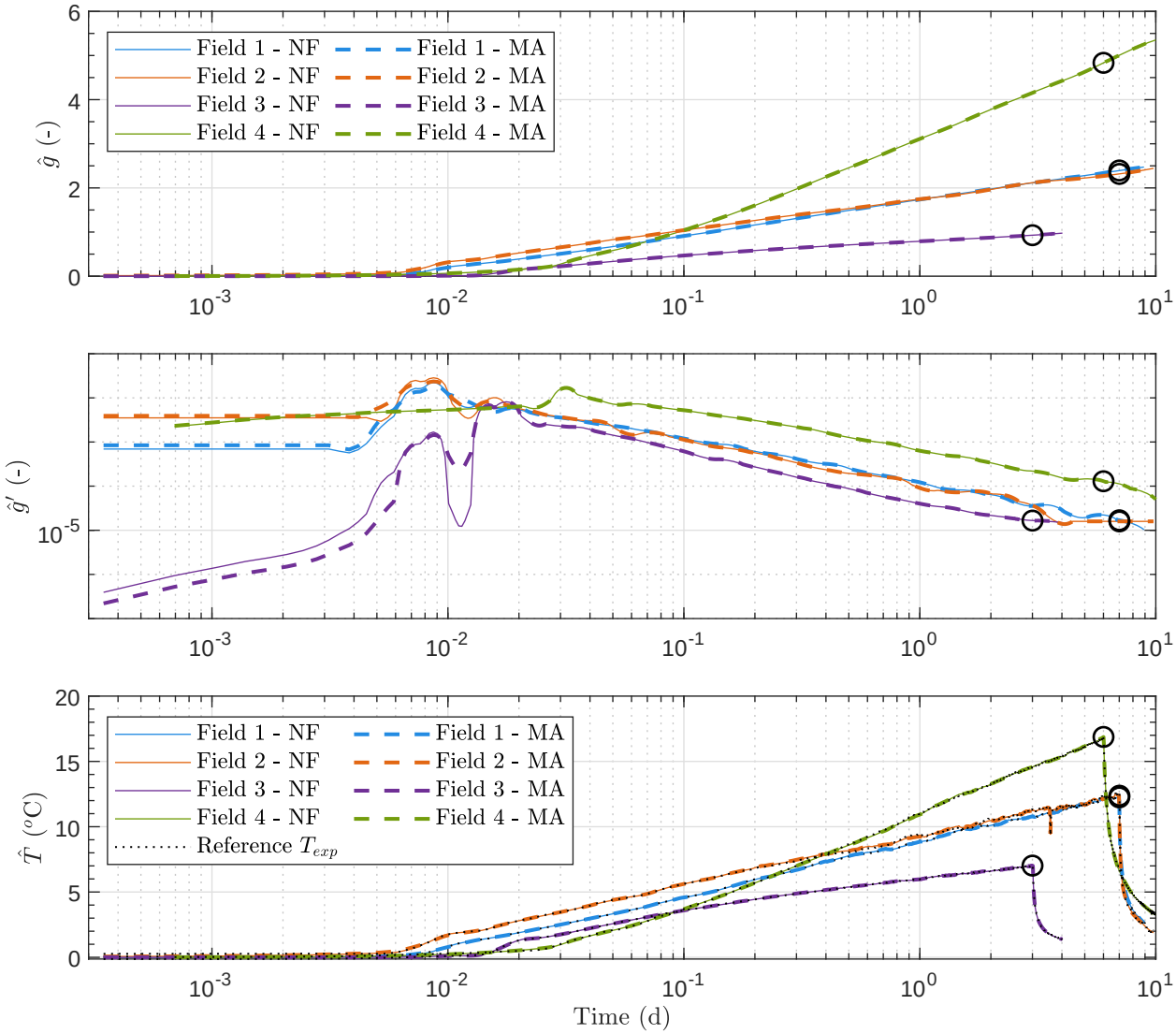

Figure 4.7 Results of the deconvolution for the field test cases without filter (NF) and with the moving average (MA) filter: (Top) $\hat{g}$, (Middle) $\hat{g}'$ and (Bottom) $\hat{T}$.

for a given flow rate. Hence, contrarily to standard g-functions, a high value for $\hat{g}$ can in fact express a high heat transfer since $Q = \rho_f C_p V \Delta T$. For example, the field test case 4 in Fig. 4.7 shows $\hat{g}$ values for $t = 10$ days at least two times higher than the other STgFs. This is mostly caused by the flow rate used in the SCW that was at least four times higher than the flow rate used in the closed-loop boreholes (see Fig. 4.13).

The numerical g'_{exp} and $\hat{g}'$ do not correspond well at early time-steps, as shown in Fig. 4.5(Middle). Before $4 \cdot 10^{-2}$d (or 58 minutes), which is a little more than one residence time in the SCW (calculated at 51 minutes), $\hat{g}'$ presents the expected characteristics for a SCW, that is a progressive increase of $\hat{g}$ (stable $\hat{g}'$), while g'_{exp} seems unstable. The expected

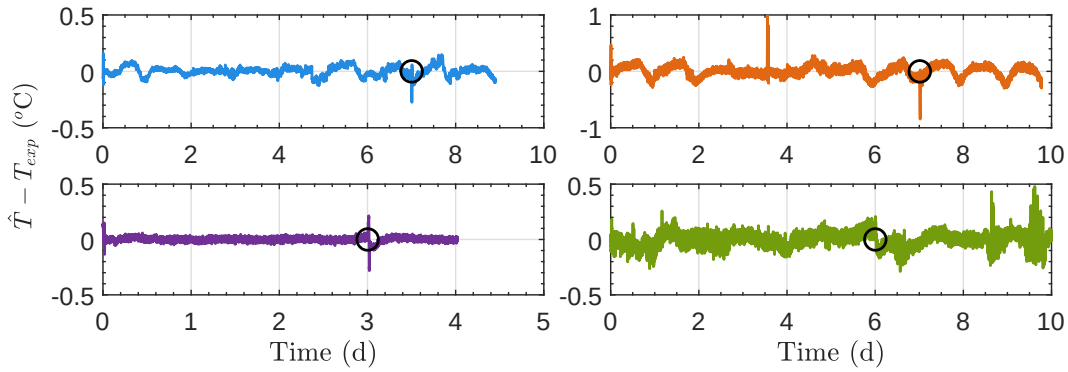

Figure 4.8 Residuals of T_{exp} for the field test cases and with the moving average (MA) filter.

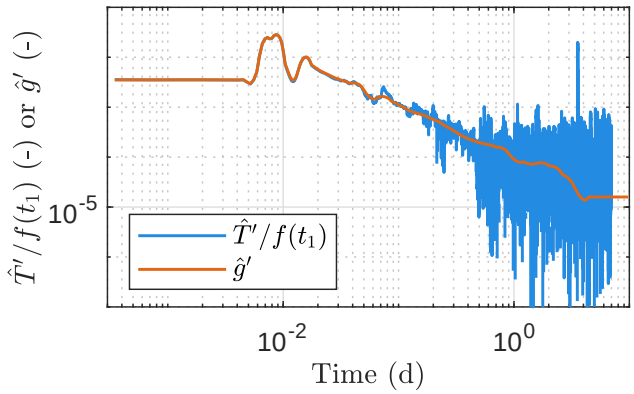

Figure 4.9 Comparison of $\hat{g}'$ and $\hat{T}'$ for field test case 2. To match $\hat{g}'$, $\hat{T}'$ is divided by the initial impulse of the incremental temperature function $f(t_1)$.

evolution of $\hat{g}'$ is due to thermal short-circuiting within the vertical pipe before the heat carrier fluid has completed its first full cycle, followed by a steeper slope. It suggests that the reference curve presents some numerical inaccuracies due, for example, to the time and spatial discretization of the numerical model used. Appart from the early time-steps, the local maximums at time $\sim 3.5 \cdot 10^{-2}$d in Fig. 4.5(Middle) are well aligned for both the reference and deconvolved curves.

Concerning the numerical test cases, the natural variations, simulated with autocorrelation between the values, are well handled by the deconvolution algorithm. The measurement errors, simulated with a white noise, are filtered by the nodes used to parametrize the STgF, the different terms included in the objective function and the constraints applied. The temperature residuals in Fig. 4.6 appear as white noise, reflecting the measurement errors added to the heating power and temperature. This would also explain the higher temperature RMSE from Table 4.4 on the numerical test cases compared to the field test cases on Table

4.5. All the temperature's RMSE are in the same range, which shows the efficiency of the method on various data sets, TRT duration and GHE type.

Concerning the field test cases, $\hat{g}$ allows precise reconstruction of the temperatures. The short power interruption of the field test case 2 is well handled even if a sharp spike can be seen on the residual of T in Fig. 4.8. This behaviour is expected, since the incremental temperature function cannot be evaluated in the case of power interruption. It also suggests that $\hat{g}$ is not much affected by a short power interruption.

Adding a low-pass filter helps lowering the RMSE between the $\hat{g}$ and g_{exp}, as displayed in Table 4.4, albeit not by a large margin, while keeping the global precision on $\hat{g}$ (Figs. 4.5(Top) and 4.7(Top)) and their derivatives (Figs. 4.5(Middle) 4.7(Middle)). This effect is impossible to assess on the field test cases, since no field g_{exp} is available. On the other hand, filtering does not appear to have a significant effect on the temperature RMSE (numerical or field), as displayed in Tables 4.4 and 4.5. Hence, filtering only appears to have benefic effect on $\hat{g}$ reconstruction.

Otherwise, there are apparent computing artefacts on some test case results. In Fig. 4.8 the residuals of the field cases 1 and 2 oscillate considerably compared to case 3. This could be linked to the stability of the heating power pattern. In Fig. 4.4, the heating power of the two first cases (i.e. top row) show larger variability compared to the two last cases (i.e. bottom row), where measurement noise seems more predominant. Hence, there seems to be a correlation between the pattern of function f and $\hat{T}$. Knowing that the STgFs all have generally the same shape, the results indicate that the reconstruction of $\hat{T}$ depends mostly on the accuracy of function f, especially when it contains abrupt changes. Indeed, the temperature residual on the field test cases have large error spike around the start of the recovery phase, even if more weights is attributed to this section of the TRT during the optimization process. Such deviations show the difficulties encountered by the algorithm to optimize the temperature and impulse function at highly varying periods. However, even considering these spikes, the residuals are relatively small and centered on 0 °C. Finally, the field cases 1 and 2 are located in the same area, but in different boreholes. Hence, the corresponding $\hat{g}$ are quite similar. The differences between 10^{-2} and $3{\cdot}10^{-1}$d are due to differences in the borehole construction for these two cases.

4.6.2 Objective function analysis

The objective function and its constraints use different variables and weights to reconstruct an accurate STgF. The optimized weights P applied to the second and third terms of the objective function (Eqs. 4.5, 4.6) are set so that the proportion of each term lies between

certain intervals: 75 to 90 % for E_T, 5 to 20 % for $E_{\hat{g}'}$ and 1 to 15 % for $E_{\hat{g}''}$. For example, the numerical test case 1 has weight of 79%, 17% and 4% respectively for E_T, $E_{\hat{g}'}$ and $E_{\hat{g}''}$. The field test case 1 has weight of 82%, 9% and 9% respectively for E_T, $E_{\hat{g}'}$ and $E_{\hat{g}''}$. Tests indicate that these intervals hand acceptable results for the tested data sets.

The weights W_T are used in the present methodology to emphasize the early time steps. It consists in a vector of length m with the first 300 points having a value of 10. The remaining points of the vector have a value of 1. Tests have been conducted on the usefulness of adding a section with high weights at the beginning of the recovery phase. However, the temperatures RMSE was not reduced and it did not improve the reproduction of g for the numerical cases. Other weighting functions could have been used, like weights decreasing exponentially or following a power law in time, but this was not tested as the adopted weights provided globally good results.

The optimization methodology remains flexible and multiple parameters can vary whilst handing good deconvolution results. To visualize the impact of certain modifications, Fig. 4.10 presents four variations on the proposed methodology with the field test case number 4: (1) the optimized approach with the appropriately weighted objective function terms, (2) the objective function containing only the residual on the temperature term ($E(t_i) = E_{\hat{T}}$), (3) the terms of the objective function have roughly the same proportion on the minimization ($E_{\hat{T},\hat{g},\hat{g}'}/E \sim$33%) and (4) using the optimized objective function, but without $C1$ and $C2$ constraints (no constraints).

Not using the set constraints $C1$ and $C2$ results in less stable first derivative for the variation number 4 (see Fig. 4.10 (top-right)). On the opposite, having roughly the same proportion on the three terms of the objective function results in the smoothest $\hat{g}$ first derivative. The early times, however, miss the recirculation period, as visible on the zoomed sections in Fig. 4.10. The variation number 2 would be the one recreating the temperature variations with the most accuracy since only the temperatures reconstruction are evaluated. However, its first derivative is not as smooth and continuous as with the optimized deconvolution parameters (variation number 1). Hence, the optimized scenario appears to fulfill the objective of the deconvolution with the most precision.

4.6.3 Position and number of nodes

The number of nodes used to parametrize the STgF affects the precision of $\hat{g}$ and $\hat{T}$. Figure 4.11 shows the impact of the number of nodes n_0 on the $\hat{g}$ and $\hat{T}$ RMSEs for the numerical test cases. When n_0 is larger than 100, the RMSE increases significantly, which can be the result of the optimization ending in a local minimum instead of a global one. Furthermore,

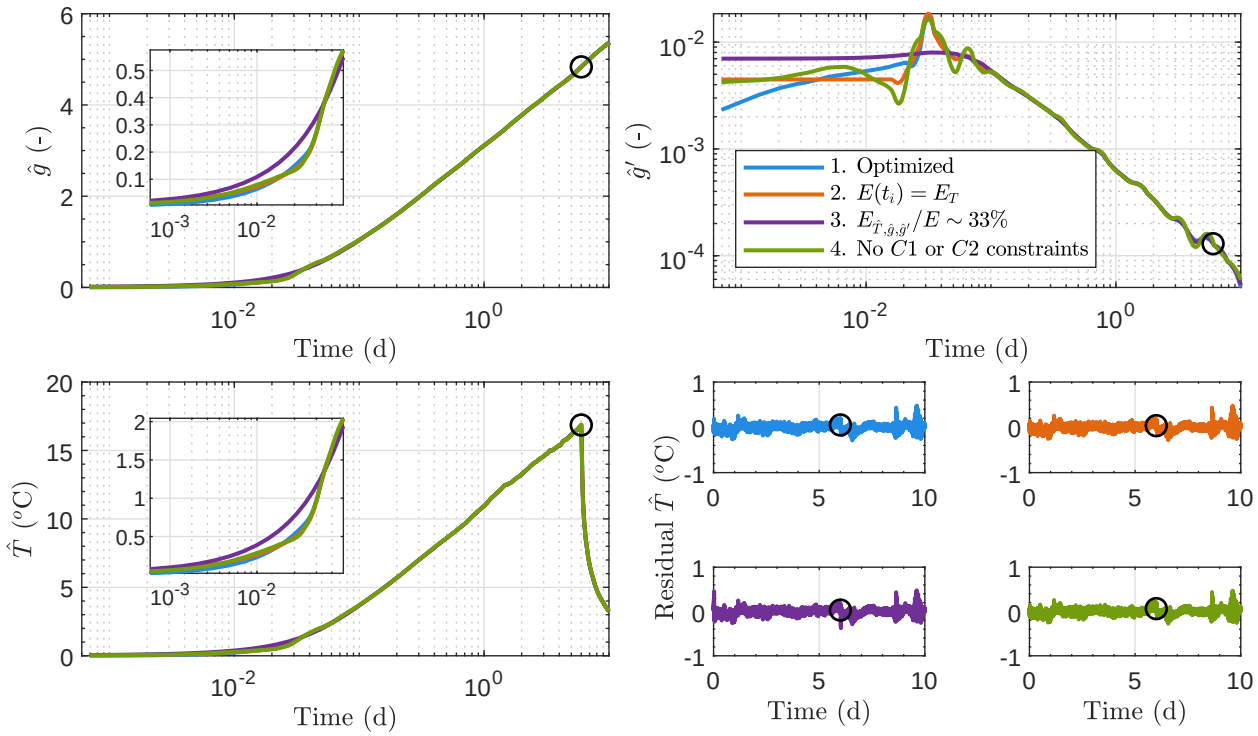

Figure 4.10 Impact of the objective function and constraints for field test case 4 with the moving average (MA) filter. (Top-left) $\hat{g}$, (Top-right) $\hat{g}'$, (Bottom-left) $\hat{T}$ and (Bottom-right) residuals on $\hat{T}$.

artefacts appear on $\hat{g}$ when the number of nodes goes over 60 (not shown), which is an appropriate higher bound for this parameter. Using less than 25 nodes prevents retrieving a $\hat{g}$ that yields an optimal accuracy on the temperature reconstruction. Hence, recommended nodes number should be between 25 and 60 for TRTs of 3 to 10 days. This recommendation is also similar to the indications of Pimonov et al. (2010) ([174], which is 10 nodes per logarithmic cycle, or around 40 nodes.

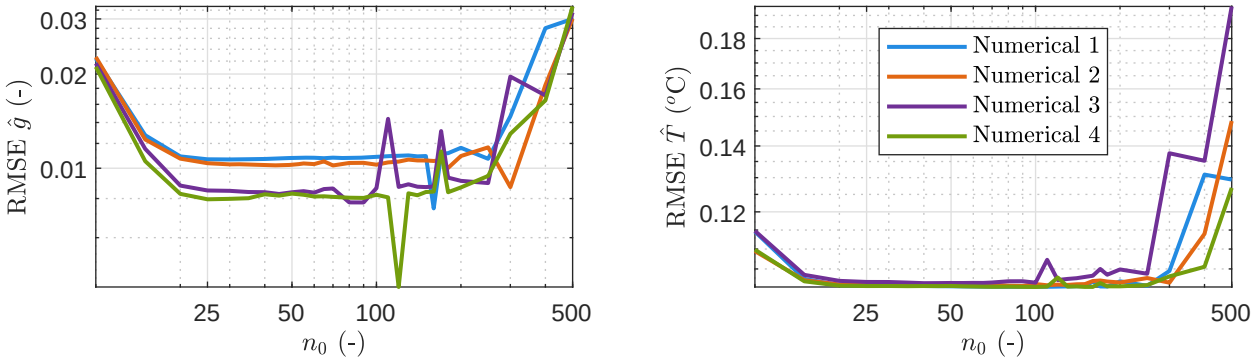

Figure 4.11 Impact of the number of nodes on the RMSE for the numerical test cases. (Left) $\hat{g}$ and (Right) $\hat{T}$.

4.6.4 Effect of undisturbed ground temperature

The variation of the initial ground temperature T_0 could create as much as 27 % uncertainty in the evaluation of the thermal resistance of the GHE [186]. Hence, to verify its impact on the deconvolution method, a sensitivity analysis was performed on this parameter for the field test cases when using the moving average filter. Figure 4.12 shows the RMSE variations for a range of undisturbed ground temperature for the field test cases. The circles are the T_0 calculated from a mean of the recirculation phase, preceding the heating phase of the TRT. Each test case presents sharp variations if T_0 is not well evaluated. Since the circles are close to the minimum of each curve, it is believed that using the mean temperature during the recirculation is an appropriate way to easily obtain the undisturbed ground temperature to be used with the deconvolution algorithm.

4.6.5 Effect of varying flow rate

Eq. 4.2 can use both the heating power and the flow rates at every time step as input. Eq. 4.2 give an incremental temperature profile when considering $Q(t_i)$ and a constant flow rate V_1. However, the use of another flow rate $V_2 \neq V_1$ would result in a different $\hat{g}$. This type of problem are now studied (see, for example, Beaudry et al. (2021) [143]). Nonetheless, as

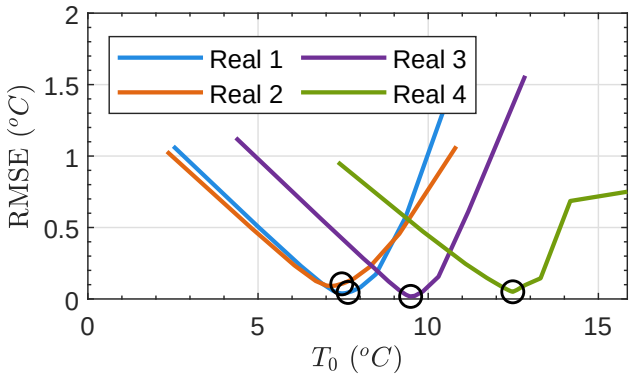

Figure 4.12 Impact of an error on the undisturbed ground temperature T_0 for the field test cases. The circles show the T_0 obtained using an average of the recirculation phase at the beginning of the TRT and used in this work.

the flow rate fluctuations are usually small, it is common to assume the flow rate as constant over the TRT duration, hence the simplification $V(t_i) = V$.

Figure 4.13 shows the measured flow rate for the four field test cases. On test case 1, 2 and 4, the variations mostly resemble a white noise effect with small to no autocorrelation between the values. Test case 3 presents a pattern that is often seen due to the power distribution in the TRT rig between heating and recovery phases. Test case 2 (top-right) shows the power interruption at around 3.5 days.

The deconvolution algorithm was tested under two scenarios: variable and constant flow rate. For the field test case 1, 2 and 4, the RMSEs were a bit larger when considering a variable flow rate. This could be attributed to the measurement errors on the flow rate. For test case 3, smaller RMSEs, albeit very similar, were obtained when using the moving average filter (0.024 °C with V and 0.020 °C with $V(t_i)$). This could stem from the stronger relation between the variation of the flow rate and the adequate incremental temperature function f to represent the temperature variations induced in the GHE. In general, similar results are obtained with either scenarios. Larger flow rate variations could, however, create large impact on $\hat{g}$. Maintaining a stable flow rate is then critical, especially since the STgF is associated to the mean flow rate measured during the TRT. Hence, temperature prediction is valid with the specified flow rate.

4.7 Conclusion

This article presented a deconvolution method that uses the entire experimental data set of a thermal response test to extract the borehole outlet short-term transfer function, without

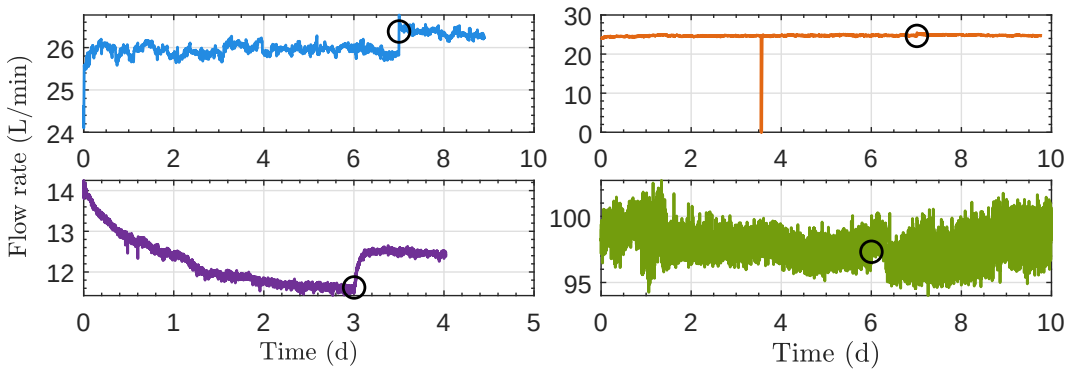

Figure 4.13 Measured flow rate for the field test cases

needing a heat transfer model. The method minimized a constrained multi-objective function on a selection of nodes that ensures smoothness of the short-term transfer function and its first derivative. The noded solution is interpolated with a piecewise cubic Hermite interpolating polynomial (PCHIP) to allow smooth reconstruction on the time steps of the thermal response test.

Numerical and field data sets were used to assert the performance, robustness and reliability of the proposed algorithm. Results show that the convolved temperatures have RMSE of 0.1 °C or lower. Filtering appears to have beneficial impacts on the reconstruction of the STgF for the numerical case whereas the temperature reconstruction remained relatively insensitive to filtering in all cases considered.

The deconvolution algorithm can handle TRT data sets from different GHE types and time-varying heat load profile with high sampling rate. Natural variations and data measurement errors were handled adequately by the proposed method. Moreover, the g-functions estimated were not significantly impacted by the occurrence on an unplanned relatively short power interruption. Further research is required to generalize the deconvolution algorithm to events inducing non-linear effects in the TRT.

4.8 CRediT authorship contribution statement

Gabriel DION: Conceptualization, Methodology, Software, Visualization, Writing - Original Draft. **Philippe PASQUIER**: Methodology, Conceptualization, Validation, Writing - Review & Editing, Supervision, Funding acquisition. **Denis MARCOTTE**: Methodology, Software, Validation, Writing - Review & Editing.

4.9 Acknowledgments

The authors wish to acknowledge the support and funding provided by the Natural Sciences and Engineering Research Council of Canada (grant number RDCPJ 530945), the Trottier Energy Institute, Hydro-Québec, FTE drilling, Marmott Energies, Richelieu Hydrogeology and Versaprofiles.

4.10 Nomenclature

β	Bleed ratio (%)
$C1$	Positive and function and its first derivative constraint (-)
$C2$	Second derivative constraint (-)
C_f	Fluid heat capacity ($\mathrm{J{\cdot}m^{-3}{\cdot}K^{-1}}$)
C_s	Soil heat capacity ($\mathrm{J{\cdot}m^{-3}{\cdot}K^{-1}}$)
C_g	Grout heat capacity ($\mathrm{J{\cdot}m^{-3}{\cdot}K^{-1}}$)
D	Half pipe spacing (m)
E	Objective function value (-)
f	Incremental temperature function (°C)
g_0	Initial borehole outlet short-term g-function (-)
g	Borehole outlet short-term g-function (-)
$\hat{g}$	Estimated borehole outlet short-term g-function (-)
g_{exp}	Numerically generated borehole outlet short-term g-function (-)
H	Borehole length (m)
k_s	Soil thermal conductivity ($\mathrm{W{\cdot}m^{-1}K^{-1}}$)
k_s	Grout thermal conductivity ($\mathrm{W{\cdot}m^{-1}K^{-1}}$)
m	Length of time array (-)
n	Length of node array (-)
P	Scalar weight on the objective function (-)
Q	Heating power (W)
r_b	Borehole radius (m)
t	Time (d)
τ	Node placement (d)
T_0	Initial ground temperature (°C)
T_{out}	GHE outlet water temperature (°C)
T	Temperature variation $T_{out} - T_0$ (°C)
$\hat{T}$	Temperature variation obtained with $\hat{g}$ (°C)

T_{exp}	Temperature variation from either numerical or field experiments (°C)
ΔT	Temperature difference between the input and output of the GHE (°C)
V	Flow rate ($m^3 \cdot s^{-1}$ or $L^3 \cdot min^{-1}$)
W	Time dependant weights (-)

CHAPITRE 5 ARTICLE 2 - MULTI-DECONVOLUTION IN NON-STATIONARY CONDITIONS APPLIED TO EXPERIMENTAL THERMAL RESPONSE TEST ANALYSIS TO OBTAIN SHORT-TERM TRANSFER FUNCTIONS

Gabriel Dion[1*], Philippe Pasquier[1], Denis Marcotte[1], Gabrielle Beaudry[1]

Science and Technology for the Built Environment, June 8th 2023

[1] Department of Civil, Geological and Mining Engineering, Polytechnique Montréal, P.O. Box 6079 Station Centre-Ville, Montréal, Canada H3C 3A7

[*] Corresponding author email: gabriel.dion@polymtl.ca

Keywords: thermal response test, deconvolution, non-stationary test, ground heat exchanger, optimization

5.1 Abstract

Thermal response test interpretation methods usually rely on the assumptions of constant operating conditions in time. However, through desired or undesired processes, these conditions often vary in time. Since interpretation is usually done with stationary methods, no current algorithm allows to account for non-stationarity in thermal response test, as encountered with varying flow rate. The goal of this article is to apply a multi-deconvolution algorithm to retrieve a set of short-term transfer functions during a thermal response test with changing operating conditions. The deconvolution algorithm uses an optimization-based technique as the inverse model, while considering non-stationarity in the forward model through a recent non-stationary convolution algorithm. By optimizing a set of nodes on each estimated short-term transfer function, precise reconstruction of the experimental temperatures is possible. Results show that temperature reconstruction is as precise as an error of 0.06 °C on numerical cases and 0.07 °C on field cases. The usable transfer function duration and an analysis of the objective function's optimum are also demonstrated. With the proposed algorithm, only the dataset of a thermal response test is needed to obtain short-term transfer functions when operating conditions are changing.

5.2 Introduction

The electrification of the building sector could create a 31.6 % energy demand increase on the electric grid capacity, at the benefit of almost 30-40 % greenhouse gas emissions reduction [198]. It is then a viable option to dampen the effect of global warming. However, to aid lessening the electric consumption growth that accompanies the building sector's electrification, adaptive technologies [199] should be used to reduce the energy consumption needed to meet a building's heating and cooling load, which can amount up to 50 % of a building's total energy consumption in cold climates [200]. In this sense, ground source heat pump (GSHP) systems could be employed, since they use up to 75 % less electricity than conventional electric resistance heaters [12]. This high efficiency allows reducing both the building's heating and cooling energy consumption, as well as the peak energy demand, which is highly impactful on the electricity grid [200]. GSHP systems employ a geothermal heat pump to connect the building to a ground heat exchanger (GHE). The latter is commonly a vertical borehole in which a heat carrier fluid circulates and exchanges heat with the ground that acts as a thermal reservoir [48]. These GHEs make heat dispersion or collection possible either by conduction in a closed-loop configuration or by conduction and advection in an open-loop configuration.

To design a GHE in accordance with the heating and cooling demand of a building, it is common to perform an *in-situ* thermal response test (TRT) [26] and to interpret the results to obtain the ground effective thermal properties [51]. A TRT consists in circulating a heated or cooled heat carrier fluid in the GHE and to measure the difference between the GHE inlet and outlet fluid temperature. This difference can then be interpreted by various methods to retrieve, mainly, the ground thermal conductivity and the borehole thermal resistance [18, 201]. Common TRT interpretation methods are generally based on direct ground response models that allow to evaluate the effects of underground heat transfer [28]. The main inputs of these models are the geometrical and thermal parameters corresponding to the investigated site (i.e., borehole radius and length, ground and borehole materials thermal conductivity and heat capacity), and their outputs are generally temperature signals describing the response of the GHE to an input heat rate. These models are mainly analytical, like the infinite or finite line source model [69, 79], numerical, like the finite volume element method [202] or the thermal resistance and capacitance method [47]. For TRT interpretation, the forward models are implemented in an inverse algorithm, in which the thermal parameters are adjusted until a good fit is achieved with the TRT experimental data [37, 105]. Known inverse algorithms used for low temperature geothermal applications are trial and errors, the graphic interpretation [24] or optimization algorithms that minimize an objective function

that are used to estimate thermal parameters [28,115,177]. The thermal parameters retrieved by inversion from TRT interpretation can in turn be used in forward models for GSHP simulation and sizing purposes.

In this regard, a common approach is to use thermal response factors, also known as g-functions [39], which describe the temperature evolution at the borehole wall given a constant unit heat impulse and therefore encompass the capability of a GHE to exchange heat with its surroundings. Additional elements that emulate the casing, grout, pipe and fluid properties can also be integrated to obtain the borehole outlet fluid temperature, which is an important design parameter. Extensive research has been carried out towards a precise evaluation of g-functions. Common methods use either a numerical simulation model [39, 40, 89], an approximation by an analytical model [124,126,127], a thermal resistance and capacity model [98,203], neural networks [98,130], a table interpolation [131] or a successive flux methodology [123, 204]. Usually, a g-function's range of validity is for time steps larger than an hour and can go up to decades. Efforts have been made to also identify shorter time steps g-functions to obtain a full response model [99, 147]. The short-term g-function (STgF) allows the simulation of rapid transient regime changes during a GSHP system operation, such as starting or stopping the geothermal heat pump. Short-term performance of a GHE is important to evaluate when optimizing the operation and performance of a GSHP simulation since rapid changes in operating conditions are mainly reflected on the short time response of the GHE [44]. It is interesting to note that this shorter period usually ranges from minutes to days, which corresponds relatively well to a TRT duration.

The generation of short-, long- or full-time scale g-functions through forward heat transfer models generally suffers from model-based approximations or long computing time. To enhance the precision and rapidity of this process, the experimental data of a TRT (for short-term g-function) or data from a GSHP system operation (for long-term g-function) can be directly implemented in a deconvolution algorithm. Such a method allows to directly retrieve the g-functions from experimental data, and therefore eliminates the need for analytical or numerical heat transfer model, as well as the biases of the associated usual simplification assumptions. So far, deconvolution algorithms applied to TRT data have been used to obtain the thermal parameters of the ground [177] or the short-term g-function (STgF) representing the fluid temperature at the outlet of a BHE [205]. In the latter case, the authors have demonstrated the precision of the so-called STgF (also referred to as transfer function) to predict the borehole's outlet fluid temperature over short time steps (i.e., less than an hour). Another test case applied the deconvolution algorithm to numerically generated year-long GSHP operations and demonstrated the possible application of this technique to recover long-term g-functions, on the condition that stationarity is maintained [206].

It is important to note that each transfer function (or g-function) is valid for a single GHE geometry and set of constant operating parameters (e.g., flow rates). This leads to consider transfer functions as part of stationary, or linear and time-invariant (LTI) systems. In such a system, two main properties are present: (1) a linear relation between the input and output and (2) a time invariance of the system [148]. For a GHE, time-varying heating power can be accounted with the load aggregation technique [120], which still respects the definition of stationarity. This technique can also be computed as a convolution [45], which supposes a LTI system. Hence, superposition and convolution in their traditional form cannot be used to interpret non-stationary systems.

In all experimental scenarios, it is feasible to obtain quasi-stationarity, even though it cannot be maintained due to outside factors. In the case of a TRT, non-stationarity occurs with a variation of the circulating flow rate or bleed flow rate in the case of standing column well (SCW) GHEs. This operating strategy consists of purging a small amount of groundwater outside of the main circulation well, which stimulates the groundwater influx at the borehole wall and thus advective heat transfer. Other factors like groundwater flow changes, material property variations with underground temperature and thawing also affect a GHE stationary operation [143]. Using a numerical forward model, non-stationarity can be considered in time-varying simulations, but at the cost of being a time-consuming and computationally heavy method [202, 207]. To avoid these issues, a hybrid methodology that considers non-stationarity in the outputs of the TRT can be employed to avoid relying on analytical or forward numerical models to interpret a TRT. Beaudry et al. (2021, 2022) [102,143] proposed an algorithm that allows to consider non-stationarity in the convolution of GHE temperatures and demonstrated their impact on GSHP simulations. In particular, it is shown that the non-stationary variation of flow rates can significantly enhance the performance and efficiency of a GSHP system. The algorithm is a non-stationary convolution that uses a set of transfer functions, each associated with its corresponding operating conditions (e.g., circulation flow rate, bleed ratio, groundwater pumping or natural variations in the hydraulic gradient). This set of transfer functions is, however, obtained using an advanced numerical model, which hinders the practical use of the method for now.

The deconvolution algorithm of Dion et al. (2022a) [205] allows to recover STgF from experimental TRT data in a stationary scenario, which alleviates the error related to simplification assumptions of forward heat transfer models. However, non-stationary operating conditions still need to be handled through computationally heavy numerical models. To the author's knowledge, only the work of Dion et al. (2022b) [206] provided an initial framework to apply deconvolution on a non-stationary TRT. The aim of this article intends to present a non-stationary deconvolution algorithm that employs the non-stationary convolution algorithm

of Beaudry et al. (2021) [143] for the precise and fast interpretation of TRTs with dynamic operating conditions and validate it through numerical and field TRT. The outputs of the proposed deconvolution algorithm are several STgFs, each one being associated with a different set of constant operating conditions, whereas a single one is obtained in stationary case [205]. The purpose of obtaining multiple STgFs from TRT is to help short-term forward simulations involving time-variant operating conditions and to improve the prediction of the corresponding response of the GHE, which is critical to a quality GSHP system design. The proposed multi-signal deconvolution algorithm is akin to an inversion problem where the optimized parameters are the nodes of the different STgFs. This flexible algorithm that can be used for both closed-loop and standing column well GHEs, in which not only the heating power can vary, but also the circulating and bleed flow rates. It is expected that such an algorithm could benefit the design process of GHEs by efficiently providing a set of precise STgFs corresponding to different operating conditions and ready for implementation in a non-stationary simulation algorithm.

5.3 Methodology

A deconvolution algorithm is an inverse problem, applicable to stationary systems, that is solved to generate a single transfer function representing the system's response to a unit impulse. The direct model is a convolution, and in deconvolution, the transfer function is optimized to fit the experimental data. Hence, a dataset retrieved from a TRT is the only input needed to identify the transfer function. The next two sections present the non-stationary deconvolution using a non-stationary convolution as a forward model. The multi-signal deconvolution hands multiple transfer functions, allowing to consider various sets of operating conditions during the TRT. The stationary deconvolution being a particular case of non-stationary cases, the method presented hereinafter is thus a more complete and flexible algorithm that can be used with a large variety of TRT datasets.

5.3.1 Forward model - Non-stationary convolution

Classical analytical approaches for TRT interpretation usually consider a constant heat load signal [69], which is often not representative of real field tests. Extensions to these analytical models consider time-varying heating power by employing the superposition principle [41, 45, 48]. This allows the variation of one input to reproduce the output. With respect to the hypothesis of an LTI system (i.e., a stationary system), the superposition principle is

expressed as a convolution product with the equation:

$$T_{out}(t) - T_0 = (f * g)(t) = \sum_{k=1}^{i} f(t_k) \cdot g(t_{i-k+1}) \tag{5.1}$$

where t is the time array of the TRT, T_{out} is the borehole outlet temperature, T_0 is the initial borehole outlet ground temperature, $f = Q(t_i) - Q(t_{i-1})$ is the incremental input function and g is the transfer function. Here, the borehole outlet temperature is used instead of the average borehole wall temperature since the transfer function is then used to simulate the GHE response to various heat load. In that way, the transfer function regroups the thermal and hydrogeological properties of the ground, the grout and the heat carrier fluid.

Eq. 5.1 supposes stationary conditions during the TRT, hence that only the heating power variation $Q(t_i)$ would affect the convolved temperature $T_{out} - T_0$ (first LTI system's property) for the whole signal duration (second LTI system's property). If more operating parameters are varied, then the system becomes non-stationary. Beaudry et al. (2021) [143] developed a non-stationary convolution algorithm able to compute precise temperature reconstruction considering multiple operating conditions throughout a TRT. The technique performs multiple convolutions using a set of transfer functions (instead of one, as in Eq. 5.1), which correspond to different operating conditions and are selected according to the segment at each time step of the TRT. Each convolved segment is then added to the final temperature variation. The non-stationary convolution's first step is represented in its discrete form by the equation:

$$T_{out}(t_i) - T_0 = (f * g_s)(t, s) = \sum_{k=1}^{i} f(t_k) \cdot g_s(t_{i-k+1}, s) \tag{5.2}$$

This equation is computed on a time vector t_i with constant time steps divided in $S = (s_1, s_2, ..., s_k)$ segments, during which various operating conditions are maintained constant. The first step in non-stationary convolution is to identify the sequence S. The number of different sets of operating conditions s_k is equal to the number of transfer functions needed. Each of these transfer functions g_{s_k} is activated when its corresponding operating conditions occur during the TRT. Hence, Eq. 5.2 is equivalent to a non-stationary combination in which delayed transfer functions are convolved with the excitation function f. This also means that the transfer functions only have to be defined until the last occurrence of their corresponding operating condition s during the TRT. This will be discussed in section *Validity period for the deconvolved STgF set*.

In general, Eq. 5.1 uses dimensionless g-function and an incremental temperature function in °C. In the approach of Beaudry et al. (2021) [143], f is normalized by 1 Watt and

is dimensionless. The units of g are °C instead of the usual dimensionless g-function of Eskilson. They, however, represent the same underlying principle in the convolution.

In the non-stationary combination of Eq. 5.2, each moment of transition between transfer functions creates a discontinuity in the temperature signal $T_{out} - T_0$. To circumvent this effect, Beaudry et al. (2021) [143] identified two transition types: a rapid (fluid residence time) or continuous (several hours) signal shift. The former occurs when a circulation flow rate change occurs within the GHE, and the latter is applied when the groundwater flow regime in the area surrounding the GHE is modified through a natural variation or a bleed flow rate change. These variations are defined by a correction function applied to the convolution, which gives the solution:

$$T_{out}(t) - T_0 = (f * g_s)(t, s) - \lambda(t, s) \tag{5.3}$$

Figure 5.1 summarizes the convolution for both stationary and non-stationary cases. The top row case has a varying heating power and a constant flow rate, which respects the stationarity, since only one input affecting the temperature evolution. Hence, a single STgF is needed to represent this case. The bottom row case shows that, for the same heating power profile as in the stationary case, each different flow rate has its corresponding transfer function. The non-stationary convolution allows to obtain the combined temperature profile according to the specific segment s_k from the multiple temperature profiles T_i.

The correction function $\lambda(t, s)$ in Eq. 5.3 allows to account for the rate of the transitions between stationary signals. The latter is related to the behavior of the transfer functions describing the system before and after the transitions and encompass different phenomena depending on the cause of non-stationarity. For example, when the circulating flow rate changes, the transition is as long as the fluid residence time in the GHE, while a transition on the bleed flow rate results in a lengthier process. Due to the limited scope of this article, interested readers are encouraged to read Beaudry et al. (2021) [143] for an in-depth explanation of the correction function and for details on the overall algorithm. In their paper, the transfer functions are computed on a numerical model that was custom-built to represent the studied site. However, developing and calibrating such a model can be rather time consuming and necessitates long computing time [208]. To avoid this issue, a non-stationary deconvolution algorithm that optimizes the multiple transfer functions is used on the experimental data of a TRT, which is the topic of the present work.

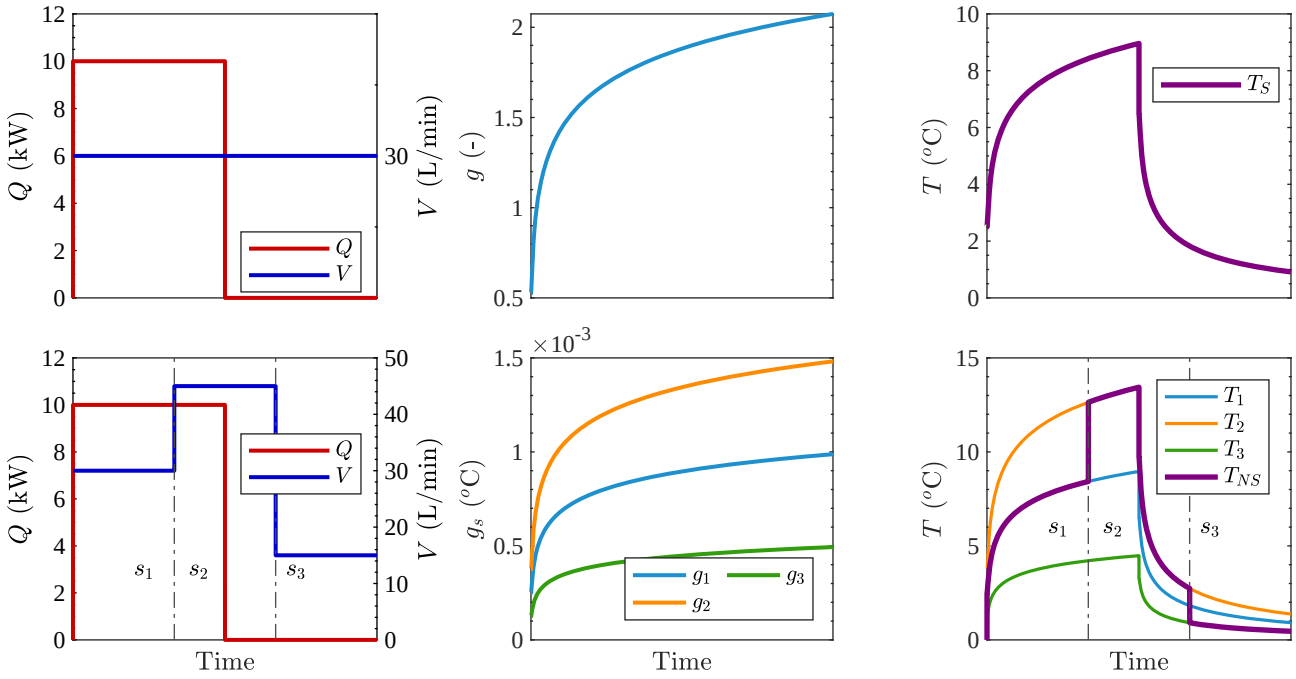

Figure 5.1 Diagram showing (top row) the convolution process for stationary and (bottom row) non-stationary cases. In stationary case, a single transfer function is needed. In non-stationary case, a function for each operating condition is needed. Then, the convolution combines the temperature profiles. Q and V are respectively the heating power and flow rate of each test, and s_i are the time-dependent segments.

5.3.2 Inverse problem - Multi-signal deconvolution

Dion et al. (2022a) [205] presented an inversion optimization algorithm that retrieved an estimated STgF ($\hat{g}$) signal, hence called a stationary deconvolution algorithm, based on the experimental data recorded during a TRT. The methodology minimizes a scalarized [111] multi-objective function in which the parameters (i.e., optimization variables) are logarithmically spaced nodes (τ_j) selected on the time array (t_i). The optimization uses the interior-point method [195], which has already shown its capability in a GSHP system sizing context [37]. The objective function is written as a summation of the Euclidean norm between: (1) the convolved and experimental temperatures using an interpolated $\hat{g}(t_i)$, (2) the first and (3) the second STgF derivatives. The first term adjusts the STgF to the experimental temperature variations, while the second and third terms are regularization terms that enhance the STgF's smoothness and its first derivative. The algorithm also uses linear inequality constraints and bounds to ensure appropriate reconstruction of $\hat{g}$. These constraints are based on known theoretical properties of a transfer function, such as being strictly positive and growing, and having an inflection point in the early time step of the STgF's first derivative.

The deconvolution algorithm presented in this paper relies on concepts from the previous one but expands its capability to include non-stationary scenarios. Hence, to retrieve multiple transfer functions $\hat{g}_s$. One limitation is that experimental data are needed to obtain the STgFs.

First STgF set estimation ($\hat{g}_{0,s}$)

To initiate an optimization problem, a first guess must be provided to the algorithm. The stationary deconvolution of Dion et al. (2022a) [205] is used on the first operating condition s_1 of the TRT to obtain $\hat{g}_0$. It is doable because non-stationarity has not yet occurred, and the stationary deconvolution is appropriate in that scenario.

This function is then extrapolated to the total length of the TRT by fitting an exponential integral function on the last part of $\hat{g}_0$. The problem is described as:

$$\hat{x}_{1,2} = \min_{x_1,x_2} \left\| \left(f * \left(x_1 \int_{x_2/t} \frac{e^{-t}}{t} dt \right) \right) - T_{exp} \right\|_2 \tag{5.4}$$

where $\| \cdot \|_2$ is the Euclidean norm of the objective function, $T_{exp} = T_{out} - T_0$ are the experimental temperatures variations and the parameters x_1 and x_2 are optimized to compute the exponential integral from the end of $\hat{g}_0$ to the total TRT duration. This transfer function $\hat{g}_0$ is only able to correctly reconstruct the experimental temperature when the operating conditions are identical to the ones present in the first segment s_1.

To go from this single STgF to an initial set of STgFs $\hat{g}_{0,s}$, $\hat{g}_0$ is repeated s_k times. Then, a multiplicative scalar applied to each function is optimized to obtain a rough solution. This process is written as:

$$\hat{a}_s = \min_{a_s} \left\| \left(f * \left(a_s \cdot \hat{g}_0 \right) \right) (t, s) - T_{exp}(t) \right\|_2 \tag{5.5}$$

where a_s is a vector with s_k scalar weights. Each value in $\hat{a}_s$ serves to adjust $\hat{g}_0$ for s_k times to have $\hat{g}_{0,s}$. Note that in this last equation, the non-stationary convolution of Eq. 5.3 is used.

This methodology leads to get a set of functions that are generally representative of the experimental temperatures. However, in that way, only the first section of the first operating conditions s_1 is truly optimized. The remaining sections on $\hat{g}_{0,s}$ will be optimized in the main optimization problem.

Main optimization

Before performing the main optimization, a set of nodes are defined on each STgF of the set $\tau_s(j),\ \forall\ S = (s_1, s_2, ..., s_k)$ and $\forall\ j = (1, 2, ..., n_j)$. The nodes $\tau_s(j)$ span from the beginning to the last occurrence of the segments s_k during the TRT. They are parameters on which an optimization process will iterate to minimize the objective function. These nodes $\tau_s(j)$ are spaced logarithmically to ensure better resolution in early time step and each function is characterized by 24 nodes, independently of the STgF time duration. To interpolate the nodes $\tau_s(j)$ with the time steps of the TRT $t_i\ \forall\ i = (1, 2, ..., n_i)$, the Piecewise Cubic Hermite Interpolating Polynomial (PCHIP) is used to preserve a signal's continuity on the first derivative.

Using the roughly optimized $\hat{g}_{0,s}\left(\tau_s(j)\right)$ as the initial guess, the main inversion iterates on the nodes of each STgF to minimize the objective function, as follows:

$$\hat{g}_s(t_i) = \arg\min_{g_s(\tau_s(j))} \left(E\left(t_1, ..., t_m\right) | C_{1,\tau}, C_2\right) \tag{5.6}$$

where E is the scalarized multi-objective function, described by Eq. 5.7, and $C_{1,\tau}$ and C_2 are constraints which will be described later in this section.

The objective function is composed of 4 weighted terms, so that each one has a certain proportion of the total objective value. All the terms use the time resolution of the TRT (i.e., $t_i,\ \forall\ i = (1, ..., n_i)$), thus requiring an interpolation of the nodes $\hat{g}_s\left(\tau_s(j)\right)$. The interpolated $\hat{g}_s\left(t_i\right)$ is then convolved, using the non-stationary convolution of Eq. 5.3 as a forward model. The Euclidean norm is employed to compute the various terms of the objective function, as described by:

$$E(t) = E_{\widehat{T}} + E_{\hat{g}'} + E_{\hat{g}''} + E_{C_{1,t}} \tag{5.7}$$

where:

$$E_{\widehat{T}} = W_1 \cdot \left\| \widehat{T}(t_i) - T_{exp}(t_i) \right\|_2 \tag{5.8}$$

$$E_{\hat{g}'} = W_2 \cdot \left\| \hat{g}'_s(t_i) \right\|_2 \tag{5.9}$$

$$E_{\hat{g}''} = W_3 \cdot \left\| \hat{g}''_s(t_i) \right\|_2 \tag{5.10}$$

$$E_{C_{1,t}} = \sum_{j=1}^{p} \sum_{i=1}^{n_i - j} \left\| \min\left(0, \hat{g}_s(t_{i+j}) - \hat{g}_s(t_i)\right) \right\|_2 \tag{5.11}$$

where $\widehat{T}$ are the convolved temperature variations obtained through the non-stationary convolution using the iterated $\hat{g}_s\left(t_i\right)$. Variables $\hat{g}'$ and $\hat{g}''$ are respectively the s_k first and second

finite difference derivatives STgFs, and are used as regularization terms to help each transfer function being smooth. Weights W_i are scalar factors that control which terms of the objective function has more influence on E and will be discussed in the section *Weights approximation*. Eq. 5.11 is a soft constraint that penalizes any negative value within each $\hat{g}'_s(t_i)$. The second summation in Eq. 5.11 passes the signal on different window lengths p to penalize severely larger negative derivatives.

Linear inequality constraints on the nodes $\hat{g}_s(\tau_s(j))$ are also added to the optimization, similarly to Dion et al. (2022a) [205], following the equations:

$$0 < \hat{g}(\tau_j) < \hat{g}(\tau_{j+1}) \; \forall \; j \in [1, n-1] \qquad (C_{1,\tau})$$

$$0 < \hat{g}'(\tau_{j+1}) < \hat{g}'(\tau_j) \; \forall \; j \in [z, n-1] \qquad (C_2)$$

Eq. $C_{1,\tau}$ computes an analogous constraint to Eq. 5.11, i.e., it penalizes any negative values of $\hat{g}_s(\tau_s(j))$. Eq. C_2 penalizes positive second derivative after the point z, identifying around 3 hours of test. This time is used to ensure a downward slope of a STgF function derivative. Note that the constraint C_2 is not added in the objective function, as is constraint C_1 in Eq. 5.11, because the values of the second derivative are small enough that they are too close to the machine precision and could result in erroneous constraint value. Figure 5.2 shows a numerically generated STgF first derivative to visualize how constraints $C_{1,\tau,t}$ and C_2 are applied.

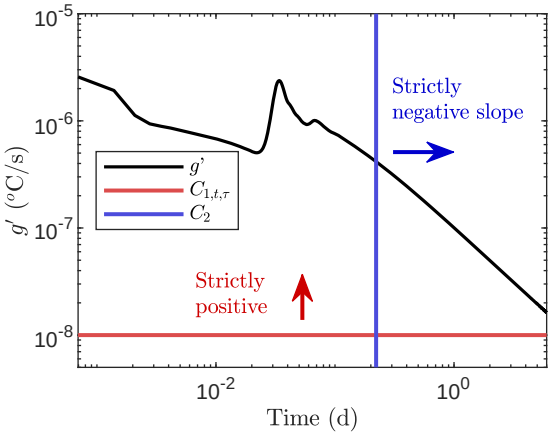

Figure 5.2 Visualization of the constraints $C_{1,\tau,t}$ and C_2 on a numerically generated STgF first derivative.

It is worth noting that the objective function and the optimization constraints differ from the ones of Dion et al. (2022a) [205]. The main differences are how the constraints are applied within the optimization. The constraint C_1 was previously only imposed on the optimization

parameters $\hat{g}_s\left(\tau_s(j)\right)$ as a *hard* constraint ($C_{1,\tau}$ in Eq. 5.6). Here, it is also passed as a *soft* constraint in the objective function ($C_{1,t}$ in Eq. 5.7). The constraint C_2 also differs from Dion et al. (2022a) [205], since only the negative slope of the first derivative is employed, as opposed to around an inflection point.

Weights approximation

In Eqs. 5.8, 5.9 and 5.10, weights W_i are set so that each term of the objective function (Eq. 5.7) respects a certain percentage of the global value of E. Usually, trial and error is used until the desired weights or a general appreciation of the converged solution are found. However, due to the complexity of the inversion problem (i.e., large number of parameters $\hat{g}_s\left(\tau_s(j)\right)$, each different deconvolution problem requires a specific set of weights W_i. It can then become impractical to use trial and errors for each case. Instead, a simple methodology to adjust the weights W_i is added after obtaining $\hat{g}_{0,s}$. First, the convolved temperature profile is obtained with $\widehat{T}_0(t_i) = \left(f * \hat{g}_{0,s}\right)(t, s)$. Second, Eq. 5.7 is computed, and the initial proportion of each term is $P_0 = E_i/E$. By manually setting the desired percentage P_{fit} of each term in Eq. 5.7, which are of 70 %, 15 % and 15 % for $E_{1\rightarrow 3}$ in this study, the corrected weights W_i are obtained by a rule of three:

$$W_{cor,i} = \frac{P_{fit}}{P_0} \tag{5.12}$$

Note that these corrected weights correspond to the desired percentage using the initial guess $\hat{g}_{0,s}$ and not the optimized $\hat{g}_s$. Still, results from various test cases have shown that the desired proportion of each term in Eq. 5.7 is generally respected.

Finally, the steps of the multi-deconvolution methodology are visualized in Figure 5.3, where the left graph shows the result of the stationary deconvolution for the first operating condition of the TRT ($\hat{g}_0$). The middle figure shows the first guess of the set by the multiplication with the $\hat{a}_s$ ($\hat{g}_{0,s}$). The right figure shows the nodes $\hat{g}_s\left(\tau_s(j)\right)$ on which the optimization iterates to enhance the fit to the experimental data. Note that if the function $\hat{g}_1$ would be called later during the TRT, nodes would be added after the result of the stationary deconvolution, hence the red dot in the blue line of the legend of Figure 5.3(right). All steps are also summarized in Figure 5.4.

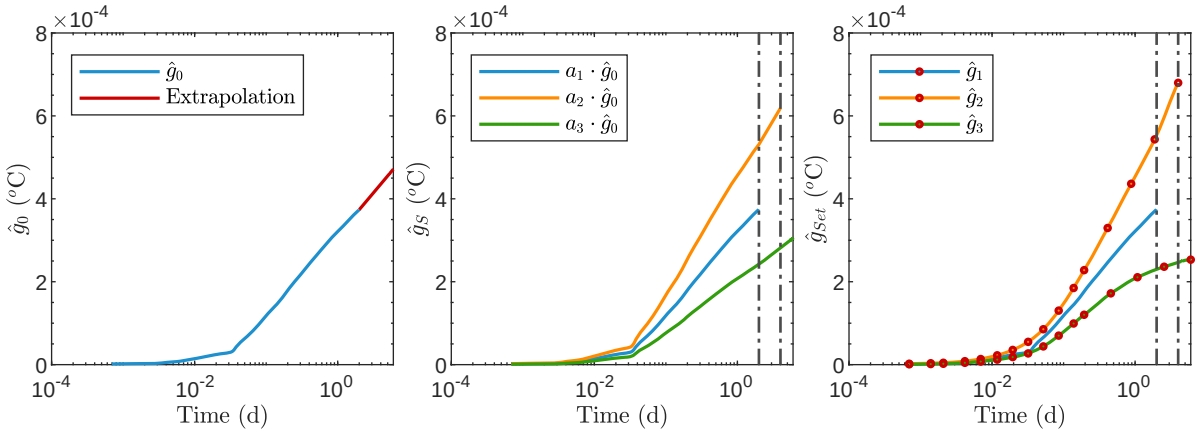

Figure 5.3 Visualization of the methodology: (left) stationary deconvolution result with extrapolation, (middle) initial guess obtained by multiplication with a fitted scalar a_s and (right) completed optimization on $\hat{g}_s\left(\tau_s(j)\right)$.

5.4 Results

To assess the precision and accuracy of the proposed multi-deconvolution algorithm, numerical and field TRT data are used. Numerical scenarios allow to compare both the TRT output temperatures as well as the STgF sets obtained with the forward numerical model and the proposed deconvolution algorithm. On the other hand, field scenarios allow to validate the accuracy of the algorithm using field datasets. Note that all the scenarios are performed on a SCW, a type of GHE that integrates important contributors to non-stationarity in their operation, such as the time variation of pumping and bleed flow rate. This type of GHE is an uncased borehole in which the circulating fluid is the groundwater. A TRT performed on a SCW hands results that are analogous to those obtained from a conventional TRT on a closed-loop GHE. Some differences are that the fluid residence time is much larger, and thus the heating power must be higher to obtain an adequate signal-to-noise ratio. In some occurrences, the integration of bleed in the test sequences can be made to provide additional information about the ground's thermal and hydraulic responses. The deconvolution algorithm can, however, be applied to any type of GHE, if the processes (i.e., operating conditions) that affect stationarity can be recorded.

5.4.1 Numerical TRTs

The numerical TRTs on a SCW are performed using a validated axisymmetric finite element model proposed by Beaudry et al. (2019) [1]. This model couples groundwater flow to heat transfer and uses a sequential resolution, which can consider dynamic operating conditions.

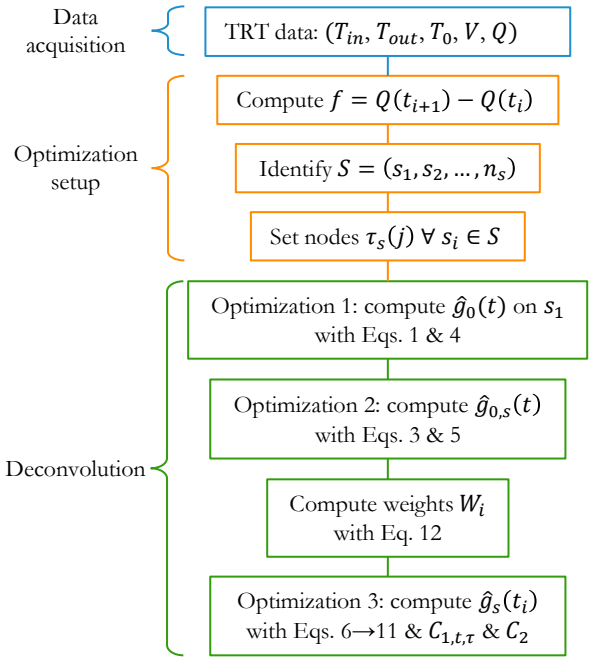

Figure 5.4 Non-stationary deconvolution steps.

It has been demonstrated that SCWs display a high efficiency [15], being strongly correlated to dynamic operating parameters, especially the bleed flow rate [102].

To test the multi-deconvolution algorithm, the numerical model was used to generate multiple synthetic TRTs, in which the main circulating flow rate $V(t)$ was maintained at a constant 100 L/min. The operating conditions variations then occur by changing the bleed flow rate $\beta(t)$. This variation is employed in the following test cases as opposed to the circulating flow rate because it has the most impact on the thermal performance of the SCW [15]. This choice has been done to highlight the effectiveness of the deconvolution algorithm to consider large variations. The undisturbed ground temperature over the whole simulation domain is set at 11 °C and a generated heating power profile Q is applied to the numerical model. Natural variations, which are auto-correlated changes happening during the TRT (e.g., electricity grid variation), are added to the heating power profile and are computed using an exponential covariance function [196]. With this modified heating power profile, the inlet and outlet temperature variations are obtained from the numerical model. In field test cases, measurement noise is also present in the data, mainly due to the data acquisition and monitoring equipment. Hence, white noise is also added to the numerical heating power profile and the simulated temperatures when using the multi-deconvolution algorithm. Most of this noise is filtered through a moving average with a window of 10 samples [205]. The use

of this simple filter enhances the signal-to-noise ratio of the deconvolved signals, enhancing the results without compromising the inputs. Table 5.1 shows the main parameters used in the numerical model, which is also detailed in Beaudry et al. (2019) [1].

Table 5.1 Borehole geometry and thermal properties of the numerical and field TRTs.

Parameters	Symbol	Unit	Value
Soil thermal conductivity	k_{gr}	W/(m·K)	2.76
Soil heat capacity	C_{gr}	MJ/(m^3·K)	2.00
Borehole radius	r_b	m	0.083
Borehole length	H	m	215.0

Two numerical TRTs of 6 days with 3 bleed rate changes ($S = (1, 2, 3)$) occurring every 2 days are first presented as verification cases for the proposed deconvolution algorithm. Each of the 3 segments involves 24 hours of heating and 24 hours of restitution. The main difference between the two tests is the sequence of bleed rates, which are set successively at 0, 10 and 20 L/min for the first TRT and at 10, 0 and 20 L/min for the second TRT.

The results of the multi-deconvolution algorithm are presented for both numerical TRTs in Figure 5.5. In this figure, the STgF and their first derivatives are superposed to their numerical counterpart and, for each TRT, the STgFs are linked to a bleed flow rate change. The indices of the g_s are the test number and the corresponding flow rate in increasing order. Hence, $\hat{g}_{1,1}$ is for the first test and 0 L/min of bleed flow rate, while $\hat{g}_{2,3}$ is for the second test and 20 L/min of bleed flow rate.

For both TRTs, the functions are mostly well fitted, with larger variations towards the end of the signals, which will be discussed in Section *Algorithm performance and precision*. The fit between convolved and experimental temperatures in Figure 5.5 results in a RMSE of 0.05 °C for both scenarios. It is worth noting that this corresponds to the expected precision of the non-stationary convolution reported by Beaudry et al. (2022) [102]. One can see that the STgFs in Figure 5.5 are not all the same length. This is due to the activation time of each function and will be discussed in Section *Validity period for the deconvolved STgF set*.

5.4.2 Field TRTs

Two validation field TRTs are also presented to assess the precision of the multi-deconvolution algorithm. The tests were performed on an experimental SCW described by Beaudry et al. (2019) [1]. Note that some descriptive parameters about the study site are in Table 5.1. Similarly to the numerical TRTs, the field tests were performed over 6 days, with 3 successive

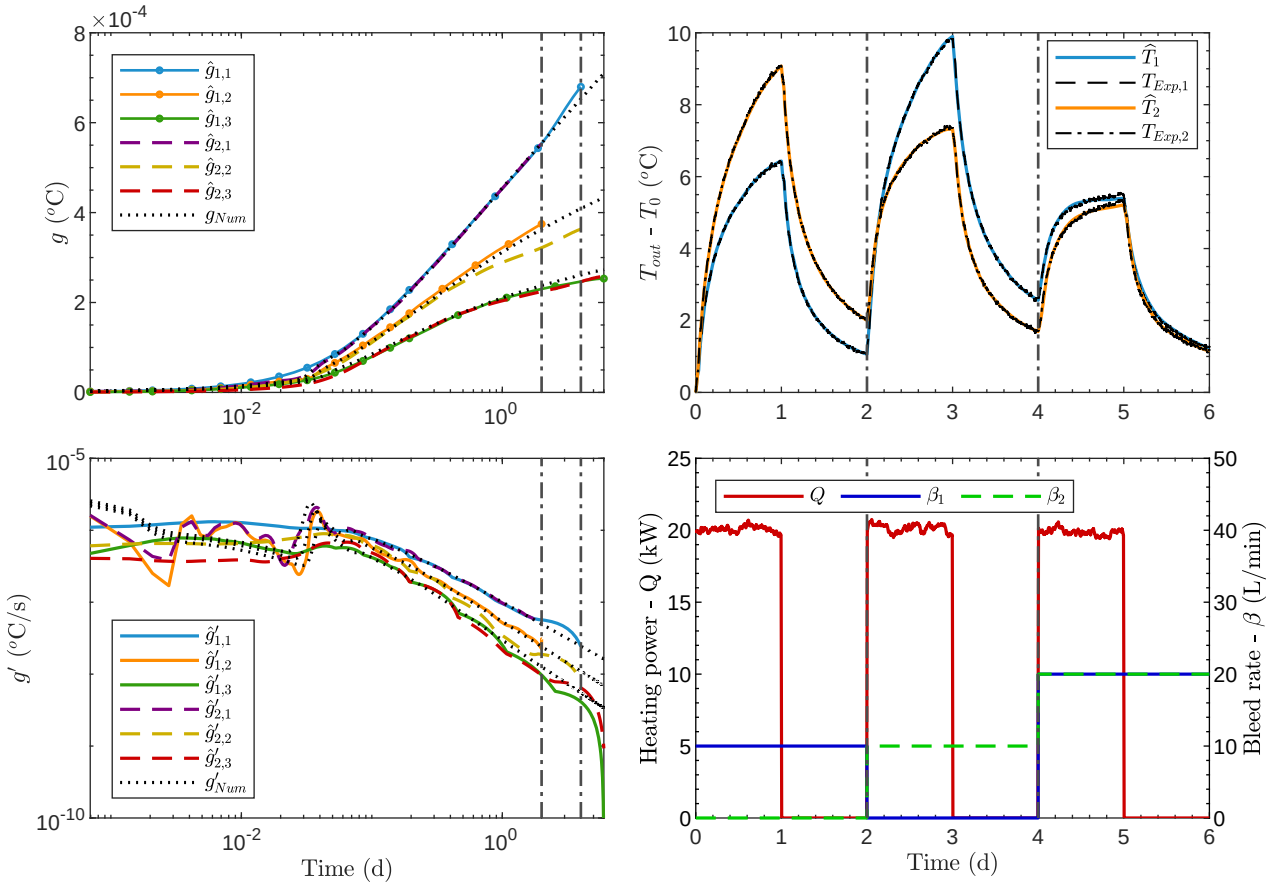

Figure 5.5 Results of the non-stationary deconvolution on two numerical TRTs with 3 operating conditions each ($S = (1, 2, 3)$). (top-left) STgF sets, (top-right) GHE outlet fluid temperature variation, (bottom-left) STgFs' first derivatives and (bottom-right) Heating power and bleed flow rates (operating conditions). For both TRTs, the circulating flow rate is of 100 L/min. The indices of $\hat{g}_s$ are the test number and the corresponding flow rate in increasing order.

different bleed rates ($S = (1, 2, 3)$). The circulation flow rate (2 % measurement error) was maintained constant at around 105±1.38 L/min and 101±1.40 L/min for TRT 1 and 2, respectively. The successive bleed ratios were of 4±0.11, 0 and 8±0.19 L/min, and 4±0.17, 6±0.40 and 8±0.39 L/min both TRTs respectively. Note that these values are lower than for the numerical test cases and were set that way to consider injection flow rate limitations at the injection well caused by a low average hydraulic conductivity. The heating power profile is computed with the specific heat formula ($Q = Vc_f\Delta T$, with $\Delta T = T_{in} - T_{out}$), using the mean flow rate and the inlet and outlet fluid temperature of the TRT. For both TRTs, a 12-hour recirculation period prior to the beginning of the heating occurred. The temperature sensors (Greystone TE200) have an accuracy of ±0.2 °C, and the resulting uncertainty on the heating power profile (errors from V and $2\Delta T$) is of ±770 W.

Figure 5.6 shows the results of the multi-deconvolution algorithm, as well as the operating conditions (i.e., measured heating power and bleed flow rates). The GHE outlet fluid temperatures signals are well reconstructed, with RMSEs of 0.07 °C and 0.05 °C, which is below the temperature recording accuracy. This may indicate a slight overfit during deconvolution, but since the heating power is computed with the temperature values, this precision is deemed adequate. Since the bleed flow rates are similar for all the field test cases, the STgFs show similar evolution in their beginning, where heat is mainly exchanged inside the GHE. Larger variations occur after 3 hours of test, where higher bleed rates (e.g., $\hat{g}_{1,3}$ and $\hat{g}_{2,3}$) correspond to lower STgF curve, showing the positive effect of bleed operations on heat transfer.

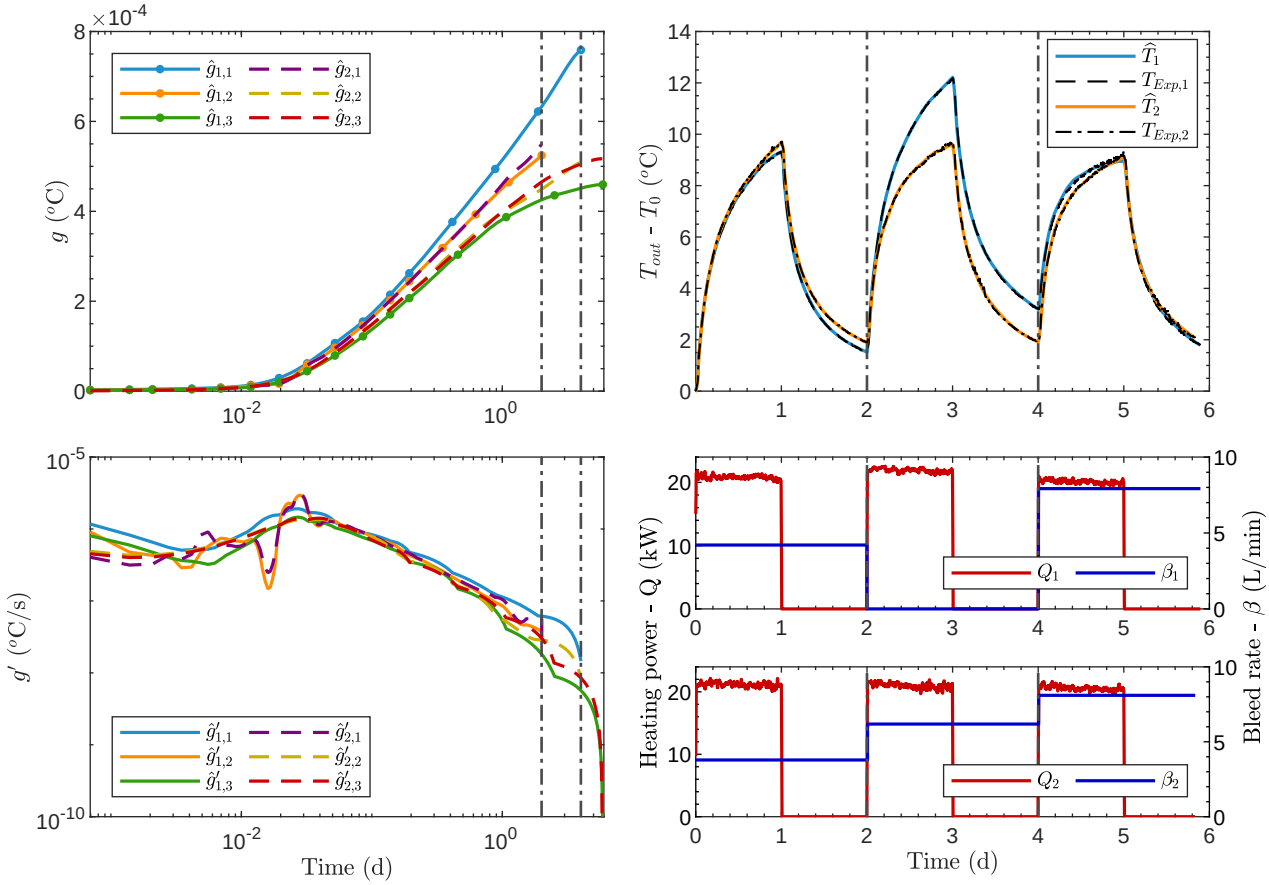

Figure 5.6 Results of the non-stationary deconvolution on two field TRTs with 3 operating conditions each ($S = (1, 2, 3)$). (top-left) STgF sets, (top-right) GHE outlet fluid temperature variation, (bottom-left) STgFs' first derivatives and (bottom-right) Heating power and bleed flow rates (operating conditions). The circulating flow rates are of 105±1.38 L/min and 101±1.40 L/min respectively. The indices of $\hat{g}_s$ are the test number and the corresponding flow rate in increasing order.

5.5 Discussion

5.5.1 Algorithm performance and precision

The results of Figs. 5.5 and 5.6 show general good accordance between reference (either numerical or field) and deconvolved TRT temperatures. However, some STgFs show larger fluctuations compared to the numerical ones.

The possible cause of these discrepancies is the initial position of an operating condition s_i. For example, on Figure 5.5 (numerical cases), the function $\hat{g}_{1,2}$, which was used to evaluate the signal $\widehat{T}_1$ when the bleed flow rate is 10 L/min (i.e., between 0 and 2 days), shows a behavior similar to that of its reference numerical counterpart. On the same figure, the function $\hat{g}_{2,2}$, which is the one used to obtain $\widehat{T}_2$ when the bleed flow is of 10 L/min (i.e., between 2 and 4 days), is noticeably less accurate. One explanation is that $\hat{g}_{1,2}$ was optimized using a stationary deconvolution, since it represents the first operating conditions of the TRT. Function $\hat{g}_{2,2}$ was optimized with the non-stationary optimization, which would be less accurate due to some limitation in the non-stationary convolution (see below). Also, larger bleed rates (from days 4 to 6 across all cases) seems to create larger variations on the transfer functions and temperature reconstruction (see $\widehat{T}_2$ in Figure 5.5(Top-right)).

Another source of error is the approximation of the circulating and bleed flow (V and β) rates by step signals, where each step is the average of the measured flow rates. This technique is used to limit the number of deconvolved STgF, since they depend on stationarity at a specific time. Indeed, if the time-varying signal was used, a STgF could be deconvolved at almost every combination of circulating and bleed flow rates. The impact of such a simplification is hard to predict on the precision of the deconvolution technique.

One way to verify the results of the deconvolution algorithm is to take a set of STgF obtained from one test, and then use it to reproduce the results of another, providing that the operating conditions sets are identical in both cases. In this case, this strategy was applied to the numerical TRTs, which share identical operating parameters but where the bleed flow rates are presented in a different order.

Figure 5.7 shows the non-stationary convolution that was computed using the deconvolved STgF set from the second numerical TRT and the succession of operating conditions of the first numerical TRT (i.e., heating power, circulating flow and bleed rates). In this figure, the red sections on the STgF are extrapolations to have the right function length for the non-stationary convolution (Eq. 5.3). The extrapolation is done with an exponential integral, as in Section *First STgF set estimation ($\hat{g}_{0,s}$)*. The RMSE between the convolved and experimental temperatures is of 0.14 °C, which is still below the temperature sensor accuracy.

However, the largest discrepancy between the 2 curves occurs at the beginning of day 5 and is of -0.45 °C. The difference between the original convolution and this one stems mainly from the deconvolution precision at late time on each STgF. Still, the STgF of a TRT can reconstruct the values of another TRT with acceptable accuracy, providing that they are on the same GHE and uses the same set of operating conditions.

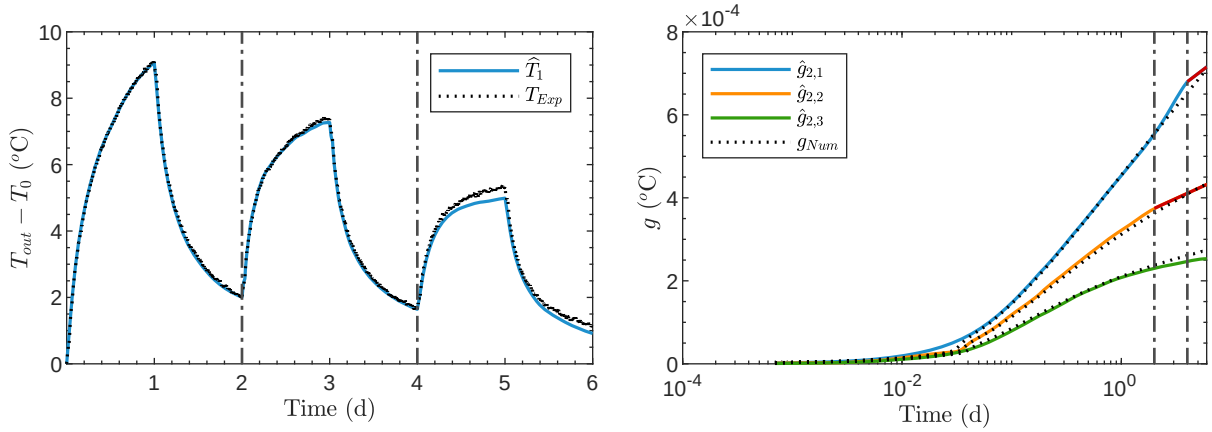

Figure 5.7 Convolution with $\hat{g}_s$ from the *second* numerical TRT to obtain the temperature of the *first* numerical TRT. Red sections on the right are extrapolated sections based on an infinite line source model.

Another source of error comes from the forward model itself (the non-stationary convolution of Beaudry et al. (2021) [143]), which the authors have identified to provide larger RMSE values in the time steps following a change in the non-stationary operating conditions. Another fact worth of mentioning is that the present work neglects consideration of the vertical temperature profile variations in T_0, which has been shown to have effects on surface temperature reconstruction [1, 102].

Lastly, numerous tests indicated that measurements noise does not impact the deconvolution results significantly. However, especially for the non-stationary cases, knowing accurately the moment a shift occurs (e.g., heating to recovery, changes between two flow rates) is important to recover STgFs precisely. Hence, TRTs that include large errors could still be interpreted, as long as the state transitions are adequately recorded. For that, signal recording at every minute and high accuracy from calibration is necessary.

5.5.2 Validity period for the devonvolved STgF set

In the non-stationary convolution (Eq. 5.3), each STgF is activated in the time period when their corresponding operating conditions occur. Then, the last occurrence of a set of operating conditions corresponds to the last time step to evaluate the associated STgF.

Hence, in a non-stationary operation, each STgF is not defined on the entire deconvolved signal (i.e., TRT duration). To demonstrate the usable length of each transfer function of the set, a simple experiment was performed.

The test performs two loops, in which the first one passes each numerically generated STgF $g_{Num,1\to3}$ showcased in Figure 5.5(top-left). The second loop manually changes a single value over the length of each STgF ($\tilde{g}$). Then, the non-stationary convolution is computed using $\tilde{g}$. At each iteration, the RMSE computed with the newly convolved temperature is compared to the RMSE with the original g_{Num} following the equation:

$$\text{rmse}\left(\widehat{T}(\tilde{g}) - T_{exp}\right) \neq \text{rmse}\left(\widehat{T}(g_{Num}) - T_{exp}\right) \tag{5.13}$$

Figure 5.8 shows the results of this test, in which the active length of each STgF is shown when each RMSE variation becomes zero. It is observed that g_1 does not affect the convolution after 2 days, which thus represents its activation time. The second STgF g_2 is active from days 2 to 4, but it impacts the convolution on the first 4 days. The third STgF g_3 is active from days 4 to 6, but this one impacts the convolution over the whole simulation period. From this demonstration, it is confirmed that each STgF is active up to the end of their last activation time (i.e., the end of the corresponding operating conditions).

Note that if the TRT duration was of 8 days and g_1 was called again from days 6 to 8 (not shown), then it would affect the convolution from the beginning to the end of day 8. In that case, nodes to optimize should be added from day 2 (i.e., end of stationary conditions solved in Section *First STgF set estimation ($\hat{g}_{0,s}$)*) to the end of the TRT, on the 8th day. Visually, the nodes would appear in an extension of the blue curve in Figure 5.3(right).

5.5.3 Objective function optimum analysis

Important factors to any optimization problem are the convergence rate and form of the objective function. Convergence analysis is performed to examine the shape of the optimum described by the objective function. Here, to examine the parameter space of the multi-deconvolution algorithm, changes to the numerically generated STgFs g_{Num} are made to visualize the impact on the objective function value. The method employed is to multiply two points (x_1, x_2), located at 1.5 and 3 days on g_1 respectively, by factors (p_1, p_2) ranging from 0.8 to 1.2. Then, an interpolation is performed between the two modified points whilst ensuring continuity of the new $\tilde{g}_1$. With the modified set $\tilde{g}_s$, the objective function of Eq. 5.7 is computed for different values of the points (p_1, p_2).

A map of the objective function value can be visualized in Figure 5.9 (left), as well as examples

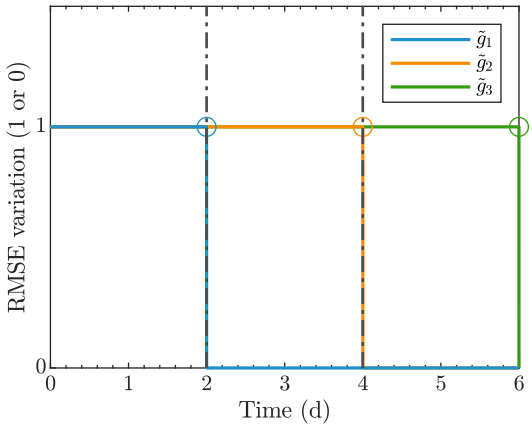

Figure 5.8 Impact on the RMSE of changing a single point on each STgF in the non-stationary convolution. Each function's active period ends when the RMSE with modification on the STgFs becomes equal to the RMSE without modification (shown by the circles).

of $\tilde{g}_2$ (right). The map is an interpolation of a 20x20 RMSEs grid between the convolved and experimental temperature. It shows smooth changes through space and is differentiable. Note that similar optimums are found by using any function in g_s and various values of x_1 and x_2.

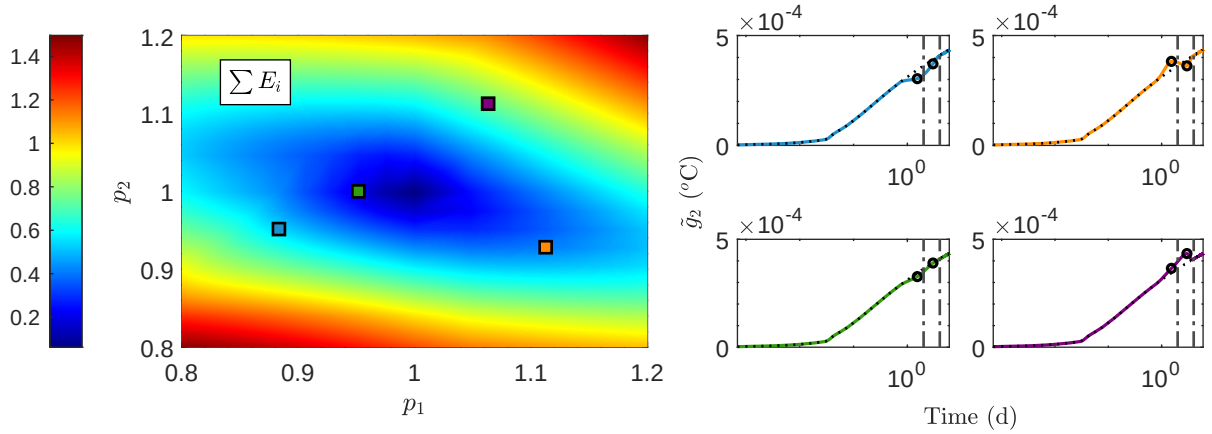

Figure 5.9 (Left) RMSE map of the multi-objective function (Eq. 5.7) computed by varying 2 points on a STgF. (Right) examples of STgF variations $\tilde{g}_2$ used to build the map. The points $x_1 \cdot p_1$ and $x_2 \cdot p_2$ (circles on the right graphs) are located on days 1.5 and 3 respectively.

Note that the RMSE map is computed with only $E_{1\to3}$, since $E_{C_{1,t}}$ is a constraint. It is omitted to visualize the optimum without its impact. Also, this map shows the impact of varying 2 nodes per function (2D). However, the number of dimensions in Eq. 5.6 is $s_k \cdot n_j = 72$, the total number of parameters. A smooth surface in 2D does not guarantee that the hypersurface is smooth in higher dimensions.

5.5.4 Computing consideration

The presented forward and inverse problem were implemented in the computing environment MATLAB (2020) [209]. The inversion algorithm is performed using the nonlinear solver `fmincon` from the optimization toolbox. Using a quasi-Newton algorithm with a L-BFGS Hessian update method [195], which is a gradient-based method, the direct model is computed at least $s_k \cdot n_j + 1$ times per iteration.

For the deconvolution algorithm, the parameters are composed of the nodes of each transfer functions $\hat{g}_s\left(\tau_s(j)\right)$ minus the nodes for the first operating condition of the TRT. Hence, for the presented cases with 24 nodes per function, the total number of parameters is 54, since the first one is computed with the stationary deconvolution. Figure 5.10 shows convergence metrics on the performance of the multi-deconvolution for the first numerical test case. A solution is found in around 100 iterations with most of the iterations computing between 55 and 64 times the direct problem.

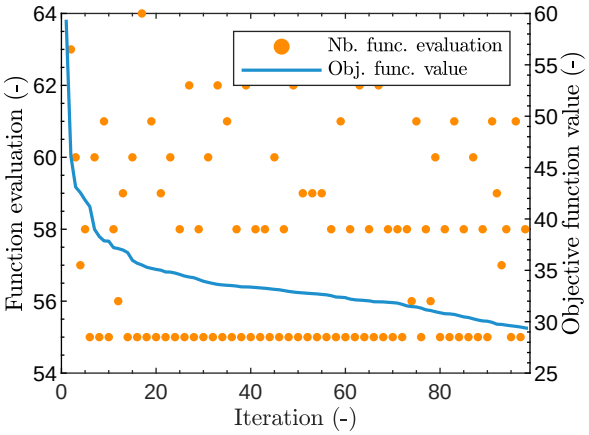

Figure 5.10 Number of function evaluations and objective function value per iteration for the numerical test 1.

In the non-stationary convolution (forward problem), if the raw heating power profile is used, each iteration is solved in about 4 to 5 seconds. In such raw data, the heating power changes at each time step, due either to natural variations or noise. Knowing that the non-stationary convolution computation speed is closely related to the number of variations in the signals (heating power, circulating flow and bleed rate), one way to speedup the computing time is by approximating the heating power profile by a step function. Figure 5.11 shows this approximation, in which each step is an average of its segment. The step changes occur when there is an abrupt change in the signal's average. With this process, the heating power profile can be reduced to around 300 variations, which speeds up the non-stationary convolution

computation from 5 seconds to 0.08 seconds. With this methodology, the deconvolution converges in less than 5 minutes for all the presented test cases.

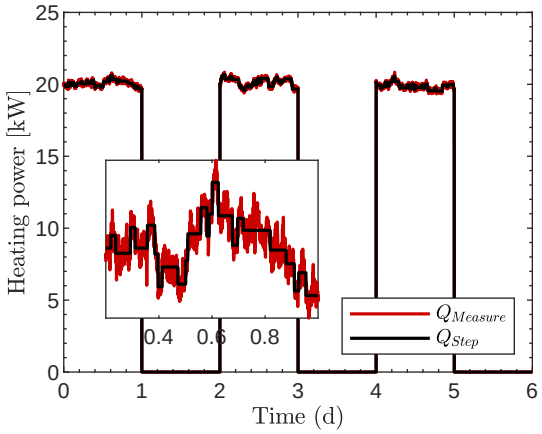

Figure 5.11 Heating power profile measurement and approximation by a step function of the numerical TRT 1.

5.6 Conclusion

Different types of GHEs feature enhanced performance if time-variant operating conditions sequences are defined according to the heating or cooling demand of a building. This strategy, however, leads to a non-stationary behavior of the thermal exchange in the GHE which can be challenging to represent in a simulation model. It has recently been demonstrated that such non-stationarity is efficiently considered by using a non-stationary convolution simulation algorithm that combines multiple transfer functions to reproduce the temperature evolution of a GHE.

This article presents a novel application of a deconvolution algorithm to non-stationary TRTs, with the aim to recover a set of experimental transfer functions representing various operating conditions occurring on a GHE. The methodology is validated on numerical and field test cases, verifying both the set of STgFs and the performance of the algorithm to reproduce experimental temperatures with RMSE of less than 0.07 °C across various test cases. The optimization-based deconvolution algorithm uses new constraints and regularization terms on the iterated STgFs. Convergence occurred in less than 5 minutes for 6 days TRTs with data sampled every minute.

This algorithm has the potential to help simulate GHEs under various operating conditions, since it has shown its ability to evaluate accurate STgFs using only experimental results and without any simulation model. The proposed algorithm could thus contribute positively to

accelerate ground source heat-pump systems design. Other applications could aim to analyze changes in transfer functions during the operation of GSHP systems. Such an analysis could highlight differences between the thermal resistances of boreholes, the ground heterogeneity, or changes in the groundwater flow regime.

5.7 Acknowledgments

The authors wish to acknowledge the support and funding provided by the Natural Sciences and Engineering Research Council of Canada (grant number RDCPJ 530945), the Trottier Energy Institute, Hydro-Québec, FTE drilling and Richelieu Hydrogeology.

5.8 Nomenclature

Acronyms

GHE	Ground heat exchanger
GSHP	Ground source heat pump
LTI	Linear time invariant
SCW	Standing column well
STgF	Short-term g-function
TRT	Thermal response test

Subcripts

0	Initial
exp	Experimental
fit	Fitted
i, j, k	Counter
Num	Numerical
out	Borehole outlet
s	Current segment (operating conditions)

Variables

a, $\hat{a}$	Vector of scalar factors (-)
β	Bleed rate ($m^3 \cdot s^{-1}$ or $L^3 \cdot min^{-1}$)
$C_{1,t,\tau}$	Strictly growing function constraint (-)

C_2	Negative first derivative slope constraint on τ_j (-)
E	Objective function value (-)
f	Incremental temperature function (W/W)
g, $\hat{g}$	Borehole outlet transfer function (°C)
λ	Non-stat. convolution correction function (°C)
n	Number of value (-)
P	Objective function terms' proportion (-)
Q	Heating power (W)
s	System segment defined by operating conditions (-)
t	Time vector (d)
τ	Node position on each STgF (d)
T, $\widehat{T}$	Temperature (°C)
V	Flow rate ($m^3 \cdot s^{-1}$ or $L^3 \cdot min^{-1}$)
W	Weights applied in the objective function (-)
x_1, x_2	Parameters of the exponential integral (-)

CHAPITRE 6 ARTICLE 3 - APPLICATION OF DECONVOLUTION TO INTERPRETATION OF DISTRIBUTED THERMAL RESPONSE TEST (DTRT) AND TO DETERMINATION OF THERMAL CONDUCTIVITY PROFILES

Gabriel Dion[1*], Philippe Pasquier[1], Denis Marcotte[1],

Applied Thermal Engineering, approved for publication on September 24th, 2023

[1] Department of Civil, Geological and Mining Engineering, Polytechnique Montréal, P.O. Box 6079 Station Centre-Ville, Montréal, Canada H3C 3A7

[*] Corresponding author email: gabriel.dion@polymtl.ca

Keywords: Distributed thermal response test, Deconvolution, Ground heat exchanger, First-order approximation, Thermal conductivity profile

6.1 Abstract

Distributed thermal response tests offer the possibility to retrieve both the effective and depth-dependent thermal conductivity profile of a ground heat exchanger. The purposes of this paper are to apply a novel deconvolution method on distributed thermal response test data, which has not been performed before, and to showcase the advantages of using short-term transfer function to calculate thermal conductivity values at each geological layer from a conventional interpretation method, which is also a novelty. To achieve that, the ground is separated in layers from which a set of transfer functions and a thermal conductivity profiles are estimated. Results show that at the ground heat exchanger outlet, the effective thermal conductivity is estimated with comparable accuracy from temperature signals and transfer functions, but for the depth-dependent thermal conductivity profile, the maximum error is reduced from 51.45 % to 3.83 % for a low thermal conductivity layer using transfer functions. A comparison between the analysis with temperature signals or transfer functions also shows the robustness of the latter to interpret tests with low flow rates. This methodology has the potential to aid decision-making when designing a ground heat exchanger field by providing a clearer representation of the heat exchange capacity of the ground at a site under study.

6.2 Introduction

A ground source heat pump (GSHP) system links a building, a geothermal heat pump and a ground heat exchanger (GHE) to heat or cool a building efficiently. In these systems, the ground is used as a stable thermal reservoir, and can be exploited by different types of GHEs. A closed-loop GHE circulates a fluid inside a U-loop, from which the heat exchange process between the fluid and the surrounding ground is conduction. An open-loop system uses the groundwater as the circulating fluid, which adds advection to the heat exchange process. To assess the local ground thermal parameters, which are critical factors when designing a GSHP system [117], thermal response tests (TRT) are usually employed. In this test, a heated (or cooled) fluid circulates in a GHE and dissipates (or accumulates) heat [26,105,210]. In a TRT, three distinct phases can be observed. First, a fluid recirculation is performed to homogenize the temperature within the borehole. Second, the fluid is heated with a water heater before being injected into the GHE. The thermal exchange within the GHE is then monitored through the fluid temperature between the inlet and outlet. Third, a recovery phase can follow the heating phase, during which fluid circulation continues while the water heater is deactivated. From this *in-situ* test, the ground effective thermal conductivity and equivalent borehole thermal resistance are evaluated [183], along with other parameters depending on the interpretation method used [105]. The aim is to estimate the ground thermal properties as accurately as possible, so as to prevent over-sizing while covering the thermal load of the associated building, hence minimizing the investment cost.

Investigating underground heterogeneities that can affect the heat transfer rate is a key element to correctly design a GSHP system [62, 211]. By using distributed temperature sensing (DTS) [60] inside a traditional U-loop GHE, or by placing thermal probes along the GHE, vertical temperature profiles are recorded in both the inlet and outlet pipes. With this setup a distributed thermal response test (DTRT) can be performed, which differs from an enhanced thermal response test (ETRT) that uses a heated fiber-optic cable [62]. When interpreting DTRT, layers with higher effective thermal conductivity are sought, since they usually relate to higher groundwater flow rate [212]. These layers can be targeted in subsequent boreholes to minimize drilling cost [213].

To obtain the effective or depth-distributed ground thermal parameters, interpretation methods are used on data from TRT or DTRT, respectively. For effective thermal parameter estimation, the most common methods are: (i)- a curve fitting between an analytical model and the GHE mean outlet temperature during a TRT (e.g., Mogensen (1983) [24], Choi et Ooka (2015) [214]), (ii)- an optimization problem, solving multiple variables with a more complex forward model (e.g., Li et Lai (2012a) [28], Pasquier (2015) [215], Beier (2019) [51]) or (iii)-

calibrating a numerical model (e.g., Brunetti et al. (2017) [90], Zarrella et al. (2018) [203], Robert et al. (2022) [91], Zhou et al. (2022) [216]).

Interpretation methods applied to a DTRT are commonly performed by a first-order approximation (FOA) using the infinite line source (ILS) model at various depths (e.g., [60, 64, 211, 217–219]) and are thoroughly reviewed in Wilke et al. (2020) [62]. The result is mainly a thermal conductivity vertical profile, calculated from the heat dispersed radially by the inlet and outlet pipes (in a U-loop configuration) between selected depths. Among recent contributions to DTRT interpretation, Beier et al. (2021) [220] studied the estimation of the ground thermal conductivity through a layer-factor model. Beier et al. (2022) [221] proposed an analytical model to simulate DTRT with geothermal gradient linked with a parameter estimation inversion algorithm and analyzed the effect of parameters identification on each layer. Ma et al. (2022) [222] assessed the impact of different heat load profiles on the thermal conductivity estimation, finding that the test duration has the largest influence. Nian et al. (2022) [223] obtained the thermal conductivity profile within 2 hours of a DTRT using a 2D analytical model coupled with a genetic algorithm. Aranzabal et al. (2020) [224] retrieved thermal conductivity profiles using Geoball and Geowire together with a numerical inversion algorithm to showcase alternative technology to the conventional DTS employing fiber-optic cables. Noteworthy other methodologies applied to the interpretation of ETRT are the use of moving infinite line source as a forward model to retrieve both the thermal conductivity and the Darcy velocity [225, 226] and the use of a multivariate linear regression to identify thermal conductivity for fine alternating layers [65].

To analyze the heat transfer in the GHE and the ground, forward models, albeit analytical or numerical, have disadvantages to characterize naturally complex underground heat transfer phenomenon. Analytical models often employ simplifying assumptions, and numerical models are long to calibrate and needs heavy computing [90]. On the other hand, approaches based on transfer functions (or g-functions) encompasses the thermal exchange capacity of the ground on time scales from minutes to years [39, 44, 147]. A transfer function define a GHE's response to a constant heating power of either 1 °C, 1 kW or 1 W/m between the inlet and outlet GHE temperature. For a specific site, transfer functions are used to simulate ground temperature under the historical heating load of the building on which a GSHP system is built. Time-varying heat loads are considered with the temporal superposition technique, either by load aggregation [120] or convolution [45, 123].

Practically, transfer functions used for simulation are obtained with analytical or numerical models, in which thermal parameters are retrieved from the TRT interpretation and the sizing parameters are varied to satisfy part of the building's heating or cooling load. Shorter transfer

functions are calculated by optimizing thermal parameters, so that simulated temperatures are fitted precisely to experimental temperatures from a TRT. To remove the use of any heat transfer models, transfer functions can be retrieved directly from the experimental data of a TRT by an inversion technique called a deconvolution [177, 205]. Such transfer functions could provide two uses, first to be added to longer g-function when simulating a GSHP system to account for short-term behavior of the GHE, and second, to provide a better temperature signal for thermal parameter interpretation with known methodology. In this regard, Beier (2020a) [177] used the ILS logarithmic derivative to recover the thermal conductivity from the transfer function of a sandbox and a field TRT, getting values with as much as 50 % *less* uncertainty. Dion et al. (2022b) [227] obtained thermal conductivity estimation from transfer functions deconvolved from experimental TRT with low variation and standard deviation between the ones from temperature signals.

Currently no work has shown how to obtain experimental depth-dependent transfer functions or their uses for TRT interpretation. A combination of both an algorithm to compute these functions through deconvolution and an analytical model solver for the thermal conductivity profile estimation could enhance layers identification for precise GHE sizing. Since the usual interpretation method is based on an analytical model with a constant heating power, then using transfer functions will be advantageous to obtain an accurate thermal conductivity, since it is one of their properties.

The goals of this paper are first, to define a deconvolution algorithm for numerical and field DTRT datasets with several geological layers to recover depth-dependent transfer functions. Second, demonstrate the benefits of using deconvolved transfer functions to obtain vertical thermal conductivity profile with common interpretation methods. This methodology will help to precisely identify ground layers' thermal properties, and subsequently help designing GHE.

6.3 Methodology

This section first presents the deconvolution algorithm applied at the GHE outlet to obtain an experimental transfer function. Then, the standard methodology based on the FOA of the ILS model is used on both the outlet temperature and the transfer function to acquire the average ground thermal conductivity. Finally, a methodology to compute the transfer function for each geological layer of a DTRT and to their corresponding thermal conductivity profile is described.

6.3.1 Deconvolution algorithm

Dion et al. (2022a) [205] proposed an inversion algorithm to retrieve a transfer function defined at the outlet of a GHE, from TRT experimental data. The obtained transfer function is as long as the TRT duration, which can be between 3 and 10 days long. These short-term g-function (STgF) represent the heat transfer occurring in the circulating fluid, the borehole and the surrounding ground of the GHE [51], as opposed to year-long ones who characterize the heat transfer in the ground and the possible interactions with adjacent GHE [99]. A deconvolution is the inverse problem of the known convolution equation [98], here defined at the GHE outlet as:

$$T_{out}(t) - T_0 = (f * g)(t) = \mathcal{F}^{-1}\left(\mathcal{F}(f) \cdot \mathcal{F}(g)\right) \tag{6.1}$$

where T_{out} is the GHE outlet temperature, t is the time series of the TRT, T_0 is the temperature at the end of the recirculation phase prior to the heating phase, g is the GHE outlet STgF and $\mathcal{F}$ and $\mathcal{F}^{-1}$ are respectively the Fourier transform and its inverse. The latter are used to convert the signals to frequency, allowing to perform a fast multiplication in the spectral domain instead of a convolution product ($*$) [45]. Function f is the incremental heat load function (or excitation function) written as:

$$f(t) = \frac{Q(t_i) - Q(t_{i-1})}{H} = q(t_i) - q(t_{i-1}) \tag{6.2}$$

where $t \equiv t_i$, Q is the heating power profile, H is the borehole length and q is the heating power profile per unit of GHE length and is equal to Q/H. If the TRT rig does not have a wattmeter, then the specific heat formula can be used to compute Q where $\Delta T = T_{in} - T_{out}$. Since the units of f are W/m, then the associated STgF will be defined for an impulse of 1 W/m. This choice is made to simplify the use of the ILS model in the next section, but the STgF could be computed with either an impulse of 1 W, 1 °C or any other constant value.

The deconvolution algorithm optimizes the position of various nodes spaced logarithmically on the transfer function, noted $\hat{g}$, so that convolved and experimental temperature signals are well adjusted, while ensuring a realistic shape of the transfer function using constraints. The concentration of nodes at the beginning of the STgF aims for an accurate early time reconstruction since it is the period with the most transient temperature evolution. With this methodology, no analytical or numerical model is used to estimate the STgF. The equations and particularities of the algorithm are presented in Appendix 6.11 and interested readers are referred to Dion et al. (2022a) [205] for more details.

6.3.2 Thermal conductivity estimation with FOA

One of the simplest and most common approaches to TRT interpretation is to fit the FOA of the ILS to the mean fluid temperature signal ($T_f = (T_{in} + T_{out})/2$) obtained from a TRT, knowing the heating power used during the heating phase [24,37]. Recent advances by Pasquier (2018) [108] extend this method to also retrieve the thermal conductivity from a TRT recovery phase, as well as the temperature derivative of both the heating and recovery phases. The interpretation of the recovery phase considers that the heat impulse is the inverse of the one during the heating phase. In this article, one of the goals is to show the gains of using transfer functions when interpreting TRT instead of using the fluid temperature. Following the work of Dion et al. (2022b) [227], both the mean fluid temperature and the outlet STgF signals can be used to recover the thermal conductivity of the ground. This section explains how to apply the FOA of the ILS model to both of these signals. It must be emphasized that the methodology of interpreting a TRT with the FOA of the ILS is employed in this article due to its accuracy, and also because it is widely used to retrieve the ground thermal conductivity from TRT data.

First, the FOA of the ILS model for both signals are:

$$T_f(t) = T_0 + \bar{q}R_b + \frac{\bar{q}}{4\pi k}\left(ln\left(\frac{4\alpha t}{r_b^2}\right) - \gamma\right) \tag{6.3}$$

and

$$g(t) = R_b + \frac{1}{4\pi k}\left(ln\left(\frac{4\alpha t}{r_b^2}\right) - \gamma\right) \tag{6.4}$$

where $\bar{q}$ is the average heating power rates per unit of length, R_b is the equivalent borehole thermal resistance, k and α are respectively the ground effective thermal conductivity and diffusivity, r_b is the borehole radius, γ is the Euler constant. One can note that Eq. 6.4 is a simplification of Eq. 6.3 where the heating power is a constant of 1 and the initial ground temperature T_0 is zero. During the interpretation, $g(t)$ in Eq. 6.4 corresponds in fact to $\hat{g}(t)$ obtained with the deconvolution algorithm.

To perform an analysis with the FOA, Eqs. 6.3 and 6.4 are linearized on a logarithm scale for times larger than $t_c = 5r_b^2/\alpha$ (where the specific heat c_p in $\alpha = k/\rho c_p$ is guessed and constant):

$$T_f(t) = m_T \cdot ln(t) + b_T \quad \forall\ t > t_c \tag{6.5}$$

and

$$g_{out}(t) = m_g \cdot ln(t) + b_g \quad \forall\ t > t_c \tag{6.6}$$

The slopes m_T and m_g of the log-linear regressions are tied to Eqs. 6.3 and 6.4 by the general expression $m = q/(4\pi k)$. The thermal conductivity values are then estimated from both the temperature and the transfer function signals with:

$$k_T = \frac{\bar{q}}{4\pi m_T} \tag{6.7}$$

and

$$k_g = \frac{1}{4\pi m_g} \tag{6.8}$$

One can already note the advantage of using the STgF to retrieve the thermal conductivity. In Eq. 6.8, the heating power is constant by construction, which is closer to the assumptions of the ILS model. Another gain of using a STgF is that if the TRT includes a recovery phase, then this portion is not used in Eqs. 6.3, 6.5 and 6.7. However, $\hat{g}(t)$ includes information from both the heating and the recovery phases.

Finally, a useful way to add robustness to the effective thermal conductivity calculation is to compute the FOA methods sequentially for increasingly long TRT duration, as is shown in Spitler et Gehlin (2015) [18] and Choi et al. (2018a) [32]. For example, Eqs. 6.5 and 6.7 are rewritten as:

$$T_f(t_j) = m_T(i) \cdot ln(t_j) + b_T(i) \quad \forall j \in [1, i] \, , t_i > 6 \text{ h} \tag{6.9}$$

and

$$k_T(i) = \frac{\bar{q}_i}{4\pi m_T(i)} \tag{6.10}$$

where $\bar{q}_i$ is the average heat load up to time i and where the index i moves from the 6-hour mark to the end of the TRT. Note that 6 hours corresponds to a typical value found for the critical time t_c in the literature [108]. Similar equations to Eqs. 6.9 and 6.10 are obtained trivially for STgFs by replacing T by g and $\bar{q}$ by 1. The thermal conductivity as a function of the TRT duration can be analyzed as a signal where the mean and standard deviations are:

$$\bar{k} = \frac{\sum_i^{n_t} k(i)}{n_t - i(1)} \quad t_i > 6 \text{ h} \tag{6.11}$$

and

$$\sigma_k = \sqrt{\frac{\sum_i^{n_t} \left(k(i) - \bar{k}\right)^2}{n_t - i(1) - 1}} \tag{6.12}$$

where $\bar{k}$ is the mean effective thermal conductivity and σ_k is the standard deviation of the effective thermal conductivity signal.

6.3.3 Distributed TRT interpretation method

Both the deconvolution algorithm and the FOA method of the previous sections are detailed to interpret data from the GHE outlet. Hence, the effective thermal conductivity represents a value over the whole GHE. By using a DTS system, a DTRT can be performed, and the subsequent interpretation allows identifying vertical thermal conductivity profiles over the GHE length, which may lead to a more precise GHE design [65]. The rest of this section addresses the deconvolution and FOA interpretation on the temperature signals at various depths in the GHE.

In this work, the soil surrounding a GHE is first separated in n_L layers, each one corresponding either to a specific geological formation in heterogeneous sites or simply a specific vertical discretization when layers are thick. The thermal conductivity identified for a layer is considered constant within a given layer, an assumption also used by Beier (2020b) [228]. Two vectors z_m and z_s can be written to identify the middle and separation depths of each layer, respectively. Fig. 6.1 shows how the layers are separated for the interpretation.

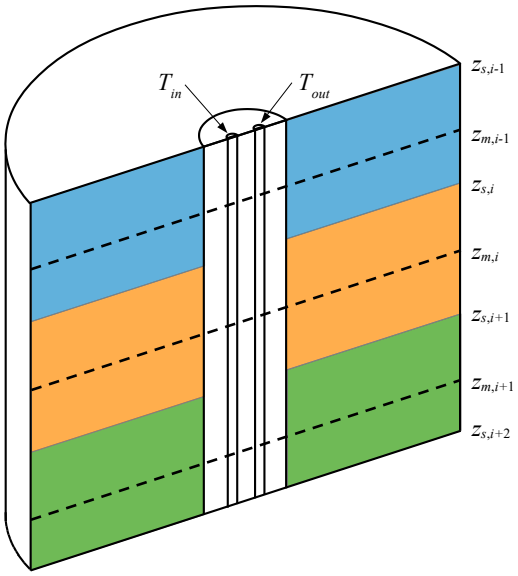

Figure 6.1 Layers and identification of their middle (z_m) and their separation (z_s).

When performing a DTRT, the number of vertical temperature recording point is highly dependent on the specific DTS system or probe used, with minimal and maximal distances between signals of 0.1 to 5 meters [62]. Hence, vertical interpolation could be needed to provide temperature signals in the specified z_m and z_s vectors. Beier (2020b) [228] used polynomial regressions of degrees 2 to 4.

With the proposed vertical discretization using the vectors z_m and z_s, the deconvolution is applied on a layer of thickness $\Delta z_{m,i} = z_{s,i+1} - z_{s,i}$. Using the temperature signal measured at depth z_m, the convolution equation is written as:

$$T_f(t, z_m) - T_0(z_m) = (f * g)\,(t, z_m) \tag{6.13}$$

The heat load profile is the addition of heat dissipated from the inlet and outlet pipes at each layer:

$$q(t, z_m) = VC_f \Delta T(t, z_m) \tag{6.14}$$

where, for a specific ground geological unit i,

$$\Delta T(t, z_{m,i}) = \frac{T_{out}(t, z_{s,i+1}) - T_{out}(t, z_{s,i})}{\Delta z_{m,i}} - \frac{T_{in}(t, z_{s,i+1}) - T_{in}(t, z_{s,i})}{\Delta z_{m,i}} \tag{6.15}$$

and V is the circulating flow rate and C_f is the fluid volumetric heat capacity. The minus sign in front of the inlet term in Eq. 6.15 ensures that the heat loss is added to the total heat dissipated for a layer.

The incremental heat load profile is then computed similarly to Eq. 6.2 as the difference of the heat load at each layer:

$$f(t, z_m) = q(t_{i+1}, z_m) - q(t_i, z_m) \tag{6.16}$$

Applying the deconvolution algorithm hands n_L STgFs noted $\hat{g}(t, z_{m,i})$. Using both the mean depth temperature $T_f(t, z_{m,i})$ and the STgFs, the analysis with the FOA can be done with Eqs. 6.3 through 6.12, but for each layer separately. The results obtained are depth dependent thermal conductivity profiles from both the interpretation of the temperature signals obtained during the DTRT and the STgFs obtained by deconvolution.

A weighted average can be computed from the depth-dependent thermal conductivity values and their corresponding layer thickness as follows:

$$\tilde{k} = \frac{\sum_{i=1}^{n_L} \Delta z_{m,i} \cdot \bar{k}(z_{m,i})}{\sum_{i=1}^{n_L} \Delta z_{m,i}} \tag{6.17}$$

Hence, this average can be compared to the effective thermal conductivity obtained at the GHE outlet. It should be noted that the *effective* thermal conductivity is a more accurate representation of the heat exchange capacity of the whole GHE compared to the *weighted average* one. The ILS model assumes that heat is emitted by an infinite line, which is not

respected for a GHE, let alone for smaller sections when analyzing a DTRT. Computing Eq. 6.17 also compounds the error of each estimation of $k(z_{m,i})$. Nevertheless, the value $\tilde{k}$ gives an indication of the effective thermal conductivity's veracity. Thus, discrepancies between $\tilde{k}$ and $\bar{k}$ should be small.

6.4 Results

In this section, the deconvolution and FOA methods presented previously are applied to the interpretation of numerically generated and field DTRTs to validate their use to obtain experimental depth-dependent STgFs and a vertical profile of thermal conductivity values.

6.4.1 Numerical DTRT

To generate numerical DTRT datasets, the 3D numerical model described by Pasquier et Marcotte (2014) [47] is modified to extract temperature signals at various depths. In this model, a single U-loop GHE is modeled using a *Heat Transfer* physics, modeled by following heat balance equation:

$$\rho c_p \frac{\partial T}{\partial t} + \rho c_p \mathbf{u} \cdot \nabla T = \nabla \cdot (k \nabla T) \tag{6.18}$$

where ρ is the material density, c_p is the specific heat capacity and $\mathbf{u}$ is a velocity vector. The latter is used to simulate a flow within the circulating pipes, and the remaining of the model transfer heat through conduction.

The ground, grout, pipes and circulating fluid materials are constructed with the physical and thermal properties summarized in Table 6.1. A thermal insulation boundary condition cuts the model in half to reduce the total number of mesh and still providing the same simulation results at a faster computing time. The main modifications to the model were to increase vertical meshing density, so that vertical temperature profiles are extracted at every meter along the GHE in both the inlet and outlet pipes. Another enhancement is to add a zone of 0.5 m in diameter around the surface of the borehole where a null heat flux boundary condition is applied, following findings from Robert et al. (2022) [91]. Two numerical DTRTs are used here, and the operating conditions used to produce them are summarized in Table 6.2.

Both numerical DTRTs are 7-day long, with a first day being a recirculation phase, prior to heating. The first DTRT (DTRT-1) has a constant (i.e., without natural variations or noise) heating power of 12 kW over the 6 remaining testing days and is used as a demonstration case. The second DTRT (DTRT-2) has 3 days of heating at 12 kW with added autocorrelated variations that simulates typical electric grid changes, and 3 days of recovery. Figure 6.2

Table 6.1 Parameters used to generate numerical DTRTs and describing the field DTRT.

Parameter	**Numerical**	**Field**
Borehole length (m)	150.00	138.99
Borehole radius (m)	0.075	0.078
Inner pipe radius (m)	0.017	0.017
Outer pipe radius (m)	0.021	0.021
Half shank spacing (m)	0.050	0.057
Ground vol. heat capacity (MJ/m^3°C)	2.40	2.25
Grout thermal conductivity (W/m°C)	0.75	1.90
Grout vol. heat capacity (MJ/m^3°C)	2.00	1.89
Pipe thermal conductivity (W/m°C)	0.40	0.74
Pipe vol. heat capacity (MJ/m^3°C)	1.9	1.8
Fluid thermal conductivity (W/m°C)	0.6	0.6
Fluid vol. heat capacity (MJ/m^3°C)	4.2	4.2
Undisturbed ground temperature (°C)	10.00	7.49
Circulating flow rate (L/min)	30.00	26.08

Table 6.2 Operating conditions applied to the numerical model to create the two numerical DTRTs.

DTRT	**Parameters**
1	$Q = 12$ kW for 6 days $k = 3$ W/m°C over the ground
2	$Q(t) = 12 \pm 0.5$ kW and $Q = 0$ kW, 3 days each $k(t) \in [1.25, 4]$ with $\tilde{k} = 2.68$ W/m°C (Fig. 6.3)

shows the simulation results for both DTRTs. The datasets to interpret are inlet and outlet temperatures profiles, as well as 2D maps of the temperature evolution as a function of time and depth, for both the inlet and outlet pipes.

Figure 6.3 presents the deconvolved STgFs, as well as the regressions obtained by the FOA interpretation on both the temperature and STgFs, for the two numerical DTRTs. The regressions are adjusted with Eqs. 6.5 and 6.6, start at a critical time t_c and finish at the end of the heating phase. Note that for DTRT-2, the regression on the temperature ends at day 3, but the regression on the STgF ends at day 6.

Table 6.3 shows the fit of the regressions through the RMSE, as well as the estimated thermal conductivity values for both DTRTs. One can note that all the RMSEs are around the same order of precision for the temperature signals and STgFs. The RMSE of DTRT-2 of 0.125 °C is correlated to the amplitude of the natural variations added to the heating power signal. This

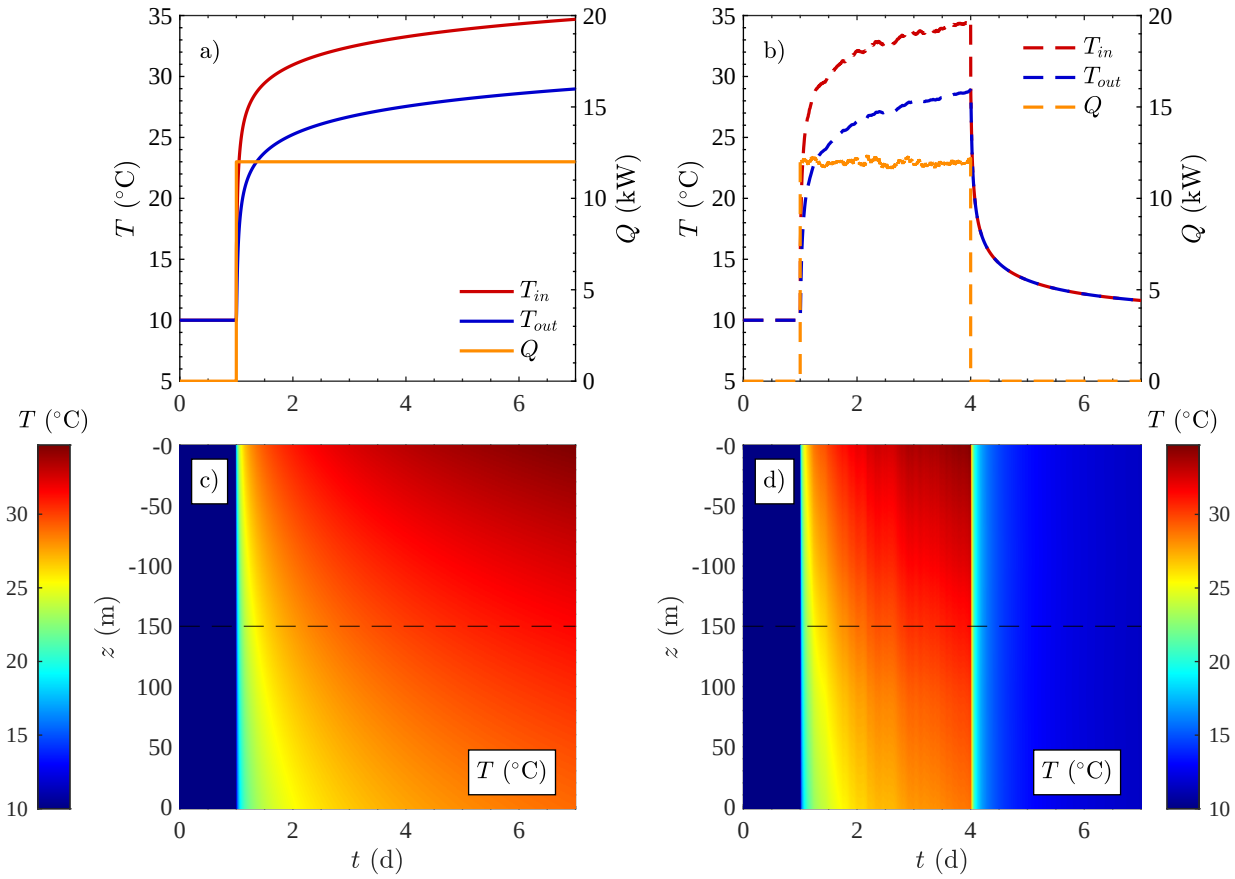

Figure 6.2 Simulated numerical DTRT results, where the DTRT-1 is in a) and c) and the DTRT-2 is in b) and d). The top row (a) and b)) presents the fluid temperature signals at the GHE inlet and outlet and the heating power profiles. The bottom row (c) and d)) shows 2D maps of fluid temperature evolution as a function of time and depth, where the top 150 m is in the inlet pipe, the bottom 150 m is in the outlet pipe, with the U-bent corresponding to the dashed line.

effect is removed by using the STgF, as noted by the RMSE of $3.3e^{-4}$, which is comparable to the one from DTRT-1.

The effective thermal conductivity values estimated from DTRT-1, reported in Table 6.3, are both approximately 1 % from the reference value used in the model ($\epsilon = (k - k_{ref})/k_{ref}$). This excellent result is expected, since all the operating conditions are maintained constant through time, so that the DTRT-1 represents an idealized situation to demonstrate the algorithm's effectiveness. For DTRT-2, the errors are larger and around 3 %, and are deemed reasonable considering the limitations of the FOA (see Section 6.5.1). The larger standard deviations observed for the DTRT-2 compared to the DTRT-1 are mainly attributed to two factors: (i)- the greater complexity of the ground thermal conductivity variation and (ii)- the

use of a heating power profile that includes variations in the simulation. An observation is that all the thermal conductivity estimations lead to thermal conductivity estimation smaller than the reference values albeit by small discrepancy. Note that all relative errors are well within common values when using the FOA method, which can go up to 26 % [36].

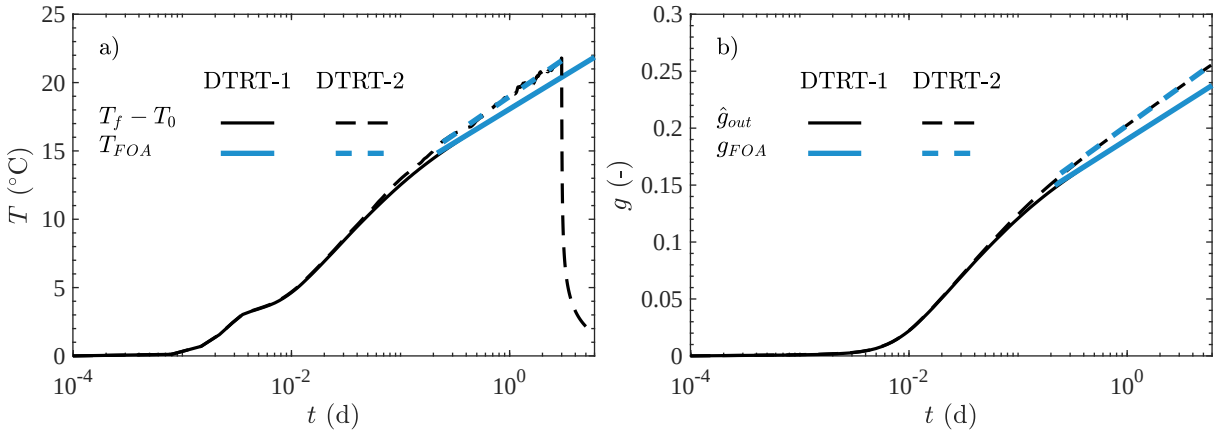

Figure 6.3 a) Results of the FOA interpretation on the temperature signals and b) the deconvolved STgFs for both numerical DTRTs.

Table 6.3 RMSE fit and effective thermal conductivity estimated with FOA on both numerical DTRTs and with the average outlet temperature and the STgF ($\epsilon = (k - k_{ref})/k_{ref}$).

DTRT	**Signal**	**RMSE (°C, -)**	k **(W/m°C)**	ϵ **(%)**
1	T_f	0.023	2.97	-1.0
	$\hat{g}_{out}$	2.9e^{-4}	2.97	-1.0
2	T_f	0.125	2.60	-3.0
	$\hat{g}_{out}$	3.3e^{-4}	2.61	-2.7

Along the GHE, the STgFs are estimated at the center (z_m) of each layer (bounded by z_s). To display relatively smooth thermal conductivity profiles, DTRT-1 is separated in 15 layers of 10 m each, which corresponds to 15 thermal conductivity estimations. Similarly, DTRT-2 is separated in 7 layers with varying thermal conductivity ranging from 1.25 to 4 W/m°C. Figure 6.4 shows the deconvolution results, as well as the thermal conductivity profiles for each DTRT.

Interpretation of DTRT with depth-dependent STgFs gives conductivity estimates closer to the model than interpretation with temperature signals. As an example, for DTRT-1, the STgFs in Fig. 6.4 a) are almost all identical, which shows that the GHE thermal parameters are constant along the GHE. For DTRT-2 (Fig. 6.4 b)), the STgFs diverges from each other

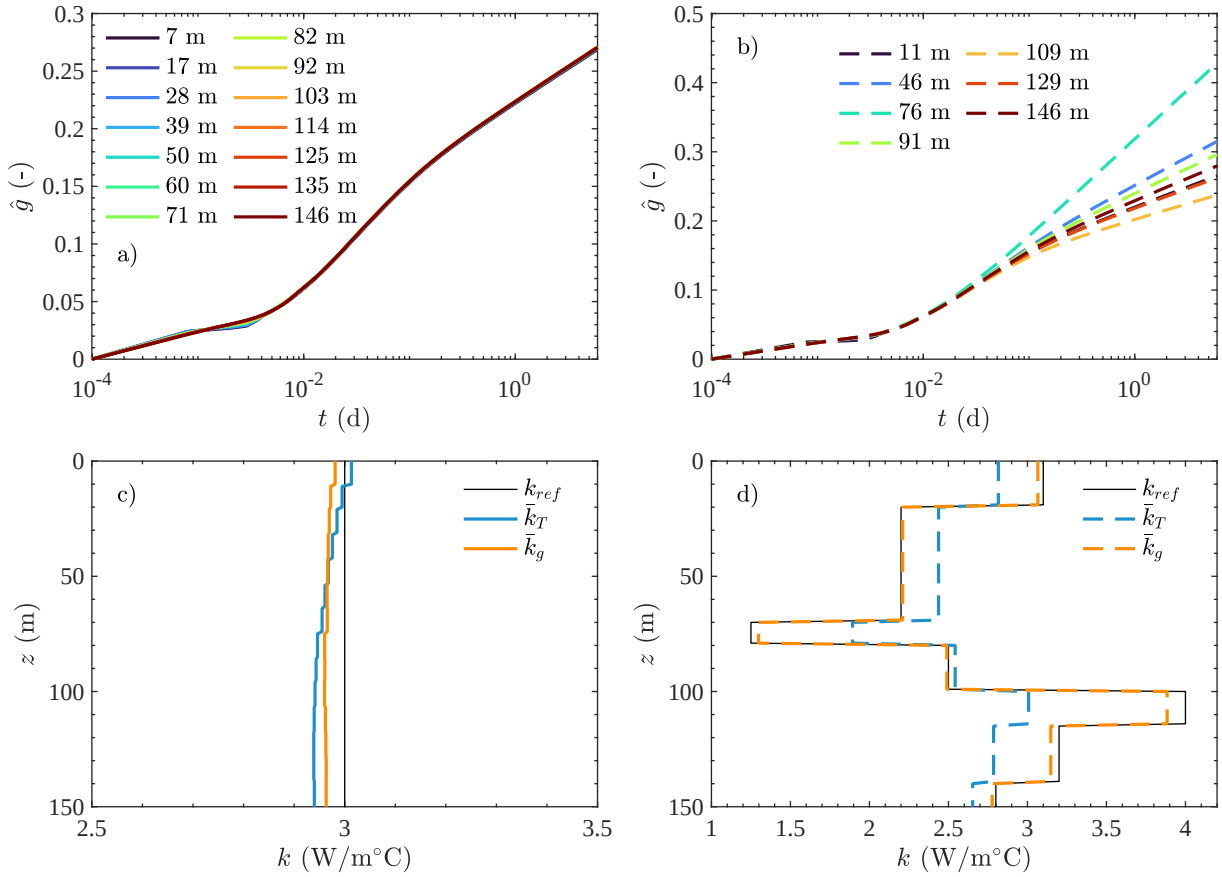

Figure 6.4 a) and b) STgFs evaluated with the deconvolution algorithm. c) and d) Thermal conductivity profiles using the average temperature and the STgFs. a) and c) are results for the DTRT-1 and b) and d) are results for the DTRT-2.

at approximately 1 hour. This time shows that the critical time of 6 hours used in Eqs. 6.9, 6.10 and 6.11 is indeed when the heat transfer occurs in the ground. Knowing that the thermal conductivity values from the borehole materials are constant along the GHE but the ground one varies as a function of depth, this indicates that the heat transfer is first affected by the GHE materials' thermal parameters (i.e., fluid, pipe and grout) and then by the thermal parameters of the ground. Beier (2020a) [177] refers to this interface as the transition between the borehole dominated and steady heat flux periods.

The thermal conductivity profiles in Fig. 6.4 c) and d) shows that the interpretation with the mean temperature is not as precise as the one with the STgFs, especially with DTRT-2. For DTRT-1, The vertical profile $\bar{k}_g$ has less deviation from the reference value than the profile $\bar{k}_T$. The latter one having a larger curvature, especially in the first half of the GHE (0-75 m). A key feature of DTRT-2 is that a time-varying heating power profile ($q(t)$) is

used during the simulation, but a time average one ($\bar{q}(t)$) is used during the interpretation (Eq. 6.3). A bias on the estimate of the thermal conductivity can therefore come from this simplification, which is removed with the depth-dependent STgFs, since the heating power is constant and equal to 1 W/m. Also, the length used for the FOA regression is doubled for the STgFs compared to the temperature signal, since the recovery phase is also characterized in the STgFs.

The maximum relative error of each profile, the location and the estimated thermal conductivity for the layer are reported in Table 6.4. Note that the larger error for the DTRT-2 is for the layer with the lowest thermal conductivity value of 1.25 W/m°C, which is the one most penalized by the relative error equation.

Table 6.4 Maximum discrepancy between estimated and reference thermal conductivity, the vertical position and the relative error for both DTRTs

DTRT	**Signal**	**Depth (m)**	$k(z_m)$	$k_{ref}(z_m)$	ϵ **(%)**
1	T_f	125	2.94	3.00	-2.04
	$\hat{g}_{out}$	103	2.96	3.00	-1.33
2	T_f	76	1.89	1.25	51.45
	$\hat{g}_{out}$	76	1.30	1.25	3.81

The numerical results demonstrate clearly that using deconvolved STgFs is beneficial to the accurate identification of the vertical conductivity values obtained with the FOA method along the borehole. At the GHE outlet, since the temperature variations are larger, the gain of using the borehole outlet STgF to estimate the effective thermal conductivity is not as clear, however.

6.4.2 Field DTRT

To further demonstrate the effectiveness of the proposed methodology, a field DTRT performed on a closed-loop GHE is also interpreted. The test was performed on a single U-loop GHE, equipped with 9 submersible probes (±0.05 °C) distributed along both the inlet and outlet pipes. The DTRT duration is of 12 days, with 3 days of recirculation, 7 days of heating and 2 days of recovery. The main borehole dimensions and operating parameters are summarized in Table 6.1. To interpret the DTRT in the middle of each geological layers (z_m), interpolated temperature signals are computed from vertical temperature profiles at each time step from the 9 probes in the U-tubes. The interpolation is based on a polynomial of degree 3, as used by Beier (2020b) [228], and hands temperature signals at all manually

set z_m and z_s depths. In this case, 4 layers are considered, according to a geological report identifying sand (0 to 11 m), red slate (11 to 31 m) and two different mudshales (31 to, 50 m and 50 to 138.99 m) along the GHE [229].

Figure 6.5 a) and b) shows the experimental temperature profiles, as well as the heating power and circulating flow rate recorded during the field DTRT. Figure 6.5 c) and d) presents deconvolution and FOA outcomes. The STgFs in the Figure 6.5 c) do not have large variations, indicating that the ground thermal conductivity values are similar along the GHE, leading to relatively similar thermal conductivity values between 2.8 to 3.15 W/m°C, as shown in Figure 6.5 d). Analogously to DTRT-2, the STgFs are superposed up until around 15 minutes, which is close to the recirculating time of 10 minutes.

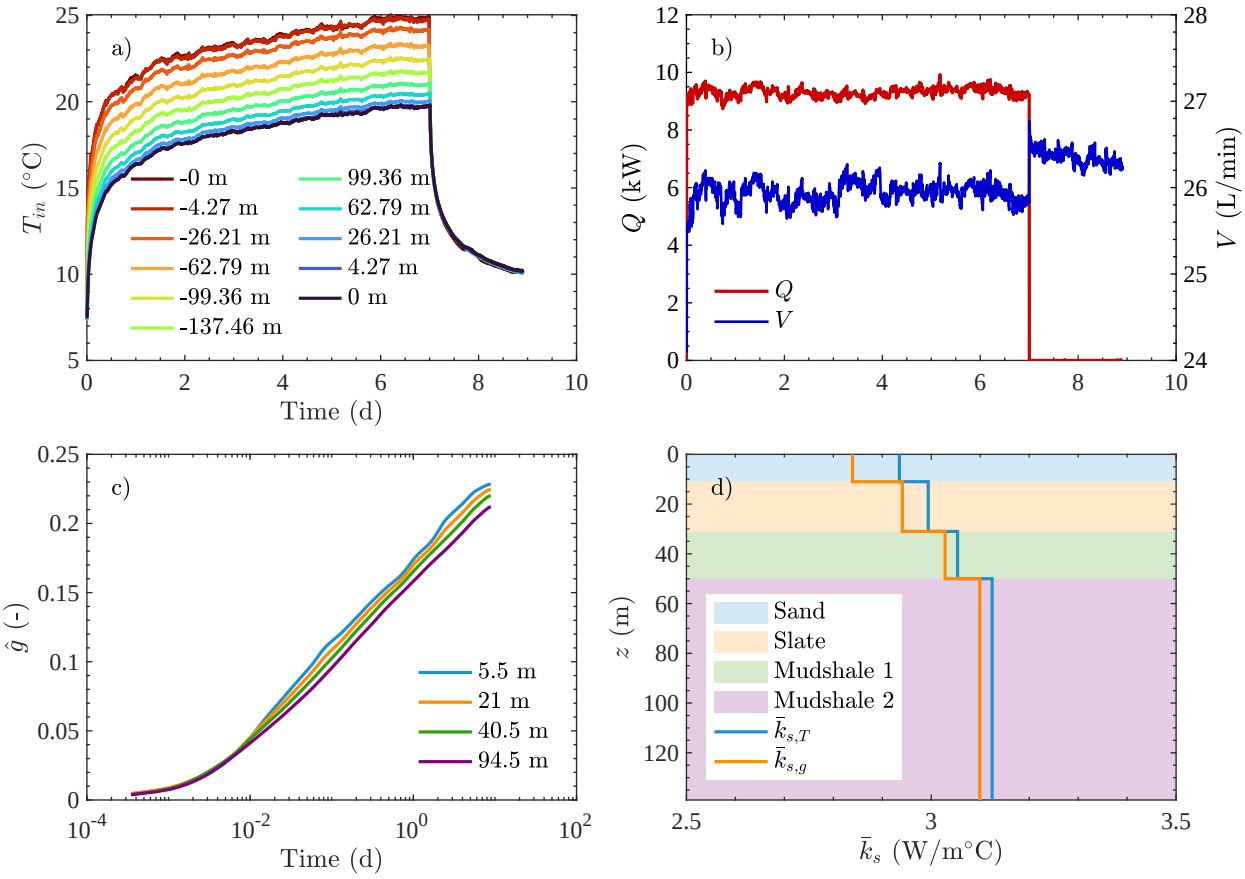

Figure 6.5 a) Field DTRT temperature signals, b) Heating power profile and circulating flow rate, c) STgFs obtained with deconvolution as a function of depth and d) thermal conductivity profiles from $T_f(t,z)$ and $\hat{g}_{out}(t,z)$

Pasquier (2015) [215] and Pasquier et Marcotte (2020) [118] studied this field TRT and found effective thermal conductivity values of 2.96 ± 0.17 W/m°C, 3.10 ± 0.14 W/m°C and 3.03

$\pm$ 0.04 W/m°C, using a finite line source model, a thermal resistance and capacity model and a Bayesian inference approach, respectively. Using the described methodology, the FOA interpretation at the GHE outlet led to an estimation of the effective thermal conductivity of $\bar{k}_T = \bar{k}_g = 3.01$ W/m°C. The depth average thermal conductivity (Eq. 6.17) are of 3.08 and 3.05 for T_f or $\hat{g}_{out}$ respectively. These last results show that the depth-average thermal conductivity estimation is also a valid methodology to obtain a guess of the effective values, with the STgF being slightly more accurate.

Figure 6.5 d) shows that the thermal conductivity estimation is systematically smaller when using the STgFs than with the temperatures. This may be explained by the average value of the circulating flow rate varying between the heating and recovery phases (Fig. 6.5 b)). The average during the heating phase is 25.95 L/min compared to 26.03 L/min for the whole DTRT duration. Using the latter value in the FOA results in an effective thermal conductivity $\bar{k}_T = 3.11$ W/m°C, an overestimation of 3.3 %. This effect is dampened when using the STgF, since both sections are used to estimate the effective thermal conductivity.

6.5 Discussion

6.5.1 Limits of the ILS model

The ILS model used in the FOA interpretation (Eqs. 6.3 and 6.4) employs a truncated series of the exponential integral equation. This truncation may lead to an error of up to 26 % on the thermal conductivity estimation [36]. Among other assumptions and simplifications of the ILS model, these include the fact that a U-tube has two line sources, as opposed to the single line source considered in the ILS model, the interactions between the heat source and the geothermal gradient are not taken into account, and that boundary conditions are omitted, hampering near-surface analysis.

One of the limitations of the current methodology is the presence of a significant geothermal gradient. In numerical simulations, the addition of a depth-dependent initial ground temperature ($T_0(z)$) leads to errors in thermal conductivity estimates correlated to the depth at which the estimation is made. The use of the ILS model (see Section 6.5.1) as opposed to a more detailed heat transfer model [35] is one possible explanation. Implementing the q_{ratio} concepts of Morchio et al. (2022, 2023) [230, 231] to the evaluation of STgFs along the GHE could help eliminate the impact of the geothermal gradient on the thermal conductivity identification.

The theoretical ILS model also assumes an infinite circulating flow rate. This assumption is not realistic in practice. However, the impact of the circulating flow rate on the thermal

conductivity can be estimated by running the numerical model several times with different flow rates. Figure 6.6 shows various thermal conductivity profiles computed with DTRT-1 inputs, but for circulating flow rates varying between 10 L/min to 50 L/min. Note that all the selected flow rates keep the Reynolds number high enough to maintain turbulent flow, which would become laminar at around 7 L/min. In such a case, the heat transfer within the fluid would only be conduction, lowering the efficiency by a large margin.

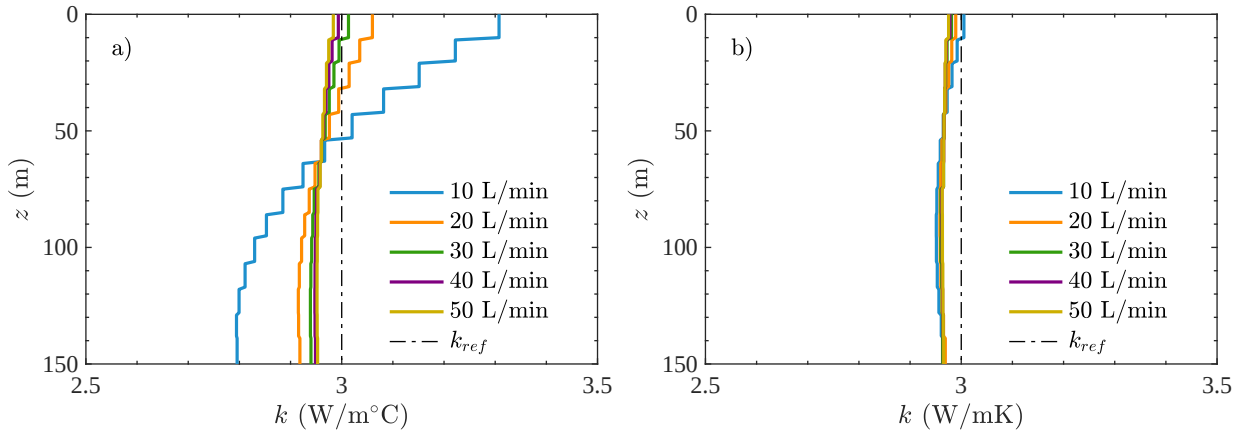

Figure 6.6 Thermal conductivity profiles when interpreting DTRT-1 with various circulating flow rates for: a) the mean temperature signals and b) the STgFs.

The first result from Fig. 6.6 is that the thermal conductivity profiles of the STgFs are much more robust to flow rate changes than the profiles with temperature signals. Second, as the circulating flow rate increases, thermal conductivity estimated values with the temperature signals approach the reference one.

It is therefore recommended that, when interpreting temperature signals from fluid flowing through pipes with diameters of 3.4 cm with the FOA method, a flow rate of at least 25 to 30 L/min must be maintained to avoid affecting the thermal conductivity estimation. Alternatively, the STgFs can be used if the flow rate is too low.

6.5.2 In depth demonstration of the algorithm for a layer

This section aims to demonstrate how using a STgF is better suited for FOA on a specific layer, rather than the temperature signal. For this, Fig. 6.7 presents the FOA results on the temperature $T_f(t, z = 76 \text{ m})$ and $\hat{g}_{out}(t, z = 76 \text{ m})$ for DTRT-2 at a depth bounded by $z_s =$ 71 and 81 m, with a thermal conductivity of 1.25 W/m°C. Each graph in the figure shows the interpreted signal (either the average temperature or the STgF), as well as the heating power profile used in the FOA.

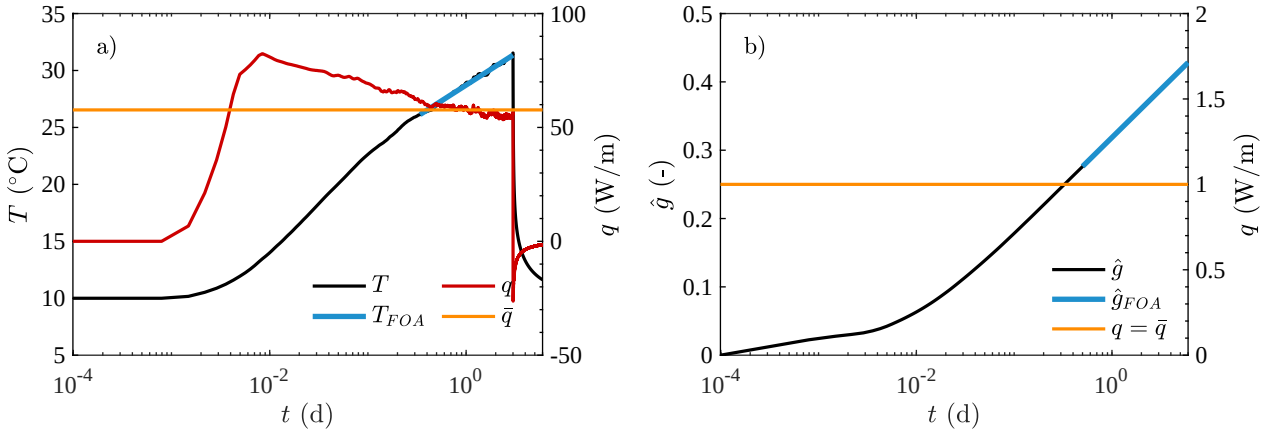

Figure 6.7 FOA interpretation on the layer centered at $z_m = 76$ m on DTRT-2 for: a) $T_f(t, z = 76\text{ m})$ and b) $\hat{g}_{out}(t, z = 76\text{ m})$

One can notice that the quality of the regressions' fit is similar for the two signals in Fig. 6.7, but that the regression on the STgF is longer, since the recovery phase is contained in the STgF. The largest difference, however, is on the heating power profile used in the FOA method. The red line in Fig. 6.7 a) is computed with Eq. 6.14, but the interpretation requires an average constant heating power $\bar{q}$ (Eqs. 6.3 and 6.7), which is shown by the orange curves in Fig. 6.7. The variations and measurement noise on both the temperature and the heat load signals are removed when using the deconvolved STgF shown in Fig. 6.7 b). The FOA interpretation is then done using a constant heating power of 1 W/m, which results in a more precise thermal conductivity estimation for this layer. The difference between the two heat load signals is at the root of the discrepancy between the evaluated thermal conductivity and the one in the numerical model.

6.5.3 FOA interpretation using temperature and STgF

When using temperature signals, measurement noise on the heating power profile leads to errors on the thermal conductivity estimation and can account for up to 25 % error on the 95 % confidence interval distribution of a calculated thermal conductivity value [36]. Using a STgF instead of temperature signals eliminates this source of errors, since the variations in the temperature and the heating power are filtered out by the deconvolution.

As discussed in Section 6.4, the FOA interpretation at the GHE outlet benefits only slightly from the use of STgFs compared to the temperature signals, provided the regression is performed on a sufficiently long signal. However, the borehole outlet STgF is not primarily used for thermal parameter identification, but to simulate the short-term response of the GHE

under varying heat load profiles.

Unlike the STgF from the GHE outlet, the set of STgFs deconvolved at different depths are not useful for further simulations, but they offer more precise thermal conductivity values than temperature signals, and offer more flexibility when deviating from assumptions used by the ILS model (see Section 6.5.1). Therefore, when attempting to identify the most thermally efficient geological layer to be reached subsequent drilling for a larger GHE field, the FOA interpretation using the STgFs is recommended.

6.5.4 Thermal conductivity precision

The uncertainty on thermal conductivity estimation with the ILS model has been studied in relation to reference values, with discrepancy ranging from 8 % to 26 % [32, 36]. To improve the certainty of the thermal conductivity value, a sequential calculation can be performed from increasingly longer signal interval [18,32]. The thermal conductivity values in this article use this methodology and results are presented from Eq. 6.11.

The thermal conductivity standard deviation (Eq. 6.12) assess the robustness of the estimation. Table 6.5 shows the standard deviation of effective and depth-dependent thermal conductivity estimations for the field DTRT. The standard deviations are all equal or less than 0.1 W/m°C, indicating high precision, but not necessarily high accuracy. Consequently, the accuracy of thermal probes must be closely monitored by calibration both before and after a TRT to correct any possible drift. Such an error would affect the quality of the calculated thermal conductivity, since in Eqs. 6.7 and 6.8 the slope of the temperature signal or the STgF is used. A constant offset on the correct temperature signal would not affect the thermal conductivity value, but would affect the value of the impulse used in the deconvolution.

Table 6.5 Standard deviations for the thermal conductivity estimations on the field DTRT

Layer	$\sigma(k_T)$ W/m°C	$\sigma(k_g)$ W/m°C
GHE outlet	0.05	0.04
Sand	0.05	0.10
Slate	0.05	0.05
Mudshale 1	0.05	0.02
Mudshale 2	0.06	0.03

6.6 Conclusion

This article described a methodology to obtain both the short-term g-function (STgF) and the thermal conductivity estimation from distributed thermal response tests (DTRT). The STgFs are obtained both at the GHE outlet, and along the ground heat exchanger. The borehole outlet STgF allows thermal conductivity estimation and to simulate the ground heat exchanger response to varying heat load profile. Depth-dependent STgFs provide insight into how the thermal exchange occurs in each geological layer, as well as depth-dependent thermal conductivity estimations.

The proposed methodology is validated with two DTRTs generated with a validated numerical model, as well as with a field DTRT recorded with 9 submersible probes along the ground heat exchanger. Numerical tests show that the methodology using a first-order approximation of the infinite line source model is valid for both temperature signals and the STgF, and highlight interesting advantages of using STgFs, such as observing the time delay for the heat transfer to impact the ground and the independence of the thermal conductivity profile to flow rate changes.

The main results of this article are that, when interpreting a DTRT, both GHE outlet temperature signals and STgF provide similar effective thermal conductivity estimations. However, interpretation to obtain the depth-dependent thermal conductivity profile is more accurate with deconvolved STgFs, because they are smooth and based on a constant heating power, which corresponds more closely to the boundary conditions of infinite line source model.

6.7 Data Availability

Matlab functions to perform the interpretation method are available upon request from Gabriel Dion.

6.8 CRediT authorship contribution statement

Gabriel Dion: Conceptualization, Methodology, Software, Visualization, Writing - Original Draft. **Philippe Pasquier**: Conceptualization, Methodology, Validation, Writing - Review & Editing, Supervision, Funding acquisition. **Denis Marcotte**: Validation, Writing - Review & Editing.

6.9 Acknowledgments

The authors wish to acknowledge the support and funding provided by the Natural Sciences and Engineering Research Council of Canada (grant number RDCPJ 530945), the Trottier Energy Institute, Hydro-Québec, FTE drilling and Richelieu Hydrogeology.

6.10 Nomenclature

Symbols

α	Thermal diffusivity (m^2/s)
b	Constant of the FOA (°C)
c	Volumetric heat capacity ($J/m^3°C$)
c_p	Specific heat capacity (J/kg°C)
C	Optimization constraint
Δ	Variation
ϵ	Relative error (-)
E	Objective function value (-)
f	Incremental heat load function (W/m)
$\mathcal{F}$, $\mathcal{F}^{-1}$	Fourier transform and it's inverse
γ	Euler's constant
g	Borehole outlet STgF (-)
$\hat{g}$	Estimated borehole outlet STgF (-)
H	Borehole length (m)
k	Thermal conductivity (W/m°C)
$\bar{k}$	Mean thermal conductivity (W/m°C)
$\tilde{k}$	Depth average thermal cond. (W/m°C)
m	Slope of the FOA (°C/s)
n	Number of elements (-)
σ	Standard deviation (-)
ρ	Density (kg/m^{-3})
Q	Heating power (W)
q	Heating power rate (W/m)
$\bar{q}$	Average heating power rate (W/m)
r	Radius (m)
R	Thermal resistance (m°C/W)
τ	Nodes time array in optimization (s)

t	Time array (s)
T	Temperature (°C)
$\widehat{T}$	Convolved temperature ($T_{out} - T_0$) (°C)
V	Flow rate (m^3/s)
W	Weights used in the objective function
x	Parameters for initial STgF guess
z	Depth along the GHE (m)

Subscripts

0	Initial
b	Borehole
c	Critical
exp	Experimental
f	Fluid
g	Short-term g-function
i	Counter
in	Borehole inlet
j	Counter
k	Thermal conductivity
L	Ground layer
m	Middle of ground layer
out	Borehole outlet
ref	Reference
s	Interface between ground layer
τ	Nodes on the STgF
t	Time steps
T	Temperature

Abbreviations

DTRT	Distributed thermal response test
DTS	Distributed temperature sensing
ETRT	Enhanced thermal response test
FOA	First-order approximation
GHE	Ground heat exchanger

GSHP	Ground source heat pump
ILS	Infinite line source
PCHIP	Piecewise cubic Hermite interpolating polynomial
RMSE	Root-mean-square error
STgF	Short-term g-function
TRT	Thermal response test

6.11 A. Deconvolution algorithm

The deconvolution algorithm presented by Dion et al. (2022a) [205] is summarized here. The goal of this algorithm is to optimize the nodes positioned on the transfer function using the following minimization:

$$\hat{g}(t) = arg\min_{\hat{g}(\tau)} \left(E(t) \mid C_1(\tau),\ C_2(\tau) \right) \tag{6.19}$$

where $\hat{g}$ is the estimated transfer function, τ is a vector of logarithmically spaces nodes on $\hat{g}$, E is the value of the multi-objective function described by Eq. 6.20 and parameters C_1 and C_2 are linear inequality constraints that $\hat{g}(\tau)$ must respect. They are used to restrict the optimization space, and are described by Eqs. C_1 and C_2.

The objective function is the sum of three different root-mean-square error (RMSE) described as:

$$\begin{aligned} E = & \sqrt{\frac{1}{n_t}\sum_{i=1}^{n_t}\left(W_1(t)\left(\widehat{T}(t) - T_{exp}(t)\right)\right)^2} + \\ & W_2\sqrt{\frac{1}{n_t}\sum_{i=1}^{n_t}\left(\hat{g}'(t)\right)^2} + \\ & W_3\sqrt{\frac{1}{n_t}\sum_{i=1}^{n_t}\left(\hat{g}''(t)\right)^2} \end{aligned} \tag{6.20}$$

and the constraints are written as:

$$0 < \hat{g}(\tau_i) < \hat{g}(\tau_{i+1}) \ \forall\ i \in [1, n_\tau - 1] \tag{C_1}$$

$$0 < \hat{g}'(\tau_{i+1}) < \hat{g}'(\tau_i) \ \forall\ i \in [j, n_\tau - 1] \tag{C_2}$$

In Eq. 6.20, $\widehat{T}$ and T_{exp} are respectively the estimated (using $\hat{g}$ in Eq. 6.1) and experimental temperature variation, equal to $T_{out} - T_0$. Functions $\hat{g}'$ and $\hat{g}''$ are respectively the first and

second derivatives of the estimated STgF. The last two terms are added as a regularization strategy to help to smooth $\hat{g}$. Similar terms are found in Beier (2020a) [177] and studied by Du et al. (2022) [232]. The latter established that regularization terms improve the parameter estimation when the number of parameters is large (i.e., 7 parameters in their case, compared to 25 to 40 nodes in this work). Parameters n_t and n_τ are the number of time steps recorded during the TRT and the number of optimization parameters (i.e., 25 to 40), respectively. Parameter $W_1(t)$ is a weighing vector, emphasizing the reconstruction of early time steps (values of 3 for the first 300 time steps and values of 1 for the remaining ones), W_2 and W_3 are scalar weights to specify the proportion of the second and third terms in the objective function. In the deconvolution implementation, $W_2 = 10$ and $W_3 = 100$, which provide proportions of 70-90 % for the first term and 5-15 % for the second and third terms. The chosen weights are based on observations made in Dion et al. (2022a) [205] and are set to obtain the best compromise between function smoothness and temperature reconstruction, without overfitting experimental data.

The constraints in Eqs. C_1 and C_2 limits $\hat{g}(\tau)$ to be strictly growing and to have a strictly downward first derivative after a certain node j, equivalent to at least 4 hours of testing. These constraints are built so that the STgF respects physical properties and accelerate the convergence rate of the optimization, since the parameters space is smaller.

In Eqs. 6.19, 6.20, C_1 and C_2, the estimated $\hat{g}$ is defined as a function of t or τ. It is stressed that the deconvolution algorithm is implemented on the optimization parameters $\hat{g}(\tau)$, but that an interpolated $\hat{g}(t)$ is used to compute Eq. 6.20, since $\widehat{T}(t)$ is computed with Eq. 6.1. The interpolator applied both in and after the optimization process is a piecewise cubic Hermite interpolating polynomial (PCHIP), because it performs better over flat regions, which is more akin to a STgF's shape [194]. Note in particular that as $\hat{g}(\tau)$ is strictly increasing thanks to C1, $\hat{g}(t)$ interpolated by PCHIP is also strictly increasing by construction.

Lastly, an initial solution as precise as possible helps an optimization problem to converge. Here, the initial guess is obtained by a rapid optimization of 2 parameters on the exponential integral equation, which describes the STgF. The algorithm minimizes the RMSE between convolved and experimental temperature signals, as follows:

$$\hat{x}_{1,2} = \min_{x_1,x_2} \sqrt{\left[\left(f * \left(x_1 \int_{x_2/t} \frac{e^{-t}}{t} dt\right)\right) - T_{exp}\right]^2} \tag{6.21}$$

Then, the initial guess passed to the main optimization is computed as:

$$\hat{g}_0(t) = \hat{x}_1 \int_{\hat{x}_2/t} \frac{e^{-t}}{t} dt \tag{6.22}$$

CHAPITRE 7 DISCUSSION GÉNÉRALE

L'objectif général de cette thèse est de développer un algorithme de déconvolution permettant d'obtenir la fonction de transfert à court terme d'un ÉCS à partir des données expérimentales d'un ERT pour aider son interprétation. Les différents sous-objectifs ciblés visent à concevoir la méthode de déconvolution et l'étoffer en la validant pour plusieurs situations variées. Ce chapitre a pour but de contextualiser les gains à employer un algorithme de déconvolution pour interpréter un ERT, ainsi que de souligner ses limites et finalement suggérer des améliorations méthodologiques à l'algorithme développé.

7.1 Bénéfices à l'utilisation de l'algorithme de déconvolution

L'algorithme de déconvolution développé au chapitre 4 (Article 1) et peaufiné aux chapitres 5 et 6 permet d'évaluation les fonctions de transfert comparé aux algorithmes proposés par Monteyne et al. (2014) [176] et Beier (2020a) [177]. Dans ce dernier, dû à la lourdeur des calculs, un échantillonnage des données doit être fait pour que l'algorithme converge rapidement. L'algorithme développé durant ce projet de recherche permet de conserver l'ensemble des données expérimentales lors de l'interprétation, en plus de converger en moins de 5 secondes pour l'ensemble des cas testés. De plus, les fonctions objectifs utilisées dans chaque article de ce projet n'utilisent pas de signal transformé, telle que la fonction objectif présentée par Beier (2020a) [177], qui lisse la dérivée des températures expérimentales.

La déconvolution est une méthode qui se distingue des approches conventionnelles, car elle ne recourt à aucun modèle de transfert thermique. Ainsi, elle n'est pas limitée par des hypothèses simplificatrices du transfert de chaleur, comme c'est le cas pour les modèles analytiques ni par de longs délais de développement et de calcul inhérents aux modèles numériques.

La liste suivante présente les gains mis en évidence par l'utilisation de la méthode de déconvolution pour différents thèmes étudiés lors de ces travaux :

Développement de l'algorithme de déconvolution

- Le patron de charge utilisé lors d'un ERT n'a pas une influence marquée sur la précision de la fonction de transfert obtenue par déconvolution.
- De courtes interruptions lors d'un ERT peuvent être interprétées par déconvolution en posant l'hypothèse que la stationnarité du système n'a pas été largement affectée.
- La déconvolution permet de modéliser le changement abrupt de température lors de l'arrivée de l'eau chauffée à la fin du temps de résidence initial du fluide caloporteur

dans l'ÉCS.

- Les fonctions de transfert des PFB et des PCP sont similaires, et les différences entre les deux correspondent principalement au débit de circulation permettant un plus grand échange thermique pour les PCP.
- La déconvolution peut être utilisée sur les données d'un ERTD, où des fonctions de transfert en fonction de la lithologie du sol sont obtenues. Dans ce cas, le système déconvolué est la chaleur émise par l'ÉCS entre deux niveaux de profondeur.
- Lors de l'opération d'un système géothermique, si les conditions d'opération sont maintenues constantes, la déconvolution stationnaire permet d'obtenir une fonction de transfert à long terme, pourvu que la mise en marche du chauffage soit enregistrée au début des signaux de température (c.-à-d. qu'au temps initial, le fluide circule dans l'ÉCS, mais le chauffage n'est pas activé) [206].

Traitement de cas non stationnaire

- Les changements de conditions d'opération peuvent être simulés à l'aide d'une convolution non stationnaire. Inversement, des fonctions de transfert peuvent être obtenues par une méthode de déconvolution non stationnaire, où chaque fonction décrit l'échange thermique de l'ÉCS pour des conditions d'opération fixes.
- La convolution non stationnaire telle que définie par Beaudry et al. (2021) [143] nécessite des fonctions de transfert aussi longues que leur dernier pas de temps durant l'ERT, c'est-à-dire, jusqu'à la dernière instance temporelle d'un ensemble de conditions d'opération. Cela indique que les fonctions de transfert déconvoluées n'ont pas toutes la même longueur.
- La méthode de déconvolution non stationnaire a été validée expérimentalement pour des données d'un PCP où l'effet de la saignée est un des paramètres affectant la stationnarité du système. La différence entre les fonctions de transfert pour différents débits de saignée montre qualitativement l'impact de cette technique sur le transfert de chaleur. Plus la saignée est importante, plus la fonction de transfert est aplatie, donc plus le transfert de chaleur est efficace.

Interprétation de fonctions de transfert

- En utilisant l'approximation de premier ordre de la SLI, la conductivité thermique effective de l'ÉCS peut être calculée à l'aide d'une fonction de transfert déconvoluée. Cette opération peut également être faite sur les données d'un ERTD pour obtenir un profil de conductivité thermique.
- Pour les signaux à la sortie de l'ÉCS, les fonctions de transfert ou les températures donnent des conductivités thermiques semblables. Ainsi, interpréter les deux types de signaux peut contribuer à la robustesse de l'estimation des paramètres thermiques.

— Une hypothèse de la SLI est que la chaleur est émise de façon constante sur une ligne infinie et radialement sur tout le modèle, qui n'est pas parfaitement respectée lors d'un ERTD. Moins le débit de circulation est élevé, plus la température varie grandement le long de l'ÉCS. L'interprétation des fonctions de transfert d'un ERTD permet d'obtenir des conductivités thermiques plus robustes qu'avec les signaux de températures, surtout lors d'un essai à faible débit de circulation.
— Une propriété intéressante des fonctions de transfert est que leur dérivée est lisse. Pasquier (2018) [108] a développé une méthode d'interprétation par une régression entre la dérivée de l'approximation de la SLI et la dérivée temporelle des températures. Cependant, les températures tendent à être trop bruitées pour être analysées efficacement avec cette méthode dès qu'un ERT dépasse quelques heures. Par construction, une fonction de transfert ainsi que sa dérivée sont lisses sur toute la longueur de l'essai déconvolué. Ainsi, appliquer cette méthode d'interprétation aux fonctions de transfert permet d'obtenir la conductivité thermique à l'aide d'une méthode supplémentaire et confirme sa valeur [227].

Ainsi, la méthode de déconvolution établie permet d'obtenir une fonction de transfert d'un ÉCS en situation stationnaire et plusieurs fonctions de transfert en situation non stationnaire. L'algorithme s'applique à la fois à la sortie de l'ÉCS, ainsi qu'en fonction de la profondeur. Il permet l'interprétation de données expérimentales d'un PBF ou d'un PCP et la conductivité thermique des ÉCS peut être calculée robustement à l'aide des fonctions de transfert.

7.2 Limitations de la méthode de déconvolution

La technique de déconvolution choisie étant basée sur une optimisation qui s'applique à des données réelles et bruitées, différentes sources d'erreurs limitent la précision et la convergence de l'algorithme. Ces effets se regroupent en deux principales catégories : les erreurs sur la prise de données et sur la méthode d'optimisation.

7.2.1 Prise de données

L'article 1 de ce projet de recherche (chapitre 4) démontre que la fonction de transfert déconvoluée n'est pas influencée significativement par du bruit d'enregistrement. En effet, filtrer les données expérimentales à l'aide d'un filtre passe-bas de type moyenne mobile ou moyenne mobile gaussienne n'apporte pas de bénéfices clairs sur la précision des fonctions de transfert ou la reconstruction des températures. Par contre, pour des données assez bruitées, l'avantage d'un filtre est que l'ajustement des températures ne se fait pas sur le bruit, mais bien sur le signal réel. Par exemple, les outils d'enregistrements des profils verticaux par fibre optique

pour les ERTD peuvent avoir de basses résolutions allant jusqu'à une erreur de ±0.5 °C.

L'article 1 discute aussi de l'impact du choix adéquat de la température initiale de l'ÉCS avant le chauffage sur la simulation des températures (voir la figure 4.12). La température initiale est sélectionnée comme une moyenne des températures lors de la recirculation du fluide dans l'ÉCS avant le chauffage. Toutefois, cela s'applique seulement pour un système où aucune perturbation thermique n'a été subie depuis un certain temps. Pour un système où les charges sont appelées dynamiquement, la température initiale du sol peut devenir difficile à estimer correctement. Un élément à intégrer à la déconvolution serait donc d'optimiser la valeur de cette température pour assurer une reconstruction adéquate des températures.

De plus, aucun des articles de ce projet de recherche ne quantifie l'effet d'une erreur systématique sur la prise de données, c'est-à-dire qui affecte la justesse des valeurs enregistrées. Ce type d'erreur aurait un impact sur l'impulsion de la fonction incrémentale de charge dans l'équation 2.8, affectant la reconstruction de la fonction de transfert et la justesse de simulations subséquentes. Il est donc prudent d'avancer qu'un tel biais doit être minimisé à l'aide d'une calibration minutieuse des capteurs, ou corrigé avant l'interprétation des données.

7.2.2 Méthode d'optimisation

À titre de rappel, la déconvolution est un problème dit *mal posé* [153], c'est-à-dire que le bruit d'enregistrement sur les données peut empêcher la bonne reconstruction de la fonction de transfert. Cet énoncé peut sembler contre-intuitif considérant les éléments mentionnés à la section précédente, mais l'emphase ici est sur la distinction entre les erreurs sur les mesures (précision) et l'erreur systématique sur toutes les mesures (justesse). Pour le problème de déconvolution rencontré en géothermie de basse température, les capteurs de températures ont une résolution numérique adéquate pour que la précision des mesures n'affecte pas la convergence de la déconvolution (±0.1 °C). Construire les fonctions de transfert avec un nombre réduit de noeuds aide aussi en ce sens, ce qui n'était pas possible avec la méthode de déconvolution matricielle présentée par Dion et al. (2021a) [233]. Néanmoins, un biais systématique entraînerait une erreur systématique sur la fonction de transfert reconstruite, affectant la précision sur toutes simulations subséquentes, ainsi que sur l'interprétation par approximation de premier ordre de la SLI.

La méthode de déconvolution retenue est basée sur une optimisation contrainte et bornée. Ces contraintes et bornes réduisent l'espace possible des paramètres, aidant à converger plus rapidement vers un l'optimum de la fonction objectif. Toutefois, il y a aussi un risque augmenté de ne pas converger. Différentes causes connues expliquent qu'un algorithme d'optimisation ne converge pas correctement, telles qu'une convergence prématurée, une faible causalité entre

les paramètres et la réponse du modèle, une fonction objectif rugueuse, des minimums locaux et un surajustement ou une simplification excessive du problème [116].

Pour la méthode de déconvolution, l'espace des paramètres est défini par l'ensemble des valeurs que peuvent avoir les noeuds de la fonction de transfert. Ainsi, il n'est pas possible de visualiser l'hypersurface de la fonction objectif pour en définir sa forme. L'analyse en 2D présentée à la figure 5.9 montre toutefois une forme souhaitable lorsque 2 noeuds varient. La complexité d'analyser la fonction objectif rend ardue l'identification d'une mauvaise convergence. Les algorithmes de déconvolution de cette thèse sont néanmoins convenablement stables en situation stationnaire. De plus, les RMSE entre les signaux de températures expérimentales et convoluées sont d'une précision compatible avec la précision des jauges de température généralement utilisées pour un ERT. Pour les cas non stationnaires, une difficulté supplémentaire à la convergence est le nombre élevé de paramètres d'optimisation, puisqu'il y a plusieurs fonctions de transfert. L'algorithme se montre toutefois stable pour un cas où quatre fonctions de transfert sont déconvoluées [206].

Des tolérances de convergence sont employées pour définir la précision que la solution de l'optimisation doit atteindre pour converger. Pour identifier ces tolérances, une approche par tâtonnement assez flexible pour converger sans surajustement et assez stricte pour ne pas trop simplifier la solution, a été utilisée. Cependant, les nombreux essais faits lors de l'élaboration de la méthode ont montré qu'il est difficile d'avoir des tolérances justes. Entre autres, si le RMSE d'un signal reconstruit est plus petit que la précision des instruments de lectures, comme rencontré dans l'article 2, cela peu indiquer un surajustement. Les termes de régularisations (par exemple, les équations 4.5 et 4.6) aident également la fonction objectif à converger en évitant l'ajustement seulement sur le signal de température.

Une dernière limitation à la méthode de déconvolution provient de la précision de la solution initiale de la fonction de transfert ($\hat{g}_0$). Pour l'instant, cette fonction est définie par une équation exponentielle intégrale sur laquelle deux paramètres sont optimisés pour ajuster les températures convoluées et expérimentales (il s'agit d'une version simplifiée comparée à celle présentée à la section 4.3.3). Ainsi, cette première solution est basée sur le modèle de la SLI. Une façon d'aider la convergence du problème serait de fournir une solution initiale encore plus exacte en employant un modèle de transfert thermique encore plus précis, tout en gardant la rapidité de calcul de la présente méthode.

7.2.3 Simulation d'un système géothermique à plusieurs puits

Les diverses méthodes de déconvolution développées durant ce projet de recherche permettent d'obtenir les fonctions de transfert à court terme d'un ÉCS d'*exploration* sur lequel un ERT

est effectué. Ces ÉCS préliminaires servent à étudier les caractéristiques du site avant de concevoir le système géothermique final. Lorsque la demande énergétique du bâtiment est assez élevée et que d'autres ÉCS sont forés, il est commun de réutiliser l'ÉCS d'exploration dans le système final, rentabilisant ainsi l'investissement dans ce puits. À noter que l'utilisation de PCP permet de réduire la longueur totale de forage d'un projet, limitant donc le nombre de puits supplémentaires devant être forés [15, 16].

La fonction de transfert déconvoluée à partir de l'ERT sur l'ÉCS d'exploration représente la réponse d'un seul puits et ne peut pas être utilisée pour simuler un système géothermique complet à plusieurs puits. Pour une simulation à court terme, simplement multiplier le puits d'exploration est une approche suffisante, puisqu'il n'y a pas d'interaction thermique entre les échangeurs. La problématique survient lorsqu'une simulation assez longue pour qu'il y ait une telle interaction est tentée. Dans ce cas, une superposition spatiale peut être envisagée pour obtenir une fonction de transfert combinant plusieurs ÉCS à partir d'une seule fonction. D'autres recherches doivent être effectuées pour valider un modèle permettant d'obtenir une fonction de transfert expérimentale effective de plusieurs puits à partir d'un ERT.

7.3 Suggestions méthodologiques et stratégiques pour l'application de la déconvolution

La méthode de déconvolution a été développée comme un outil permettant d'aider l'interprétation des ERT. Ainsi, cette section a pour but d'identifier où des actions peuvent être posées pour assurer une utilisation adéquate de la déconvolution, maximisant ainsi les bénéfices de la méthode.

D'abord, une procédure typique pour concevoir un système géothermique incluant la déconvolution peut être décrite telle qu'à la figure 7.1. Dans cette dernière, la déconvolution se retrouve à l'étape d'interpréter les données d'essais (Étape 3). On peut ensuite utiliser la fonction de transfert à court terme et les paramètres thermiques obtenus avec celle-ci pour simuler et dimensionner le système géothermique (Étape 4). Les étapes de la figure 7.1 peuvent s'appliquer autant sur des PBF que sur des PCP, mais pour ce dernier, l'effet de l'écoulement souterrain est notablement plus important. Ainsi, l'essai de pompage doit être effectué pour ce type d'ÉCS. De plus, l'utilisation de la fibre optique ou d'un appareil équivalent pour mesurer un profil vertical de température est recommandé pour aider à localiser la ou les unités géologiques à atteindre lors du forage pour de futurs ÉCS. Le reste de la présente section décrit plusieurs stratégies à appliquer aux Étape 2 et Étape 3 de la figure 7.1 pour assurer la bonne exécution de la méthode de déconvolution, ainsi que des considérations concernant l'Étape 4.

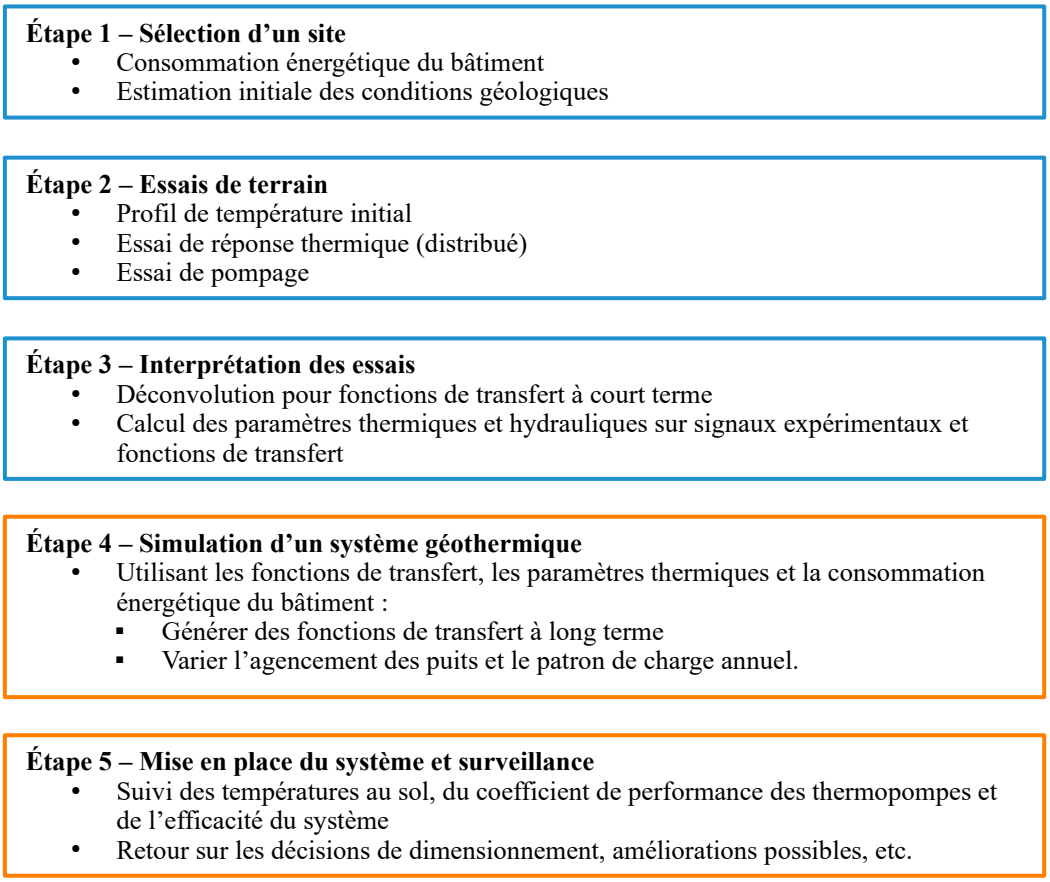

FIGURE 7.1 Étapes pour concevoir un système géothermique impliquant une méthode de déconvolution lors de l'interprétation des essais.

À propos de l'Étape 2, maintenir un état stationnaire est primordial pour interpréter un ERT avec succès à l'aide de la déconvolution, de même que pour la plupart des méthodes d'interprétation d'ailleurs. Pour être stationnaires, les conditions d'opération doivent demeurer les plus constantes possible tout au long de l'essai. Pour des changements marqués, la déconvolution non stationnaire peut être employée. Néanmoins, pour chaque segment entre les transitions d'états, les conditions d'opération doivent tout de même rester stables. Une situation typique à éviter pendant un ERT survient lorsque le débit de circulation varie dès l'activation de l'élément chauffant, un phénomène attribuable à la grande demande énergétique qui divise la répartition du courant électrique dans l'unité d'ERT. Pour prévenir cet effet, le recours à des contrôles et à un système approprié dans l'unité d'ERT sont essentiels. Les interruptions ont aussi un impact sur la stationnarité du système. L'article 1 (chapitre 4) présente la méthode de déconvolution comme permettant l'interprétation d'un ERT malgré une interruption. Il est à noter que ce point est valide lorsque cette dernière est courte. En

effet, si le débit de circulation est arrêté, le *système* définit par l'ÉCS où un fluide circule ne respecte plus les conditions de stationnarité. En résumé, les bonnes pratiques pour effectuer un ERT sont de bien calibrer les capteurs avant et après l'essai, s'assurer d'une circulation en continu pendant l'essai et d'éviter le changement lent des conditions d'opérations. Ces points sont aussi valides pour les essais de pompage.

Concernant l'Étape 3 sur les stratégies d'interprétation d'un ERT, une moyenne mobile peut être utilisée comme filtre passe-bas lorsque les erreurs d'enregistrement sur les données expérimentales sont trop élevées. Si un filtre est employé, la fenêtre ne doit comprendre que quelques points autour du point filtré pour ne pas déformer le signal d'origine. La méthode de déconvolution stationnaire optimise environ 25 et 50 noeuds et a des tolérances fixées pour généralement converger lorsque des données d'ERT sont utilisées. Toutefois, l'utilisateur doit rester à l'affût et modifier ces valeurs si l'algorithme ne converge pas. Ensuite, il est recommandé d'appliquer les méthodes d'interprétation pour obtenir les paramètres thermiques et hydrauliques à la fois sur les données expérimentales et sur les fonctions de transfert pour assurer leur identification robuste. En cas de différences, la valeur retenue peut être soit une moyenne des valeurs obtenues ou celle qui entraine un dimensionnement conservatif de l'ÉCS.

À l'égard de l'Étape 4 sur la simulation d'un système géothermique, la fonction de transfert à court terme peut être jointe à une fonction à long terme obtenue d'un modèle de transfert de chaleur tel que la source linéique finie. Ainsi, les températures à l'ÉCS peuvent être validées pour une ou plusieurs années d'opération à l'aide du profil de la demande énergétique du bâtiment.

Finalement, en intégrant la déconvolution à l'interprétation d'un ERT, les données expérimentales de ce dernier sont davantage valorisées par l'utilisation et l'interprétation des fonctions de transfert. Ainsi, cette méthodologie permet d'aider au dimensionnement précis d'un système géothermique.

7.4 Applications de la méthode de déconvolution

Durant les travaux de ce projet de recherche, la déconvolution a été appliquée à des données expérimentales de températures entourant l'exploitation d'un ÉCS par des ERT. Toutefois, comme mis en évidence à la section 2.3.1, la déconvolution est une technique utilisée dans divers domaines des géosciences.

Pourvu que les données à déconvoluer sous-entendent la même physique de phénomène qu'un ERT, la méthode développée au cours de ce projet a le potentiel d'être utilisée pour différents types d'essais. Entre autres, les essais de pompages (EDP) respectent ces paramètres, en

plus d'être un essai type à réaliser pour concevoir un système géothermique, tel que décrit à l'Étape 2 de la figure 7.1. Lors d'un tel essai, l'eau souterraine est pompée d'un puits d'exploration et les rabattements sont mesurés au puits. L'interprétation de cet essai permet de calculer la conductivité hydraulique effective du sol entourant le puits. Ainsi, une fonction de transfert hydraulique décrirait la réponse en rabattement du puits sous une impulsion unitaire et constante de pompage. Cette fonction serait, par construction, strictement positive et croissante. À titre d'exemple, la figure 7.2 montre l'application de la déconvolution à un essai de pompage. Ainsi, il pourrait être bénéfique d'incorporer une déconvolution à la fois des données d'un EDP et d'un ERT pour interpréter adéquatement les essais de terrain réalisés pour dimensionner un ÉCS.

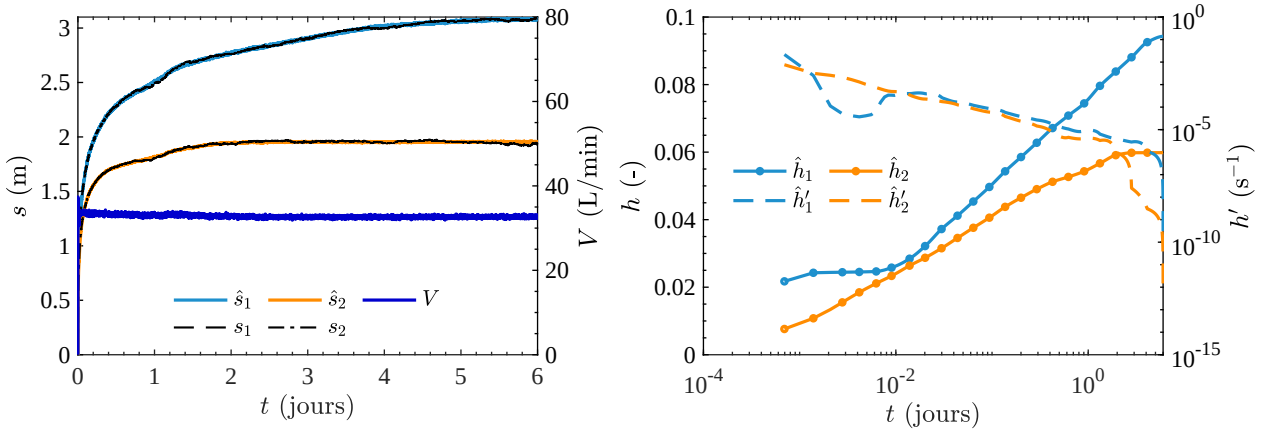

FIGURE 7.2 Déconvolution d'un essai de pompage à l'aide de la méthode de déconvolution développée pour interpréter un essai de réponse thermique.

La déconvolution pourrait aussi être utilisée pour obtenir des fonctions de transfert sur des systèmes géothermiques déjà en marche. Ce faisant, les coefficients de performance du système pourraient être évalués en comparant les fonctions de transfert pour différentes périodes de temps. L'évolution de la performance thermique d'un système géothermique pourrait être suivie au fil du temps, ce qui permettrait d'anticiper les périodes de maintenance des équipements. Ainsi, la déconvolution a le potentiel d'être utilisée à l'Étape 5 de la figure 7.1 pour la surveillance du système géothermique.

CHAPITRE 8 CONCLUSION

Les systèmes géothermiques de basse température permettent de réduire la quantité d'énergie utilisée pour chauffer et climatiser un bâtiment, grâce à l'efficacité énergétique des thermopompes géothermiques. La conception de ces systèmes est néanmoins un processus complexe. Suivant l'évaluation des besoins énergétiques du bâtiment, un échangeur de chaleur souterrain est dimensionné pour répondre le plus adéquatement possible à cette demande. Ce dimensionnement est fait à l'aide des paramètres thermiques du sol qui sont communément obtenus en interprétant un essai de réponse thermique. À l'aide de ces paramètres, des simulations sont effectuées pour valider le nombre, les dimensions et l'agencement des échangeurs de chaleur souterrains composant le système géothermique.

Les méthodes d'interprétation des essais de réponse thermique utilisent un modèle de transfert de chaleur pour reproduire les processus d'échange thermique dans l'échangeur de chaleur souterrain et le sol. Ces processus sont résumés par les paramètres thermiques du site étudié, qui sont identifiés durant l'interprétation pour reproduire les températures expérimentales de l'essai de réponse thermique. Les fonctions de transfert représentent un modèle de transfert de chaleur qui émule la réponse thermique de l'échangeur de chaleur souterrain sous une charge unitaire et constante, tout en intégrant les paramètres thermiques de l'échangeur de chaleur souterrain et du sol. En les employant, la simulation des températures à la sortie de l'échangeur de chaleur souterrain en fonction d'un patron de chauffage est possible. Une limite à l'utilisation des fonctions de transfert est qu'il est nécessaire d'utiliser un modèle de transfert de chaleur analytique ou numérique pour les produire. L'objectif de ces travaux de recherche est de proposer une méthode permettant d'obtenir les fonctions de transfert sans ces modèles.

8.1 Synthèse des travaux

Les travaux de ce projet de recherche ont permis de répondre à l'objectif général qui est de proposer une méthode de déconvolution flexible, précise et performante s'appliquant aux données expérimentales d'un essai de réponse thermique afin d'obtenir une fonction de transfert à court terme à la sortie d'un échangeur de chaleur souterrain.

La méthode par optimisation retenue reprend des idées provenant de plusieurs domaines des géosciences tels que mis en évidence dans la revue de littérature (chapitre 2). Cette méthode, qui est présentée dans le premier article (chapitre 4), obtient des fonctions de transfert à

court terme expérimentales pour des échangeurs de chaleur souterrains de type puits en boucle fermée ou puits à colonne permanente ainsi que pour différents patrons de chauffage, répondant ainsi à l'objectif spécifique 1. L'algorithme de déconvolution a d'abord été validé expérimentalement sur des essais de réponse thermique où les conditions d'opération sont stationnaires.

Pour considérer les variations des conditions d'opération lors d'un essai de réponse thermique, l'utilisation d'une convolution non stationnaire a ensuite été utilisée au second article (chapitre 5) pour mettre en place une déconvolution qui obtient plusieurs fonctions de transfert en fonction des changements d'état lors d'un essai de réponse thermique. Ce faisant, la déconvolution peut s'appliquer à des situations beaucoup plus près de l'opération d'un système géothermique en marche, remplissant ainsi l'objectif spécifique 2.

Pour aider au dimensionnement et au design d'un système géothermique, le troisième article (chapitre 6) utilise la déconvolution pour obtenir une fonction de transfert et une estimation de la conductivité thermique pour chaque unité géologique du sol au site étudié. La distribution verticale de la conductivité thermique selon la profondeur d'un échangeur de chaleur souterrain permet d'aider à identifier la profondeur appropriée à atteindre lors du forage d'autres échangeurs de chaleur souterrain pour un système géothermique à plusieurs puits, atteignant ainsi l'objectif spécifique 3.

Finalement, des articles de conférences ont alimenté la robustesse de la déconvolution stationnaire en l'appliquant avec succès aux données d'une année d'opération d'un système géothermique pour un cas numérique [206] et ont montré que la dérivée lisse des fonctions de transfert peut être utilisée pour obtenir une estimation des paramètres thermiques avec des essais de réponse thermique d'une durée de 24 heures [227]. De plus, la déconvolution non stationnaire a été validée sur un long essai de réponse thermique de 30 jours [206].

8.2 Contributions originales

L'originalité des travaux présentés est exprimée par la proposition d'une méthode de déconvolution novatrice pour interpréter un essai de réponse thermique. Dans un premier temps, les fonctions de transfert à court terme peuvent désormais être obtenues en utilisant uniquement les données expérimentales d'un essai de réponse thermique, qu'il soit stationnaire ou non. Dans un second temps, ces fonctions peuvent être interprétées, permettant le calcul des propriétés thermiques du sol et de l'échangeur de chaleur souterrain.

La contribution originale de la méthode de déconvolution proposée au chapitre 4 comparée à l'approche de Beier (2020a) [177] est que l'ensemble des données expérimentales sont utilisées

lors de l'optimisation, sans échantillonnage. De plus, la fonction de transfert expérimentale est explicitée (comparé aux travaux de Monteyne et al. (2014) [176]) et elle est directement utilisable pour simuler la réponse de l'échangeur de chaleur souterrain, puisqu'elle retire la température initiale du puits. Aussi, la déconvolution permet d'obtenir la fonction de transfert sans utiliser de modèle de transfert thermique analytique ou numérique.

Auparavant, la simulation de la réponse non stationnaire d'un échangeur de chaleur souterrain devait se faire à l'aide d'un modèle numérique complexe. À l'aide de la méthode de déconvolution non stationnaire présentée au chapitre 5, les fonctions de transfert peuvent maintenant être obtenues directement à l'aide des données expérimentales d'un essai de réponse thermique, et ce autant pour les puits en boucle fermée que pour les puits à colonne permanente.

Finalement, les méthodes usuelles d'interprétation des essais de réponse thermique traitent les signaux de températures pour calculer les propriétés thermiques du sol et de l'échangeur de chaleur souterrain. Ensuite, les fonctions de transfert sont évaluées à l'aide de ces propriétés. Les contributions mises de l'avant au chapitre 6 permettent d'obtenir les propriétés thermiques effectives du puits à l'aide des fonctions de transfert déconvoluées. De plus, l'approche présentée permet d'évaluer le profil vertical de conductivité thermique pour chaque unité géologique de façon robuste à l'aide des fonctions de transfert.

8.3 Utilisations de la déconvolution et applications futures

Cette dernière section vise à résumer les situations dans lesquelles la méthode de déconvolution a été utilisée au cours de ce projet de recherche, ainsi que de suggérer certains axes de recherche et applications futures. La liste suivante énumère sur quel type de données la déconvolution a été appliquée :

- Des essais de réponse thermique (réguliers et distribués) stationnaires et non stationnaires entre 4 et 10 jours pour des échangeurs de chaleur souterrains de type puits en boucles fermées et puits à colonne permanente (chapitres 4, 5, 6)
- Des simulations numériques de l'opération d'un puits à colonne permanente d'une durée de 1 an en conditions stationnaires [206]
- Un essai de réponse thermique expérimental de 30 jours d'un puits à colonne permanente avec des conditions d'opération non stationnaires [206]

Les développements futurs de l'algorithme de déconvolution devront viser à augmenter la performance et à intégrer plus de paramètres à l'optimisation. Par exemple, ajouter l'obtention de la température initiale avant une période de chauffage aiderait à assurer que le premier noeud de la fonction de transfert déconvoluée ait une valeur de zéro. En pratique,

le noeud est près de zéro, mais sous certaines conditions, il peut y avoir un écart, créant une fonction non réaliste. Aussi, il serait important de renforcer l'algorithme face à des effets tels que des données trouées. Deux scénarios peuvent alors être étudiés : un essai de réponse thermique qui a une interruption prolongée et lorsque les données ne sont pas enregistrées ou récupérables, mais que le système est néanmoins en opération. Finalement, une application intéressante serait d'intégrer une méthode stochastique, telle que l'inférence bayésienne, à l'évaluation de chaque noeud d'une fonction de transfert pour identifier l'incertitude sur la fonction obtenue.

Les utilités de la déconvolution pourraient être étendues pour considérer la simulation de systèmes géothermiques à plusieurs puits à partir d'un seul ÉCS. L'argument principal limitant la pertinence de la déconvolution pour éventuellement simuler dynamiquement un champ d'échangeurs de chaleur souterrain est que la fonction de transfert obtenue n'est valide que pour les conditions d'opération de l'essai de réponse thermique. Ainsi, un prochain axe de recherche serait de valider une méthode combinant spatialement les fonctions de transfert d'un champ d'échangeurs de chaleur souterrains. À court terme, il n'y a pas d'interaction thermique entre les puits, mais à long terme, ces interactions doivent être examinées en fonction de la configuration du champ d'échangeurs.

Finalement, la déconvolution pourrait avoir un rôle de contrôle et d'analyse de la performance d'un système géothermique en fonction. L'étude de l'évolution temporelle des fonctions de transfert permet une interprétation simplifiée de l'efficacité d'un système géothermique, comparée aux profils de température. Pour un système géothermique en fonction, ces dernières sont très variables. Il est donc difficile de jauger l'évolution de l'efficacité globale du système dans le temps. Un sujet de recherche futur serait d'utiliser la déconvolution pour analyser la performance d'un champ d'échangeurs de chaleur souterrain en marche à l'aide des fonctions de transfert. Par exemple, comparer les fonctions de transfert pour un ÉCS d'année en année pour une même période et les mêmes conditions d'opération. À noter que dans ce cas, un défi serait d'avoir les impulsions de températures à des moments similaires pour reconstruire les fonctions de transfert sur des périodes semblables. À terme, cette idée pourrait être étendue à un système de surveillance des performances du système qui serait intégré au système d'enregistrement des données. Ainsi, l'évaluation de la fonction de transfert se ferait en temps réel. Une alerte pourrait être émise lorsqu'il y a une différence significative entre la fonction de transfert présente et celle d'une période similaire. Cette différence peut être attribuable à la diminution de la performance du système.

RÉFÉRENCES

[1] G. Beaudry, P. Pasquier et D. Marcotte, “The impact of rock fracturing and pump intake location on the thermal recovery of a standing column well : model development, experimental validation, and numerical analysis,” *Science and Technology for the Built Environment*, vol. 25, n°. 8, p. 1052–1068, sept. 2019. [En ligne]. Disponible : https://www.tandfonline.com/doi/full/10.1080/23744731.2019.1648133

[2] S. Fawzy *et al.*, “Strategies for mitigation of climate change : a review,” *Environmental Chemistry Letters*, vol. 18, n°. 6, p. 2069–2094, nov. 2020. [En ligne]. Disponible : https://doi.org/10.1007/s10311-020-01059-w

[3] IEA, “CO2 Emissions in 2022,” International Energy Agency, Paris, Rapport technique, 2023. [En ligne]. Disponible : https://www.iea.org/reports/co2-emissions-in-2022

[4] C. A. Horowitz, “Paris Agreement,” *International Legal Materials*, vol. 55, n°. 4, p. 740–755, août 2016, publisher : Cambridge University Press. [En ligne]. Disponible : https://www.cambridge.org/core/journals/international-legal-materials/article/abs/paris-agreement/1EC0C66C41C86DE533D3BD777B997B16

[5] Loi Canadienne, “Loi canadienne sur la responsabilité en matière de carboneutralité,” Gouvernement du Canada, Lois codifiées L.C. 2021, ch. 22, mai 2023. [En ligne]. Disponible : https://laws.justice.gc.ca/PDF/C-19.3.pdf

[6] Gouvernement du Québec, *Gagnant pour le Québec, gagnant pour la planète : plan pour une économie verte 2030. Politique-cadre d’électrification et de lutte contre les changements climatiques.* Québec (Québec) : Ministère de l’environnement et de la lutte contre les changements climatiques, 2020, oCLC : 1333529825. [En ligne]. Disponible : https://cdn-contenu.quebec.ca/cdn-contenu/adm/min/environnement/publications-adm/plan-economie-verte/plan-economie-verte-2030.pdf

[7] IEA, “Renewables 2022,” International Energy Agency, Paris, Rapport technique, déc. 2022.

[8] Gouvernement du Québec, “Plan de mise en œuvre 2023-2028 du Plan pour une économie verte 2030,” Gouvernement du Québec, Rapport technique, 2023, iSBN 978-2-550-91029-9. [En ligne]. Disponible : https://cdn-contenu.quebec.ca/cdn-contenu/adm/min/environnement/publications-adm/plan-economie-verte/plan-mise-oeuvre-2023-2028.pdf

[9] J. Dion *et al.*, “Vers un Canada carboneutre : s’inscrire dans la transition globale.” Institut canadien pour des choix climatiques, Rapport technique, févr. 2021.

[10] J. Whitmore et P.-O. Pineau, “État de l’énergie au Québec 2023,” Chaire de gestion du secteur de l’énergie, HEC Montréal, Rapport technique, févr. 2023. [En ligne]. Disponible : https://energie.hec.ca/eeq/

[11] IEA, “Heat Pumps,” International Energy Agency, Paris, Rapport technique, 2022. [En ligne]. Disponible : https://www.iea.org/reports/heat-pumps

[12] A. Mustafa Omer, “Ground-source heat pumps systems and applications,” *Renewable and Sustainable Energy Reviews*, vol. 12, n°. 2, p. 344–371, févr. 2008. [En ligne]. Disponible : https://www.sciencedirect.com/science/article/pii/S1364032106001249

[13] T. You *et al.*, “An overview of the problems and solutions of soil thermal imbalance of ground-coupled heat pumps in cold regions,” *Applied Energy*, vol. 177, p. 515–536, sept. 2016. [En ligne]. Disponible : https://linkinghub.elsevier.com/retrieve/pii/S0306261916307218

[14] P. Cui *et al.*, “Advances in ground heat exchangers for space heating and cooling : Review and perspectives,” *Energy and Built Environment*, oct. 2022. [En ligne]. Disponible : https://www.sciencedirect.com/science/article/pii/S2666123322000733

[15] Z. D. O’Neill, J. D. Spitler et S. J. Rees, “Performance Analysis of Standing Column Well Ground Heat Exchanger Systems,” *ASHRAE Transactions*, vol. 112(2), p. 12 (633–643), 2006.

[16] P. Pasquier *et al.*, “Standing column wells,” dans *Advances in Ground-Source Heat Pump Systems*. Elsevier, 2016, p. 269–294. [En ligne]. Disponible : https://linkinghub.elsevier.com/retrieve/pii/B9780081003114000108

[17] C. Lee, “Thermal performance of a standing column well geothermal heat exchanger system using re-injection of bleeding water,” *Geothermics*, vol. 82, p. 73–80, nov. 2019. [En ligne]. Disponible : https://linkinghub.elsevier.com/retrieve/pii/S0375650519301245

[18] J. D. Spitler et S. E. A. Gehlin, “Thermal response testing for ground source heat pump systems—An historical review,” *Renewable and Sustainable Energy Reviews*, vol. 50, p. 1125–1137, oct. 2015. [En ligne]. Disponible : http://www.sciencedirect.com/science/article/pii/S1364032115005328

[19] H. J. L. Witte, G. J. van Gelder et J. D. Spitler, “In Situ Measurement of Ground Thermal Conductivity : The Dutch Perspective,” *ASHRAE Transactions*, vol. 108, p. 21, 2002.

[20] S. Rees, *Advances in Ground-Source Heat Pump Systems*. Elsevier, mai 2016. [En ligne]. Disponible : https://www.elsevier.com/books/advances-in-ground-source-heat-pump-systems/rees/978-0-08-100311-4

[21] R. Moghanni, A. Hakkaki-Fard et S. K. Hannani, “A comprehensive study on the performance of vertical ground-coupled heat pumps,” *Geothermics*, vol. 110, p. 102674, mai 2023. [En ligne]. Disponible : https://www.sciencedirect.com/science/article/pii/S0375650523000287

[22] ASHRAE, *2021 ASHRAE Handbook - Fundamentals*. American Society of Heating Refrigerating and Air-Conditioning Engineers Inc. (ASHRAE, 2021. [En ligne]. Disponible : http://ezaccess.libraries.psu.edu/login?url=https://app.knovel.com/hotlink/toc/id:kpASHRAEZ2/2021-ashrae-handbook?kpromoter=marc

[23] C. Sáez Blázquez *et al.*, “Comparative Analysis of Different Methodologies Used to Estimate the Ground Thermal Conductivity in Low Enthalpy Geothermal Systems,” *Energies*, vol. 12, n°. 9, p. 1672, mai 2019. [En ligne]. Disponible : https://www.mdpi.com/1996-1073/12/9/1672

[24] P. Mogensen, “Fluid to duct wall heat transfer in duct system heat storages,” dans *Fluid to duct wall heat transfer in duct system heat storages*. Stockholm, Sweden : Swedish Council for Building Research, juin 1983, p. 652–657. [En ligne]. Disponible : http://cat.inist.fr/?aModele=afficheN&cpsidt=9388418

[25] W. A. Austin, C. Yavuzturk et J. D. Spitler, “Development of an In-Situ System and Analysis Procedure for Measuring Ground Thermal Properties,” *ASHRAE Transactions*, vol. 106, n°. 1, p. 365–379, 2000.

[26] S. Gehlin, “Thermal response test : method development and evaluation,” Doctoral Thesis, Luleå University of Technology, Luleå, 2002. [En ligne]. Disponible : http://urn.kb.se/resolve?urn=urn:nbn:se:ltu:diva-18433

[27] J. Raymond *et al.*, “A Review of Thermal Response Test Analysis Using Pumping Test Concepts,” *Groundwater*, vol. 49, n°. 6, p. 932–945, 2011. [En ligne]. Disponible : https://onlinelibrary.wiley.com/doi/abs/10.1111/j.1745-6584.2010.00791.x

[28] M. Li et A. C. Lai, “Parameter estimation of in-situ thermal response tests for borehole ground heat exchangers,” *International Journal of Heat and Mass Transfer*, vol. 55, n°. 9-10, p. 2615–2624, avr. 2012. [En ligne]. Disponible : https://linkinghub.elsevier.com/retrieve/pii/S0017931011007496

[29] Natural Resources Canada, “Ground-Source Heat Pumps (Earth-Energy Systems),” mars 2017, last Modified : 2017-03-27 Library Catalog : www.nrcan.gc.ca Publisher : Natural Resources Canada. [En ligne]. Disponible : https://www.nrcan.gc.ca/energy/publications/efficiency/heating-heat-pump/6833

[30] N. Mattsson, G. Steinmann et L. Laloui, “Advanced compact device for the in situ determination of geothermal characteristics of soils,” *Energy and*

Buildings, vol. 40, nº. 7, p. 1344–1352, janv. 2008. [En ligne]. Disponible : https://linkinghub.elsevier.com/retrieve/pii/S0378778807002952

[31] F. Bozzoli *et al.*, "Short-time thermal response test based on a 3-D numerical model," *Journal of Physics : Conference Series*, vol. 395, p. 012056, nov. 2012. [En ligne]. Disponible : http://stacks.iop.org/1742-6596/395/i=1/a=012056?key=crossref.d60f759197de05fcbc3c61875947c6cd

[32] W. Choi *et al.*, "Bayesian inference for thermal response test parameter estimation and uncertainty assessment," *Applied Energy*, vol. 209, p. 306–321, janv. 2018. [En ligne]. Disponible : https://linkinghub.elsevier.com/retrieve/pii/S0306261917314459

[33] S. Javed, J. D. Spitler et P. Fahlén, "An Experimental Investigation of the Accuracy of Thermal Response Tests Used to Measure Ground Thermal Properties." *ASHRAE Transactions*, vol. 117, nº. 1, 2011.

[34] ANSI/CSA/IGSHPA, "ANSI/CSA/IGSHPA C448 SERIES-16 (R2021) Design and Installation of Ground Source Heat Pump Systems for Commercial and Residential Buildings," CSA Group, Rapport technique, 2016.

[35] X. Zhang *et al.*, "Comparison of Four Methods for Borehole Heat Exchanger Sizing Subject to Thermal Response Test Parameter Estimation," *Energies*, vol. 12, nº. 21, p. 4067, oct. 2019. [En ligne]. Disponible : https://www.mdpi.com/1996-1073/12/21/4067

[36] W. Mazzotti Pallard et A. Lazzarotto, "Thermal response tests : A biased parameter estimation procedure ?" *Geothermics*, vol. 97, p. 102221, 2021. [En ligne]. Disponible : https://www.sciencedirect.com/science/article/pii/S0375650521001784

[37] N. BniLam et R. Al-Khoury, "Parameter identification algorithm for ground source heat pump systems," *Applied Energy*, vol. 264, p. 114712, avr. 2020. [En ligne]. Disponible : https://linkinghub.elsevier.com/retrieve/pii/S0306261920302245

[38] X. Zhang *et al.*, "Thermal response tests for the identification of soil thermal parameters : A review," *Renewable Energy*, déc. 2020. [En ligne]. Disponible : https://www.sciencedirect.com/science/article/pii/S0960148120319546

[39] P. Eskilson, "Thermal Analysis of Heat Extraction Boreholes," Thèse de doctorat, Lund Inst. of Tech., Sweden, janv. 1987.

[40] C. Yavuzturk et J. D. Spitler, "A Short Time Step Response Factor Model for Vertical Ground Loop Heat Exchangers," *ASHRAE Transactions*, vol. 105(2), p. 12 (475–485), 1999.

[41] J. Claesson et A. Dunand, *Heat extraction from the ground by horizontal pipes : a mathematical analysis*, ser. Document / Swedish Council for Building Research ; D1 :1983. Stockholm : Swedish Council for Building Research, 1983.

[42] L. Lamarche et P. Pasquier, “Higher-order temporal scheme for ground heat exchanger analytical models,” *Geothermics*, vol. 78, p. 111–117, mars 2019. [En ligne]. Disponible : https://linkinghub.elsevier.com/retrieve/pii/S0375650518301524

[43] J. Spitler, J. Cook et X. Liu, “_USRecent experiences calculating g-functions for use in simulation of ground heat exchangers,” *_USGeothermal Resources Council Transactions*, vol. 44, 2020, accepted : 2022-04-26T18 :35 :39Z Publisher : Geothermal Resources Council. [En ligne]. Disponible : https://shareok.org/handle/11244/335285

[44] S. Javed et J. Claesson, “New Analytical and Numerical Solutions for the Short-term Analysis of Vertical Ground Heat Exchangers,” *ASHRAE Transactions*, vol. 117, n°. 1, p. 3–12, 2011.

[45] D. Marcotte et P. Pasquier, “Fast fluid and ground temperature computation for geothermal ground-loop heat exchanger systems,” *Geothermics*, vol. 37, n°. 6, p. 651–665, déc. 2008. [En ligne]. Disponible : http://www.sciencedirect.com/science/article/pii/S0375650508000552

[46] L. Lamarche, “A fast algorithm for the hourly simulations of ground-source heat pumps using arbitrary response factors,” *Renewable Energy*, vol. 34, n°. 10, p. 2252–2258, oct. 2009. [En ligne]. Disponible : https://www.sciencedirect.com/science/article/pii/S0960148109000731

[47] P. Pasquier et D. Marcotte, “Joint use of quasi-3D response model and spectral method to simulate borehole heat exchanger,” *Geothermics*, vol. 51, p. 281–299, juill. 2014. [En ligne]. Disponible : https://linkinghub.elsevier.com/retrieve/pii/S0375650514000182

[48] J. D. Spitler et M. Bernier, “2 - Vertical borehole ground heat exchanger design methods,” dans *Advances in Ground-Source Heat Pump Systems*, S. J. Rees, édit. Woodhead Publishing, janv. 2016, p. 29–61. [En ligne]. Disponible : https://www.sciencedirect.com/science/article/pii/B9780081003114000029

[49] M. Cimmino et M. Bernier, “Experimental determination of the g-functions of a small-scale geothermal borehole,” *Geothermics*, vol. 56, p. 60–71, juill. 2015. [En ligne]. Disponible : http://www.sciencedirect.com/science/article/pii/S0375650515000371

[50] S. Gehlin et B. Nordell, “Determining undisturbed ground temperature for thermal response test,” *ASHRAE Transactions*, vol. 109, n°. 1, p. 151–156, 2003, conference Name : Winter meeting of the American Society of Heating, Refrigerating and Air-Conditioning Engineers : 26/01/2003 - 29/01/2003. [En ligne]. Disponible : http://urn.kb.se/resolve?urn=urn:nbn:se:ltu:diva-40540

[51] R. A. Beier, “Insights into parameter estimation for thermal response tests on borehole heat exchangers,” *Science and Technology for the Built Environment*, vol. 25, n°. 8, p. 947–962, 2019, publisher : Bellwether Publishing, Ltd.

[52] L. Jacques, P. Pasquier et D. Marcotte, “Influence of Measurement and Model Error on Thermal Response Test Interpretation,” *Geothermal Energy*, p. 7, 2014.

[53] W. Choi, H. Kikumoto et R. Ooka, “New perspectives in thermal performance test : Cost-effective apparatus and extended data analysis,” *Energy and Buildings*, vol. 180, p. 109–121, déc. 2018. [En ligne]. Disponible : https://www.sciencedirect.com/science/article/pii/S0378778818308569

[54] ——, “Critical comparison between thermal performance test (TPT) and thermal response test (TRT) : Differences in heat transfer process and extractable information,” *Energy Conversion and Management*, vol. 199, p. 111967, nov. 2019. [En ligne]. Disponible : http://www.sciencedirect.com/science/article/pii/S0196890419309732

[55] R. A. Beier, “Analysis of thermal response tests on boreholes with controlled inlet temperature versus controlled heat input rate,” *Geothermics*, vol. 94, p. 102099, juill. 2021. [En ligne]. Disponible : https://www.sciencedirect.com/science/article/pii/S0375650521000596

[56] J. Raymond *et al.*, “A Novel Thermal Response Test Using Heating Cables,” dans *World Geothermal Congress 2010*. Bali, Indonesia : World Geothermal Congress, 2010, p. 10.

[57] J. Raymond et L. Lamarche, “Development and numerical validation of a novel thermal response test with a low power source,” *Geothermics*, vol. 51, p. 434–444, juill. 2014. [En ligne]. Disponible : http://www.sciencedirect.com/science/article/pii/S0375650514000212

[58] J. Raymond, L. Lamarche et M. Malo, “Field demonstration of a first thermal response test with a low power source,” *Applied Energy*, vol. 147, p. 30–39, juin 2015. [En ligne]. Disponible : https://linkinghub.elsevier.com/retrieve/pii/S0306261915001543

[59] J. Acuña, P. Mogensen et P. M. Ab, “DISTRIBUTED THERMAL RESPONSE TEST ON A U-PIPE BOREHOLE HEAT EXCHANGER,” *Applied Energy*, vol. 109, p. 8, 2009.

[60] J. Acuña et B. Palm, “Distributed thermal response tests on pipe-in-pipe borehole heat exchangers,” *Applied Energy*, vol. 109, p. 312–320, sept. 2013. [En ligne]. Disponible : http://www.sciencedirect.com/science/article/pii/S0306261913000330

[61] M. I. Vélez Márquez *et al.*, “Distributed Thermal Response Tests Using a Heating Cable and Fiber Optic Temperature Sensing,” *Energies*, vol. 11, n°. 11, p. 3059, nov. 2018. [En ligne]. Disponible : https://www.mdpi.com/1996-1073/11/11/3059

[62] S. Wilke *et al.*, “Advanced thermal response tests : A review,” *Renewable and Sustainable Energy Reviews*, vol. 119, p. 109575, mars 2020. [En ligne]. Disponible : https://www.sciencedirect.com/science/article/pii/S136403211930783X

[63] V. F. Bense *et al.*, "Distributed Temperature Sensing as a downhole tool in hydrogeology," *Water Resources Research*, vol. 52, n°. 12, p. 9259–9273, 2016. [En ligne]. Disponible : https://agupubs.onlinelibrary.wiley.com/doi/abs/10.1002/2016WR018869

[64] Y. Sakata, T. Katsura et K. Nagano, "Multilayer-concept thermal response test : Measurement and analysis methodologies with a case study," *Geothermics*, vol. 71, p. 178–186, janv. 2018. [En ligne]. Disponible : https://linkinghub.elsevier.com/retrieve/pii/S0375650516301365

[65] G. Dalla Santa *et al.*, "Repeated ETRTs in a Complex Stratified Geological Setting : High-Resolution Thermal Conductivity Identification by Multiple Linear Regression," *Journal of Geotechnical and Geoenvironmental Engineering*, vol. 148, n°. 4, 2022. [En ligne]. Disponible : http://dx.doi.org/10.1061/(ASCE)GT.1943-5606.0002724

[66] H. J. Witte, "Error analysis of thermal response tests," *Applied Energy*, vol. 109, p. 302–311, sept. 2013. [En ligne]. Disponible : https://linkinghub.elsevier.com/retrieve/pii/S0306261912008653

[67] R. Beier, "Equivalent Time for Interrupted Tests on Borehole Heat Exchangers," *HVAC&R Research*, vol. 14, n°. 3, p. 489–505, mai 2008. [En ligne]. Disponible : http://www.tandfonline.com/doi/abs/10.1080/10789669.2008.10391021

[68] J. Luo *et al.*, "A novel approach to the analysis of thermal response test (TRT) with interrupted power input," *Energies*, vol. 13, n°. 19, 2020, publisher : MDPI AG.

[69] L. R. Ingersoll *et al.*, "Heat conduction with engineering, geological, and other applications," *University of Wisconsin Press*, 1954.

[70] H. S. Carslaw et J. C. Jaeger, "Conduction of heat in solids," *Oxford : Clarendon Press, 1959, 2nd ed.*, 1959.

[71] W. Choi *et al.*, "Bayesian inference of structural error in inverse models of thermal response tests," *Applied Energy*, vol. 228, p. 1473–1485, oct. 2018. [En ligne]. Disponible : https://linkinghub.elsevier.com/retrieve/pii/S0306261918310171

[72] L. Lamarche, "Short-term behavior of classical analytic solutions for the design of ground-source heat pumps," *Renewable Energy*, vol. 57, p. 171–180, sept. 2013. [En ligne]. Disponible : https://linkinghub.elsevier.com/retrieve/pii/S0960148113000839

[73] H. Y. Zeng, N. R. Diao et Z. H. Fang, "A finite line-source model for boreholes in geothermal heat exchangers," *Heat Transfer ?Asian Research*, vol. 31, n°. 7, p. 558–567, nov. 2002. [En ligne]. Disponible : http://doi.wiley.com/10.1002/htj.10057

[74] L. Lamarche et B. Beauchamp, "A new contribution to the finite line-source model for geothermal boreholes," *Energy and Buildings*, vol. 39, n°. 2, p. 188–198, févr. 2007. [En ligne]. Disponible : https://linkinghub.elsevier.com/retrieve/pii/S0378778806001824

[75] T. V. Bandos *et al.*, “Finite line-source model for borehole heat exchangers : effect of vertical temperature variations,” *Geothermics*, vol. 38, n°. 2, p. 263–270, juin 2009. [En ligne]. Disponible : https://linkinghub.elsevier.com/retrieve/pii/S0375650509000054

[76] D. Marcotte *et al.*, “The importance of axial effects for borehole design of geothermal heat-pump systems,” *Renewable Energy*, vol. 35, n°. 4, p. 763–770, avr. 2010. [En ligne]. Disponible : https://linkinghub.elsevier.com/retrieve/pii/S0960148109004108

[77] J. Claesson et S. Javed, “An analytical method to calculate borehole fluid temperatures for time-scales from minutes to decades,” dans *ASHRAE Transactions*, vol. 117, Montreal, QC, Canada, 2011, p. 279 – 288, iSSN : 00012505 Issue : PART 2.

[78] M. Cimmino, M. Bernier et F. Adams, “A contribution towards the determination of g-functions using the finite line source,” *Applied Thermal Engineering*, vol. 51, n°. 1-2, p. 401–412, mars 2013. [En ligne]. Disponible : https://linkinghub.elsevier.com/retrieve/pii/S135943111200573X

[79] X. Zhang *et al.*, “Improvement on an analytical finite line source model considering complex initial and boundary conditions : Part 1, model development and validation,” *Energy and Buildings*, vol. 198, p. 1–10, sept. 2019. [En ligne]. Disponible : https://linkinghub.elsevier.com/retrieve/pii/S0378778818326136

[80] M. G. Sutton, D. W. Nutter et R. J. Couvillion, “A Ground Resistance for Vertical Bore Heat Exchangers With Groundwater Flow,” *Journal of Energy Resources Technology*, vol. 125, n°. 3, p. 183–189, août 2003. [En ligne]. Disponible : https://doi.org/10.1115/1.1591203

[81] N. Diao, Q. Li et Z. Fang, “Heat transfer in ground heat exchangers with groundwater advection,” *International Journal of Thermal Sciences*, vol. 43, n°. 12, p. 1203–1211, déc. 2004. [En ligne]. Disponible : http://www.sciencedirect.com/science/article/pii/S1290072904001139

[82] P. Pasquier et L. Lamarche, “Analytic expressions for the moving infinite line source model,” *Geothermics*, vol. 103, p. 102413, 2022. [En ligne]. Disponible : https://www.sciencedirect.com/science/article/pii/S0375650522000657

[83] N. Molina-Giraldo *et al.*, “A moving finite line source model to simulate borehole heat exchangers with groundwater advection,” *International Journal of Thermal Sciences*, vol. 50, n°. 12, p. 2506–2513, déc. 2011. [En ligne]. Disponible : https://linkinghub.elsevier.com/retrieve/pii/S129007291100192X

[84] J. Hu, “An improved analytical model for vertical borehole ground heat exchanger with multiple-layer substrates and groundwater flow,” *Applied Energy*, vol. 202, p. 537–549, sept. 2017. [En ligne]. Disponible : https://www.sciencedirect.com/science/article/pii/S0306261917307006

[85] T. V. Bandos, K. Martin-Escudero et J. M. Sala-Lizarraga, “Evaluation of modified Hantush’s function : A tool for parametric study with the finite line-source model,” *Geothermics*, vol. 113, p. 102751, sept. 2023. [En ligne]. Disponible : https://www.sciencedirect.com/science/article/pii/S0375650523001050

[86] A. Puy et A. Saltelli, “Mind the hubris : complexity can misfire,” oct. 2022, arXiv :2207.12230 [cs, math]. [En ligne]. Disponible : http://arxiv.org/abs/2207.12230

[87] P. Cui, H. Yang et Z. Fang, “Numerical analysis and experimental validation of heat transfer in ground heat exchangers in alternative operation modes,” *Energy and Buildings*, vol. 40, n°. 6, p. 1060–1066, janv. 2008. [En ligne]. Disponible : https://linkinghub.elsevier.com/retrieve/pii/S0378778807002319

[88] V. Wagner *et al.*, “Numerical sensitivity study of thermal response tests,” *Renewable Energy*, vol. 41, p. 245–253, mai 2012. [En ligne]. Disponible : https://linkinghub.elsevier.com/retrieve/pii/S0960148111006033

[89] P. Monzó *et al.*, “A novel numerical approach for imposing a temperature boundary condition at the borehole wall in borehole fields,” *Geothermics*, vol. 56, p. 35–44, 2015. [En ligne]. Disponible : https://www.sciencedirect.com/science/article/pii/S0375650515000346

[90] G. Brunetti *et al.*, “A computationally efficient pseudo-3D model for the numerical analysis of borehole heat exchangers,” *Applied Energy*, vol. 208, p. 1113–1127, déc. 2017. [En ligne]. Disponible : https://linkinghub.elsevier.com/retrieve/pii/S0306261917313247

[91] S. Robert, P. Pasquier et A. Nguyen, “Impact of layered heterogeneity on thermal response test interpretation performed on a standing column well operated without bleed,” *Geothermics*, vol. 101, p. 102353, mai 2022. [En ligne]. Disponible : https://www.sciencedirect.com/science/article/pii/S0375650522000074

[92] F. Eppner, P. Pasquier et P. Baudron, “A coupled thermo-hydro-geochemical model for standing column well subject to CO 2 degassing and installed in fractured calcareous aquifers,” *Geomechanics for Energy and the Environment*, vol. 11, p. 14–27, sept. 2017. [En ligne]. Disponible : https://linkinghub.elsevier.com/retrieve/pii/S2352380816301186

[93] L. Cerclet, B. Courcelles et P. Pasquier, “Thermohydrochemical Model to Identify the Impact of Bleed Flow on Calcite Scaling in a Standing Column Well,” Copernicus Meetings, Rapport technique EGU23-17433, févr. 2023, conference Name : EGU23. [En ligne]. Disponible : https://meetingorganizer.copernicus.org/EGU23/EGU23-17433.html

[94] V. Laroche, P. Pasquier et B. Courcelles, “Integration of standing column wells in urban context : A numerical investigation-case in the City of Montreal,” *Sustainable Cities and Society*, vol. 78, p. 103513, 2022. [En ligne]. Disponible : https://www.sciencedirect.com/science/article/pii/S2210670721007794

[95] D. Bauer *et al.*, “Thermal resistance and capacity models for borehole heat exchangers,” *International Journal of Energy Research*, vol. 35, n°. 4, p. 312–320, mars 2011. [En ligne]. Disponible : http://doi.wiley.com/10.1002/er.1689

[96] P. Pasquier et D. Marcotte, “Short-term simulation of ground heat exchanger with an improved TRCM,” *Renewable Energy*, vol. 46, p. 92–99, oct. 2012. [En ligne]. Disponible : https://linkinghub.elsevier.com/retrieve/pii/S0960148112002017

[97] A. Nguyen, P. Pasquier et D. Marcotte, “Thermal resistance and capacity model for standing column wells operating under a bleed control,” *Renewable Energy*, vol. 76, p. 743–756, avr. 2015. [En ligne]. Disponible : https://linkinghub.elsevier.com/retrieve/pii/S0960148114008118

[98] P. Pasquier, A. Zarrella et R. Labib, “Application of artificial neural networks to near-instant construction of short-term g-functions,” *Applied Thermal Engineering*, vol. 143, p. 910–921, oct. 2018. [En ligne]. Disponible : https://linkinghub.elsevier.com/retrieve/pii/S1359431118305921

[99] A. Laferrière *et al.*, “Development and validation of a full-time-scale semi-analytical model for the short- and long-term simulation of vertical geothermal bore fields,” *Geothermics*, vol. 86, p. 101788, juill. 2020. [En ligne]. Disponible : http://www.sciencedirect.com/science/article/pii/S0375650518303122

[100] J. D. Spitler *et al.*, “R&D Studies Applied To Standing Column Well Design,” Oklahoma State University, Oklahoma State University, Rapport technique ASHRAE 1119-RP, juill. 2002.

[101] C. Yavuzturk et A. D. Chiasson, “Performance analysis of U-tube, concentric tube, and standing column well ground heat exchangers using a system simulation approach,” dans *ASHRAE Transactions*, vol. 108 PART 1, Atlantic City, NJ, United states, 2002, p. 925 – 938, iSSN : 00012505.

[102] G. Beaudry *et al.*, “Flow rate control in standing column wells : A flexible solution for reducing the energy use and peak power demand of the built environment,” *Applied Energy*, vol. 313, p. 118774, mai 2022. [En ligne]. Disponible : https://www.sciencedirect.com/science/article/pii/S0306261922002203

[103] Y. Cui *et al.*, “A comprehensive review on 2D and 3D models of vertical ground heat exchangers,” *Renewable and Sustainable Energy Reviews*, vol. 94, p.

84–114, oct. 2018. [En ligne]. Disponible : https://linkinghub.elsevier.com/retrieve/pii/S1364032118304088

[104] A. Franco et P. Conti, "Clearing a Path for Ground Heat Exchange Systems : A Review on Thermal Response Test (TRT) Methods and a Geotechnical Routine Test for Estimating Soil Thermal Properties," *Energies*, vol. 13, n°. 11, p. 2965, janv. 2020, number : 11 Publisher : Multidisciplinary Digital Publishing Institute. [En ligne]. Disponible : https://www.mdpi.com/1996-1073/13/11/2965

[105] X. Zhang *et al.*, "Thermal response tests for the identification of soil thermal parameters : A review," *Renewable Energy*, vol. 173, p. 1123–1135, août 2021. [En ligne]. Disponible : https://linkinghub.elsevier.com/retrieve/pii/S0960148120319546

[106] A. Tarantola, *Inverse Problem Theory and Methods for Model Parameter Estimation*. Society for Industrial and Applied Mathematics, janv. 2005. [En ligne]. Disponible : http://epubs.siam.org/doi/book/10.1137/1.9780898717921

[107] M. Ahmadfard et M. Bernier, "A review of vertical ground heat exchanger sizing tools including an inter-model comparison," *Renewable and Sustainable Energy Reviews*, vol. 110, p. 247–265, août 2019. [En ligne]. Disponible : https://linkinghub.elsevier.com/retrieve/pii/S1364032119302576

[108] P. Pasquier, "Interpretation of the first hours of a thermal response test using the time derivative of the temperature," *Applied Energy*, vol. 213, p. 56–75, mars 2018. [En ligne]. Disponible : https://linkinghub.elsevier.com/retrieve/pii/S0306261918300229

[109] C. Zhang *et al.*, "A review on thermal response test of ground-coupled heat pump systems," *Renewable and Sustainable Energy Reviews*, vol. 40, p. 851–867, déc. 2014. [En ligne]. Disponible : https://linkinghub.elsevier.com/retrieve/pii/S1364032114006947

[110] J. W. Chinneck, *Practical optimization : a gentle introduction*. Carleton University, Ottawa, Canada : Carleton University, 2006. [En ligne]. Disponible : https://www.optimization101.org/

[111] G. Eichfelder, *Adaptive Scalarization Methods in Multiobjective Optimization*, ser. Vector Optimization. Berlin, Heidelberg : Springer Berlin Heidelberg, 2008. [En ligne]. Disponible : http://link.springer.com/10.1007/978-3-540-79159-1

[112] H. Sayyaadi, E. H. Amlashi et M. Amidpour, "Multi-objective optimization of a vertical ground source heat pump using evolutionary algorithm," *Energy Conversion and Management*, vol. 50, n°. 8, p. 2035–2046, août 2009. [En ligne]. Disponible : https://linkinghub.elsevier.com/retrieve/pii/S0196890409001253

[113] S. Huang, Z. Ma et F. Wang, "A multi-objective design optimization strategy for vertical ground heat exchangers," *Energy and Buildings*, vol. 87, p. 233–242,

janv. 2015. [En ligne]. Disponible : https://linkinghub.elsevier.com/retrieve/pii/S0378778814009554

[114] A. H. Keshavarzzadeh *et al.*, "Multi-objective evolutionary-based optimization of a ground source heat exchanger geometry using various optimization techniques," *Geothermics*, vol. 86, p. 101861, juill. 2020. [En ligne]. Disponible : https://www.sciencedirect.com/science/article/pii/S0375650519304857

[115] P. Pasquier, A. Zarrella et D. Marcotte, "A multi-objective optimization strategy to reduce correlation and uncertainty for thermal response test analysis," *Geothermics*, vol. 79, p. 176–187, mai 2019. [En ligne]. Disponible : https://linkinghub.elsevier.com/retrieve/pii/S0375650518301706

[116] T. Weise *et al.*, "Why Is Optimization Difficult ?" dans *Nature-Inspired Algorithms for Optimisation*, J. Kacprzyk et R. Chiong, édit. Berlin, Heidelberg : Springer Berlin Heidelberg, 2009, vol. 193, p. 1–50, series Title : Studies in Computational Intelligence. [En ligne]. Disponible : http://link.springer.com/10.1007/978-3-642-00267-0_1

[117] D. Marcotte et P. Pasquier, "On the estimation of thermal resistance in borehole thermal conductivity test," *Renewable Energy*, vol. 33, n°. 11, p. 2407–2415, nov. 2008. [En ligne]. Disponible : https://linkinghub.elsevier.com/retrieve/pii/S0960148108000372

[118] P. Pasquier et D. Marcotte, "Robust identification of volumetric heat capacity and analysis of thermal response tests by Bayesian inference with correlated residuals," *Applied Energy*, vol. 261, p. 114394, mars 2020. [En ligne]. Disponible : http://www.sciencedirect.com/science/article/pii/S0306261919320811

[119] L. Jacques et P. Pasquier, "Obtaining the hydraulic and thermal properties of the main hydrostratigraphic units surrounding a standing column well using a thermal response test," *Journal of Hydrology*, vol. 623, p. 129823, août 2023. [En ligne]. Disponible : https://www.sciencedirect.com/science/article/pii/S0022169423007655

[120] M. A. Bernier *et al.*, "A Multiple Load Aggregation Algorithm for Annual Hourly Simulations of GCHP Systems," *HVAC&R Research*, vol. 10, n°. 4, p. 471–487, oct. 2004, publisher : Taylor & Francis_eprint : https ://www.tandfonline.com/doi/pdf/10.1080/10789669.2004.10391115. [En ligne]. Disponible : https://www.tandfonline.com/doi/abs/10.1080/10789669.2004.10391115

[121] J. Claesson et S. Javed, "A load-aggregation method to calculate extraction temperatures of borehole heat exchangers," *ASHRAE Transactions*, vol. 118, n°. 1, p. 530–540, janv. 2012, publisher : American Society of Heating, Refrigerating, and Air-Conditioning Engineers, Inc. (ASHRAE). [En ligne]. Dispo-

nible : https://go.gale.com/ps/i.do?p=AONE&sw=w&issn=00012505&v=2.1&it=r&id=GALE%7CA295268257&sid=googleScholar&linkaccess=abs

[122] M. S. Mitchell et J. D. Spitler, "Characterization, testing, and optimization of load aggregation methods for ground heat exchanger response-factor models," *Science and Technology for the Built Environment*, vol. 25, n°. 8, p. 1036–1051, sept. 2019, publisher : Taylor & Francis _eprint : https ://doi.org/10.1080/23744731.2019.1648936. [En ligne]. Disponible : https://doi.org/10.1080/23744731.2019.1648936

[123] P. Pasquier et D. Marcotte, "Efficient computation of heat flux signals to ensure the reproduction of prescribed temperatures at several interacting heat sources," *Applied Thermal Engineering*, vol. 59, n°. 1-2, p. 515–526, sept. 2013. [En ligne]. Disponible : https://linkinghub.elsevier.com/retrieve/pii/S1359431113004328

[124] M. Cimmino et M. Bernier, "A semi-analytical method to generate g-functions for geothermal bore fields," *International Journal of Heat and Mass Transfer*, vol. 70, p. 641–650, mars 2014. [En ligne]. Disponible : https://linkinghub.elsevier.com/retrieve/pii/S0017931013009915

[125] A. Lazzarotto, "A methodology for the calculation of response functions for geothermal fields with arbitrarily oriented boreholes – Part 1," *Renewable Energy*, vol. 86, p. 1380–1393, févr. 2016. [En ligne]. Disponible : https://linkinghub.elsevier.com/retrieve/pii/S0960148115303359

[126] B. Dusseault, P. Pasquier et D. Marcotte, "A block matrix formulation for efficient g-function construction," *Renewable Energy*, vol. 121, p. 249–260, juin 2018. [En ligne]. Disponible : https://linkinghub.elsevier.com/retrieve/pii/S096014811731296X

[127] M. Cimmino, "A finite line source simulation model for geothermal systems with series- and parallel-connected boreholes and independent fluid loops," *Journal of Building Performance Simulation*, vol. 11, n°. 4, p. 414–432, juill. 2018. [En ligne]. Disponible : https://www.tandfonline.com/doi/full/10.1080/19401493.2017.1381993

[128] ——, "Semi-Analytical Method for g-Function Calculation of bore fields with series- and parallel-connected boreholes," *Science and Technology for the Built Environment*, vol. 25, n°. 8, p. 1007–1022, 2019, publisher : Taylor & Francis_eprint : https ://doi.org/10.1080/23744731.2019.1622937. [En ligne]. Disponible : https://doi.org/10.1080/23744731.2019.1622937

[129] E. Zanchini, C. Naldi et M. Dongellini, "Dimensionless fluid-to-ground thermal response of single-line bore fields with isothermal fluid," *Applied Thermal Engineering*, vol. 233, p. 121210, oct. 2023. [En ligne]. Disponible : https://www.sciencedirect.com/science/article/pii/S1359431123012395

[130] B. Dusseault et P. Pasquier, “Efficient g-function approximation with artificial neural networks for a varying number of boreholes on a regular or irregular layout,” *Science and Technology for the Built Environment*, p. 1–13, août 2019. [En ligne]. Disponible : https://www.tandfonline.com/doi/full/10.1080/23744731.2019.1634932

[131] M. Fossa et A. Priarone, “Constant temperature response factors for fast calculation of sparse BHE field g-functions,” *Renewable Energy*, vol. 131, p. 1236–1246, 2019. [En ligne]. Disponible : https://www.sciencedirect.com/science/article/pii/S0960148118309339

[132] E. Zanchini et S. Lazzari, “Temperature distribution in a field of long Borehole Heat Exchangers (BHEs) subjected to a monthly averaged heat flux,” *Energy*, vol. 59, p. 570–580, sept. 2013. [En ligne]. Disponible : https://linkinghub.elsevier.com/retrieve/pii/S0360544213005380

[133] ——, “New g-functions for the hourly simulation of double U-tube borehole heat exchanger fields,” *Energy*, vol. 70, p. 444–455, juin 2014. [En ligne]. Disponible : https://linkinghub.elsevier.com/retrieve/pii/S0360544214004356

[134] J. R. Cullin et J. D. Spitler, “A computationally efficient hybrid time step methodology for simulation of ground heat exchangers,” *Geothermics*, vol. 40, n°. 2, p. 144–156, juin 2011. [En ligne]. Disponible : https://linkinghub.elsevier.com/retrieve/pii/S0375650511000046

[135] C. Yavuzturk, J. D. Spitler et S. J. Rees, “A Transient Two-Dimensional Finite Volume Model for the Simulation of Vertical U-Tube Ground Heat Exchangers,” *ASHRAE Transactions*, vol. 105(2), p. 465–474, 1999.

[136] P. Hu *et al.*, “A method and case study of thermal response test with unstable heat rate,” *Energy and Buildings*, vol. 48, p. 199–205, mai 2012. [En ligne]. Disponible : https://linkinghub.elsevier.com/retrieve/pii/S0378778812000539

[137] M. Li et A. C. Lai, “Analytical model for short-time responses of ground heat exchangers with U-shaped tubes : Model development and validation,” *Applied Energy*, vol. 104, p. 510–516, avr. 2013. [En ligne]. Disponible : https://linkinghub.elsevier.com/retrieve/pii/S0306261912007763

[138] D. Marcotte et P. Pasquier, “Unit-response function for ground heat exchanger with parallel, series or mixed borehole arrangement,” *Renewable Energy*, vol. 68, p. 14–24, août 2014. [En ligne]. Disponible : https://linkinghub.elsevier.com/retrieve/pii/S0960148114000524

[139] J. Wei *et al.*, “A new method for calculation of short time-step g-functions of vertical ground heat exchangers,” *Applied Thermal Engineering*, vol. 99, p. 776–783,

avr. 2016. [En ligne]. Disponible : http://www.sciencedirect.com/science/article/pii/S1359431116300552

[140] F. Cruz-Peragon *et al.*, "Extending capabilities of Thermal Response Tests in vertical ground heat exchangers : An experiment-based local short-time temperature response factor," *Applied Thermal Engineering*, vol. 178, p. 115606, sept. 2020. [En ligne]. Disponible : http://www.sciencedirect.com/science/article/pii/S135943112033088X

[141] X. Xu et J. D. Spitler, "Modeling of Vertical Ground Loop Heat Exchangers with Variable Convective Resistance and Thermal Mass of the Fluid," dans *10th International Conference on Thermal Energy Storage-EcoStock*, Pomona, NJ, USA, mai 2006, p. 8.

[142] Y. Brussieux et M. Bernier, "_USHybrid model for generating short-time g-functions," *_USInternational Ground Source Heat Pump Association*, 2018, accepted : 2018-08-28T17 :58 :46Z Publisher : International Ground Source Heat Pump Association. [En ligne]. Disponible : https://shareok.org/handle/11244/301548

[143] G. Beaudry, P. Pasquier et D. Marcotte, "A fast convolution-based method to simulate time-varying flow rates in closed-loop and standing column well ground heat exchangers," *Renewable Energy*, avr. 2021. [En ligne]. Disponible : https://www.sciencedirect.com/science/article/pii/S0960148121005632

[144] M. De Rosa *et al.*, "A novel TRNSYS type for short-term borehole heat exchanger simulation : B2G model," *Energy Conversion and Management*, vol. 100, p. 347–357, août 2015. [En ligne]. Disponible : https://linkinghub.elsevier.com/retrieve/pii/S0196890415004689

[145] M. S. Mitchell et J. D. Spitler, "An Enhanced Vertical Ground Heat Exchanger Model for Whole-Building Energy Simulation," *Energies*, vol. 13, n°. 16, p. 4058, janv. 2020, number : 16 Publisher : Multidisciplinary Digital Publishing Institute. [En ligne]. Disponible : https://www.mdpi.com/1996-1073/13/16/4058

[146] R. A. Beier et M. D. Smith, "Minimum duration of in-situ tests on vertical boreholes," *ASHRAE Transactions*, vol. 109, p. 475, 2003, publisher : American Society of Heating, Refrigeration and Air Conditioning Engineers, Inc.

[147] M. Li *et al.*, "Full-scale temperature response function (G-function) for heat transfer by borehole ground heat exchangers (GHEs) from sub-hour to decades," *Applied Energy*, vol. 136, p. 197–205, déc. 2014. [En ligne]. Disponible : http://www.sciencedirect.com/science/article/pii/S030626191400960X

[148] C. L. Phillips, J. M. Parr et E. A. Riskin, *Signals, systems, and transforms*, 4e éd. Upper Saddle River, NJ : Pearson/Prentice Hall, 2008, oCLC : ocn133465573.

[149] C. Montagud, J. M. Corberán et A. Montero, "In situ optimization methodology for the water circulation pumps frequency of ground source heat pump systems,"

Energy and Buildings, vol. 68, p. 42–53, janv. 2014. [En ligne]. Disponible : https://www.sciencedirect.com/science/article/pii/S0378778813006105

[150] D. Del Col *et al.*, "Energy efficiency in a ground source heat pump with variable speed drives," *Energy and Buildings*, vol. 91, p. 105–114, mars 2015. [En ligne]. Disponible : https://www.sciencedirect.com/science/article/pii/S0378778814011219

[151] A. Zarrella, G. Emmi et M. De Carli, "A simulation-based analysis of variable flow pumping in ground source heat pump systems with different types of borehole heat exchangers : A case study," *Energy Conversion and Management*, vol. 131, p. 135–150, janv. 2017. [En ligne]. Disponible : https://www.sciencedirect.com/science/article/pii/S019689041630975X

[152] C. Beurcq, "CONTROL STRATEGIES FOR STANDING COLUMN WELLS IN COLD CLIMATE," Thèse de doctorat, Polytechnique de Montréal, Montréal, Canada, 2018.

[153] M. Hermanns et S. Ibáñez, "On the ill-posedness of the g-function model for the thermal response of geothermal heat exchangers," *International Journal of Thermal Sciences*, vol. 138, p. 285–292, avr. 2019. [En ligne]. Disponible : http://www.sciencedirect.com/science/article/pii/S129007291830810X

[154] O. Yilmaz, *Seismic Data Analysis : Processing, Inversion, and Interpretation of Seismic Data*. Society of Exploration Geophysicists, janv. 2001. [En ligne]. Disponible : https://library.seg.org/doi/book/10.1190/1.9781560801580

[155] N. Wiener, *Extrapolation, Interpolation, and Smoothing of Stationary Time Series, with Engineering Applications*. Martino Fine Books, août 1949. [En ligne]. Disponible : https://books.google.ca/books?id=bqFnngEACAAJ

[156] K. L. Peacock et S. Treitel, "PREDICTIVE DECONVOLUTION : THEORY AND PRACTICE," *GEOPHYSICS*, vol. 34, n°. 2, p. 155–169, avr. 1969. [En ligne]. Disponible : http://library.seg.org/doi/10.1190/1.1440003

[157] R. Neelamani, H. Choi et R. Baraniuk, "Wavelet-based deconvolution for ill-conditioned systems," dans *1999 IEEE International Conference on Acoustics, Speech, and Signal Processing. Proceedings. ICASSP99 (Cat. No.99CH36258)*. Phoenix, AZ, USA : IEEE, 1999, p. 3241–3244 vol.6. [En ligne]. Disponible : http://ieeexplore.ieee.org/document/757532/

[158] ——, "Wavelet-domain regularized deconvolution for ill-conditioned systems," dans *Proceedings 1999 International Conference on Image Processing (Cat. 99CH36348)*, vol. 1, oct. 1999, p. 204–208 vol.1.

[159] G. F. Margrave, M. P. Lamoureux et D. C. Henley, "Gabor deconvolution : Estimating reflectivity by nonstationary deconvolution of seismic data," *GEOPHYSICS*, vol. 76,

n°. 3, p. W15–W30, mai 2011. [En ligne]. Disponible : http://library.seg.org/doi/10.1190/1.3560167

[160] M. Oktariena et W. Triyoso, "Gabor Deconvolution as Preliminary Method to Reduce Pitfall in Deeper Target Seismic Data," *IOP Conference Series : Earth and Environmental Science*, vol. 132, p. 012022, mars 2018. [En ligne]. Disponible : https://iopscience.iop.org/article/10.1088/1755-1315/132/1/012022

[161] M. Radad, A. Gholami et H. R. Siahkoohi, "S-transform with maximum energy concentration : Application to non-stationary seismic deconvolution," *Journal of Applied Geophysics*, vol. 118, p. 155–166, juill. 2015. [En ligne]. Disponible : https://linkinghub.elsevier.com/retrieve/pii/S0926985115001445

[162] W. Deng *et al.*, "Seismic-Q Compensation by Iterative Time-Domain Deconvolution," *Remote Sensing*, vol. 15, n°. 3, 2023. [En ligne]. Disponible : https://www.mdpi.com/2072-4292/15/3/648

[163] G. F. Margrave, "Theory of nonstationary linear filtering in the Fourier domain with application to time-variant filtering," *Geophysics*, vol. 63, n°. 1, p. 244–259, févr. 1998. [En ligne]. Disponible : https://doi.org/10.1190/1.1444318

[164] F. Sonnenwald, V. Stovin et I. Guymer, "Configuring Maximum Entropy Deconvolution for the Identification of Residence Time Distributions in Solute Transport Applications," *Journal of Hydrologic Engineering*, vol. 19, n°. 7, p. 1413–1421, juill. 2014. [En ligne]. Disponible : http://ascelibrary.org/doi/10.1061/%28ASCE%29HE.1943-5584.0000929

[165] ——, "Deconvolving Smooth Residence Time Distributions from Raw Solute Transport Data," *Journal of Hydrologic Engineering*, vol. 20, n°. 11, p. 04015022, nov. 2015. [En ligne]. Disponible : http://ascelibrary.org/doi/10.1061/%28ASCE%29HE.1943-5584.0001190

[166] A. G. Meresescu *et al.*, "Water Residence Time estimation by 1D deconvolution in the form of a l2-regularized inverse problem with smoothness, positivity and causality constraints," *Computers & Geosciences*, vol. 115, p. 105–121, juin 2018. [En ligne]. Disponible : http://www.sciencedirect.com/science/article/pii/S0098300417306544

[167] S. P. Neuman *et al.*, "Developing a new deconvolution technique to model rainfall-runoff in arid environments," *Water Resources Research Center, University of Arizona*, 1982. [En ligne]. Disponible : http://hdl.handle.net/10150/305311

[168] S. P. Neuman et D. A. Gardner, "Determination of aquitard/aquiclude hydraulic properties from arbitrary water-level fluctuations by deconvolution," *Ground Water*, vol. 27, n°. 1, p. 66 – 76, 1989.

[169] O. A. Cirpka *et al.*, “Analyzing Bank Filtration by Deconvoluting Time Series of Electric Conductivity,” *Ground Water*, vol. 45, n°. 3, p. 318–328, mai 2007. [En ligne]. Disponible : http://doi.wiley.com/10.1111/j.1745-6584.2006.00293.x

[170] F. J. Kuchuk, M. Onur et F. Hollaender, *Pressure transient formation and well testing : convolution, deconvolution and nonlinear estimation*, 1er éd., ser. Developments in petroleum science. Amsterdam : Elsevier, 2010, n°. 57, oCLC : 730293412.

[171] T. von Schroeter *et al.*, “Deconvolution of well test data as a nonlinear total least squares problem,” dans *SPE Annual Technical Conference and Exhibition*. Society of Petroleum Engineers, 2001.

[172] M. M. Levitan, “Practical Application of Pressure-Rate Deconvolution to Analysis of Real Well Tests,” *Society of Petroleum Engineers*, vol. 8, n°. 2, p. 113–121, avr. 2005, https ://onepetro.org/REE/article-pdf/8/02/113/2569093/spe-84290-pa.pdf. [En ligne]. Disponible : https://doi.org/10.2118/84290-PA

[173] M. Onur *et al.*, “An Investigation of Recent Deconvolution Methods for Well-Test Data Analysis,” *SPE Journal*, vol. 13, n°. 02, p. 226–247, juin 2008. [En ligne]. Disponible : http://www.onepetro.org/doi/10.2118/102575-PA

[174] E. Pimonov *et al.*, “A new pressure/rate-deconvolution algorithm to analyze wireline-formation- tester and well-test data,” *SPE Reservoir Evaluation and Engineering*, vol. 13, n°. 4, p. 603 – 613, 2010. [En ligne]. Disponible : http://dx.doi.org/10.2118/123982-PA

[175] M. Onur et F. J. Kuchuk, “A New Deconvolution Technique Based on Pressure-Derivative Data for Pressure-Transient-Test Interpretation,” *SPE Journal*, vol. 17, n°. 01, p. 307–320, mars 2012. [En ligne]. Disponible : https://onepetro.org/SJ/article/17/01/307/198109/A-New-Deconvolution-Technique-Based-on-Pressure

[176] G. Monteyne, S. Javed et G. Vandersteen, “Heat transfer in a borehole heat exchanger : Frequency domain modeling,” *International Journal of Heat and Mass Transfer*, vol. 69, p. 129–139, févr. 2014. [En ligne]. Disponible : https://www.sciencedirect.com/science/article/pii/S0017931013008752

[177] R. A. Beier, “Deconvolution and convolution methods for thermal response tests on borehole heat exchangers,” *Geothermics*, vol. 86, p. 101786, 2020. [En ligne]. Disponible : http://www.sciencedirect.com/science/article/pii/S0375650519303190

[178] D. Bourdet, J. Ayoub et Y. Pirard, “Use of Pressure Derivative in Well Test Interpretation,” *SPE Formation Evaluation*, vol. 4, n°. 02, p. 293–302, juin 1989. [En ligne]. Disponible : http://www.onepetro.org/doi/10.2118/12777-PA

[179] IEA, “Energy Technology Perspectives 2020,” International Energy Agency, Paris, Rapport technique, 2020. [En ligne]. Disponible :

https://iea.blob.core.windows.net/assets/7f8aed40-89af-4348-be19-c8a67df0b9ea/Energy_Technology_Perspectives_2020_PDF.pdf

[180] ——, "World Energy Balances 2020," International Energy Agency, Paris, Rapport technique, 2020. [En ligne]. Disponible : https://www.iea.org/data-and-statistics/data-product/world-energy-balances

[181] ——, "Sustaibable Recovery," International Energy Agency, Paris, Rapport technique, 2020. [En ligne]. Disponible : https://iea.blob.core.windows.net/assets/c3de5e13-26e8-4e52-8a67-b97aba17f0a2/Sustainable_Recovery.pdf

[182] I. Sarbu et C. Sebarchievici, "General review of ground-source heat pump systems for heating and cooling of buildings," *Energy and Buildings*, vol. 70, p. 441–454, févr. 2014. [En ligne]. Disponible : https://www.sciencedirect.com/science/article/pii/S0378778813007858

[183] R. Wagner et C. Clauser, "Evaluating thermal response tests using parameter estimation for thermal conductivity and thermal capacity," *Journal of Geophysics and Engineering*, vol. 2, n°. 4, p. 349–356, déc. 2005. [En ligne]. Disponible : https://academic.oup.com/jge/article/2/4/349-356/5078234

[184] F. Bozzoli *et al.*, "Estimation of soil and grout thermal properties through a TSPEP (two-step parameter estimation procedure) applied to TRT (thermal response test) data," *Energy*, vol. 36, n°. 2, p. 839–846, févr. 2011. [En ligne]. Disponible : https://linkinghub.elsevier.com/retrieve/pii/S0360544210007218

[185] R. A. Beier et M. D. Smith, "Borehole thermal resistance from line-source model of in-situ tests," *Ashrae Transactions*, vol. 108, p. 212, 2002.

[186] W. Choi, R. Choudhary et R. Ooka, "Development of chiller-attached apparatus for accurate initial ground temperature measurement : Insights from global sensitivity analysis of thermal response tests," *Energy and Buildings*, p. 110841, févr. 2021. [En ligne]. Disponible : https://www.sciencedirect.com/science/article/pii/S0378778821001250

[187] R. A. Beier, "Use of temperature derivative to analyze thermal response tests on borehole heat exchangers," *Applied Thermal Engineering*, vol. 134, p. 298–309, avr. 2018. [En ligne]. Disponible : https://linkinghub.elsevier.com/retrieve/pii/S1359431117357502

[188] M. Li, L. Zhang et G. Liu, "Step-wise algorithm for estimating multi-parameter of the ground and geothermal heat exchangers from thermal response tests," *Renewable Energy*, vol. 150, p. 435–442, mai 2020. [En ligne]. Disponible : https://linkinghub.elsevier.com/retrieve/pii/S0960148119320191

[189] J. Jia, W. Lee et Y. Cheng, “Field demonstration of a first constant-temperature thermal response test with both heat injection and extraction for ground source heat pump systems,” *Applied Energy*, vol. 249, p. 79–86, sept. 2019. [En ligne]. Disponible : https://linkinghub.elsevier.com/retrieve/pii/S0306261919308050

[190] C. Zhang *et al.*, “Computational methods for ground thermal response of multiple borehole heat exchangers : A review,” *Renewable Energy*, vol. 127, p. 461–473, nov. 2018. [En ligne]. Disponible : https://linkinghub.elsevier.com/retrieve/pii/S0960148118305081

[191] I. R. Maestre *et al.*, “A new RC and g-function hybrid model to simulate vertical ground heat exchangers,” *Renewable Energy*, vol. 78, p. 631–642, juin 2015. [En ligne]. Disponible : https://linkinghub.elsevier.com/retrieve/pii/S0960148115000634

[192] M. Li et A. C. K. Lai, “New temperature response functions (G functions) for pile and borehole ground heat exchangers based on composite-medium line-source theory,” *Energy*, vol. 38, n°. 1, p. 255–263, févr. 2012. [En ligne]. Disponible : http://www.sciencedirect.com/science/article/pii/S0360544211007985

[193] S. W. Smith, *The scientist and engineer’s guide to digital signal processing*. San Diego (Calif.) : California Technical Pub., 1999, oCLC : 493473234.

[194] F. N. Fritsch, “Piecewise Cubic Hermite Interpolation Package. Final specifications,” Lawrence Livermore National Lab., CA (USA), Rapport technique UCID-30194, août 1982. [En ligne]. Disponible : https://www.osti.gov/biblio/6838406

[195] R. H. Byrd, M. E. Hribar et J. Nocedal, “An Interior Point Algorithm for Large-Scale Nonlinear Programming,” *SIAM Journal on Optimization*, vol. 9, n°. 4, p. 877–900, janv. 1999. [En ligne]. Disponible : http://epubs.siam.org/doi/10.1137/S1052623497325107

[196] J.-P. Chilès et P. Delfiner, *Geostatistics : Modeling Spatial Uncertainty*. John Wiley & Sons, 2012.

[197] H. J. Blinchikoff et A. I. Zverev, *Filtering in the time and frequency domains*. Raleigh, NC : SciTech Pub, 2006, oCLC : ocn252816793.

[198] B. Tarroja *et al.*, “Translating climate change and heating system electrification impacts on building energy use to future greenhouse gas emissions and electric grid capacity requirements in California,” *Applied Energy*, vol. 225, p. 522–534, 2018. [En ligne]. Disponible : https://www.sciencedirect.com/science/article/pii/S0306261918306962

[199] J. J. Saastamoinen, “Heating energy reduction of buildings in cold climates,” *Energy and Buildings*, vol. 21, n°. 3, p. 219–227, janv. 1994. [En ligne]. Disponible : http://www.sciencedirect.com/science/article/pii/037877889490037X

[200] Dunsky Energy Consulting, “The economic value of ground source heat pumps for build- 584 ing sector decarbonization : review of a recent analysis estimating the cots of electrifica- 585 tion in Canada,” Dunsky Energy Consulting, Rapport technique, 2020.

[201] H. Witte, “In situ estimation of ground thermal properties,” dans *Advances in Ground-Source Heat Pump Systems*. Elsevier, 2016, p. 97–116. [En ligne]. Disponible : https://linkinghub.elsevier.com/retrieve/pii/B9780081003114000042

[202] E. Abu-Nada *et al.*, “Modeling of a geothermal standing column well,” *International Journal of Energy Research*, vol. 32, n°. 4, p. 306–317, mars 2008. [En ligne]. Disponible : http://doi.wiley.com/10.1002/er.1355

[203] A. Zarrella *et al.*, “A comparison of numerical simulation methods analyzing the performance of a ground-coupled heat pump system,” *Science and Technology for the Built Environment*, vol. 24, n°. 5, p. 502–512, 2018.

[204] A. Nguyen et P. Pasquier, “A successive flux estimation method for rapid g-function construction of small to large-scale ground heat exchanger,” *Renewable Energy*, vol. 165, p. 359–368, mars 2021. [En ligne]. Disponible : https://linkinghub.elsevier.com/retrieve/pii/S0960148120316402

[205] G. Dion, P. Pasquier et D. Marcotte, “Deconvolution of experimental thermal response test data to recover short-term g-function,” *Geothermics*, vol. 100, p. 102302, 2022. [En ligne]. Disponible : https://www.sciencedirect.com/science/article/pii/S0375650521002583

[206] G. Dion *et al.*, “_USStationary and non-stationary deconvolution to recover long-term transfer functions,” dans *_USResearch Conference Proceedings*. Las Vegas, Nevada, USA : International Ground Source Heat Pump Association, déc. 2022, accepted : 2022-12-04T21 :40 :35Z. [En ligne]. Disponible : https://shareok.org/handle/11244/336826

[207] S. J. Rees *et al.*, “A Study of Geothermal Heat Pump and Standing Column Well Performance,” *ASHRAE Transactions*, vol. 109, Part 1., p. 12, 2004.

[208] X. Yu *et al.*, “Development of an efficient numerical model and analysis of heat transfer performance for borehole heat exchanger,” *Renewable Energy*, vol. 152, p. 189–197, juin 2020. [En ligne]. Disponible : https://linkinghub.elsevier.com/retrieve/pii/S0960148120300495

[209] MATLAB, *Version 9.8.0.1323502 (R2020a)*. Natick, Massachusetts : The MathWorks Inc., 2020.

[210] A. Galgaro, G. Dalla Santa et A. Zarrella, “First Italian TRT database and significance of the geological setting evaluation in borehole heat exchanger

sizing," *Geothermics*, vol. 94, p. 102098, juill. 2021. [En ligne]. Disponible : https://www.sciencedirect.com/science/article/pii/S0375650521000584

[211] A. McDaniel *et al.*, "Distributed thermal response test to analyze thermal properties in heterogeneous lithology," *Geothermics*, vol. 76, p. 116–124, nov. 2018. [En ligne]. Disponible : https://www.sciencedirect.com/science/article/pii/S0375650517303383

[212] H. Wang *et al.*, "Thermal performance of borehole heat exchanger under groundwater flow : A case study from Baoding," *Energy and Buildings*, vol. 41, n°. 12, p. 1368–1373, déc. 2009. [En ligne]. Disponible : https://linkinghub.elsevier.com/retrieve/pii/S0378778809001820

[213] R. B. Roka *et al.*, "A systematic review on shallow geothermal energy system : a light into six major barriers," *Soils and Rocks*, vol. 46, n°. 1, oct. 2022. [En ligne]. Disponible : https://soilsandrocks.com/sr-2023-007622

[214] W. Choi et R. Ooka, "Interpretation of disturbed data in thermal response tests using the infinite line source model and numerical parameter estimation method," *Applied Energy*, vol. 148, p. 476–488, juin 2015. [En ligne]. Disponible : https://linkinghub.elsevier.com/retrieve/pii/S0306261915003992

[215] P. Pasquier, "Stochastic interpretation of thermal response test with TRT-SInterp," *Computers & Geosciences*, vol. 75, p. 73–87, févr. 2015. [En ligne]. Disponible : https://linkinghub.elsevier.com/retrieve/pii/S0098300414002519

[216] Y. Zhou, Z.-x. Zheng et G.-s. Zhao, "Analytical models for heat transfer around a single ground heat exchanger in the presence of both horizontal and vertical groundwater flow considering a convective boundary condition," *Energy*, vol. 245, p. 123159, avr. 2022. [En ligne]. Disponible : https://www.sciencedirect.com/science/article/pii/S0360544222000627

[217] V. Soldo, L. Boban et S. Borović, "Vertical distribution of shallow ground thermal properties in different geological settings in Croatia," *Renewable Energy*, vol. 99, p. 1202–1212, déc. 2016. [En ligne]. Disponible : https://www.sciencedirect.com/science/article/pii/S0960148116307236

[218] H. Liu *et al.*, "Distributed Thermal Response Multi-Source Modeling to Evaluate Heterogeneous Subsurface Properties," *Groundwater*, 2021, publisher : Wiley Online Library.

[219] Y. Sakata *et al.*, "Evaluating variability of ground thermal conductivity within a steep site by history matching underground distributed temperatures from thermal response tests," *Energies*, vol. 14, n°. 7, 2021, publisher : MDPI AG.

[220] R. A. Beier, M. Fossa et S. Morchio, "Models of thermal response tests on deep coaxial borehole heat exchangers through multiple ground layers," *Applied*

Thermal Engineering, vol. 184, p. 116241, févr. 2021. [En ligne]. Disponible : https://www.sciencedirect.com/science/article/pii/S1359431120337200

[221] R. A. Beier, S. Morchio et M. Fossa, "Thermal response tests on deep boreholes through multiple ground layers," *Geothermics*, vol. 101, p. 102371, mai 2022. [En ligne]. Disponible : https://www.sciencedirect.com/science/article/pii/S0375650522000244

[222] Y. Ma *et al.*, "Influence of Different Heat Loads and Durations on the Field Thermal Response Test," *Energies*, vol. 15, n°. 22, p. 8759, janv. 2022, number : 22 Publisher : Multidisciplinary Digital Publishing Institute. [En ligne]. Disponible : https://www.mdpi.com/1996-1073/15/22/8759

[223] Y. Nian *et al.*, "Estimation method for layered ground thermal conductivity using genetic algorithm based on a 2-D heat transfer model," *Energy and Buildings*, vol. 258, p. 111841, mars 2022. [En ligne]. Disponible : https://www.sciencedirect.com/science/article/pii/S0378778822000123

[224] N. Aranzabal *et al.*, "Novel instruments and methods to estimate depth-specific thermal properties in borehole heat exchangers," *Geothermics*, vol. 86, p. 101813, juill. 2020. [En ligne]. Disponible : https://www.sciencedirect.com/science/article/pii/S0375650519300318

[225] M. Antelmi *et al.*, "Thermal and hydrogeological aquifers characterization by coupling depth-resolved thermal response test with moving line source analysis," *Energy Conversion and Management*, vol. 225, p. 113400, déc. 2020. [En ligne]. Disponible : https://www.sciencedirect.com/science/article/pii/S0196890420309353

[226] B. Zhang *et al.*, "Estimation of Groundwater Flow Rate by an Actively Heated Fiber Optics Based Thermal Response Test in a Grouted Borehole," *Water Resources Research*, vol. 59, n°. 1, janv. 2023. [En ligne]. Disponible : https://onlinelibrary.wiley.com/doi/10.1029/2022WR032672

[227] G. Dion, P. Pasquier et D. Marcotte, "Recovery of ground thermal conductivity from experimental short-term transfer function and its time derivative," dans *European Geothermal Congress 2022*, Berlin, Germany, oct. 2022, p. 7. [En ligne]. Disponible : https://europeangeothermalcongress.eu/proceedings-egc-2022/

[228] R. A. Beier, "Thermal response tests on deep borehole heat exchangers with geothermal gradient," *Applied Thermal Engineering*, vol. 178, p. 115447, sept. 2020. [En ligne]. Disponible : http://www.sciencedirect.com/science/article/pii/S1359431120306992

[229] Golder Associés Ltée, "Thermal Performance Evaluation of a GeoExchange Well Installed with GEOperform HDPE pipes," Golder Associés Ltée, Montréal, Canada, Research report 08-1223-0083, juin 2009.

[230] S. Morchio, M. Fossa et R. A. Beier, "Study on the best heat transfer rate in thermal response test experiments with coaxial and U-pipe borehole heat exchangers," *Applied Thermal Engineering*, vol. 200, p. 117621, janv. 2022. [En ligne]. Disponible : https://www.sciencedirect.com/science/article/pii/S1359431121010486

[231] S. Morchio *et al.*, "A Spectral Method Aimed to Explain Qratio as the Dominant Parameter When the Infinite Line Source Model is Applied to Interpret the Thermal Response Test Data," *SSRN Electronic Journal*, 2023. [En ligne]. Disponible : https://www.ssrn.com/abstract=4329775

[232] Y. Du *et al.*, "Tikhonov regularization stabilizes multi-parameter estimation of geothermal heat exchangers," *Energy*, p. 125479, sept. 2022. [En ligne]. Disponible : https://www.sciencedirect.com/science/article/pii/S0360544222023611

[233] G. Dion, P. Pasquier et D. Marcotte, "Least squares deconvolution of experimental thermal response test data to recover short-term transfer function," dans *2nd Canadian Geothermal Students' Day*. Winnipeg, Canada : University of Manitoba, juin 2021, p. 4. [En ligne]. Disponible : https://www.researchgate.net/profile/Gabriel-Dion/publication/360076522_Least_squares_deconvolution_of_experimental_thermal_response_test_data_to_recover_short-term_transfer_function/links/62a79073c660ab61f8794f7a/Least-squares-deconvolution-of-experimental-thermal-response-test-data-to-recover-short-term-trans pdf

[234] P. Bujok *et al.*, "Assessment of the influence of shortening the duration of TRT (thermal response test) on the precision of measured values," *Energy*, vol. 64, p. 120–129, janv. 2014. [En ligne]. Disponible : https://linkinghub.elsevier.com/retrieve/pii/S0360544213010499

[235] Z. Han *et al.*, "Study on the influence of the identification model on the accuracy of the thermal response test," *Geothermics*, vol. 72, p. 316–322, mars 2018. [En ligne]. Disponible : http://www.sciencedirect.com/science/article/pii/S0375650517302596

[236] Y. D. Liu et R. A. Beier, "Required duration for borehole test validated by field data," *ASHRAE Transactions*, vol. 115, n°. 2, p. 782–793, 2009, publisher : American Society of Heating, Refrigerating, and Air-Conditioning Engineers ….

[237] F. Robert et L. Gosselin, "New methodology to design ground coupled heat pump systems based on total cost minimization," *Applied Thermal Engineering*, vol. 62, n°. 2, p. 481–491, janv. 2014. [En ligne]. Disponible : https://linkinghub.elsevier.com/retrieve/pii/S1359431113005589

[238] G. Beaudry, P. Pasquier et D. Marcotte, "Hydrogeothermal characterization and modelling of a standing column well experimental installation," dans *Proceedings of the*

IGSHPA Research Track 2018. International Ground Source Heat Pump Association, sept. 2018, p. 1–10. [En ligne]. Disponible : https://hdl.handle.net/11244/301593

ANNEXE A ARTICLE DE CONFÉRENCE 1 - LEAST SQUARES DECONVOLUTION OF EXPERIMENTAL THERMAL RESPONSE TEST DATA TO RECOVER SHORT-TERM TRANSFER FUNCTION

Gabriel Dion[1*], Philippe Pasquier[1], Denis Marcotte[1]

2nd Canadian Geothermal Students' Day, June 21-22 2021

[1] Department of Civil, Geological and Mining Engineering, Polytechnique Montréal, P.O. Box 6079 Station Centre-Ville, Montréal, Canada H3C 3A7

Abstract

The short-term transfer function of a geothermal heat exchanger is a key element for the design of a geoexchange system since it allows dynamic simulation of the system. In practice, the transfer function is generated with computing thermal models that emulate the thermal behavior of a ground heat exchanger. However, there is currently no method to directly retrieves the short-term transfer function from an experimental data set provided by a thermal response test. A least squares deconvolution method is proposed for this purpose. The proposed method can be applied to time-varying heating load on the full thermal response test data. Test cases done on noisy synthetic and real data sets were analyzed and showed the robustness of the method. Results indicate that filtering the signal with a single pre-processing step prior to deconvolution allowed to recover a transfer function within a relative error of 1%. Deconvolution being fully data-driven, no analytical model is used to represent the ground heat transfer processes. By avoiding the simplifying assumption of an analytical model, this new method improves the construction of the short-term transfer function and should lead to better simulation of ground source heat pump systems.

A.1 Introduction

When sizing a Ground Heat Exchanger (GHE), it is common to rely on first-order approximation (FOA) to obtain the thermal parameters of the ground. The original method uses a graphic interpretation method [24], but recent research enhanced this approach by also using the temperature derivative [108]. Instead of estimating the thermal parameters of the ground, it is common to use the g-function proposed by Eskilon (1987) [39], which describes the long-term thermal behaviour of the GHE. A g-function is a signal that is the equivalent

of an impulse function (also named transfer function) and it represents the response of a system to a unit impulse signal at the initial time [193]. In practice, it corresponds to the response of a GHE to a constant heat impulse of either 1 °C, 1W or 1W/m for the duration of the TRT [138].

The classical g-function can only be applied with large time steps. To consider smaller ones, Yavuzturk et Spitler (1999) [40] developed a short-time transfer function. The evaluation of these transfer functions received considerable research attention in recent years [44, 98, 140] because they can predict the dynamic thermal evolution of the geothermal system. This effect is crucial when considering the transient heat demand from the building and outside temperature variations. Short-term g-functions (STgFs) are usually retrieved with the interpretation of data sets obtained during a thermal response test (TRT). The interpretation models are either analytical or numerical.

Using analytical equations to represent the STgF leads to model errors, added to the usual errors encountered in a TRT [66]. Hence, using directly the experimental data to extract the STgF is advantageous as it avoids incorporating model errors. To this regard, a precedent contribution used a FOA to extract the thermal parameters of the ground and then compute the STgF [140]. Also, a logarithmic thinned time selection of the experimental data was used in to recover a temperature transfer function [177]. However, no proposed method uses the entire data set of a TRT to acquire the STgF.

Obtaining the STgF with the entire data set of a TRT is akin to a deconvolution problem. The aim of this paper is to present a regularized, weighted least squares deconvolution algorithm that can be applied to time-varying heat flux to recover the STgF of a GHE.

A.2 Methods

The convolution equation can be expressed in the time domain by Eq. A.1 [98]:

$$T_{out}(t_i) - T_0 = (f * g)(t_i) = \sum_{j=1}^{i} f(t_j) g(t_{i-j+1}) \tag{A.1}$$

where T_{out} [°C] is the outlet GHE fluid temperature, T_0 [°C] is the undisturbed ground temperature, g [-] is the unknown borehole outlet STgF to be evaluated in the deconvolution process and f [°C] is the incremental heat load function that can be calculated with Eq. A.2:

$$f(t) = \Delta T(t_i) - \Delta T(t_{i-1}) = \frac{Q(t_i) - Q(t_{i-1})}{V(t_i) C_m \rho_f} \tag{A.2}$$

where Q [W] is the heat flux injected or extracted from the circulating fluid, V [m^3 s^{-1}] is the fluid circulating flow rate (which can also be taken as constant), C_m [J kg^{-1} K^{-1}] is the specific heat capacity of the fluid and ρ_f [kg m^{-3}] is the density of the fluid.

Equation A.1 can be expressed as a matrix multiplication representing the solution of a linear system of equations, with $\boldsymbol{F}$ a Toeplitz triangular inferior matrix composed of the vector f.

$$\Delta \boldsymbol{T} = \boldsymbol{F} \cdot \hat{\boldsymbol{g}} \tag{A.3}$$

$$\begin{bmatrix} \Delta T(t_1) \\ \Delta T(t_2) \\ \vdots \\ \Delta T(t_n) \end{bmatrix} = \begin{bmatrix} f(t_1) & 0 & \dots & 0 \\ f(t_2) & f(t_1) & \ddots & \vdots \\ \vdots & f(t_2) & \ddots & 0 \\ f(t_n) & \dots & \dots & f(t_n) \end{bmatrix} \begin{bmatrix} \hat{g}(t_1) \\ \hat{g}(t_2) \\ \vdots \\ \hat{g}(t_n) \end{bmatrix} \tag{A.4}$$

The linear system of Eq. A.3 has n unknown and n equations. It can then be solved directly. However, since experimental data have reading errors and $\hat{g}$ has intrinsic properties, a common method to solve Eq. A.3 is to solve the least squares between the left and right side of the equation with added constraints [35, 37]. Hence, the problem tries to minimize the objective function:

$$\hat{g} = \arg\min_{g} \|(f * g) - \Delta T\|_2^2 \tag{A.5}$$

It is common to add a regularization term to ensure smoothness of the response function, like the time derivative of the evaluated function, as described at Eq. A.6:

$$\hat{g} = \arg\min_{g} \|(f * g) - \Delta T\|_2^2 + \lambda \left\| \frac{dg}{dt} \right\|_2^2 \tag{A.6}$$

where λ is the relative weight of the STgF derivative ($\lambda > 0$). Increasing this parameter enhances the smoothness of $\hat{g}$ at the expense of the precision (goodness of fit). Using Eq. A.3 in Eq. A.6, it is possible to explicit the calculation of the objective function $J(\hat{\boldsymbol{g}})$, as show in Eq. A.8, where the derivative of the STgF is expressed by a matrix multiplication ($\boldsymbol{D}\hat{\boldsymbol{g}}$). The solution is a direct computation of the STgF as shown in Eq. A.9. Matrix $\boldsymbol{D}$ of

size (n-1) by n is the first-order finite difference matrix, as described in Eq. A.7:

$$\boldsymbol{D} = \begin{bmatrix} -1 & 1 & 0 & \dots & 0 \\ 0 & -1 & 1 & \ddots & \vdots \\ \dots & \ddots & \ddots & \ddots & 0 \\ 0 & \dots & 0 & -1 & 1 \end{bmatrix} \tag{A.7}$$

$$J(\hat{\boldsymbol{g}}) = (\boldsymbol{F}\hat{\boldsymbol{g}} - \Delta\boldsymbol{T})^T (\boldsymbol{F}\hat{\boldsymbol{g}} - \Delta\boldsymbol{T}) + \lambda (\boldsymbol{D}\hat{\boldsymbol{g}})^T (\boldsymbol{D}\hat{\boldsymbol{g}}) \tag{A.8}$$

To minimize the least squares of the previous equation, the partial derivative of J with respect to $\hat{g}$ should equal 0 at the minimum, leading to Eq. A.9:

$$\hat{g} = \left(\boldsymbol{F}^T\boldsymbol{F} + \lambda\boldsymbol{D}^T\boldsymbol{D}\right)^{-1} \boldsymbol{F}^T\Delta\boldsymbol{T} \tag{A.9}$$

which is a regularized weighted deconvolution algorithm that extracts a STgF.

Since this algorithm uses experimental data, the results are affected by noise on the recording variables [66]. To limit noise impact, a low-pass filter can be applied since recording error are of high frequency. The moving average or the Gaussian window moving average are both excellent filters for time-domain data set [193].

The methodology to obtain a STgF with a deconvolution algorithm is summarized below:

1. Retrieve the heat flux Q, the circulating flow V, the initial ground temperature T_0 and the outlet GHE temperature T_{out} from a TRT.
2. Since V is on the denominator of Eq. A.2, change every 0 value for a small value close to the machine precision.
3. Calculate the temperature variation $T_{out} - T_0$.
4. Apply either a moving average or a Gaussian window moving average on $T_{out} - T_0$ and Q.
5. Calculate the incremental heat load function f with Eq. A.2.
6. Construct the Toeplitz matrix $\boldsymbol{F}$ and sparse matrix $\boldsymbol{D}$.
7. Set the λ factor to 0.5 at first and adjust its value subsequently according to the smoothness of the deconvolve STgF.
8. Solve the Eq. A.9

A.3 Results

The deconvolution algorithm was applied to different numerical and experimental data sets on both closed loop and standing column well systems. Here, only the results of a real TRT performed on a standing column well are deconvolved to obtain the STgF. Figure A.1 shows the experimental data extracted from the TRT. The undisturbed ground temperature T_0 is equal to 12.35 °C and retrieved with a recirculation test prior to the TRT.

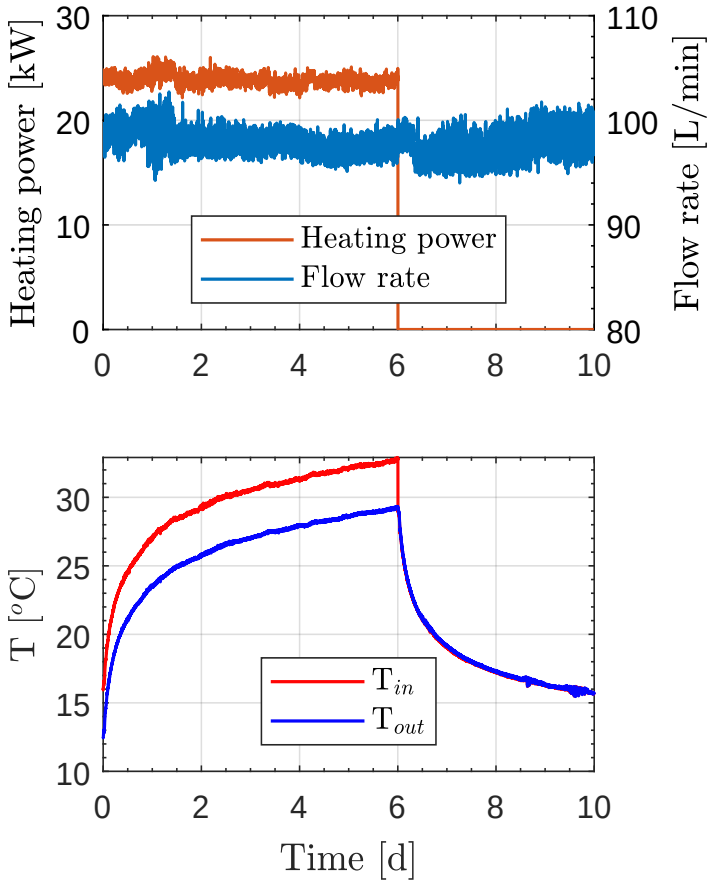

Figure A.1 Experimental data (Q, V, T_{in}, T_{out}) for a TRT performed on a standing column well. The value T_0 is equal to 12.35 °C [1].

After solving Eq. A.9, the STgF obtained can be convolved with Eq. A.1 and the convolved temperature variations is compared with the initial temperature variations to assess the performance of the method [45, 123].

Fig. A.2 shows the results of the deconvolution and the subsequent convolution to obtain the original temperature variations retrieve from the TRT. Table A.1 shows the root-mean-square-error (RMSE) between the convolved temperature variations and the reference tem-

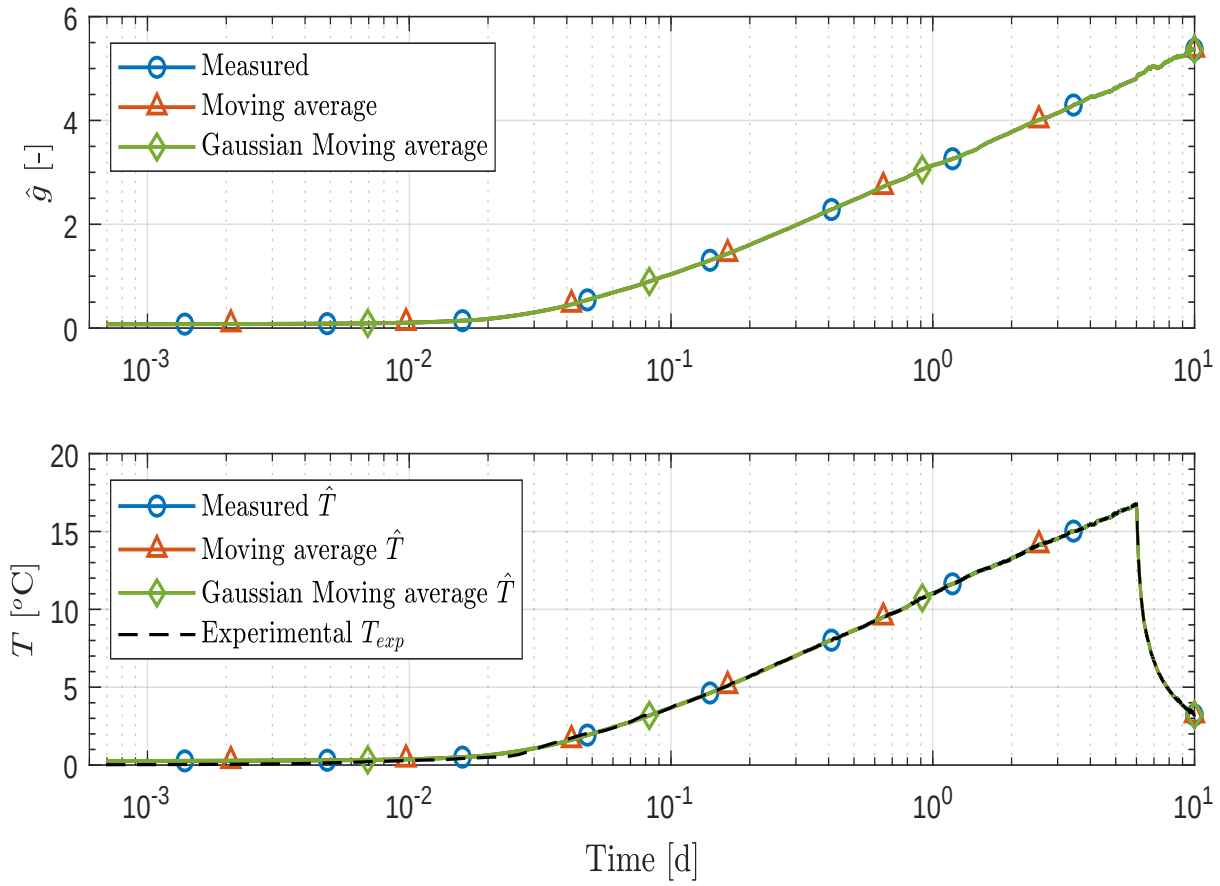

Figure A.2 Deconvolved STgF (top), convolved and reference temperature variation $T_{out} - T_0$ (bottom). Forms are present to differentiate the curves.

perature variation obtained with the TRT.

A.4 Discussion

The STgF on Fig. A.2 shows satisfactory results regarding the robustness of the proposed deconvolution method. All the curves are close to each other, with minimal deviation according to the different approaches used. This last statement is also confirmed when the STgF are compared to the reference temperature variation as is shown in Table A.1. Usually, the moving average filter helps lowering the RMSE in the time domain since high frequency are attenuated, but on this test case, only the Gaussian moving average allows greater precision on the reconstructed STgFs.

The algorithm induces some error toward the end of the STgF. Since the definition of a transfer function is the response of a system under a unit impulse at initial time, two main

Table A.1 RMSE between convolve and reference temperature variations. Convolution uses the deconvolved STgF.

Approac	**RMSE** [°C]
1. Measured	0.009
2. Moving average	0.011
3. Gaussian moving average	0.006

properties can be inferred: (1) the transfer function must be strictly positive and (2) the derivative of the transfer function should always be greater than 0. This comes with the realistic assumption that the transfer function should be smooth and continuous. Although the STgF shown have good form, the smoothness and positive derivative are not respected toward the end, especially at the start of the restitution phase.

The parameter λ can be changed to enhance the smoothing effect, but at the cost of the precision on the reconstructed STgF. Tests indicate that optimal values are between 0.5 and 1. The lowest RMSE will be obtained with $\lambda = 0$, since it cancels the regularization. Hence, it is apparent to resolving the Eq. A.3 directly with Eq. A.5.

It is worth pointing out that the algorithm was applied successfully on a variety of other TRT data set with various effects as power interruption and different GHE type. The precedent deconvolution algorithm is implemented on the software package MATLAB [209]. The computation of Eq. A.9 is heavy for long TRT since the construction of matrix $\boldsymbol{F}$ requires high Random-access memory (RAM) usage. For example, on an array of length n=25 000, the RAM can go as high as 23 Gb of and computing time is around 3.5 minutes. The computation cost is proportional to n^2.

A.5 Conclusion

This paper presents a regularized weighted deconvolution algorithm to obtain the STgF from the experimental data set of a TRT. The proposed algorithm shows good promise in retrieving the STgF without model error since no analytical or numerical model is applied to reconstruct the STgF.

Future works should aim at stabilizing the STgF reconstruction, improve efficiency and provide more validation against various experimental test cases.

ANNEXE B ARTICLE DE CONFÉRENCE 2 - RECOVERY OF GROUND THERMAL CONDUCTIVITY FROM EXPERIMENTAL SHORT-TERM TRANSFER FUNCTION AND ITS TIME DERIVATIVE

Gabriel Dion[1*], Philippe Pasquier[1], Denis Marcotte[1]

European Geothermal Congress 2022, October 17-21 2022

[1] Department of Civil, Geological and Mining Engineering, Polytechnique Montréal, P.O. Box 6079 Station Centre-Ville, Montréal, Canada H3C 3A7

Keywords: Short-term g-function, temperature derivative, ground thermal conductivity, thermal response test, signal deconvolution

Abstract

The ground thermal conductivity is one of the main parameters employed to size ground heat exchangers. It is usually obtained by interpreting the data retrieved from a thermal response test. This test can be interpreted using a convolution equation, which uses a dimensionless transfer function that represents the heat transfer capability of the ground heat exchanger under a known constant impulse. Recent advances have made it possible to extract the short-term transfer function and its first derivative from the experimental data recovered from a thermal response test by utilizing a deconvolution algorithm. It is shown in this paper that the thermal conductivity can be retrieved from the deconvolved transfer function by using known first-order approximation models. Results show that the estimated ground thermal conductivity obtained with the transfer function is within range with the one obtains with the temperature signal. An analysis also presents a way to obtain more robust thermal conductivity after only 1 day of TRT by computing the regression on an increasingly long interval.

B.1 Introduction

Ground source heat pump (GSHP) systems are 3 to 5 times more efficient than resistance heating [12]. This efficiency is a notable benefit when attempting to reduce the electricity consumption and CO_2 emission of buildings. These systems can dampen the impact of buildings' heating and cooling load by connecting a ground heat exchanger (GHE) to a geothermal heat pump. These two components allow heat exchange between the ground and

a building.

To size a GHE according to the heat load demands of the building, the ground thermal parameters, mainly the ground thermal conductivity and the borehole thermal resistance [28] are used. They are commonly obtained with a thermal response test (TRT) [25]. This test consists in circulating a heated or cooled fluid in a GHE and record the difference between the fluid temperature at the GHE entrance and exit. The difference between these temperatures can then be interpreted to retrieve the ground thermal parameters. Common ways to obtain these thermal parameters or to study TRT use analytical equations representing the underground heat transfer [216] or numerical modelling of the studied site [31, 88, 91].

To speed up both the TRT realization and further interpretation, various studies were made to minimize the TRT duration [108, 234–236]. Recently, Pasquier (2018) [108] presented many first-order approximations (FOA) methods that use the time derivative of the fluid temperature to retrieve the ground thermal conductivity within 10 % of a reference value. One limitation of the temperature time derivative is that it is sensitive to measurement noise and other temperature variations that are inherent to real field test.

To alleviate the noise impact on the TRT interpretation, the transfer function or g-function of a GHE can be employed, since it represents the ground and borehole thermal exchange capability under a unit excitation impulse. By definition, these functions are noiseless [39,40]. In the case of a GHE, the transfer functions are akin to performing a TRT using a unit excitation of 1 °C (or heating power of 1 W or 1 W/m). Then, the short-term transfer function would be the borehole outlet temperature. Such short-term g-functions (STgF) are well suited to use with a FOA to recover the thermal conductivity of the GHE since they are noiseless and not impacted by heating variations occurring during a TRT. This has not yet been demonstrated.

This article presents an adaptation of the methodology of Pasquier (2018) [108] that used FOA methods on the temperature of a TRT. The goal is to recover the thermal conductivity from a TRT by applying selected FOA methods using both the STgF and its first derivative obtained with a deconvolution algorithm. The practicality of this procedure is enhanced when using an efficient method to retrieve the STgF, like the recent deconvolution algorithms of Beier (2020a) [177] or Dion et al. (2022a) [205]. The thermal conductivity can be calculated with accuracy using solely the data outputs of a TRT.

B.2 Methodology

This section briefly presents the deconvolution algorithm used to retrieve the STgF of a GHE [205] and one of the FOAs developed by Pasquier (2018) [108].

B.2.1 Deconvolution algorithm to recover STgF

Using the outlet temperature measured during a TRT, the heat transfer that occurred during the test can be written with a convolution product as:

$$T_{out}(t) - T_0 = (f * g)(t) = \sum_{j=1}^{i} f(t_j) \cdot g(t_{i-j+1}) \tag{B.1}$$

where t is the time vector, T_{out} is the borehole outlet fluid temperature, T_0 is the undisturbed ground temperature, g is the borehole outlet STgF and f is the incremental temperature function written as:

$$f = \Delta T(t_i) - \Delta T(t_{i-1}) = \frac{Q(t_i) - Q(t_{i-1})}{V C_p \rho} \tag{B.2}$$

where ΔT is the difference between the inlet and outlet fluid temperature, Q is the heating power, V is the circulating flow rate, C_p is the specific fluid capacity and ρ is the density. Following Dion et al. (2022a) [205], the deconvolution algorithm used to recover an estimated STgF ($\hat{g}$) is the solution to an inverse problem where the goal is to minimize an objective function written as:

$$\hat{g}(t) = \arg\min_{\hat{g}} \left(E(t) | C_1(\tau), C_2(\tau)\right) \tag{B.3}$$

where $\hat{g}$ is the estimated STgF and E is the multi-objective function to be minimized and described with:

$$E = E_T + E_{\dot{g}} + E_{\ddot{g}} \tag{B.4}$$

$$E_T = \left\| W \cdot \left(\widehat{T}(t) - T_{exp}(t)\right) \right\|_2 \tag{B.5}$$

$$E_{\dot{g}} = P_{\dot{g}} \cdot \left\| \hat{\dot{g}}(t) \right\|_2 \tag{B.6}$$

$$E_{\ddot{g}} = P_{\ddot{g}} \cdot \left\| \hat{\ddot{g}}(t) \right\|_2 \tag{B.7}$$

In Eq. B.4 through Eq. B.7, $\|.\|_2$ is the Euclidean norm, $\widehat{T}$ and T_{Exp} are respectively the convolved and experimental temperatures equal to $T_{out} - T_0$ for the whole TRT signal (including heating and recovery phases), $\hat{\dot{g}}$ and $\hat{\ddot{g}}$ are respectively the first and second derivatives of the estimated STgF and act as regularization terms, W is a vector that emphasizes the early temperature by having a larger value at the beginning and smaller one afterwards, and P are

weights that allow the objective function to modulate which term of the objective function is prioritized in the minimization. In this work, W is a vector of values of 10 for the first 300 points and values of 1 for the remaining points. Considering Eq. B.5 to have an equivalent weight of 1, $P_{\dot{g}}$=10 and $P_{\ddot{g}}$=100. This leads to general proportions after optimization of 80%, 10% and 10% for Eq. B.5, Eq. B.6 and Eq. B.7 respectively.

In Eq. B.3, C_1 and C_2 are constraints imposed on the inverse problem so that $\hat{g}(\tau)$ respects mathematical properties. These properties are respectively:

$$0 < \hat{g}(\tau_j) < \hat{g}(\tau_{j+1}) \ \forall j \in [0, n-1] \tag{B.8}$$

$$\begin{aligned} 0 < \hat{\dot{g}}(\tau_j) < \hat{\dot{g}}(\tau_{j+1}) \ \forall j \in [0, z-1] \\ 0 < \hat{\dot{g}}(\tau_{j+1}) < \hat{\dot{g}}(\tau_j) \ \forall j \in [z, n-1] \end{aligned} \tag{B.9}$$

In the previous two equations, τ_j are a set of nodes, generally around 40, that spread logarithmically on $\hat{g}$ and on which the inversion algorithm iterates. This methodology allows to fit the STgF curve on a more representative vector of points, lightening the computation load and enhancing the smoothing and regularity of the estimated STgF. Eq. B.8 is a positivity and strictly growing constraints imposed on the STgF. In the algorithm, the positivity constraint is set as a lower bound and the strictly growing part is imposed by a linear inequality constraint enforcing a positive first derivative. Eq. B.9 is a constraint on the STgF first derivative so that it respects a logical evolution of the function. The shape of the first derivative should have a growing part early on the function, and a decreasing part afterwards. The second constraint represents this evolution from both sides of the maximum value z. These values will be observable later in the article.

B.2.2 Unconstrained and constrained first-order approximations of the temperature

The aim of the first-order approximation is to use an analytical model to retrieve the thermal conductivity and the borehole thermal resistance of the temperature acquired during a TRT [24]. The model is usually a truncated version of the infinite line source (ILS) model expressed as a power series [69]. The interpretation is conducted on the fit between the model and the experimental temperature, through a linear regression. The temperature using the ILS can be written as:

$$T_f(t) = T_0 + qR_b + \frac{q}{4\pi k_s}\left(ln\left(\frac{4\alpha t}{r_b^2}\right) - \gamma\right) \tag{B.10}$$

where T_f is the mean fluid temperature, q is the normalized power over the borehole length, R_b is the borehole thermal resistance, k_s and α are respectively the ground thermal conductivity and diffusivity, r_b is the borehole radius and γ is the Euler constant.

The two thermal parameters can be computed by expressing Eq. B.10 in a logarithmic linear relation of the form $T_f = m \cdot ln(t) + b$, where the slope is $m = q/4\pi k_s$ and the intercept is $b = T_0 + qR_b + q(ln(4\alpha/r_b^2) - \gamma)/4\pi k_s$. Using the slope, the thermal conductivity is computed with:

$$k_s = \frac{q}{4\pi m} \tag{B.11}$$

In the previous equation, the slope is calculated from a critical time $t_c = 5r_b^2/\alpha$, after which the temperature regression usually has a good fit with the experimental data. Pasquier (2018) [108] showed that, using the derivative of the temperature, shorter TRTs could be performed while retrieving thermal parameters with adequate precision. To do that, first the derivative of the ILS can be written as:

$$\dot{T}_f(t) = \frac{q}{4\pi k_s t} e^{\frac{-r_b^2}{4\alpha t}} \tag{B.12}$$

where $\dot{T}_f$ is the time derivative of the mean fluid temperature during the heating phase. As time increases, the term $-r_b^2/4\alpha t$ tends rapidly to zero and can be neglected. The FOA using the temperature derivative of a heating phase in a TRT can be expressed using the logarithm of the temperature derivative as:

$$ln\left(\dot{T}_f(t)\right) = -ln(t) + ln\left(\frac{q}{4\pi k_s}\right) \tag{B.13}$$

With Eq. B.13 as a logarithmic linear expression, the thermal conductivity can be expressed as:

$$\dot{k}_s = \frac{q}{4\pi e^{\dot{b}}} \tag{B.14}$$

Using Eq. B.13 and Eq. B.14 to fit the experimental temperature derivatives can lead to adequate approximation of the thermal conductivity. However, the slope of -1 cannot always be maintained in this unconstrained expression, which negatively impacts the accuracy of the method. To constrain the slope to a value of -1, a constraint is applied to Eq. B.13, so that the following equation is respected:

$$\frac{1}{n}\sum_{i=1}^{n}\left(ln\left(\dot{T}_f(t_i)\right) + ln(t_i) - \dot{b}\right) \to 0 \tag{B.15}$$

here n is the number of points in the time vector. Using the previous equation:

$$\tilde{b} = \frac{1}{n}\sum_{i=1}^{n}\left(ln\left(\dot{T}_f(t_i)\right) + ln(t_i)\right) \tag{B.16}$$

which finally hands the thermal conductivity calculation with a constrained approach:

$$\tilde{k}_s = \frac{q}{4\pi e^{\tilde{b}}} \tag{B.17}$$

Pasquier (2018) [108] recommended to perform the regression fitting between an interval of 4 to 16 residence time ($t_r = 2\pi r_{in}^2 H/V$).

B.2.3 Application of FOAs to STgF

Eq. B.10 through Eq. B.17 are written for borehole temperature variation (i.e., $EWT - LWT$) during the heating phase of TRT. In a similar way, the borehole outlet STgF expresses the dimensionless evolution of the temperature underground under a known heating unit impulse. Hence, Eq. B.10 through Eq. B.17 and their analysis are still valid when used with STgFs. The main difference is that the "heating power" is a constant of 1 W. This has the advantage of removing the uncertainty of varying heating power throughout a TRT. Figure B.1 shows that, compared to measured temperature, the derivative of a transfer function is smooth in time, since the "heating power" is constant in time. In this figure, it is also possible to see that the general usable region on which to perform a regression (i.e., where the noise is not too strong) is longer with the STgF than with the temperature.

B.3 Results

B.3.1 Data sets used for the demonstration

The previous algorithms were applied on a variety of experimental STgFs and temperature obtained through field TRTs. Here the method's precision assessment is presented on two field TRTs of respectively 8.9 and 9.8 days, performed on closed-loop GHE. Table B.1 shows the characteristics of each GHE and the TRT flow rates, while Figure B.2 illustrates the inlet and outlet fluid temperatures and the heating powers. It is worth noting that the second TRT presents a power interruption at about 85 hours.

Using the temperature, heating power, and knowing the average flow rate for both TRTs, the deconvolution algorithm was used by minimizing Eq. B.3 to retrieve a STgF for each TRT. Figure B.3 shows the resulting functions and their derivatives. The algorithm iterated

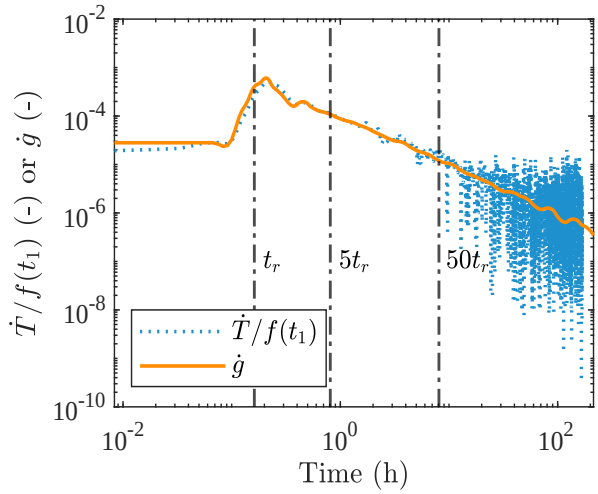

Figure B.1 Visualization of the smoothness of a STgF first derivative compared to a temperature derivative during the heating phase from a TRT. Value $f(t_1)$ is the initial heat input, used to normalize the temperature derivative to the StgF.

Table B.1 GHE borehole geometry, thermal properties, and average flow rate for the presented TRTs.

TRT	**Borehole radius**	**Borehole length**	**Half-pipe spacing**	**Pipe thermal conductivity**	**Residence time**	**Critical time**	**Flow rate**
	m	m	m	W/(m K)	h	h	L/min
1	0.075	152.4	0.029	0.74	0.16	6.7	26.7
2	0.075	152.4	0.029	0.41	0.17	6.1	24.7

on 38 nodes, spaced logarithmically, as shown by the circles in Figure B.3. In this figure, the squares on the derivatives are the location of the variable z in Eq. B.9 (constraint C_2). Note that the TRTs recovery phases are included in the STgFs, since these phases are included in the deconvolution process. Hence, the lengths of the STgFs are the same as the whole TRT duration.

The initial fluid residence time is visible on the STgFs of Figure B.3, and corresponds to the time before the arrival of the heated fluid to the GHE outlet. It also corresponds to the time just before the STgF derivative maximum value. The temperature rises apparent before the residence time is mostly due to conduction between the inlet and outlet of the GHE. One can also observe that the power interruption at 85 hours is absent from the STgF of Figure

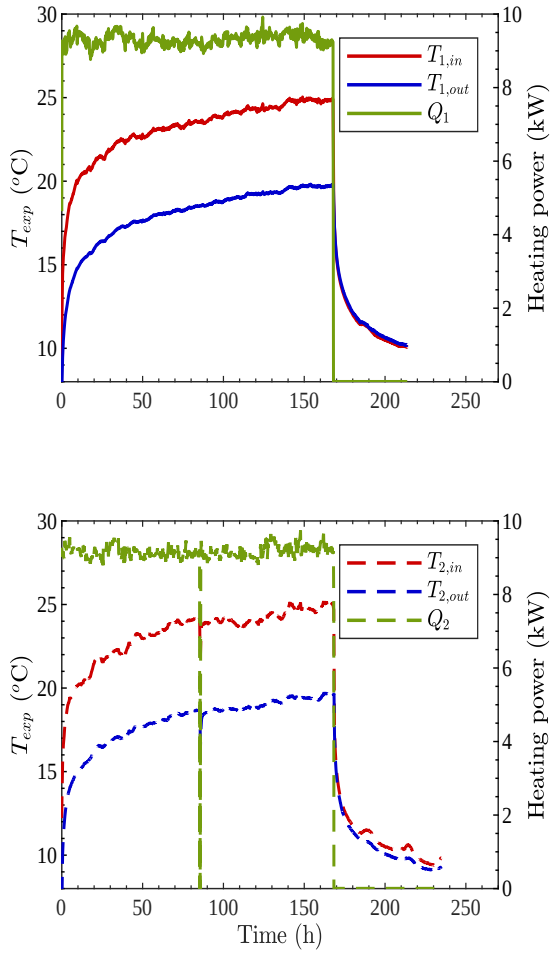

Figure B.2 Measured inlet and outlet fluid temperature and heating power for respectively the (top) first and (bottom) second TRT analyzed.

B.3. This is an advantage of the deconvolution algorithm to provide continuous and smooth functions as compared to the experimental temperature.

B.3.2 FOA on the temperature

The thermal conductivity was estimated by FOA on the heating phases only for both TRTs, using Eq. B.11 on the temperature (T) and Eq. B.17 on the temperature derivative ($\dot{T}$). The thermal conductivity values computed with the regressions are reported in Table B.2.

Figure B.4 shows the regression applied on both set of curves (T and $\dot{T}$). A first observation is that there is no overlap between the regressions on the temperature (T), where $t > t_c$, and the temperature derivative ($\dot{T}$), where $4t_r < t < 16t_r$. These bounds on the derivatives are the ones recommended by Pasquier (2018) [108] and correspond to around 0.68 to 2.65 hours

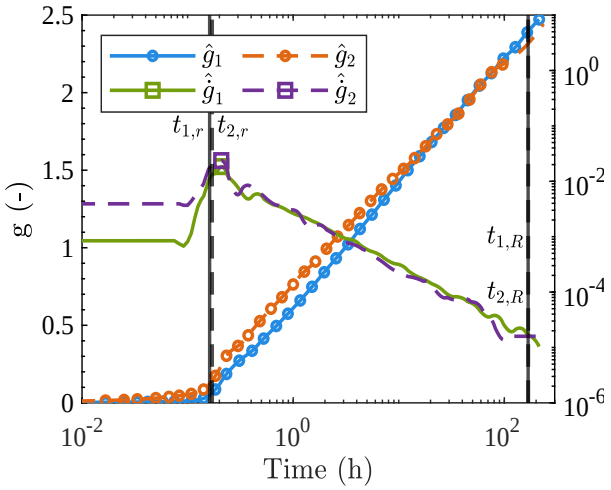

Figure B.3 Measured inlet and outlet fluid temperature and heating power for respectively the (top) first and (bottom) second TRT analyzed.

Table B.2 Regression parameters and thermal conductivity estimation using FOA methods on the temperatures, the STgFs and their respective derivatives.

Regression model	Phase	Data for regression	k TRT 1 (W/mk)	k TRT 2 (W/mk)
Eq. B.11 on T	Heating	$t > t_c$	3.02	3.31
Eq. B.17 on $\dot{T}$	Heating	$4t_r < t < 16t_r$	3.04	2.97
Eq. B.11 on g	Whole TRT	$t > t_c$	3.06	3.32
Eq. B.17 on $\dot{g}$	Whole TRT	$t > 4t_r$	3.11	3.27

of test. The thermal conductivity values present in Table B.2 are quite similar for the TRT 1 but diverges more for the TRT 2. This could be due to the relatively small sample used for the FOA computation on $\dot{T}$.

B.3.3 FOA on the STgFs

The FOA methods can be used on STgFs, as they represent the thermal response of the ground under a unit heating impulse. Hence, by using Eq. B.11 and Eq. B.17, approximations of the thermal conductivity are obtained and reported in Table B.1. Figure B.5 shows the regression fit on the STgFs and their derivative for the two TRTs.

For both TRTs, the regression on the StgF (g) are similar to the ones on the temperature (T). However, one can see that, compared to the regression of the temperature derivative, most

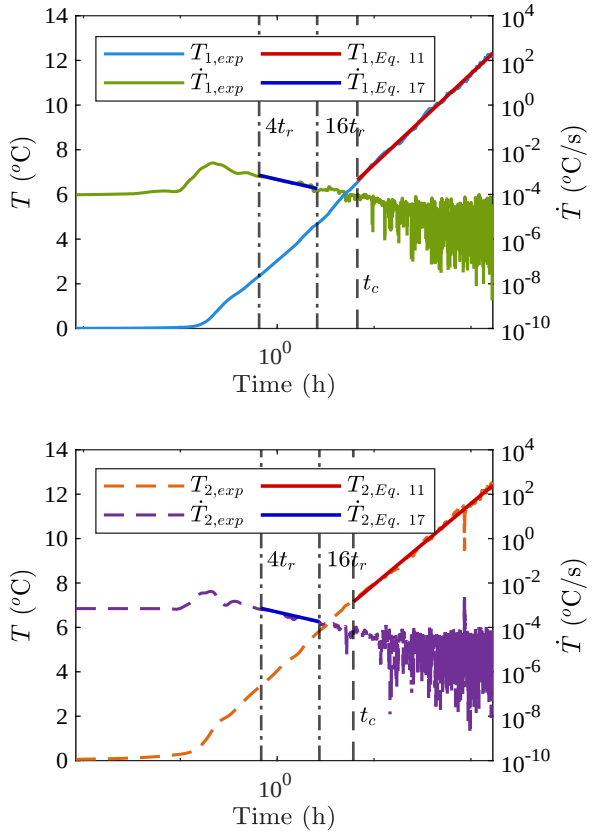

Figure B.4 FOA approximation on the experimental temperature from respectively the TRT 1 (top) and TRT 2 (bottom). The regression curves are over the duration used to evaluate the thermal conductivity.

of the signal can be used to approximate the thermal conductivity from the STgF derivative ($\dot{g}$) ($t > 4t_r$). With this, the thermal conductivity values obtained are closer to the ones obtained with the other methods. Note that both regressions on the STgF are not affected by the power interruption for the TRT 2.

B.3.4 Thermal conductivity for various TRT duration

One of the advantages of using temperature derivative cited by Pasquier (2018) [108] is that an adequate precision can be obtained with shorter TRT duration, namely within the first 3 hours of a TRT (i.e., between 4 and 16 residence time). The absence of noise on STgFs and their derivatives allows to use longer intervals for the regression, even until the recovery

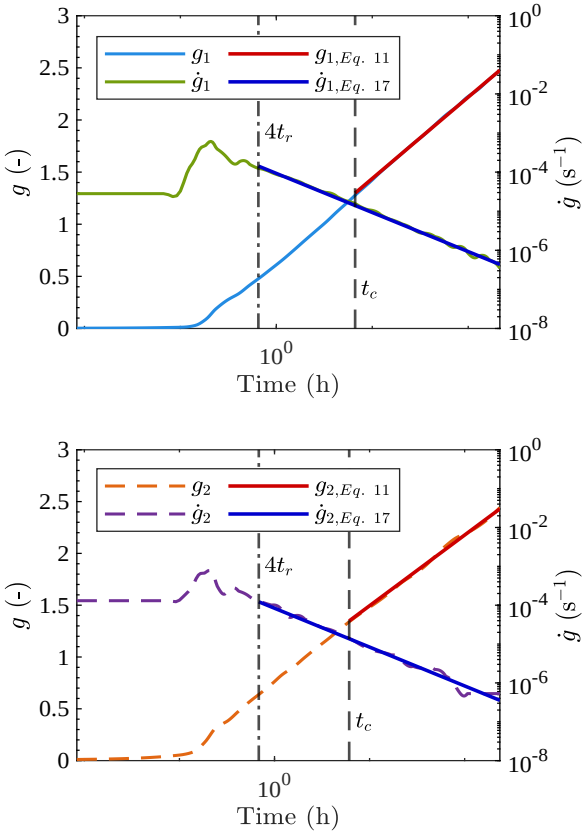

Figure B.5 FOA approximation on the transfer functions deconvolved from respectively the TRT 1 (top) and TRT 2 (bottom). The regression curves are over the duration used to evaluate the thermal conductivity.

phase of TRT. However, good approximation can be obtained with shorter periods than the full TRT, as can be seen by using the STgF derivative ($\dot{g}$).

To assess if shorter TRT can be used to obtain adequate thermal conductivity values from either the temperature or the STgF, the FOA methods (Eq. B.11 and Eq. B.17) were applied on increasingly long regression intervals on both TRTs. The intervals all start at a value of $4t_r$ and ends at the end of the heating phase for T, at $16t_r$ for $\dot{T}$ and the end of the TRT for both g and $\dot{g}$.

Figure B.6 shows the evolution of the ground thermal conductivity as a function of the interval duration. The means and standard deviations for each curve are reported in Table B.3. For the first TRT, the thermal conductivity is quite stable with a standard deviation

of less than 0.11 W/mK for all the interval duration's. The second TRT presents a larger variation on the analysis of $\dot{g}$. It can be due to the shape of the derivative that is not as stable at the end of the TRT (as can be seen in Figure B.6). Table B.3 also shows the mean and standard deviation for each test if only the regressions between 16 residence time and 24 hours are used. This is done to highlight the fact that by performing this analysis, a test of 24 hours would hand satisfactory thermal conductivity deviations.

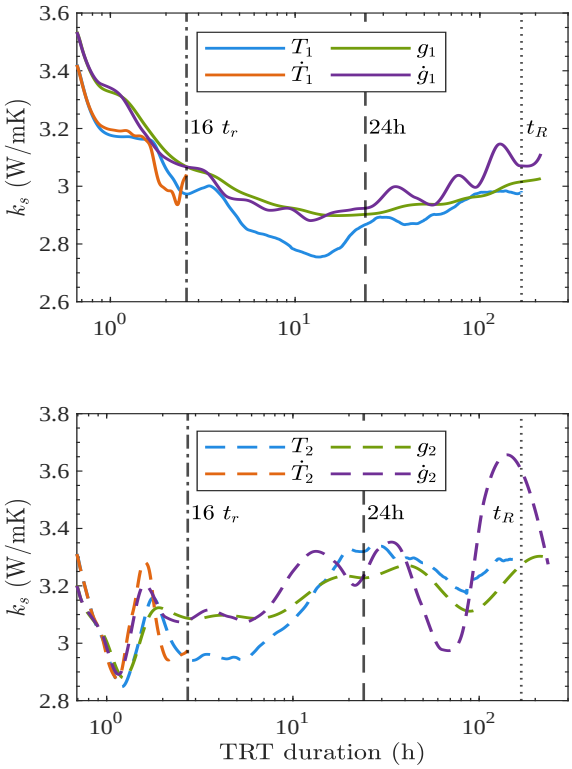

Figure B.6 Thermal conductivity evolution as a function of the regression length for (top) the TRT 1 and (bottom) the TRT 2.

B.4 Discussion

B.4.1 Global precision of the method

Figure B.6 shows the thermal conductivities for both TRTs and the four selected FOAs (i.e., Eq. B.11 and Eq. B.17 on T and g). It can be observed that all the values stay reasonably close to one another as the regression interval gets longer. A similar analysis is reported in

Table B.3 Mean and standard deviation of the thermal conductivity evolution's of Figure B.6 for the whole array and before 24 hours of test.

k_s	**TRT**	**T** Eq 11	Eq 17	**g** Eq 11	Eq 17
Mean	1	2.93	3.11	2.98	3.04
	2	3.25	3.04	3.22	3.37
Std	1	0.06	0.11	0.05	0.07
	2	0.08	0.12	0.07	0.22
Mean	1	2.93	-	2.93	2.92
$(16t_r < t < 24h)$	2	3.25	-	3.17	3.22
Std	1	0.06	-	0.04	0.04
$(16t_r < t < 24h)$	2	0.07	-	0.06	0.08

Spitler et Gehlin (2015) [18], explaining that it is improbable to have an explanation of why the values varies with an upward trend after the first 15 hours. The tests presented here shows a similar phenomenon, which leads to generally smaller thermal conductivity when the mean is taken over the entire signals in Figure B.6, as shown in Table B.3. This could lead to more conservative thermal conductivity values on similar cases.

In this sense, the analysis of the evolution of the thermal conductivity as shown in Figure B.6 could be a useful way to identify if a given value is close or not to the average of all the value that can be obtained throughout a TRT. It could then be a simple step to add in a TRT interpretation to ensure appropriate estimate of the thermal conductivity.

The advantage of using STgFs and their derivative with a FOA method is apparent with the usable length of the test used in the regression on the derivative methods. More specifically, to perform the regression from as early as 4 residence time, up until the end of a TRT. It can however be seen that, for both tests in Figure B.6, the thermal conductivity value varies more after 24 hours. This is due to the quality of the derivative obtained after the deconvolution process.

B.4.2 Analysis with varying regression length

In Table B.3, the mean thermal conductivity for each test and each method are usually of the same order. This is corroborated by their respective standard deviations. In the goal of finding an appropriate TRT duration to have an adequate thermal conductivity estimation, one could try to optimize the range within which the standard deviation of the curves in Figure B.6 would be lower. However, it is impractical for engineering purposes, since one the

TRT is done, the whole length can be used.

As an example, the mean and standard deviation are presented at the end of Table B.3 for a regression period between 16 residence time and 24 hours. Values could not be calculated for $\dot{T}$, since the derivative is too noisy during that interval. The value shows that the standard deviations are lower than using the whole array. This arbitrary time could be a first approach to use this methodology when interpreting a TRT for more robust thermal conductivity values.

B.5 Conclusion

This article presents the application of first-order approximation methods on short-term transfer functions retrieved by a deconvolution algorithm from a TRT data set. The goal is to recover the thermal conductivity value of the ground. The FOA methods are applied on the temperature and its derivative, or similarly on the STgF and its derivative, for two TRTs performed on closed-loop GHE. The results show that either the STgF or its first derivative can be used to recover a thermal conductivity close to the value obtained with the temperature of a TRT.

An advantage of using the STgF is that the heating power is a known constant, which is better simulated by analytical equations used in FOA. It also alleviates the temperature derivative noise impact, since the STgF derivative is noiseless. It is also shown that the impact of a power interruption could be overcome, since the deconvolution algorithm can handle such cases and still return smooth functions. This leads to more flexibility on the regression interval used to compute the thermal conductivity.

Finally, it has been shown that, by computing the thermal conductivity with various regression lengths, a profile can be made, helping the assessment of the effective thermal conductivity. As a base method, the average thermal conductivity can be calculated between 16 residence time and 1 day, giving more conservative values for the test cases. Then, the necessary time of a TRT could be reduced to 24 hours to assess the effective thermal conductivity, which is a gain from the common 72 hours long test.

ANNEXE C ARTICLE DE CONFÉRENCE 3 - STATIONARY AND NON-STATIONARY DECONVOLUTION TO RECOVER LONG-TERM TRANSFER FUNCTIONS

Gabriel Dion[1*], Philippe Pasquier[1], Denis Marcotte[1], Gabrielle Beaudry[1]

IGSHPA 2022 - Research Track, December 6-8 2022

[1] Department of Civil, Geological and Mining Engineering, Polytechnique Montréal, P.O. Box 6079 Station Centre-Ville, Montréal, Canada H3C 3A7

Abstract

To design a ground heat exchanger, simulations are frequently used. One way to perform simulations is to use the well-known g-functions to obtain the ground temperature. These functions are usually obtained by analytical or numerical models, which limits the precision or takes long simulation time. Recent advances show that the short-term g-functions can also be retrieved by a deconvolution algorithm. However, the known deconvolution algorithm is only validated for a set of operating parameters and duration of less than 10 days. A first objective of this article is to demonstrate that longer g-functions can be retrieved with such an algorithm. Then, a second objective is to extend the application of the deconvolution to consider time varying operating parameters throughout a ground heat exchanger's operation. To achieve those objectives, the deconvolution will be first applied to various numerical year-long simulations of a ground source heat pump system with stationary conditions. Then, an extended multi-signal deconvolution will be applied to a non-stationary thermal response test of 30 days. Both tests show adequate temperature reconstruction with RMSE of less than 0.05 °C and 0.2 °C for the first and second scenarios respectively.

C.1 Introduction

Employing a geothermal heat pump connected to a ground heat exchanger (GHE) can significantly reduce a building's heating and cooling energy consumption, affecting positively the building sector's carbon emission [12, 182]. To design a GHE, simulations employing g-functions are commonly performed to compute the ground temperature [39]. These functions describe the time evolution of the ground temperature along the borehole length to a unit impulse signal, and are generally used to find the borehole temperatures under a vary-

ing heating load [133]. Various methods were developed to compute these functions. They rely on analytical [78, 138, 139, 204], polynomial [133], numerical [237] or block matrix [126] methodology. All these methods have limitations in some ways, either by assumption on analytical model or high computation cost to retrieve the site-specific g-function.

Recent advances have made it possible to use a deconvolution algorithm to obtain the short-term g-function (STgF) from the experimental data of a thermal response test (TRT) [177, 205]. Such an algorithm does not require a direct analytical or numerical model and directly uses the experimental data to obtain the STgF. Another advantage is that defining the STgF at the borehole outlet, as done by Dion et al. (2022) [205], incorporates the thermal conductivity and capacity of the ground and of the GHE (e.g., casing, grout, pipe, and fluid). Such deconvolution algorithm performs an inversion on a set of nodes, so that the convolved temperatures are closest to their experimental counterparts. At publishing time, the deconvolution algorithm has not been used to obtain g-functions longer than periods or time representative of TRTs (e.g., 3 to 10 days).

Often, the heating power and the flow rate will vary to accommodate a heating demand, creating a system that is non-stationary through time. Recent advances in convolution algorithms allow to consider such non-stationary conditions and hands high quality results with both flow rate and heating power variations [143]. To resolve such situations, several transfer functions are used (one for each state encountered) and convolved under the assumption of non-stationarity. Using such an approach, Beaudry et al., (2022) [102] observed that including non-stationarity can ensure adequate ground temperatures and reduce peak demand to the electricity network.

On currently operating systems, temperatures at the inlet and outlet of a GHE are often available. However, matching these temperatures with a model is usually difficult because the input parameters used to design the GHE are often inaccurate, obtained with erroneous assumptions or do not consider heterogeneity. Therefore, using a calibrated model to evaluate the future response of a GHE under various operating parameters, analyze the performance and durability of a GHE or understanding a GHE's interaction with a nearby system is still a challenge. An alternative could be to use the experimental long-term g-function of a GHE and use it for simulations. Obtaining such experimental long-term g-function has never been done before.

The goals of this article are twofold: first to apply the single-deconvolution algorithm of Dion et al., (2022) [205] to long GSHP system operation to obtain long-term g-function. Second, to provide an extension to the deconvolution algorithm of Dion et al. (2022) [205] to recover a set of transfer functions corresponding to the different operating parameters in a GHE,

occurring during the operation of a GSHP system.

C.2 Methodology

A deconvolution algorithm is simply the inverse of a convolution. Both convolution and deconvolution are usually only applied to stationary systems (e.g., a GHE with constant flow and bleed rates). It is, however, possible to consider non-stationarity, for which the specific case is stationarity. This section first presents the non-stationary convolution used for GSHP system and then, the deconvolution algorithm.

C.2.1 Non-Stationary Convolution (forward problem)

The forward model is based on the convolution equation, which is described with the equation:

$$T_{out}(t) - T_0 = (f * g)(t) = \sum_{j=1}^{i} f(t_j) \cdot g(t_{i-j+1}) \tag{C.1}$$

In this equation, f in is the excitation function and corresponds to the heating power change $f = Q(t_i) - Q(t_{i-1})$. T_0 is the initial ground temperature and T_{out} is the GHE borehole outlet temperature. The variable g is a transfer function, which corresponds to the variation of a system to a unit impulse. In the case of a GSHP system, it is the GHE response to an impulse of 1 W throughout the length of the operation period. Hence, by normalizing f by 1 W, the units of g are °C, which differs from the dimensionless g-function of Eskilson (1987) [39]. Hereinafter, the expression transfer function will be used to avoid misunderstanding but the underlying concept is the same.

Eq. C.1 is valid for a steady circulation flow or bleed rate, which describes the state of the GHE operation. To account for state changes, during operation, Beaudry et al. (2021) [143] incorporated a time dependence to the transfer function of Eq. C.1, $g(t_{i-j+1}, t)$. In that way, the convolved borehole outlet temperature becomes a combination of the excitation function convolved by the corresponding transfer function. In that form, the combination results in discontinuous signal at the state changes. To correct the signal, a correction function is added to the convolution so that, for each state transition, a corresponding state variation is applied. To the interested reader, the non-stationary convolution is described in greater details in Beaudry et al. (2021) [143].

It is worth mentioning that the accuracy of the non-stationary convolution is within a mean-absolute-error of less than 0.06 °C on the operating temperature of a GSHP system. Hence, the method has a high accuracy, but is not an exact solution, as would be a stationary

convolution.

C.2.2 Stationary or Non-Stationary Signal Deconvolution (inverse problem)

The deconvolution algorithm is akin to an optimization problem, in which the parameter to be optimized is the transfer function in Eq. C.1. This section presents an extension to the algorithm of Dion et al., (2022) [205] to deconvolve a set of transfer functions for the non-stationary case instead of a single one in a stationary scenario. The algorithm is closely related to the original one and can also be used for single-signal deconvolution.

Using a non-stationary convolution, multiple transfer functions can be obtained. To achieve that, a set of nodes τ_j (between 20 and 40 per function), spaced logarithmically on each transfer function, are selected as the optimization parameters. To reconcile the nodes τ_j and the time array t of the GSHP system operation, a piecewise cubic Hermite interpolation polynomial (PCHIP) is performed on each transfer function before the non-stationary convolution. The goal of the inversion is then to optimize the nodes values of each transfer function, so that the non-stationary convolution is close to the experimental operation temperatures $T = T_{out} - T_0$. The goal to attain is:

$$\hat{g}_{Set}(t) = \arg\min_{\hat{g}(\tau_j)} \left(\left\| \left(\widehat{T} - T_{Exp} \right)(t) \right\|_2 | C_1, C_2 \right) \tag{C.2}$$

In the previous equation, $\hat{g}_{Set}$ is the estimated transfer functions obtained by deconvolution, τ_j are the nodes selected on each transfer function, t is the time vector, $\widehat{T}$ is the estimated temperature obtained by non-stationary convolution, T_{Exp} is the experimental temperature. Finally, $\|.\|$ is the l_2 norm.

In Eq. C.2, the parameters C are positive derivative and negative second derivative constraints applied to each node of each transfer function. The first constraint is to impose the fact that the transfer function must be increasing with time. The second constraint reflects the general observation that the temperature is slowly reaching a steady state under a constant heating power. This is enforced by constraining the slope of the transfer function's first derivative to be strictly negative after a certain point. The two following equations describe the constraints, which are implemented in the optimization as linear inequality equations on the nodes.

$$0 < \hat{g}(\tau_j) < \hat{g}(\tau_{j+1}) \; \forall \; j \in [1, n-1] \tag{C_1}$$

$$0 < \hat{g}'(\tau_{j+1}) < \hat{g}'(\tau_j) \; \forall \; j \in [z, n-1] \tag{C_2}$$

where z is the node τ_j from which the first derivative has a negative slope.

To ensure faster convergence, a first approximation of the optimization problem is required. Here, an initial guess of the transfer function set used by the main optimization algorithm is obtained with the use of 2 subsequent inversion problems. The first one assumes a stationary state and fits a single transfer function based on an exponential integral equation, of the form $\tilde{g}_0(x_1, x_2, t) = x_1 \int_(x_2)^{\frac{e^{-t}}{t}} dt$ with x_1 and x_2 being the optimization parameters, to the experimental temperature: $\hat{g}_0(t_i) = \min_{x_1,x_2} \|(f(t) * \tilde{g}_o(x_1, x_2, t)) - T_{Exp}(t)\|_2$. The temperatures with this method are not well reproduced in a non-stationary scenario, since only one set of circulating flow and bleed rates (i.e., state) is considered. To enhance the fit, one transfer function per state $\hat{g}_s$ can be obtained by scaling the initial function $\hat{g}_0$ by coefficients a_s, i.e., $\hat{g}_s(t) = a_s \cdot \hat{g}_0(t)$. The coefficients a_s are obtained through the minimization with non-stationary convolution: $a_s = \min_{a_s} \|(f * (a(s) \cdot \hat{g}_0))(t) - T_{Exp}(t)\|_2$. The main optimization will then use the set of $\hat{g}_s(\tau_j)$ evaluated at nodes τ_j for each state s as the initial solution.

C.3 Validation scenarios

To assess the performance of the proposed deconvolution algorithm and to fulfill the objective of the paper, two test cases are used. The first one is a set of four year-long numerical simulations with different sets of constant operating parameters of a GSHP system using a SCW. This case will be used to obtain long-term transfer functions with the stationary deconvolution. The second case is a field TRT of 30 days with time-varying circulating flow and bleed rates. This case will employ the deconvolution to retrieve an experimental set of transfer functions with the non-stationary deconvolution.

The stationary case is made using the numerical model based on the work of Beaudry et al., (2022) [102] on a system with 5 SCWs. The recordings have time steps of one hour, over a year of operation. Four simulations were generated, each using different constant sets of operating circulating flow and bleed rates, as described in Table C.1. Each state is described by its respective numerically generated transfer function. Then, temperatures T_{out} are generated by applying a superposition principle (or convolution) to the known ground heating power profile and the numerical transfer functions. These signals are then used in a stationary deconvolution to obtain the long-term transfer function.

The non-stationary case has samplings at every minute and is performed on the SCW site described by Beaudry et al. (2018, 2019) [1, 238], which was built in Varennes, Quebec. The SCW is 215 m deep and an injection well of 150m was dug at about 10 m from the main well to receive the bled flow rate. The TRT was performed in July 2019 and varies the heating power, the circulating and bleed rates to stimulate the well under non-stationary operating conditions. In total, 4 successive states occur during the TRT and are described in Table

Table C.1 Circulating flow and bleed rates for the four different states used for the stationary and non-stationary cases.

Test case	**Flow Rate**	g_1	g_2	g_3	g_4
Stationary	Circulating (L/min)	326	408	489	568
	Bleed (L/min)	65	82	98	170
Non-stationary	Circulating (L/min)	71	71	145	145
	Bleed (L/min)	0	7	0	15

C.1. Two different circulating flow rates are used, and a bleed flow rate of approximately 10% is activated in the middle of each sequence. To minimize the impact of high frequency noise on the data, a moving average filter with a window of 10 points was used on both the temperature and heating power of the field TRT. For both test cases, the physical parameters are reported in Table C.2.

Table C.2 Thermal properties of the numerical model used for the stationary (left) and non-stationary (right) cases.

Parameter	**Symbol**	**Unit**	**Ground**	**Pipe**	**Water**
Volumetric Heat Capacity	ρC_p	kJ m^{-3} K^{-1}	2160 | 2070	2000 | 2174	4187 | 4176
Porosity	n	-	0.01 | 0.02	0 | 1e-05	1 | 1
Thermal Conductivity	k	W m^{-1} K^{-1}	3.99 | 2.78	0.45 | 0.42	0.57 | 0.59
Hydraulic Conductivity	K	m s^{-1}	6.5e-5 | 5.7e-7	1e-9 | 1e-09	1000 | 1000
Specific storage	S_s	m^{-1}	1e-4 | 6.4e-4	4e-6 | 4e-10	4e-6 | 4e-10

C.4 Results

C.4.1 Stationary case – Simulated temperatures

In Figure C.1, the results of the stationary deconvolution applied to four different simulations are presented. It can be noted that both the transfer functions and the temperature are reproduced with great accuracy. The RMSE of the various transfer functions are all less than 0.001 °C/W and the RMSE of the 4 temperature fits are of less than 0.044 °C. In all cases, the constraints C_1 and C_2 are always respected. Indeed, each case shows strictly growing transfer functions and strictly downward first derivative slope from the beginning of the transfer functions, showing that the value z in the constraint C_2 can be taken as the first hour of operation. The larger deviations on the curves are at the end of the functions and mostly visible on the derivatives. All the stationary deconvolution converged in under 30 seconds.

C.4.2 Non-Stationary Case – Experimental Temperatures

In Figure C.2, the results of the non-stationary deconvolution applied to the TRT experimental data are shown, with the associated temperature RMSE being of 0.19 °C. One can notice that the transfer functions are not all the same length. Instead, they are only illustrated on their respective activation time. This means that, for example, the function corresponding to the first state (i.e., flow rate of 71 L/min and bleed rate of 0 L/min) is only used for the first 8 days of the TRT. The second function, corresponding to the second state (i.e., flow rate of 71 L/min and bleed rate of 7 L/min), is used on the first 16 days since the first 8 days impact the temperature between 8 and 16 days. The vertical lines on Figure C.2 shows the ending moment of each transfer function.

The algorithm converged in only 57 iterations and 35 minutes but had difficulty to enforce the C_2 constraint, as can be seen in Figure C.2 c). This could be explained by the difficulty of the algorithm to find a global minimum due to the large number of nodes to optimize. Indeed, each function has 22 nodes, which amount to 88 parameters to estimate on a test composed of 43200 data points.

C.5 Discussion

The results show that both the stationary and non-stationary deconvolution algorithms are quite good at reproducing the temperature of either the year-long simulation or the long field TRT. This stems from the use of the temperature as the sole factor in the objective

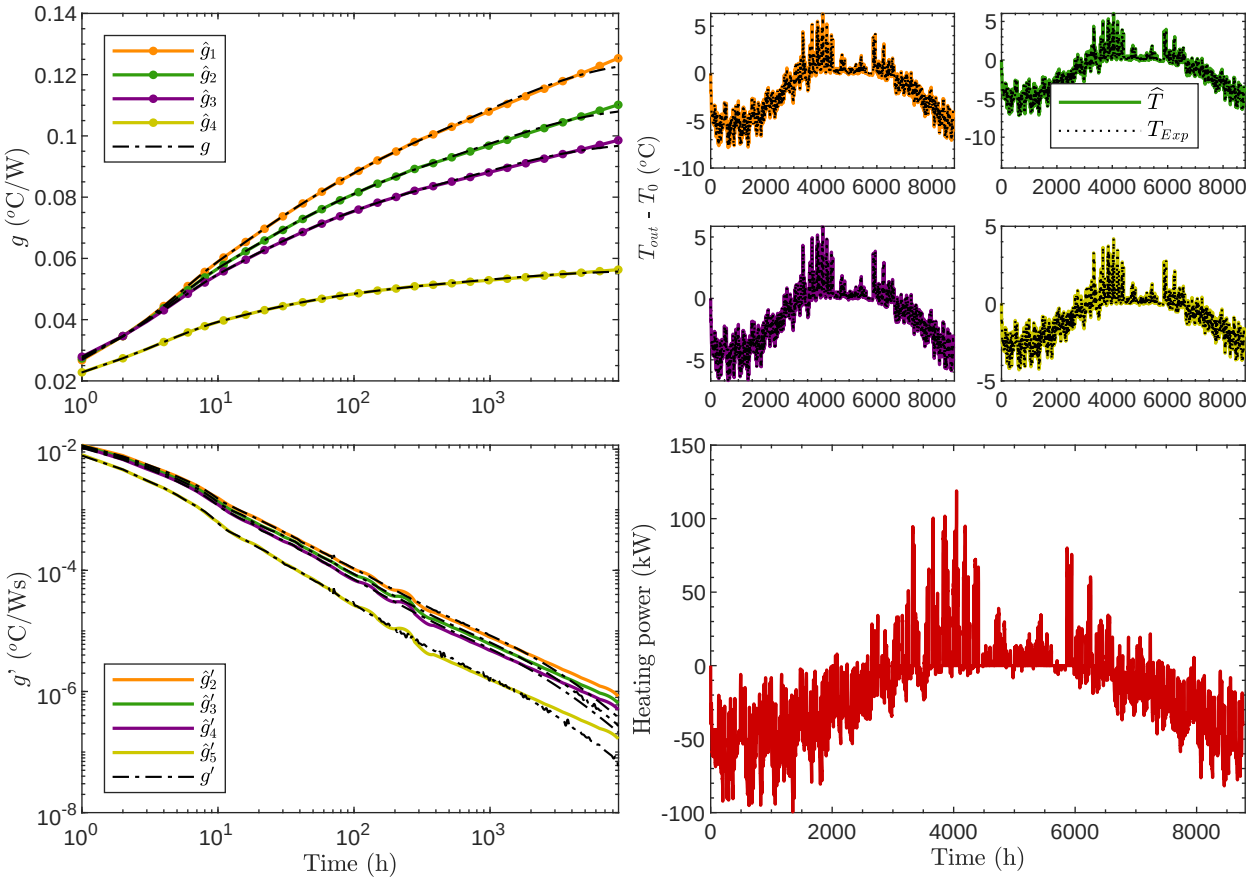

Figure C.1 Stationary deconvolution results on 4 numerical test cases using the same heating power profile. a) and c) Deconvolved and numerical transfer functions and their derivatives respectively. b) Convolved and simulated temperatures. d) Heating power profile used in each deconvolution. The dots in a) show the nodes τ_j. The RMSE for the 4 cases are respectively: 0.04, 0.04, 0.03 and 0.01 °C.

function of Eq. C.2. In the stationary deconvolution algorithm, the transfer functions show a great fit with the numerical ones. Although the experimental ones are not available for the TRT, the transfer functions are not as smooth as expected. This could stem from the way the optimization problem is set to optimize only the temperature fit. Note, however, that the fluctuations of the first derivative appear visually exaggerated using a log-log scale. One way to smooth the transfer function could be to add regularization terms to the objective function.

Also, it is noticeable that the constraint C_2 described at Eq. C_2 is not always respected during the non-stationary deconvolution. This is apparent by the slope of the transfer function first derivatives that are not always negative after around 3 hours of test. This last value was

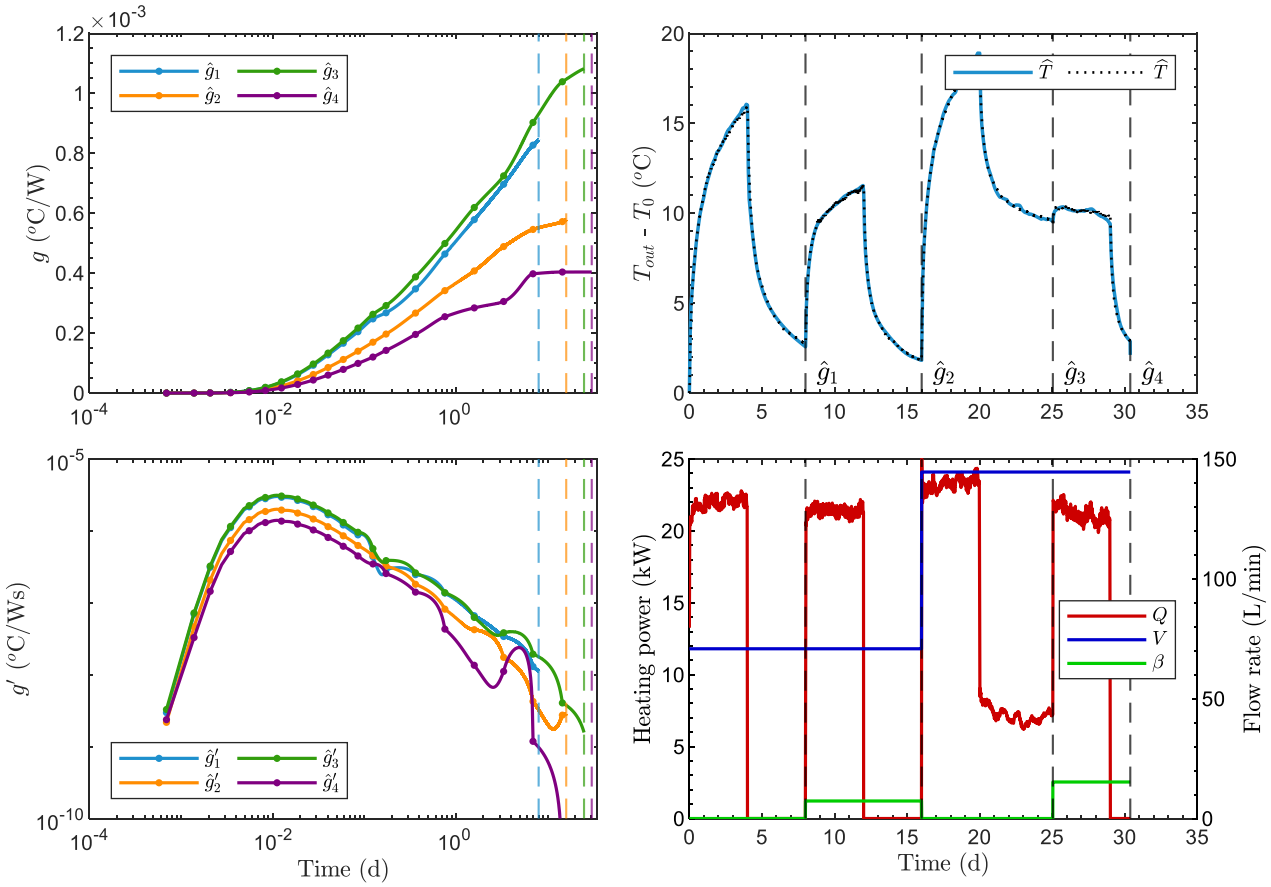

Figure C.2 Non-stationary deconvolution result on an experimental TRT with 4 successive states. a) and c) Length dependent deconvolved transfer functions and their derivatives respectively. b) Convolved and experimental temperatures. d) Heating power (Q) profile, circulating flow (V) and bleed (β) rates used in each deconvolution. The dots on the curves in a) show the location of the nodes τ_j. The temperature RMSE is 0.19 °C.

taken arbitrarily, to ensure that the TRT was in a relative steady state. In that section of the transfer function, the first derivative's slope should be strictly downward, as can be seen in the stationary deconvolution in Figure C.1. In Figure C.2, some functions show positive first derivative at long times, even if the nodes show a downward trend for these times. Indeed, PCHIP interpolation ensures that g is increasing but not that its derivative behaves as desired. This shows the complexity of the inversion problem, and that further work is needed to obtain in non-stationary case transfer functions with all the desired properties.

It is worth noting that for both stationary and non-stationary deconvolution, the measurement errors of the flow and bleeding flow rates are simplified to continuous or step signals. The flow rates shown in Figure C.2 are segmented averages of their measured signals. However,

these signals are affected by natural variation and measurement errors. This simplification is used to ensure that a limited number of transfer functions are deconvolved. Otherwise, there could be as much transfer functions as data point in the flow rates signals. The impacts of such a simplification are hard to estimate but are to be considered when analyzing deconvolution results.

Finally, an aspect limiting the fit in the non-stationary case is the precision of the forward model. In Beaudry et al. (2021) [143], it is mentioned that the non-stationary convolution method has higher residuals within the fluid residence time due to slight imprecision in the correction function. Also, vertical temperature profiles are not considered in the current application of the forward model. This could represent an additional error since it was demonstrated that it has a significant influence on the groundwater temperature along the borehole wall in SCW operations [1].

C.6 Conclusion

In this article, a deconvolution algorithm was used both in stationary and non-stationary conditions to recover transfer functions related to the operating parameters occurring in the GHE. The stationary deconvolution showed that long-term transfer functions can be obtained, and the application of non-stationary deconvolution was demonstrated on an experimental test case. It has been shown that the experimental temperature can be recovered with temperature fits with accuracies of less than 0.05 °C with stationary deconvolution and 0.2 °C with non-stationary deconvolution.

This algorithm has the potential to help GHE response simulation by providing a way to obtain experimental transfer functions on both stationary and non-stationary scenarios. The extension of the deconvolution toward non-stationary situations makes the algorithm more flexible and applicable to a larger set of situations that can be encountered in field application, such as GSHP systems that have been operating for several years or with time-varying flow rates. In this case, the deconvolution can be applied to validate the performance of the system.

C.7 ACKNOWLEDGMENTS

The authors wish to acknowledge the support and funding provided by the Natural Sciences and Engineering Research Council of Canada (grant number RDCPJ 530945), the Trottier Energy Institute, Hydro-Québec, FTE drilling, Marmott Energies, Richelieu Hydrogeology and Versaprofiles.

C.8 Nomenclature

C.8.1 Variables

a	Scalar weights to roughly adjust $\hat{g}_{0,s}$ (-)
β	Bleed flow rate (L/min)
C	Constraint applied on the nodes in the optimization problem (-)
f	Incremental heating power function (W)
g	Transfer function (°C/W)
τ	Nodes used as optimization parameters (-)
Q	Heating power (W)
T	Temperature (°C)
V	Circulating flow rate (L/min)

C.8.2 Subscripts

Exp	Experimental
0	Initial
out	Borehole outlet
s	State identifier
Set	Group of transfer functions